General Disclaimer

One or more of the Following Statements may affect this Document

NASA CR-
144446

◆ VOUGHT SYSTEMS DIVISION
LTV AEROSPACE CORPORATION

P.O. BOX 5907 · DALLAS, TEXAS 75222

FINAL REPORT
for

NASA/JSC CONTRACTS NAS9-13074 AND NAS9-13506

DEVELOPMENT AND PARAMETRIC EVALUATION
OF THE
PROTOTYPE 2 AND 3 FLASH EVAPORATORS

Report T157-76

18 July 1975

Submitted by:
VOUGHT SYSTEMS DIVISION
LTV Aerospace Corporation
Dallas, Texas

To

NATIONAL AERONAUTICS AND SPACE ADMINISTRATION
Johnson Space Center
Houston, Texas

Prepared by:

C. W. Hixon

C. W. Hixon

J. B. Dietz

J. B. Dietz

Approved by:

Ray French

Ray French - Supervisor
ECS Group

TABLE OF CONTENTS

LIST OF FIGURES (CONT'D)

LIST OF FIGURES (CONT'D)

LIST OF TABLES

1.0 SUMMARY

The development of the Prototype 2 and 3 flash evaporator heat sinks which vaporize an expendable fluid to cool a heat transport fluid loop is reported herein. The units developed utilize Freon 21 as the heat transport fluid and water as the expendable fluid to meet the projected performance requirements of the Space Shuttle for both on-orbit and ascent/re-entry operations. The evaporant is pulse-sprayed by on-off control onto heat transfer surfaces containing the transport fluid and exhausted to the vacuum environment through fixed area exhaust ducts.

The objectives of the effort reported herein were the design, development testing and extensive system testing of two flight prototype flash evaporator configurations which can meet the projected Shuttle performance requirements. The work was performed for NASA-JSC by the Vought Systems Division of the LTV Aerospace Corporation under contracts NAS9-13074 and NAS9-13506.

Element, component, and system feasibility testing was conducted to provide basic design data and to verify the approach used for the development of the two Prototype evaporators. The element/feasibility testing included: nozzle testing to obtain spray pattern data for use in heat transfer surface configuration design; spray droplet impingement and evaporation data obtained to better define heat transfer surface-interface performance capabilities and interactions; feasibility demonstration of a top-off evaporator system configuration with the evaporator equipped with a long exhaust duct and supersonic nozzles; system feasibility tests for an evaporator constructed from heat exchanger core to verify its use as the heat transport surface for the Prototype 2 and 3 units; and heat exchanger core element tests to obtain design data.

Design trade and optimization studies were performed to identify the configuration and construction of the Prototype evaporators. The system approach selected utilized separate units in each of the dual Freon loops, and employed load partitioning, between top-off and re-entry units, to minimize potential Shuttle installation weight and reduce installation volume. Two evaporators constructed of 18.5 fins per inch rectangular, lanced fin aluminum heat exchanger core with a cylindrical configuration were designed and fabricated. The units were 380 mm (15 inch) in diameter with cylindrical sidewalls 216 mm (8.5 in.) high with a single layer of heat exchanger core, and were compatible with a number of spray nozzle designs and deposition rates. The two units had different bottom-plate configurations so that both solid cone and hollow cone spray nozzles and

different duct entry locations could be evaluated in test. The Prototype evaporators weighed less than 2.2 Kg (5 lbs) each. An integrated valve/nozzle design was developed which resulted in a hold up volume of less than 0.15 cc to minimize ice chip buildup during cyclic operation. A backplate fabricated from plexiglas was constructed to aid in visual observation of the evaporators during operation.

The Prototype evaporators were extensively system tested both individually and in a Shuttle installation configuration. Early tests indicated flow maldistribution in both evaporators caused by core design and fabrication anomalies This was attributed to flow stagnation at core splice intersections in the circular bottom plate section. The circular bottom plates were redesigned to eliminate these flow stagnation areas, fabricated, and retrofitted to the Prototype 2 and 3 sidewalls.

The modified Prototype flash evaporators were then successfully tested to verify the design and demonstrate application to meeting the Shuttle performance requirements. The load partitioning approach was demonstrated with evaporation efficiencies of 98% for both the high and low temperature unit configurations. Nozzle location optimization testing indicated that the evaporator volume could be reduced 35% over the "as-fabricated" volume. With the evaporator and "on-off" controller configured for the Shuttle top-off mode, the evaporator system demonstrated outlet temperature control within $\pm$ 1.1°K ($\pm$ 2°F) of the set point for inlet temperature rate changes of 1.6°K/min (2.8°F/min). In the Shuttle re-entry mode, the evaporator system with the two units in series demonstrated control stability with outlet temperature control to $\pm$ 1.1°K ($\pm$ 2°F) with inlet temperature rate changes of up to 5.5°K/min (10°F/min).

A failure mode and effects analysis (FMEA) was performed for a proposed Shuttle flash evaporator system. Fault detection failure isolation equipment was defined for the evaporator system. The results of the study indicated that no single failure in the evaporator system would result in a condition that does not meet the fail-safe reliability criteria.

The Prototype 2 and 3 flash evaporators developed met the objective of the program and demonstrated the capability to meet the system performance requirements for use on the Space Shuttle. The design and fabrication of optimized flight representative units which meet the finalized Shuttle installation as well as performance requirements is recommended as the next phase in flash evaporator development.

2.0   INTRODUCTION/BACKGROUND

The Spraying Flash Evaporator is a recent concept for an expendable heat sink. A device of this type directs a sprayed liquid onto a dry heated surface where it is evaporated in single droplet fashion. The latent heat is provided by a circulating transport fluid which flows through the heat exchange surface. The Spraying Flash Evaporator provides (1) a simple design offering high reliability, (2) control by supply rate pulse modulation, (3) low acceleration sensitivity, (4) capability of multifluid evaporation, (5) long life expectancy, and (6) low weight. Because of these features the evaporator is a candidate for Space Shuttle use, and its development is being pursued by NASA.

Exploratory tests were conducted under NASA Contract NAS9-11254 in 1970-71 to determine the feasibility of evaporation by direct spray impingement on a heated wall. The tests, demonstrated: (a) that evaporation fluxes of 2.52 watt/cm^2 (8,000 BTU/hr-ft^2) were possible, (b) evaporant utilization of 90 percent for water, (c) transport fluid temperature control of $\pm$ 3°K ($\pm$ 5°F) at a 227°K (40°F) set point. Reference 1 documents the results of these studies.

Based on the results of these feasibility tests, the design, development and testing of a laboratory prototype flash evaporator which incorporated the size, construction, flow and temperature conditions expected for Space Shuttle application was pursued under NASA Contract NAS9-12026. The resulting Prototype I evaporator, shown in Figure F-1 was designed to reject the Shuttle Phase B heat load of 14.6 kW (50,000 BTU/hr), underwent a successful five week test program that demonstrated (a) outlet temperature control to 277°K $\pm$ 3° (40°F $\pm$ 5°), (b) dormant to active operation with no start up or shut down sequences, (c) 95% evaporative efficiency for water, and (d) performance insensitively to evaporator orientation, evaporant supply pressure, transport fluid flow rate, or use of active or redundant transport/evaporant system. These results are reported in detail in References 2 and 3.

To further investigate the basic spray evaporation technology and to improve the fabrication/construction of the flash evaporator, the Prototype 2 flash evaporator development program was initiated and pursued under Contract NAS9-13074. The objectives of the Prototype 2 program as initially planned were: (a) investigate nozzle spray patterns experimentally to find the effect of internal geometry on droplet size and spatial distribution; (b) study droplet

impingement and evaporation phenomena using high speed photography; and (c) pursue design and fabrication improvements for the Prototype 2 evaporator. (These included: valve/nozzle integration to reduce the liquid hold-up volume, the use of seamless drawn extruded tubing to eliminate tube splitting during brazing, elimination of salt pot brazing, and improved fabrication tooling.)

As the Prototype 2 program progressed, the Shuttle heat loads became better defined at much higher values than originally anticipated, the requirement for radiator "top-off" on-orbit with vapor exhaust through a supersonic nozzle was identified, and dual Freon coolant loop operation was baselined. To accommodate these changes, the Prototype 2 evaporator was redesigned based on optimization studies which led from the original wound tube heat transfer surface to one employing compact heat exchanger core to reduce weight and volume of the device. Additionally, the Prototype I evaporator was modified and extensively tested at NASA-JSC during this program to demonstrate the device applicability for meeting radiator top off requirements.

The Prototype 3 flash evaporator program was undertaken concurrently with the Prototype 2 design to investigate alternate flash evaporator configurations and to extensively test both prototype flash evaporators. The program, performed under NASA contract NAS9-13506, investigated: heat exchanger configuration, exhaust duct configuration, failure detection/fault isolation requirements, and component/system operational characteristics.

The results of both the Prototype 2 and 3 flash evaporator development programs have been integrated into this single report in order to present all data from element/feasibility testing, design optimization studies, and system testing which are applicable to both devices. The work was performed for the NASA-JSC Crew Systems Division under the technical direction of Mr. Frank Collier by the Vought Systems Division of the LTV Aerospace Corporation.

3.0 ELEMENT/FEASIBILITY TESTING

Element, component and system feasibility testing was conducted during the program to provide basic design data and to demonstrate feasibility of the approach for the development of the Prototype 2 and 3 flash evaporators. The results of these tests are summarized in the subsections that follow.

3.1 Nozzle Development Testing

The spray nozzle has been demonstrated to be a critical factor in the evaporator design. Nozzle configurations have been observed to produce a combined droplet size, distribution, and supply rate such that local accumulations of frost result independent of surface temperature. Additionally, non-uniform spray patterns, spray adherence to the nozzle face, and evaporant supply pressure limitations can plague the evaporator operation. During the development of the Prototype 2 and 3 flash evaporators and the Prototype I modification program, extensive nozzle testing was performed to find an acceptable combination of nozzle spray characteristics with various configurations of evaporator heat transfer geometry.

The various nozzle configurations selected for evaluation during the program (shown in Figure 3-1) encompassed a wide range of capacities, spray patterns, and flow geometries. Nozzles with water flow capacities from 16 to 100 lbs/hr consistent with expected spacecraft supply pressures were tested. In addition to hollow cone spray patterns tested previously in the Prototype I program, nozzles with solid cone were evaluated in conjunction with six different potential heat exchanger core configurations. Two techniques were used in evaluating spray pattern/droplet distribution: (1) "implied distribution" using the surface temperature profiles of the Prototype I flash evaporator; and (2) direct analyses obtained from optical observations of a nozzle sprayed into an evacuated bell jar.

The data obtained from the nozzle testing was reduced and put into a useful format for the designer having to select a nozzle or nozzles for a particular evaporator heat exchanger core shape. This data is presented in Appendix A along with a description of the two techniques used to obtain the data.

(a) DELAVAN COOLING TOWER NOZZLE
(b) SPRAYING SYSTEM CO. ATOMIZING NOZZLE
(c) SPRAYING SYSTEM CO. FULLJET NOZZLE
(d) SPRAYING SYSTEM CO. FULLJET NOZZLE
(e) DELAVAN OIL BURNER NOZZLE
(f) SPRAYING SYSTEM CO. WHIRLJET NOZZLE
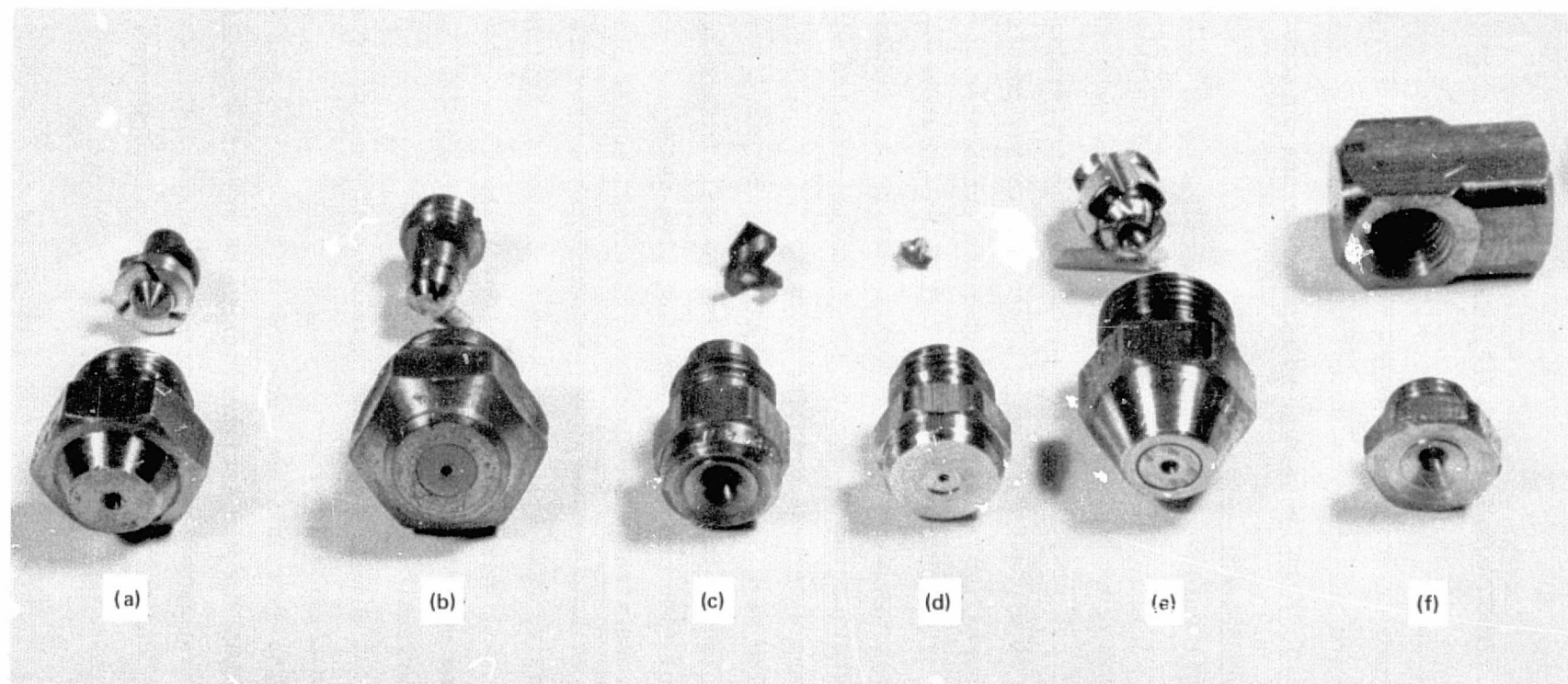
FIGURE 3-1 SPRAY NOZZLE CONFIGURATIONS EVALUATED

3.2 Spray Impact/Vaporization Testing

A series of spray impact/vaporization tests were conducted to get a
better understanding of the spray impact/evaporation/surface interface phenomena
under a wide range of simulated evaporator operating conditions. The tests
were conducted in three parts in conjunction with a NASA-JSC consultant,
Dr. J. J. Rizza. The specific objectives of these tests were: to observe, with
the aid of high-speed photography, the impacts of droplets striking a target
placed at various locations within the spray pattern produced by typical flash
evaporator nozzle; to observe, again with the aid of high-speed photography,
the subsequent droplet vaporization process; and to make quantitative measurements
of the superficial heat flux produced by the spray impact/vaporization process.
In the pursuit of these objectives, the parameters investigated included ambient
chamber pressure, surface temperature, spray impact angle, and surface location
in the spray.

The test set-up used is shown in Figure 3-2. A small target, electrically
heated, was used to simulate an evaporator segment. The target was placed in
the spray field of the baseline Prototype 2 nozzle (WDA-14-90° Delavan oil
burner nozzle). A Red Lake camera with a 10,000 fps capability was used to
record the interaction of the droplets with the heated surface.

The first series of tests, conducted in August 1972 under the direction
of Dr. Rizza, were performed at simulated chamber pressures of 133 N/m^2 (1 mmHg).
The photographic results of the six test conditions run at camera speeds of
5000 fps showed that: 1) considerable splattering and bounce of incoming droplets
occurred during impact (the smaller droplets were apparently frozen due to the
low chamber pressures); 2) larger liquid droplets formed ice caps while on the
target surface which tended to blow off during droplet evaporation; 3) incoming
droplet velocities were 20 m/sec as predicted. Dr. Rizza's observation and
explanation of the phenomena are reported in Reference 10.

Based on these results and on further data that the Prototype I flash
evaporator operated at 506 N/m^2 (3.8 mmHg), a second series of tests were con-
ducted by Dr. F. K. McGinnis of VSD during March 1973. These test results are
reported in detail in Appendix B and are summarized below. Based on analyses
of high speed photography data, a variety of phenomena appear present in the
impact/evaporation process. At any instant, sublimation, nucleate boiling, ice
cap ejection, and mass agglomeration may be occurring simultaneously. However,
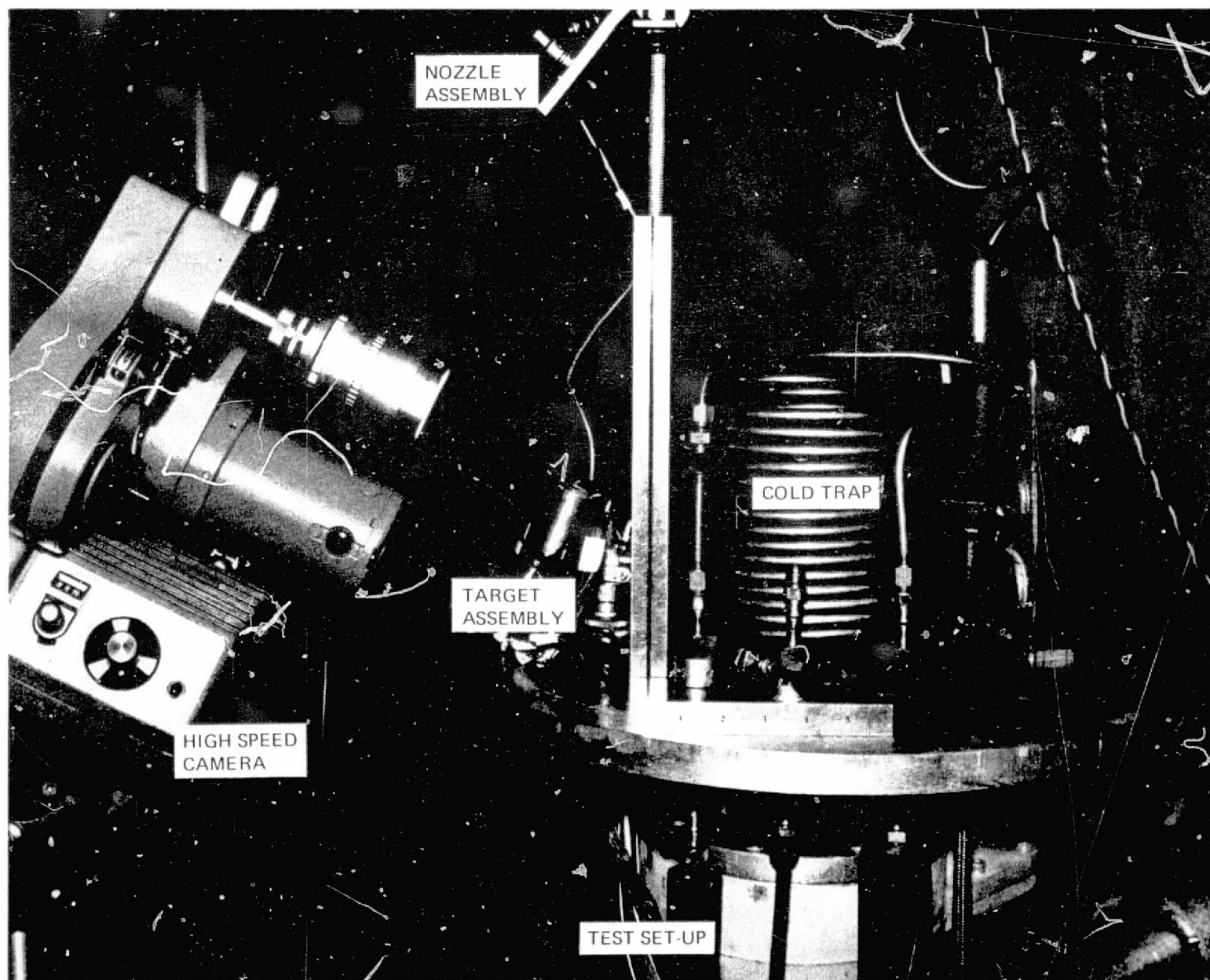
FIGURE 3—2 BELL JAR ELEMENT TEST SET-UP

the efficiency of the phase change process appears to deviate from 100% only under extreme conditions: i.e., surface temperatures sufficiently high to produce significant droplet bounce and splatter, or surface temperature sufficiently low, and pressure sufficiently high to cause surface flooding. Based upon spraying heat flux values inferred from target-transient response, it appears that droplet bounce/splatter becomes significant at surface temperature in excess of 338.71°K (150°F). A surface flooding boundary is postulated in Figure 3-3 which allows heat fluxes in excess of 63122 J/m^2-sec (20,000 BTU/ft^2-hr) at a surface temperature of 277.59°K (40°F). The range of 100%-efficient operating condition is quite wide.

A third series of tests were conducted under direction of Dr. Rizza in August 1973 with much lower camera speeds (600 fps) in order to observe the evaporation phenomena in more detail. In addition, a target constructed of cold plate heat exchanger core was used to better simulate the type of surface expected in the evaporator. Formation of bubbles in the larger liquid droplets on the surface which grow and eventually blow the droplets to pieces were noted at normal evaporator surface temperatures. It was also observed that the lower the target surface temperature, the better the liquid droplet spreads and wets the surface. At higher temperatures, an impacting droplet tended to break apart locally during the initial evaporation with the net effect of producing greater wetting of the surface and increasing heat transfer. Details of these tests are presented by Dr. Rizza in Reference 10.
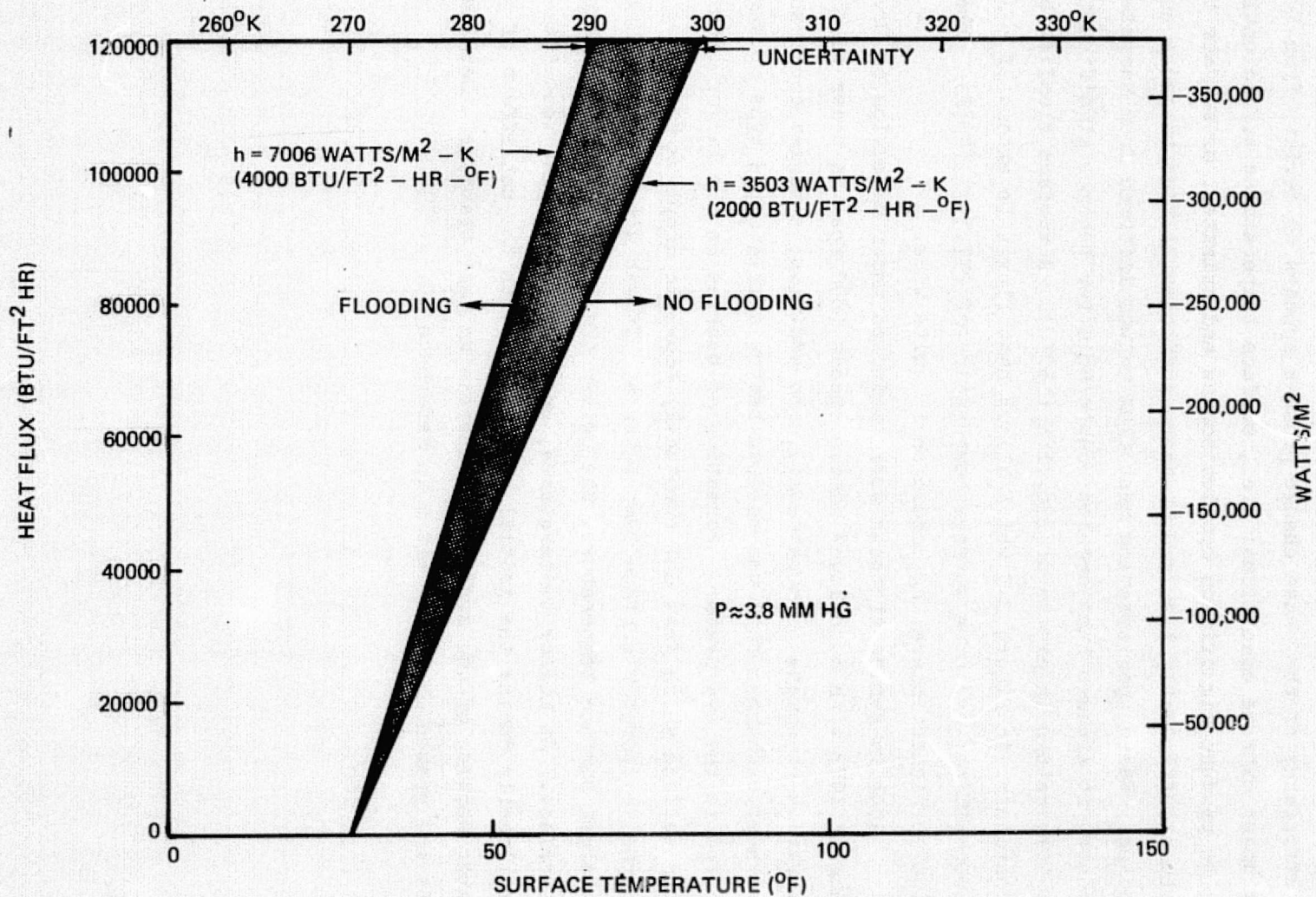
FIGURE 3–3 FLOODING BOUNDARY DEFINITION

3.3   Top-Off Evaporator Feasibility Testing

Simulated Shuttle active thermal control system testing was conducted at NASA Johnson Space Center during the summer of 1973 using a modified Prototype I Flash Evaporator as an expendable cooling device. The system tested, shown schematically in Figure 3-4, included 8 modular radiators, simulated fuel cell water supply, water storage tank, and an expendable cooling device. The modified Flash Evaporator was to demonstrate feasibility of the device application to "top-off" the radiator system during adverse orbital conditions and to dump excess fuel cell water produced during the mission. (The excess water is dumped on command from a water tank sensor which changes the mix temperature of the radiators.)

The 14.6 kW (50,000 BTU/hr) Prototype I evaporator was modified during the program to provide 4.69 kW (16,000 BTU/hr) of radiator top-off cooling. The exact performance requirements and flow conditions the device had to meet were:

Transport Fluid Requirements:

Fluid : Freon 21

Flowrate : 1000 Kg/hr (2200 lb/hr)

Heat Load Range: 0 to 4.69 kW (0 to 16K BTU/hr)

Inlet Temperature Range : 277.5 to 294°K (40° to 70°F)

Redundant Transport Loop Capability Required

Evaporant Fluid Requirements:

Evaporant : Deionized Water

Flowrate : 7.26 Kg/hr (16 lb/hr)

Supply Pressure : 0 to 3.5 Kp/cm^2 (0 to 50 psig)

Supply Temp : ambient 275 to 305°K (35° to 90°F)

Evaporator Chamber Operation Pressure : 5.2 x 10^{-3} Kp/cm^2 (3.8 mmHg)

Redundant Evaporant Supply Valve Capability Required

A Delavan 4.0-B-90° spray nozzle was selected and integrated into the metering valve to provide the proper spray distribution to achieve the desired performance. The backcone was modified to reduce overall evaporator volume to simulate the top-off device size expected on an actual design. Additionally, the evaporator was outfitted with a 75 mm (3-in) diameter by 1.83 m (6-ft.) long duct with two 45° bends to simulate Shuttle installation. Transport fluid lines were

8 RADIATOR PANELS

BANK CIRCUIT

PRIME CIRCUIT

INLET TEMP 285–345°K

MIX TEMP CONTROLLED TO 278,284 OR 295°K BASED ON WATER TANK LEVEL

MIXING VALVE

TANK LEVEL INDICATORS

H_2O TANK

H_2O FROM FUEL CELLS 0.45–5.9 KG/HR

EXPENDABLE COOLING DEVICE

NOZZLE

OUTLET TEMP CONTROLLED TO 278°K

HEAT LOAD AND PUMPS 1000 KG/HR 2.05 TO 20.5 KW
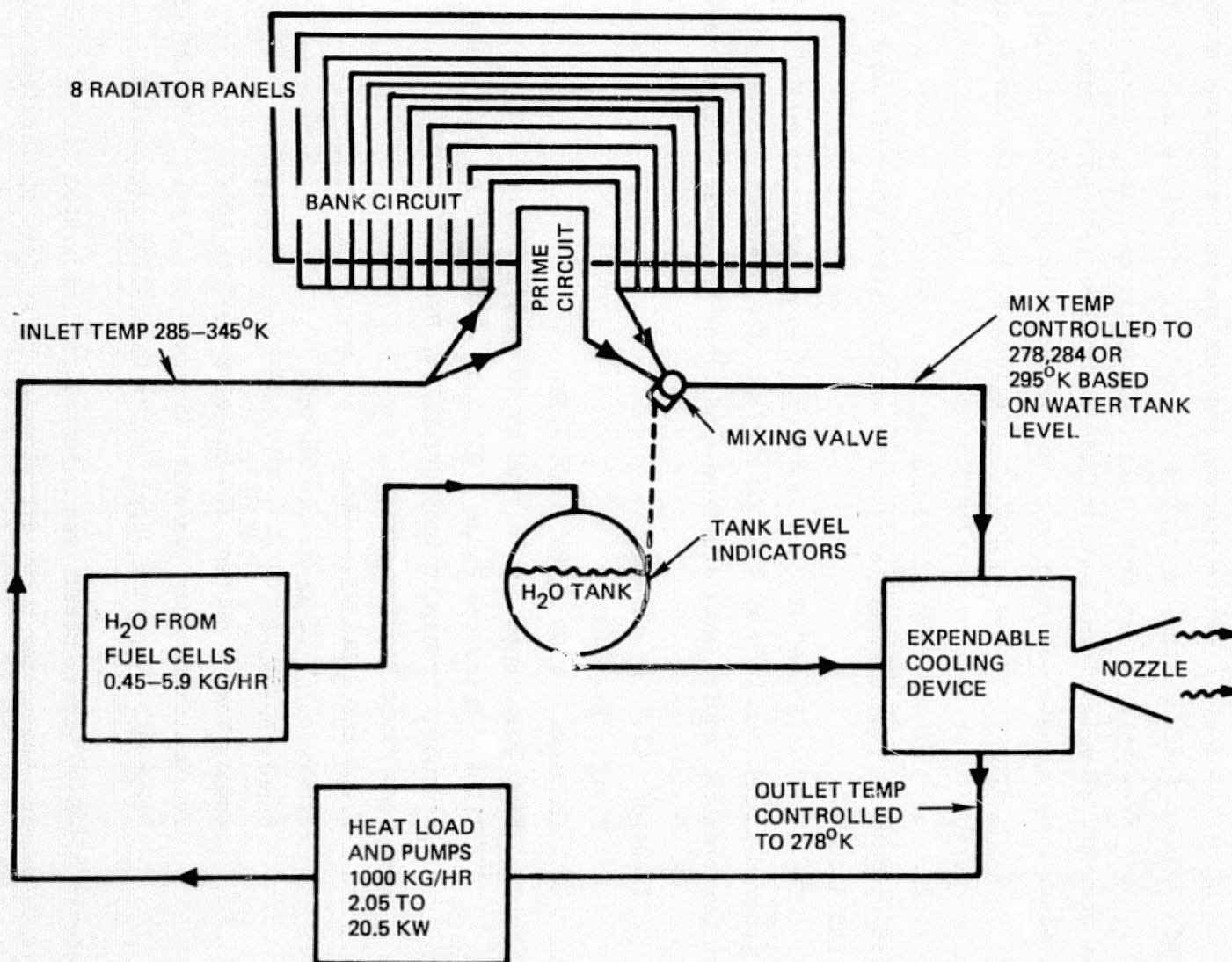
FIGURE 3–4 INTEGRATED RADIATOR EXPENDABLE COOLING SYSTEM SCHEMATIC

attached to the duct to prevent ice from depositing on the exhaust duct walls. The modified flash evaporator as installed in the NASA-JSC Chamber A is shown in Figures 3-5 and 3-6. Supersonic, plug, and sonic vapor exhaust nozzles, shown in Figure 3-7, were mated to the end of the duct to evaluate water vapor plume back-scattering on Shuttle surfaces.

The active thermal control system testing was performed under NASA contract NAS9-10534 and has been reported in detail in References 4, 5 and 6. The following is a summary of the pertinent results which are considered germane to the Prototype 2 and 3 development programs. The testing consisted of limit-case performance profiles and typical mission heat loads and environment conditions. The results of the Flash Evaporator operation are summarized in Figure 3-8 and Table 3-1. The test results demonstrated: (1) outlet temperature control with a set point of 278.6°K (42°F) with a temperature range of 276° to 280°K (37° to 44°F); (2) efficient operation with 100% evaporation efficiency for evaporator and exhaust duct combination; (3) stability of the evaporator control system for rapid transient changes in inlet temperature due to radiator mix temperature change; (4) repeated dormant to active device operation on command of the outlet temperature sensor; and (5) the evaporator performance is insensitive to the type of vapor exhaust nozzle utilized. The exhaust nozzle test data indicated that water vapor impingement could be reduced by a factor of 3 to 10 using a supersonic nozzle and by a factor of 25 to 100 for the plug nozzle over a sonic nozzle condition.

The testing verified the concept of the active thermal control system utilizing a flash evaporator to "top off" the space radiators. Based on these tests, the Shuttle baseline thermal control system was modified to include the "top off" evaporator to provide thermal control and to manage excess water.

SUBLIMATOR
SUPERSONIC NOZZLE
[52.1 CM (20.5") DIA AT EXIT]

FLASH EVAPORATOR
SUPERSONIC NOZZLE
[17.8 CM (7") DIA AT EXIT]

EXHAUST DUCT

EXHAUST DUCT

SUBLIMATORS
(HIDDEN)

MODIFIED PROTOTYPE I
FLASH EVAPORATOR
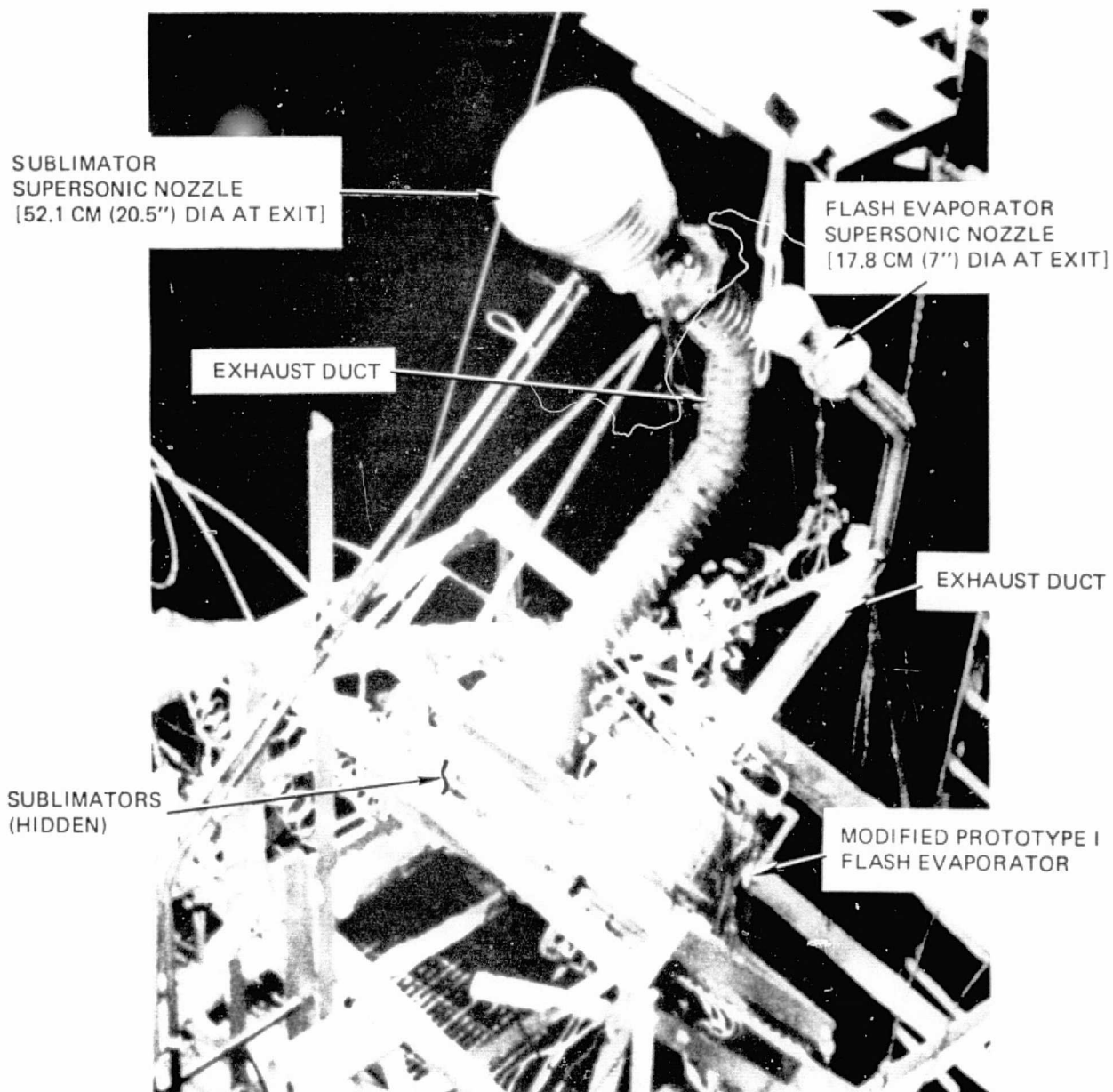
FIGURE 3–5 INSTALLATION FOR INTEGRATED SYSTEM TEST

FLASH EVAPORATOR
SUPERSONIC EXHAUST
NOZZLE

SUBLIMATOR SUPERSONIC
EXHAUST NOZZLE

7.6 CM (3") DIA
FLASH EVAP
EXHAUST DUCT
(HEATED BY AXIAL
FREON 21 FLUID
TUBES)

20.3 CM (8") DIA
SUBLIMATOR
EXHAUST DUCT
(HEATED BY SPIRAL
WOUND FLUID FREON
21 TUBES)

PROTOTYPE I
FLASH EVAPORATOR
[MODIFIED TO 4690 WATTS
(16000 BTU/HR)]

SUBLIMATOR – DUCT
TRANSITION SECTION
(UNHEATED)

LM SUBLIMATORS (2)
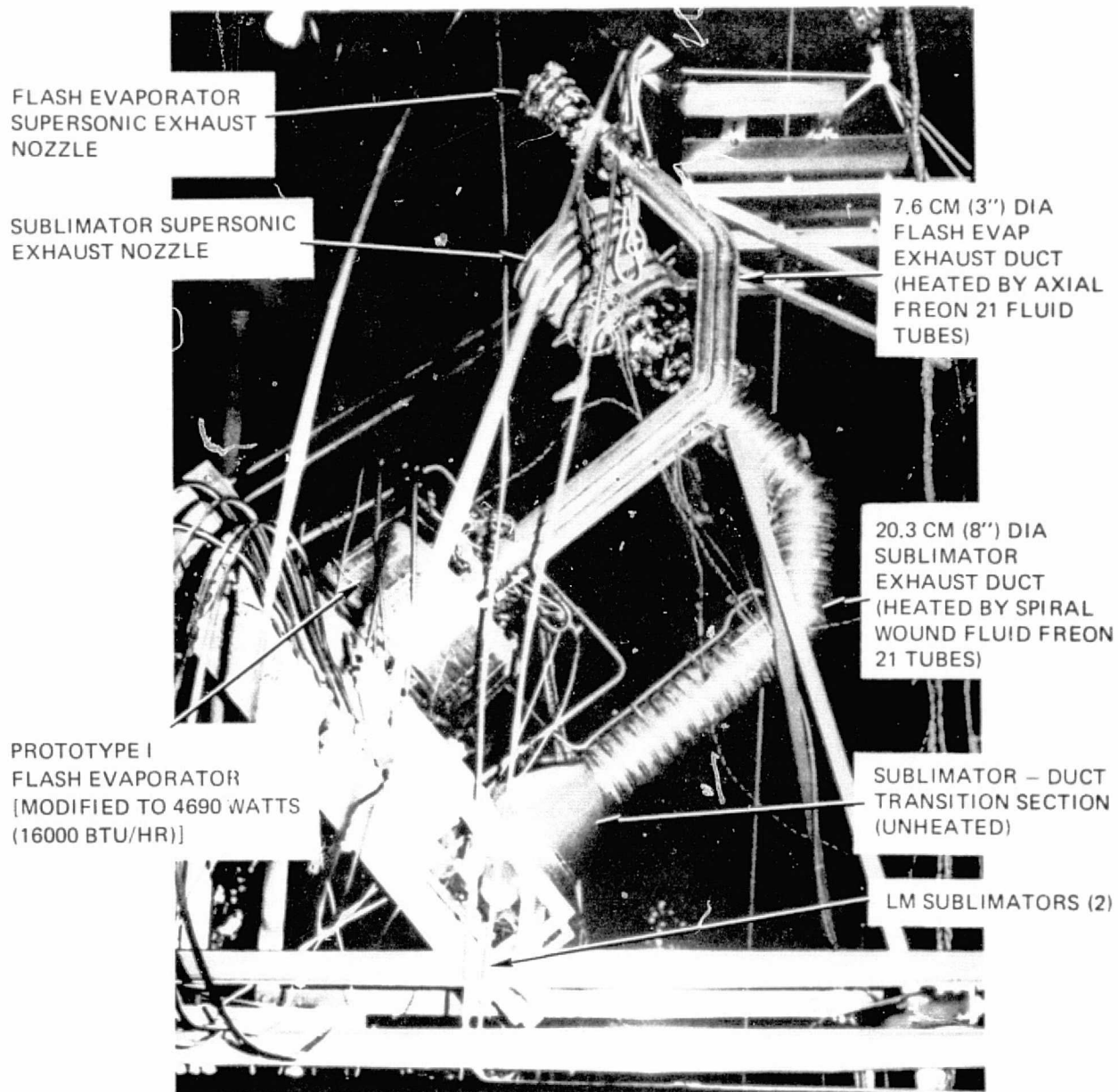
FIGURE 3–6 INSTALLATION FOR INTEGRATED SYSTEM TEST

SONIC

SUPERSONIC

PLUG
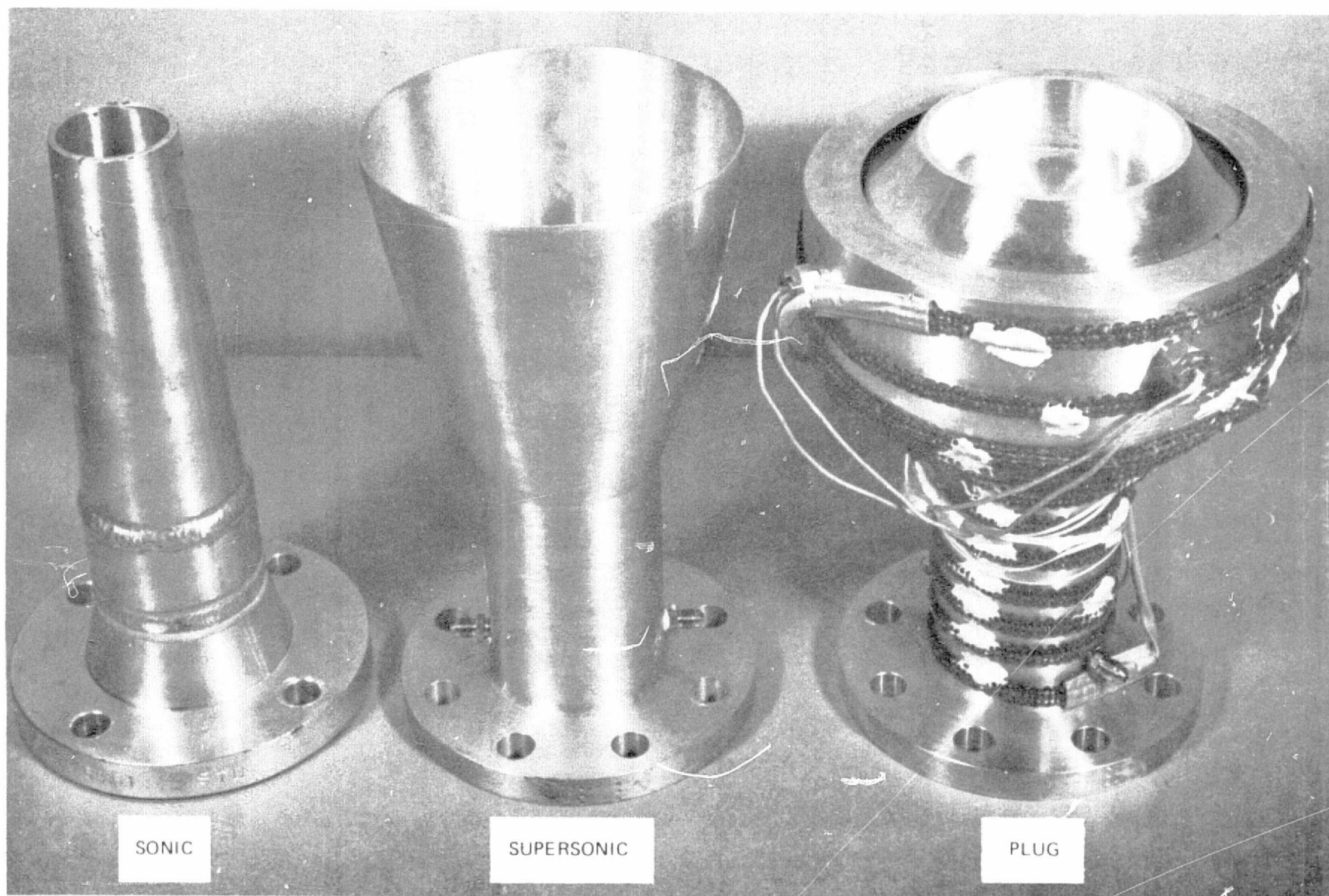
FIGURE 3-7 WATER VAPOR EXHAUST NOZZLE
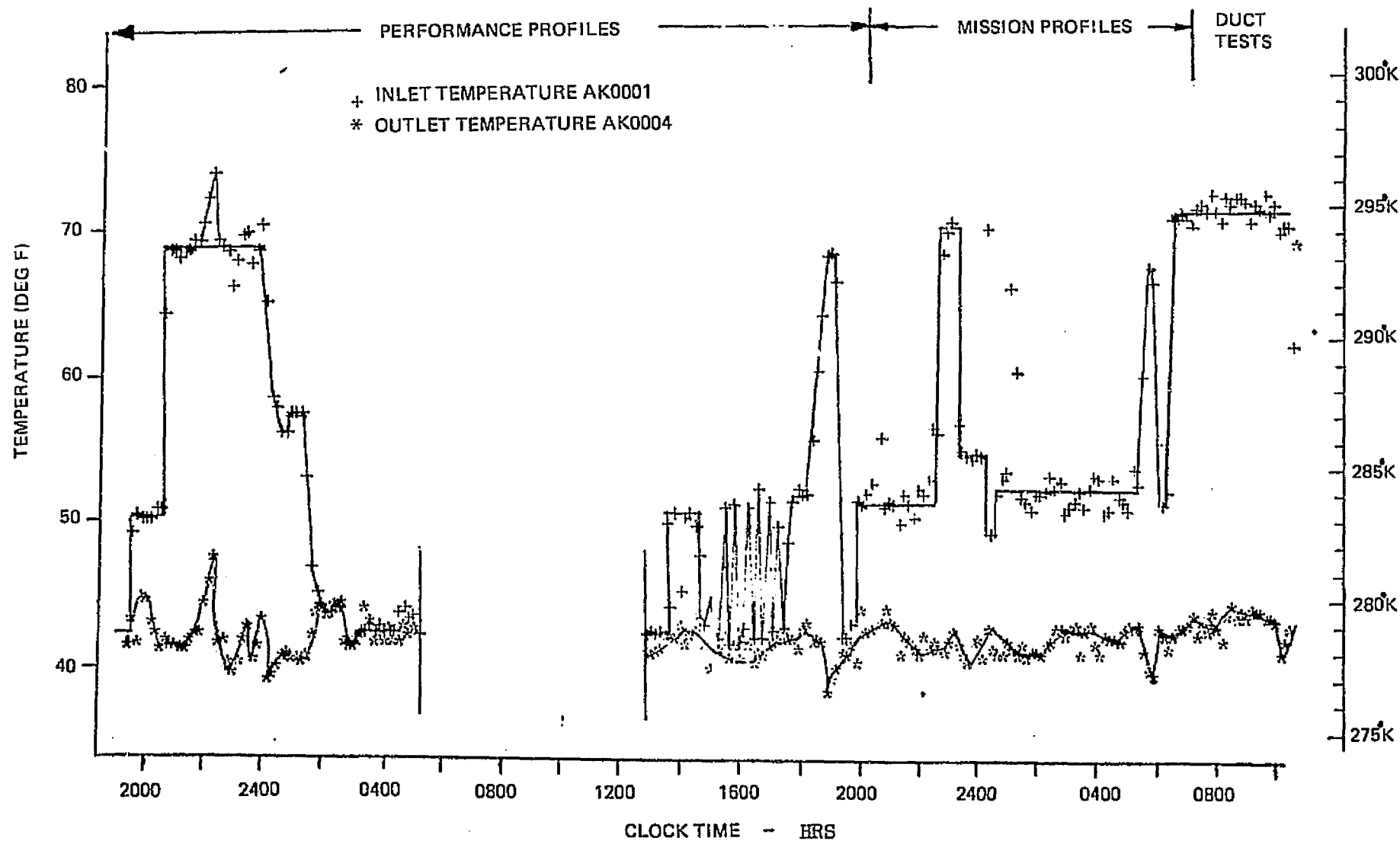
FIGURE 3–8 FLASH EVAPORATOR INLET AND OUTLET FREON TEMPERATURES

TABLE 3–1 FLASH EVAPORATOR PERFORMANCE SUMMARY

SUPERSONIC EXHAUST NOZZLE

TIME	AVERAGE WATER FLOW LB/HR	DUCT INLET °F	F. E. INLET °F	F. E. OUTLET TEMP. OSCILLATION RANGE, °F	MAX F. E. INTERNAL PRESS., MM	CYCLE TIME, SEC	
						ON	OFF
18:10	2.0	44.1	44.0	39.5 TO 41.5	3.0	5	30
19:04	16.0	72.9	69.9	42.2	3.56	—	—
20:05	8.3	56.3	54.9	39.9 TO 41.5	3.31	14	15
20:35	5.1	48.4	47.7	39.0 TO 40.8	3.1	8	22
21:31	2.8	44.7	44.4	37.9 TO 40.8	3.0	7	35
22:00	15.7	71.0	68.5	42.6	3.35	—	—

AVERAGE H_{FG}: 1030 (WITH DUCT)
950 (WITHOUT DUCT)

SONIC EXHAUST NOZZLE

TIME	AVERAGE WATER FLOW LB/HR	DUCT INLET °F	F. E. INLET °F	F. E. OUTLET TEMP. OSCILLATION RANGE, °F	MAX F. E. INTERNAL PRESS., MM	CYCLE TIME, SEC	
						ON	OFF
8:52	15.8	72.3	69.7	42.2	4.1	—	—
9:09	8.0	54.4	53.5	38.8 TO 40.4	4.08	15	15
9:44	5.3	48.4	47.5	38.4 TO 39.0	3.89	11	22
10:14	2.9	44.1	43.8	37.5 TO 40.2	3.78	7	33
10:37	1.6	42.2	42.4	38.1 TO 40.8	3.71	5	42
11:15	16.0	74.6	71.9	44.4	3.98	—	—

AVERAGE H_{FG}: 1025 (WITH DUCT)
940 (WITHOUT DUCT)

NOTES: 1. F.E. — FLASH EVAPORATOR
2. H_{FG} — H_2O LATENT HEAT OF VAPORIZATION, BTU/LB

3.4   Cold Plate Evaporator Feasibility Testing

After thorough review of Prototype I wound tube design and fabrication approach, an evaporator weight reduction and fabrication simplification program was undertaken in October 1973 by the application of current state-of-the-art cold plate heat exchanger technology. Element and system feasibility tests utilizing surplus lunar module cold plate heat exchangers were undertaken to demonstrate the validity of the design approach, and to identify any potential problem areas.

Element tests demonstrated the cold plate evaporative capabilities for single and double layer heat transfer surfaces. The system tests using the cold plate evaporator shown in Figure 3-9 demonstrated device operation for non-optimum designed core with a 4 to 1 weight reduction per unit heat transfer area when compared to the Prototype I device. Additionally, the cold plate evaporator demonstrated: high evaporant efficiencies, insensitivity to exhaust port location, operation with both hollow and solid cone nozzles, and operation with on/off and predictor/corrector heat load control techniques. Based on the results of this testing, the baseline evaporator design for the Prototype 2 and 3 was changed from the wound tubular configuration to one utilizing a cold plate surface configuration. Detailed results of the cold plate evapor tor testing are described in Appendix C.

EVAPORANT VALVE

EXHAUST PORTS (TYP)

VOUGHT SYSTEMS DIVISION
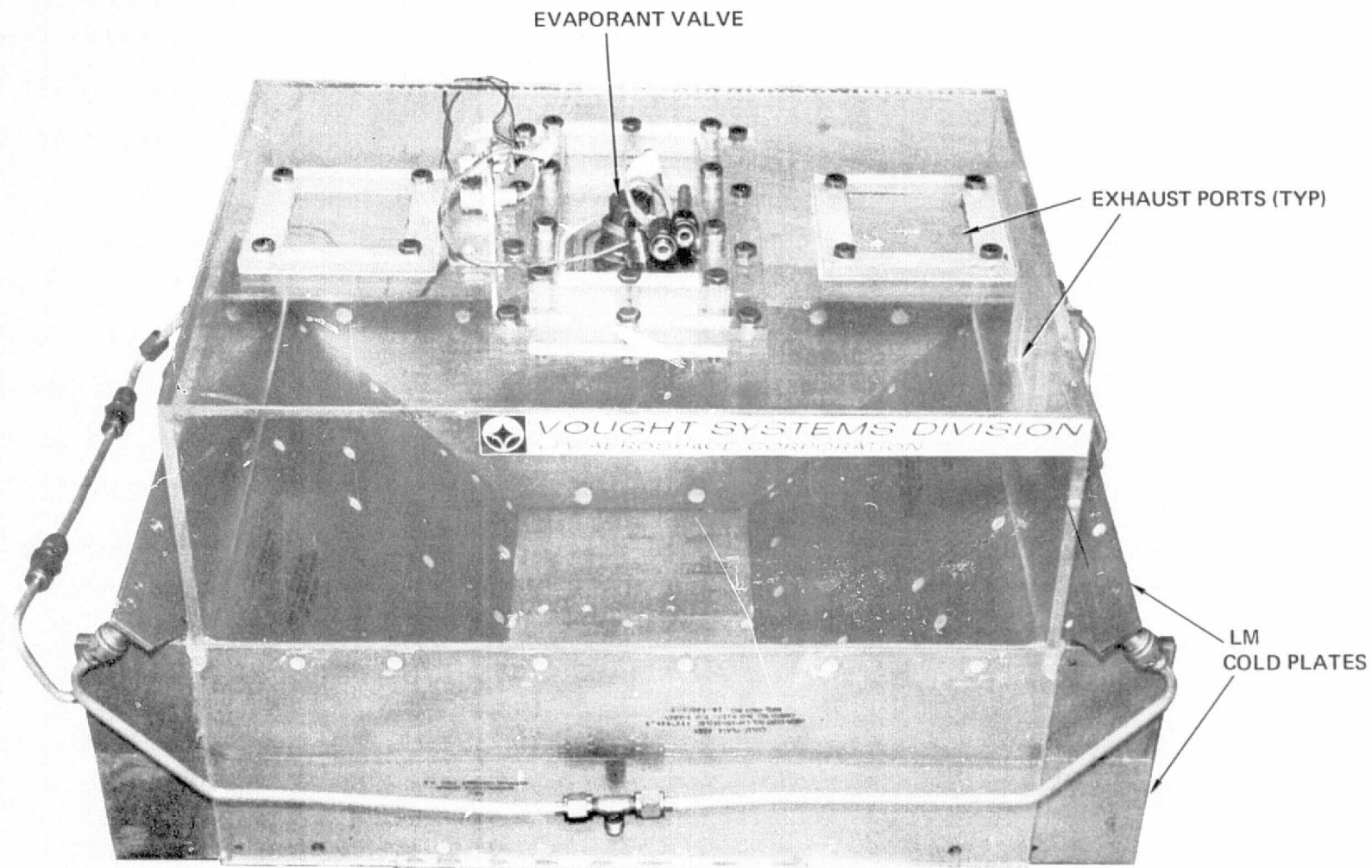
LM COLD PLATES

FIGURE 3—9 COLD PLATE EVAPORATOR

3.5   Heat Exchanger Core Element Testing

Based on the results of element and system testing described in Section 3.4 and Appendix C, the Prototype 2 and 3 designs baselined the use of compact heat exchanger core for the heat transfer surface in order to reduce weight and simplify fabrication. The heat exchanger core selected underwent a series of element tests in early 1974 to verify performance data and to investigate various methods of manifolding. These tests are described in this section.

3.5.1   Pressure Drop Tests

Prototype 2 and 3 flash evaporator heat transfer surfaces baselined United Aircraft Products fin material designated as G-core (18.5R - .1/.1-1/8 (L)-.005). G-core is a rectangular, lanced fin core and can be flowed through parallel to the fins (EASYWAY) or perpendicular to the fins (HARDWAY). EASYWAY flow results in the lowest pressure drop but is susceptible to flow maldistribution. HARDWAY flow appears very uniform across the flow width and although the pressure drop is significantly greater than EASYWAY, the magnitude was uncertain. Therefore, tests were conducted to verify the available EASYWAY pressure drop data and determine the HARDWAY pressure drop.

The test was conducted on a one foot square piece of G-core initially manifolded to flow EASYWAY. Water was used as the system fluid to create pressure drops which were readily measureable. A U-tube manometer containing Meriam blue (s.g. 1.75) was used to measure all the EASYWAY flow pressure drop. Figure 3-10 shows the pressure tap locations for EASYWAY flow.

For the HARDWAY flow, the test panel was configured as shown in Figure 3-10(b). This configuration involved cutting off the EASYWAY manifolds and original core close-outs which reduced the overall panel size. The pressure taps were located on the panel centerlines with 76.2 mm (3 inch) separation. Only pressure drops (HARDWAY flow) between taps 1, 2 and 3 could be measured with the manometer; all other pressure drop measurements were made with two Bell and Howell pressure transducers with digital readout.

The test results for the EASYWAY flow are shown in Figure 3-11 compared to manufacturer's available data. Limitations on the pump prevented obtaining data in the high flow range, however the data obtained is sufficient to verify the available data. The larger deviation between available data and the VSD test data at the lower flow rates can be partially attributed to the accuracy of the instrumentation measuring these small pressure drops (0.7 p/cm^2 or .01 psi).

15.9 mm O.D. - 0.89 mm wall
[⅝" - .035" (TYP)]

INLET

EFFECTIVE FLOW WIDTH 29.9 CM (11.75")

+1

7.6 CM (TYP)

+4 +2 +5

30.5 CM (12")

E.W.

+3

OUTLET

a. EASYWAY

INLET

EFFECTIVE FLOW WIDTH 27.9 CM (11.0")

+4

+3 +2 +1

H.W.

29.9 CM (11.75")

+5

OUTLET
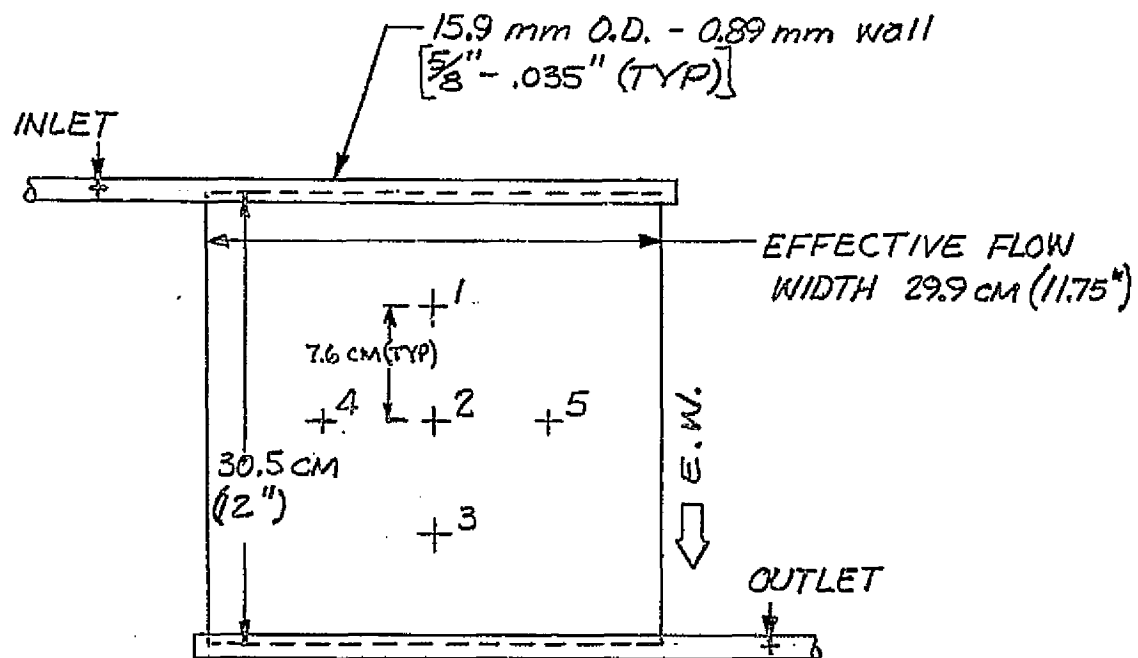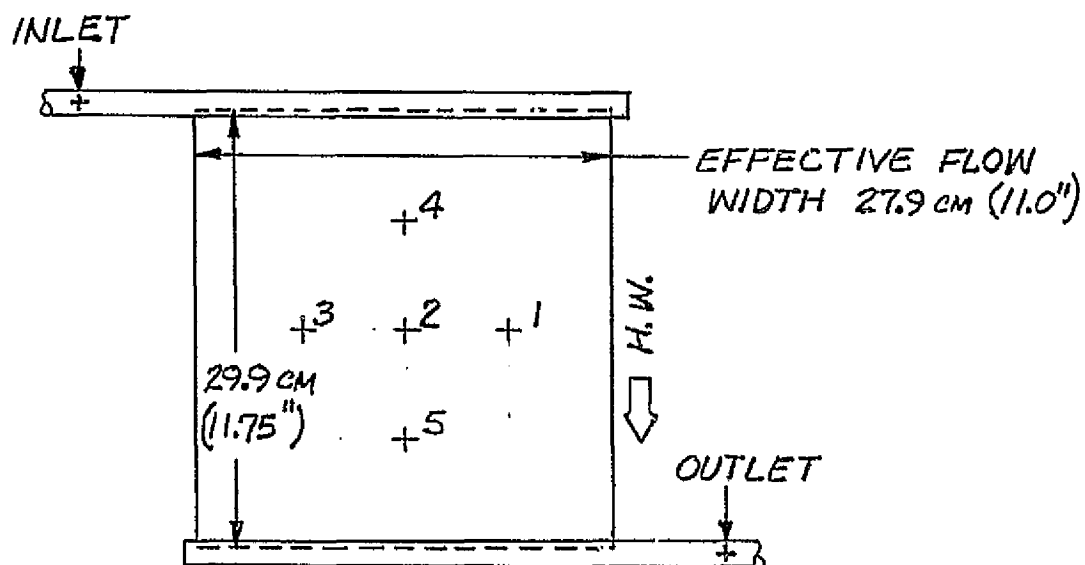
b. HARDWAY

FIGURE 3-10 TEST ARTICLE PRESSURE TAP LOCATIONS
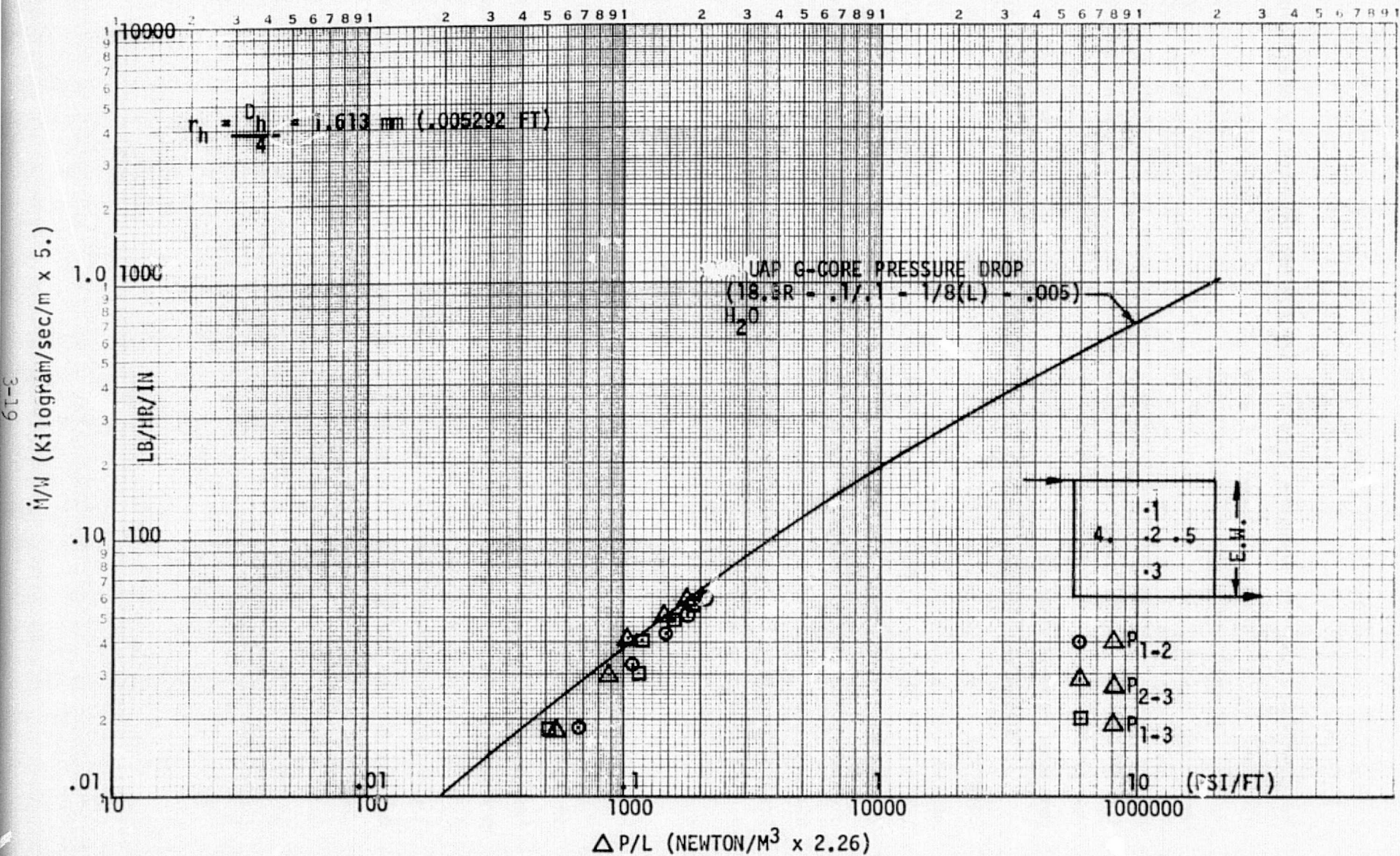
FIGURE 3-11 TEST ARTICLE EASYWAY PRESSURE DROP

The EASYWAY flow core pressure drop is very low as reported by the manufacturer's data and is recommended for EASYWAY pressure drop calculations.

Figure 3-12 presents the HARDWAY flow core pressure drop measured by VSD. The data has been corrected to reflect the smaller dimensions of the HARDWAY panel. The VSD tests measured HARDWAY pressure drop is 650 times greater than the EASYWAY pressure drop at a flow per unit width of .263 gm/sec/mm (53 pph/in.). The HARDWAY pressure drop is very large and its use should be avoided where small pressure drop is desired.

Since the HARDWAY pressure drop was 20 times larger than expected, a cursory look was undertaken to determine causes of the high pressure drop. The best estimate of a HARDWAY hydraulic radius ($r_h = \frac{Ac}{WP}$) is .115 mm (.0003788 ft.) versus 1.613 mm (.005292 ft.) for EASYWAY, a factor of 14. Inspection of typical lanced-fin material revealed burrs and metal smears which would tend to decrease the flow cross-section and increase predsure drop. The test panel probably has a similar burr problem. The test apparatus is verified by the EASYWAY data and the ΔP transducers were checked with the manometer. The HARDWAY pressure drop for the G-core should be considered 650 times the ΔP_{EW}.

3.5.2 Conductance/Evaporation Testing

The test article described above was tested in the EASYWAY configuration to investigate core conductance (UA) as a function of evaporant flowrate and coolant outlet temperature, and to look for flooding, cold spots and other signs of flow maldistribution. The 0.093 m^2 single layer heat exchanger core was tested with Freon 21 as the transport fluid. Two manifold configurations were evaluated: Configuration 1 is flow in and out adjacent corners and configuration 2 is the flow in and out diagonal corners. Flowrates ranged between .756 and 3.024 kg/sec (600 and 2400 pph) with inlet temperatures from 281.4 to 322 degrees Kelvin (47-120°F). Evaporator flow was constant at .02 kg/sec (16 pph) with a 4.00-B-90° nozzle, with a 259932 N/m^2 (23 psig) supply pressure. The nozzle was positioned in the center of the plate at a height of 305 mm (12 inches) for a series of runs and then lowered to 178 mm (7 inches) to have total spray impingement on the core.
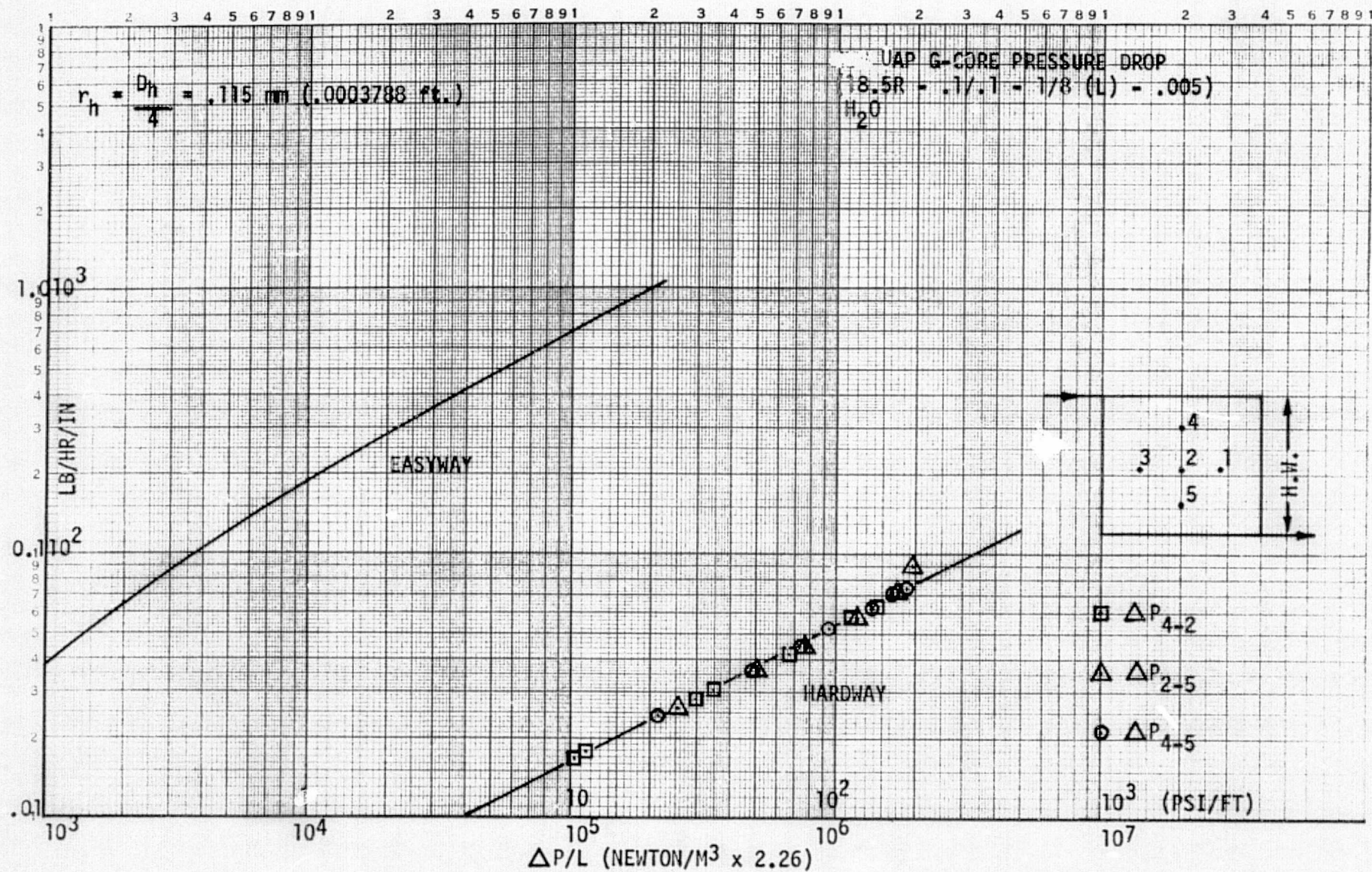
FIGURE 3-12   TEST ARTICLE HARDWAY PRESSURE DROP

Figures 3-13 and 3-14 present the test data for the onset-of-icing for configurations 1 and 2, respectively. Onset-of-icing was calculated based on the core conductance of Figure 3-15, the evaporation rate data of Figure 3-16 and solving the following equation for outlet temperature.

$$mCp(T_{in} - T_{out}) = U_{CORE}(T_{out} - T_{surf}) = U_{EVAP}(T_{surf} - T_{set})$$

(U_{EVAP} is calculated from the slope of the evaporation line of Figure 3-16 and is equal to 11626 $\frac{W}{m^2{}^oK}$ or 2045 BTU/hr-ft^2-^{o}F).

Agreement between calculated T_{out} for icing and the test data demonstrates that the core conductance and evaporation data are known to sufficient accuracy to predict when icing will occur and that Figures 3-15 and 3-16 can be used for design calculations. The spray deposition rate corresponding to Figure 3-13 and 3-14 was 0.0136 Kg/sec-m^2 (8 pph/ft^2)(maximum) evenly sprayed over the entire surface. The spray deposition in the form of a calculated surface temperature versus heat rejection capability is presented in Figure 3-3 to show agreement with the previously defined flooding boundary in Section 3.2

A device capable of evaporating 0.0136 kg/sec-m^2 (8 pph/ft^2) (maximum) spray deposition can evaporate a much higher spray rate if the outlet temperature is allowed to increase. For example, if the outlet temperature is used as the basis for determining the maximum spray rate and is allowed to increase from 277.5^{o}K (40°F) to 294°K (70°F) while a constant water saturation temperature of 272°K (30°F) is maintained, the spray rate can be increased 4 times [(70-30)/(40-30)]. The proper size nozzle was not available to provide the high spray deposition rate desired. To get the heavier spray, the nozzle was lowered to seven inches above the plate. Figure 3-17 presents the test data for the nozzle at seven inches from the core in configuration 1. The disparity between predicted and measured T_{out} is due to uncertanity in the concentration of the spray in an annulus about the plate center while the corners received no spray.

FIGURE 3-13

"ONSET-OF-ICING" CORE OUTLET TEMPERATURE
305 mm (12") NOZZLE HEIGHT

3-23
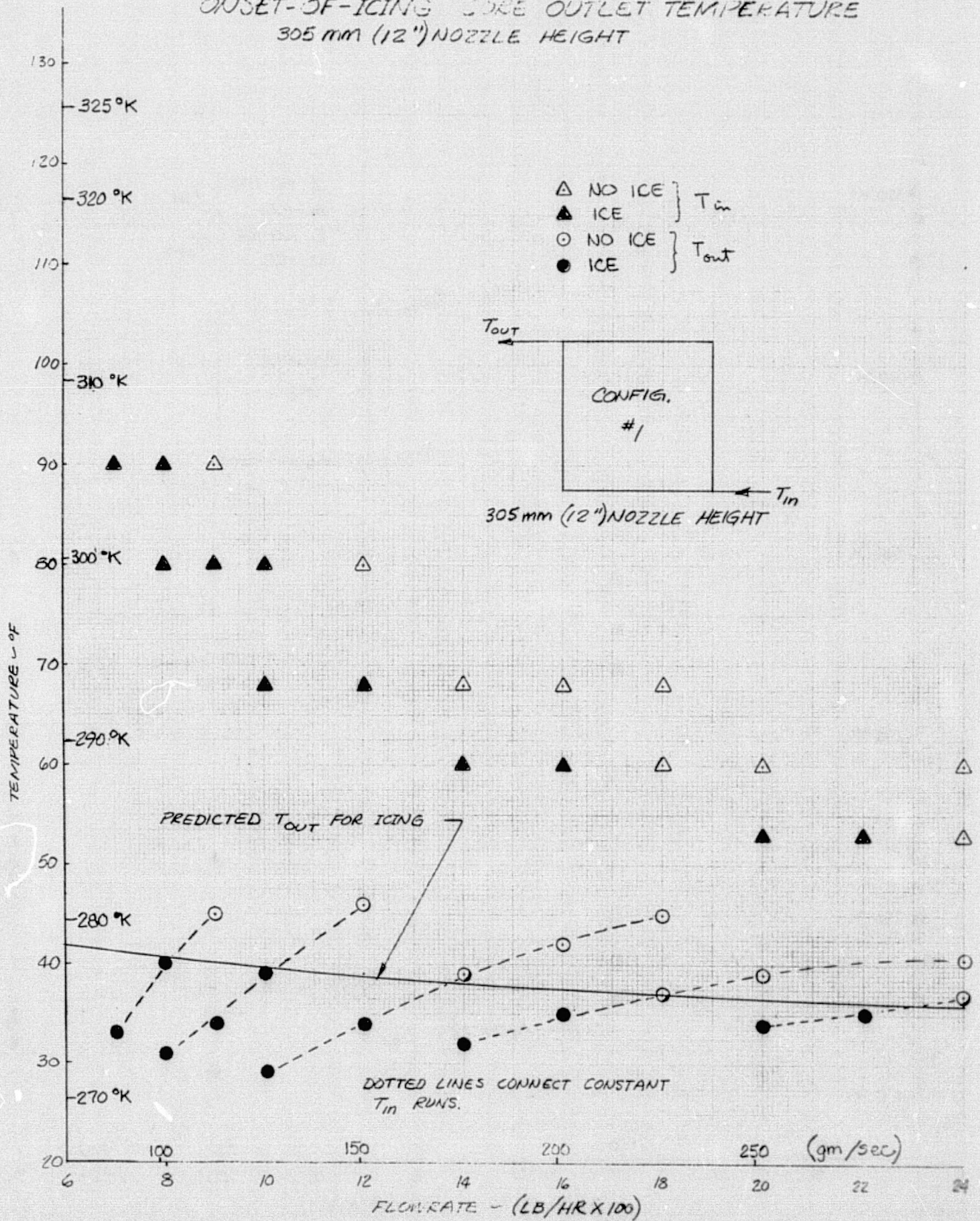
FIGURE 3-14
"ONSET-OF-ICING" CORE OUTLET TEMPERATURE
305 mm (12") NOZZLE HEIGHT
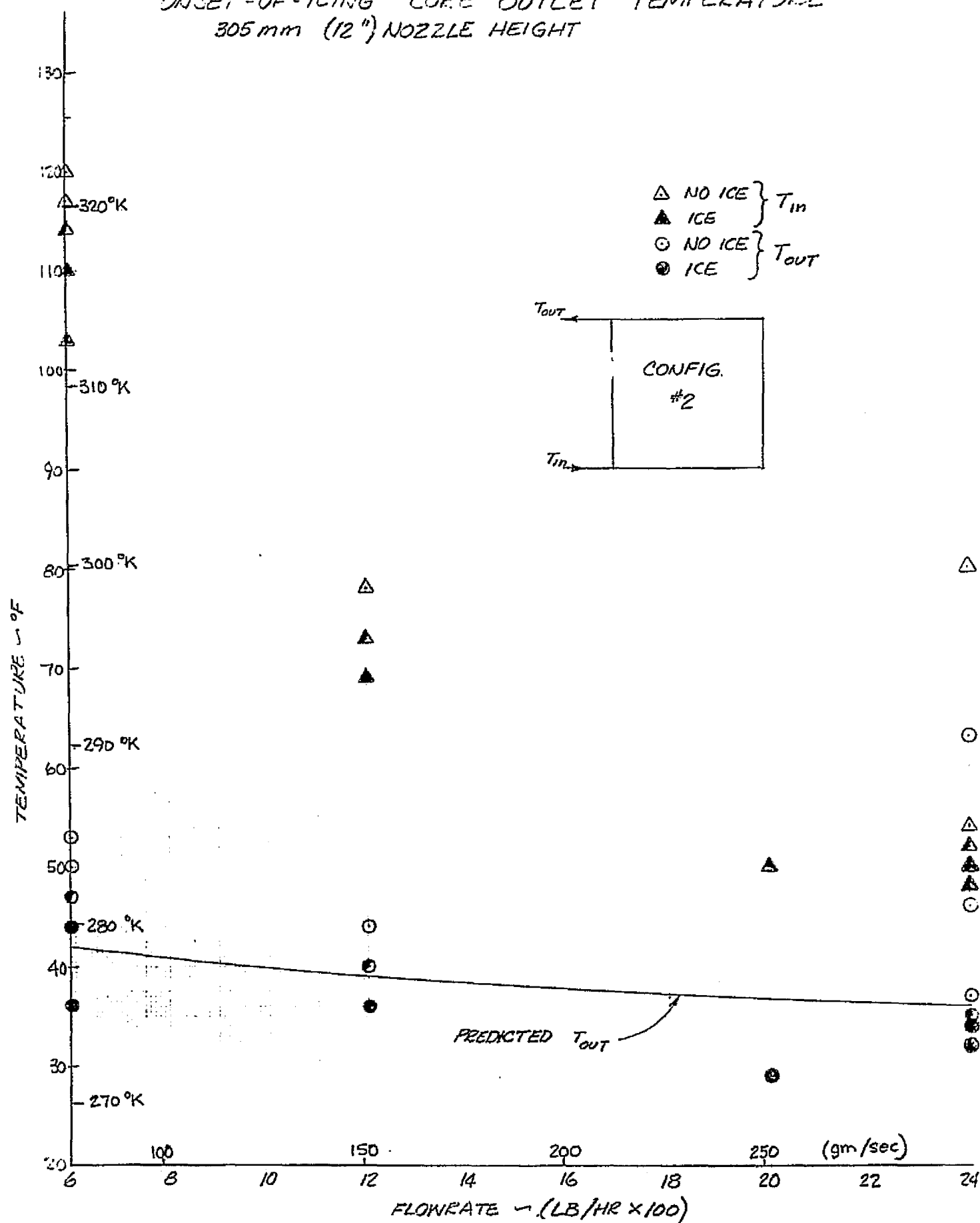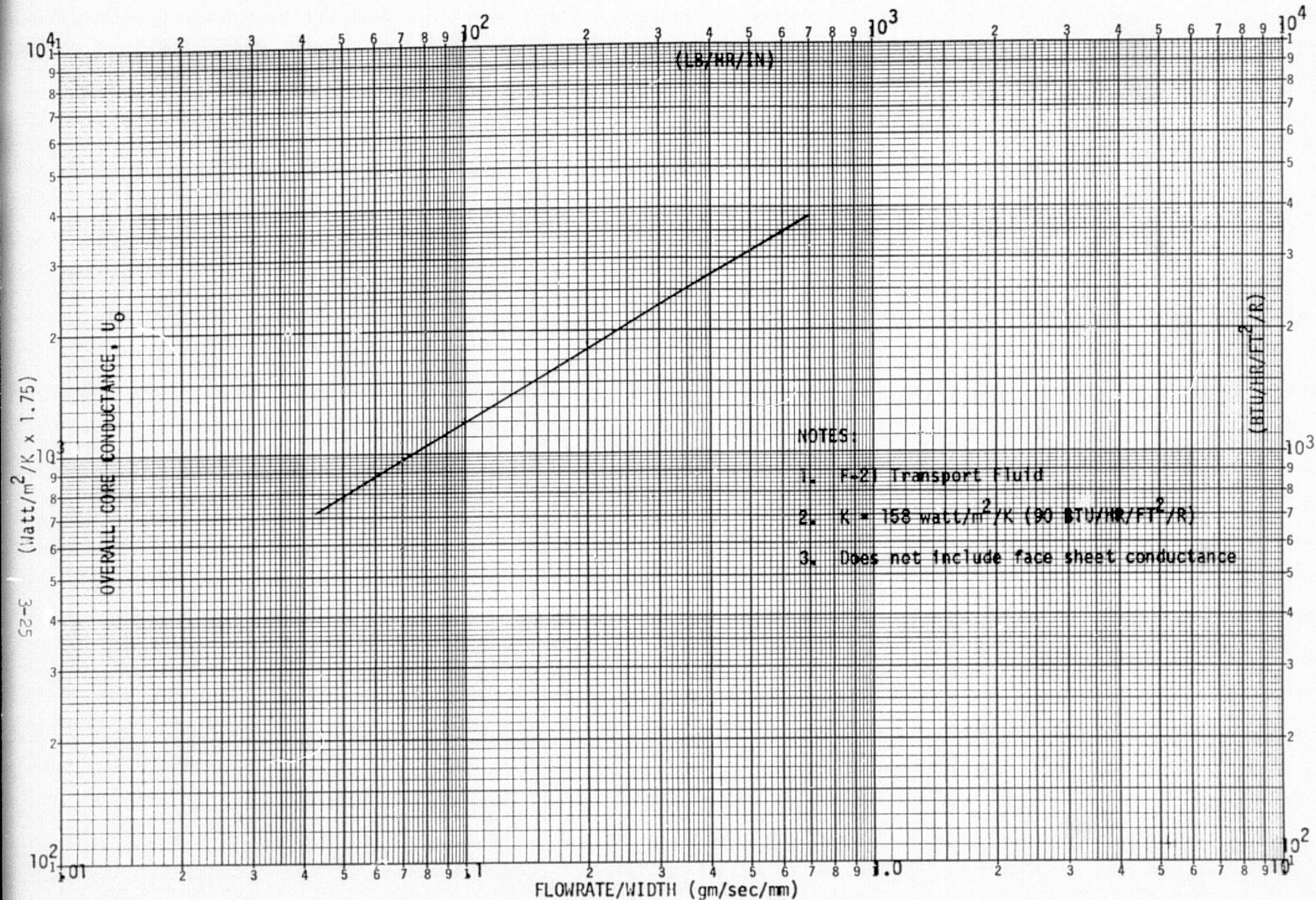
FIGURE 3-15 UAP G-CORE CONDUCTANCE

FIGURE 3-16 FLOODING BOUNDARY

UNCERTAINTY

$P = 462 \ N/m^2$
$(3.47 \ mm \ Hg)$

FLOODING ← → NO FLOODING

⊕ ICING
△ NO ICING } *

$T_{SURF} = T_{SAT} + \dfrac{Q/A}{11626}$

*G-CORE SPRAY TEST WITH
$453 - 480 \ NEWTON/m^2$,
$(3.4 - 3.6 \ mm \ Hg)$

Q/A (Btu/HR/FT²)

Q/A (WATT/M²)

SURFACE TEMPERATURE (°K)

3-26
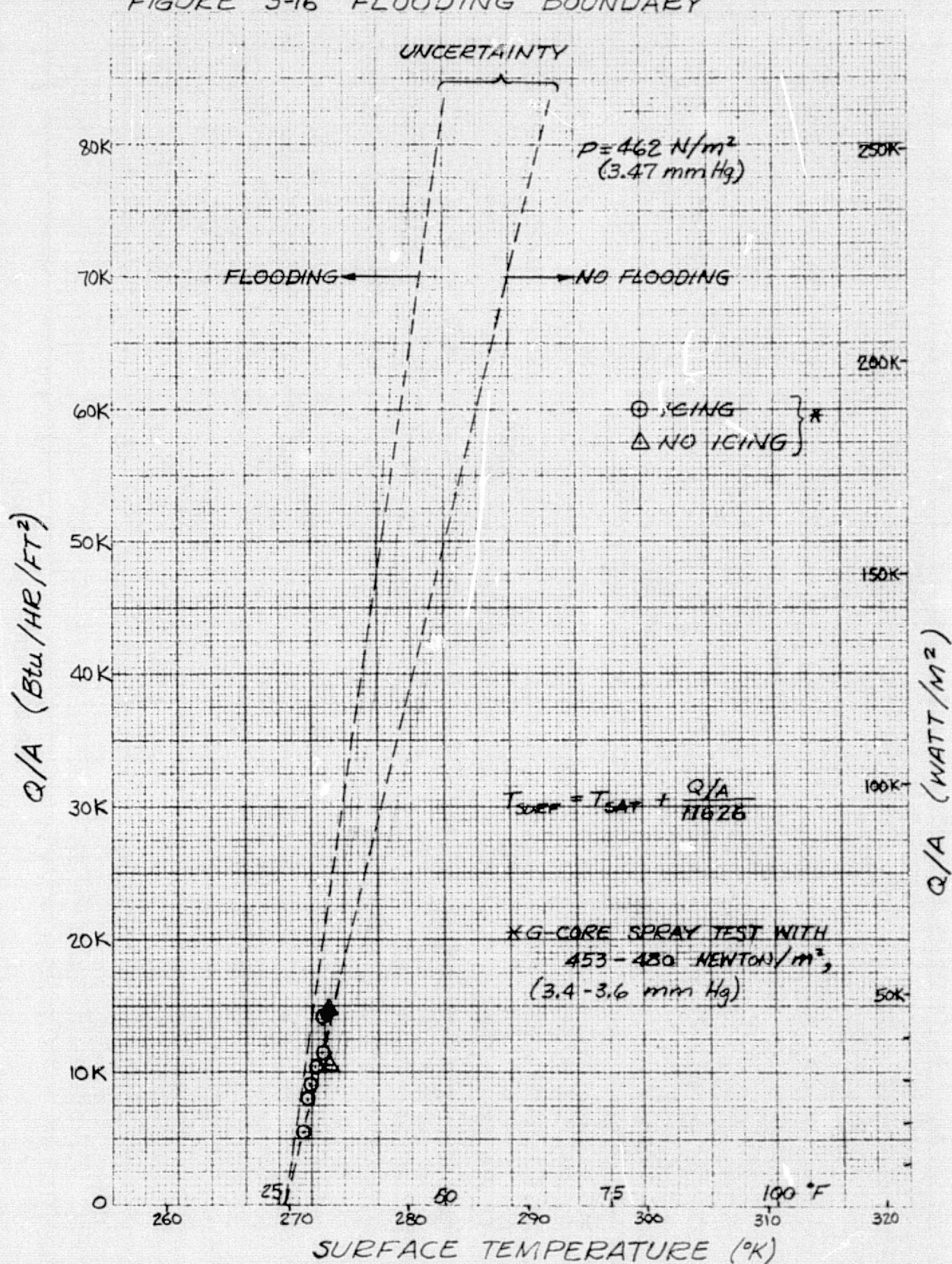
FIGURE 3-17
"ONSET OF ICING" COIL OUTLET TEMPERATURE
178 mm (7") NOZZLE HEIGHT
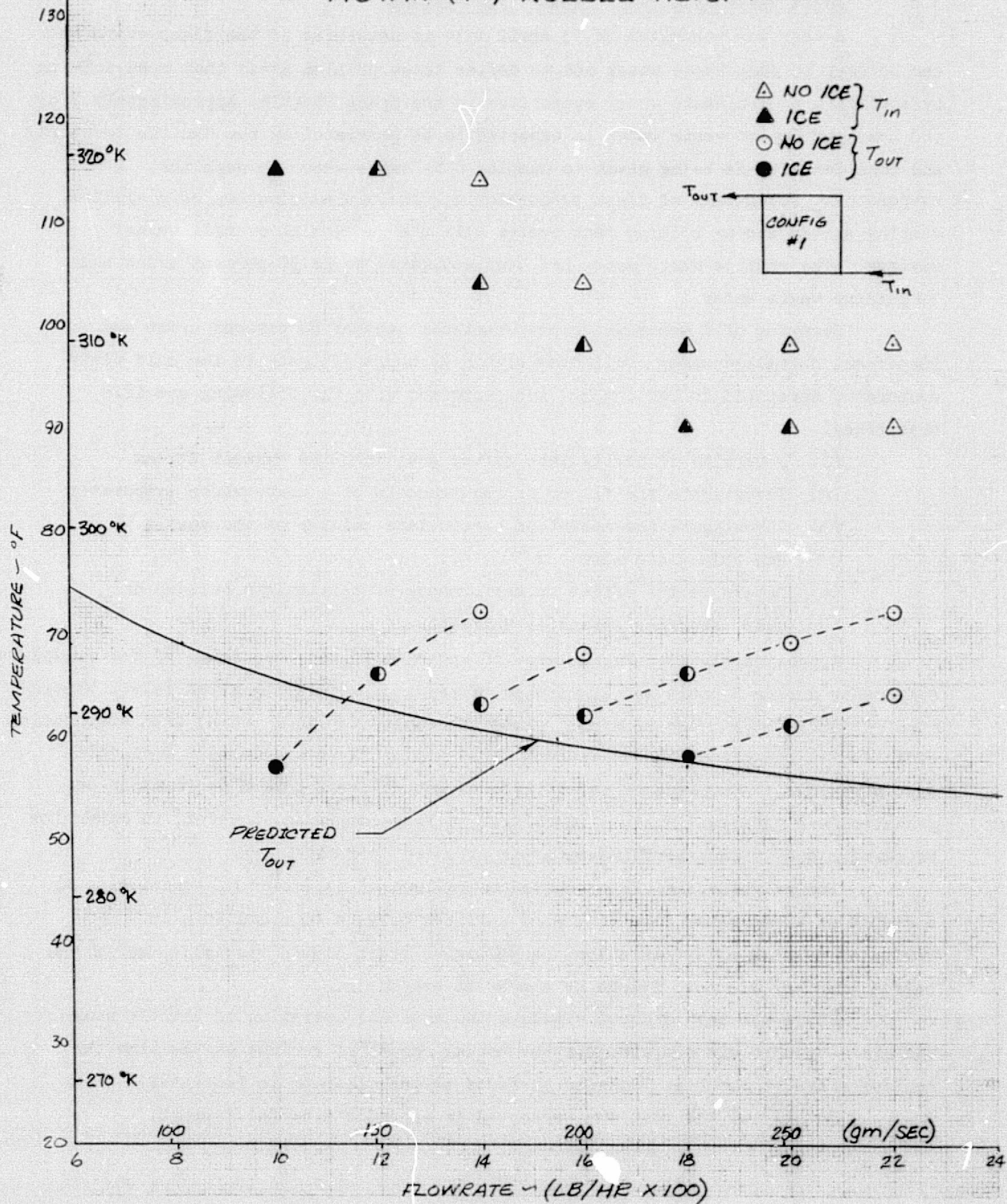
3.6 Waste Water Evaporator Feasibility Testing

A test was conducted on 23 April 1974 to determine if the flash evaporator can be used to dump waste water and to define those problem areas that need solving by application of a waste water evaporator in the Space Shuttle. Approximately 27Kg (60 lbs) per day of waste water is expected to be generated by the Shuttle occupants and consideration is being given to dumping this waste water through the evaporator. Advantages of flash evaporator use include elimination of a special dumping system and/or holding tank system with the subsequent overall weight savings. The Shuttle waste water has been estimated to be 50 percent urine and 50 percent waste water.

Spraying of a waste water evaporant composed of 50 percent urine and 50 percent distilled water (collected within 24 hours of test) in the cold plate evaporator described in Section 3.4 was performed with the following specific objectives.

(1) Determine if particulate matter gets into the exhaust stream

(2) Investigate the filtering requirements of a waste water evaporator

(3) Investigate the amount of particulate buildup on the nozzle and cold plate surfaces

(4) Determine the effect on performance of particulate buildup on evaporator heat transfer surfaces

Approximately 13.5 Kg (30 lbs) of waste water was evaporated by the coldplate evaporator during 2 hours and 20 minutes of testing. Operating at an inlet temperature of 308°K (95°F), the transport fluid was cooled to 280°K (45°F) with evaporation efficiencies between 87 and 92 percent. The impinging spray caused a froth and left a residue on the heat transfer surfaces but no trend toward performance degradation was noticed. Further investigation is recommended, however, to determine if residue does effect performance after extended operation.

The valve/nozzle/filter showed no buildup of solids or malfunctioning as a result of waste water flow with a 60 μ filter only, a 60 μ and 10 μ in series or pulsing spray operation. A yellowish brown liquid was collected in the baffle trap and did not freeze or appear to evaporate.

Since the test did not simulate the extended operation of Shuttle usage, the clean-up also did not simulate the actual amount of residue or the time the residue stays on the heat transfer surfaces before clean-up is initiated.

Details of the test are presented in Appendix D of this report.

4.0 PROTOTYPE 2 AND 3 DESIGN

The flash evaporator has undergone an evolutionary process in which the important criteria of weight, volume, and cost have been reduced while retaining high efficiency. The Prototype 2 unit design was initially planned to be a refinement of the Prototype I wound tube device with improvements in fabrication technique, nozzle performance, valve/nozzle interaction, and reduction in volume. The design of this device is reported in Appendix F. During the final design review at NASA in March 1973, it was decided to forego fabrication of this unit, however, since heat load requirements of the Shuttle had become better defined at higher values, and the need for a top-off evaporator to supplement radiator heat rejection became identified. It was also desired to optimize the device weight by fabricating the unit from state-of-the-art compact heat exchanger core based on the results of the analysis of Ref. 2 in 1972 and the cold plate evaporator testing reported in Section 3.2.

The design of the Prototype 3 evaporator was undertaken concurrently with the Prototype 2 unit to investigate alternatives to device, as well as system, configuration. During these design studies, the Shuttle Freon Coolant Loop also evolved from a single loop operation (with a completely redundant loop in a standby mode) approach to a dual loop operation (two identical fluid loops operating continuously) concept. Design considerations used to evolve the Prototype 2 and 3 designs which meet the dual Freon loop heat rejection requirements for the Shuttle are described in this Section.

4.1 Design Requirements

The baseline and alternate Shuttle Freon coolant systems in consideration during the period of Prototype 2 and 3 evaporator design are shown schematically in Figures 4-1 and 4-2. The evaporator performance requirements, tabulated on these figures, indicate a wide range of temperature conditions and flow conditions to be accommodated by the Prototype 2 and 3 designs in order to simulate the potential Shuttle application of the devices.

4.2 Load Partitioning

In addition to the thermal performance requirements, the on-orbit water vapor generated by the evaporator must be ejected overboard from the Shuttle through "non-reacting" supersonic nozzles located on either side of the Shuttle. Connecting the non-reacting nozzles is a steam duct which is attached to the evaporator.
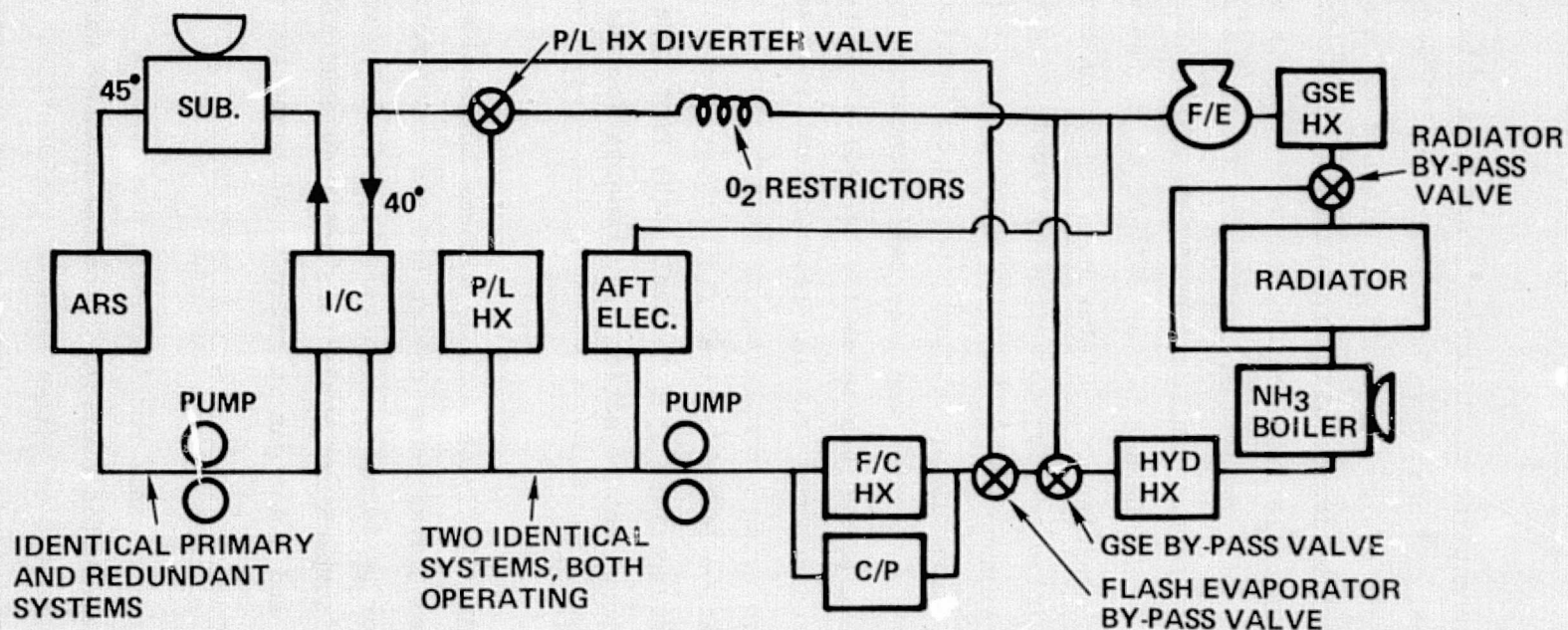
NORMAL OPERATION (SINGLE LOOP OPERATION)

	Q (BTU/HR)	FLOWRATE (LB/HR)	INLET TEMP (°F)	OUTLET TEMP (°F)
TOP-OFF EVAPORATOR				
BOOST & RE-ENTRY	24,500	400 EACH SYSTEM (715 IN OPERATING SYSTEM)	160 (174)	40
ON-ORBIT	12,500 (NOM.)	1800 EACH SYSTEM (3600 IN OPERATING SYSTEM)	53.6 (46.8)	40

FIGURE 4—1   BASELINE SHUTTLE CONFIGURATION SCHEMATIC

NOTE: ONLY ONE LOOP SHOWN FOR SIMPLICITY
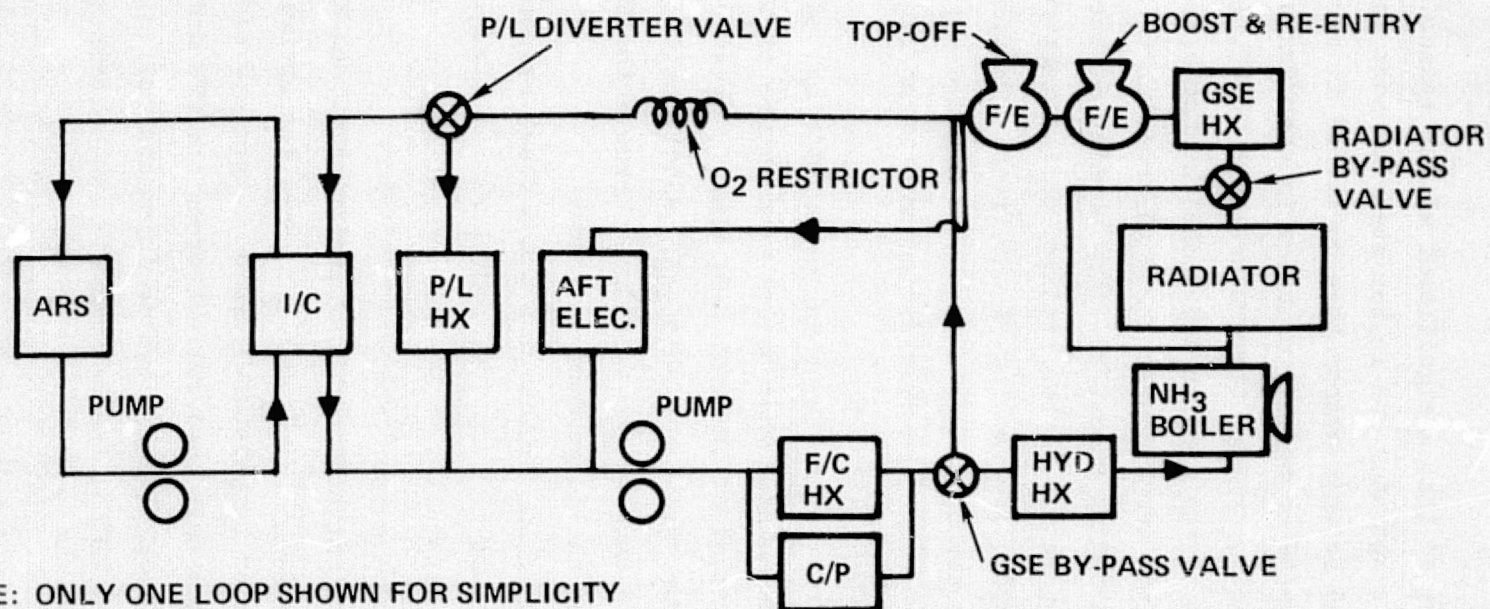
NORMAL OPERATION (SINGLE LOOP OPERATION)	FLOWRATE (LB/HR)	Q (B/H)	TIN (°F)	TOUT (°F)
FLASH EVAPORATOR				
BOOST	1800 PER SYSTEM (3600 PER OPERATING SYS)	92,647	140.5	40
ON-ORBIT	1800 PER SYSTEM (3600 PER OPERATING SYS)	12,500	53.6	40

FIGURE 4—2   ALTERNATE SHUTTLE CONFIGURATION SCHEMATIC

Preliminary design studies indicated that a significant weight reduction of approximately 27 Kg (60 lbs) in the evaporator and in the steam exhaust duct could be made by "partitioning" the load between evaporators connected in series. This approach utilizes two evaporator units connected in series in each Freon loop as shown in Figure 4-3: the upstream unit, or high temperature unit (HTU), is utilized only during the ascent/re-entry portion of the mission and cools the Freon from its maximum temperature to an intermediate temperature; the downstream unit, or low temperature unit (LTU), is utilized during ascent/re-entry portion of the mission to cool Freon from the intermediate temperature to the required outlet temperature, and during orbit to provide all the evaporative cooling of the Freon. The LTU is connected to the non-reacting duct/supersonic nozzle system to exhaust water vapor while the HTU's are connected to a short overboard duct since there is no requirement during ascent/re-entry for thrust nullification.

The primary advantage in load partitioning the flash evaporator system is a reduction in overall weight and volume. The higher outlet temperature of the HTU results in greater evaporation potential of the unit and, thus , greater spray deposition per unit area of heat transfer surface is obtained. Additionally, as can be seen in Figure 4-3, the amount of duct weight is reduced because the HTU duct installation has shorter lengths of the large diameter duct.

The approach taken in the design of the Prototype 2 and 3 flash evaporators was to baseline load partitioning. The use of identical configuration high and low temperature units for potential shuttle installation was also baselined in order to reduce hardware design and verification costs. For identical HTU and LTU configurations, optimization of load partitioning can be obtained from the curves in Figures 4-4 and 4-5. From Figure 4-4, the optimum HTU outlet temperature (and thus LTU inlet temperature) can be determined based on system inlet and outlet temperature. Thus heat load split between the HTU and LTU can be obtained from Figure 4-5. For example, for a system inlet and outlet temperature of 332°K and 277.4°K (120°F and 40°F), the optimum HTU outlet temperature would be 288.6°K (60°F).
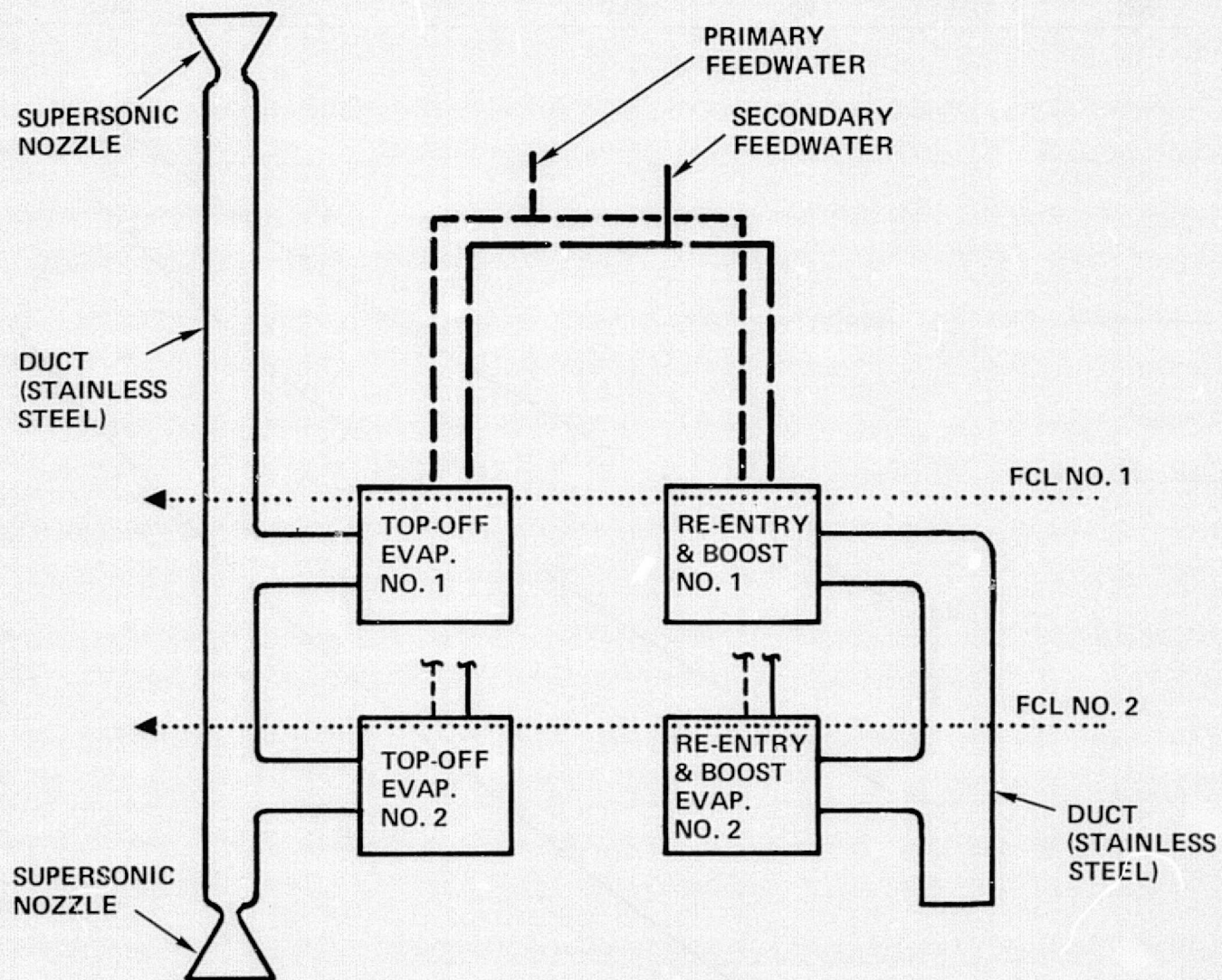
FIGURE 4-3   FLASH EVAPORATOR SYSTEM WITH LOAD PARTITIONING
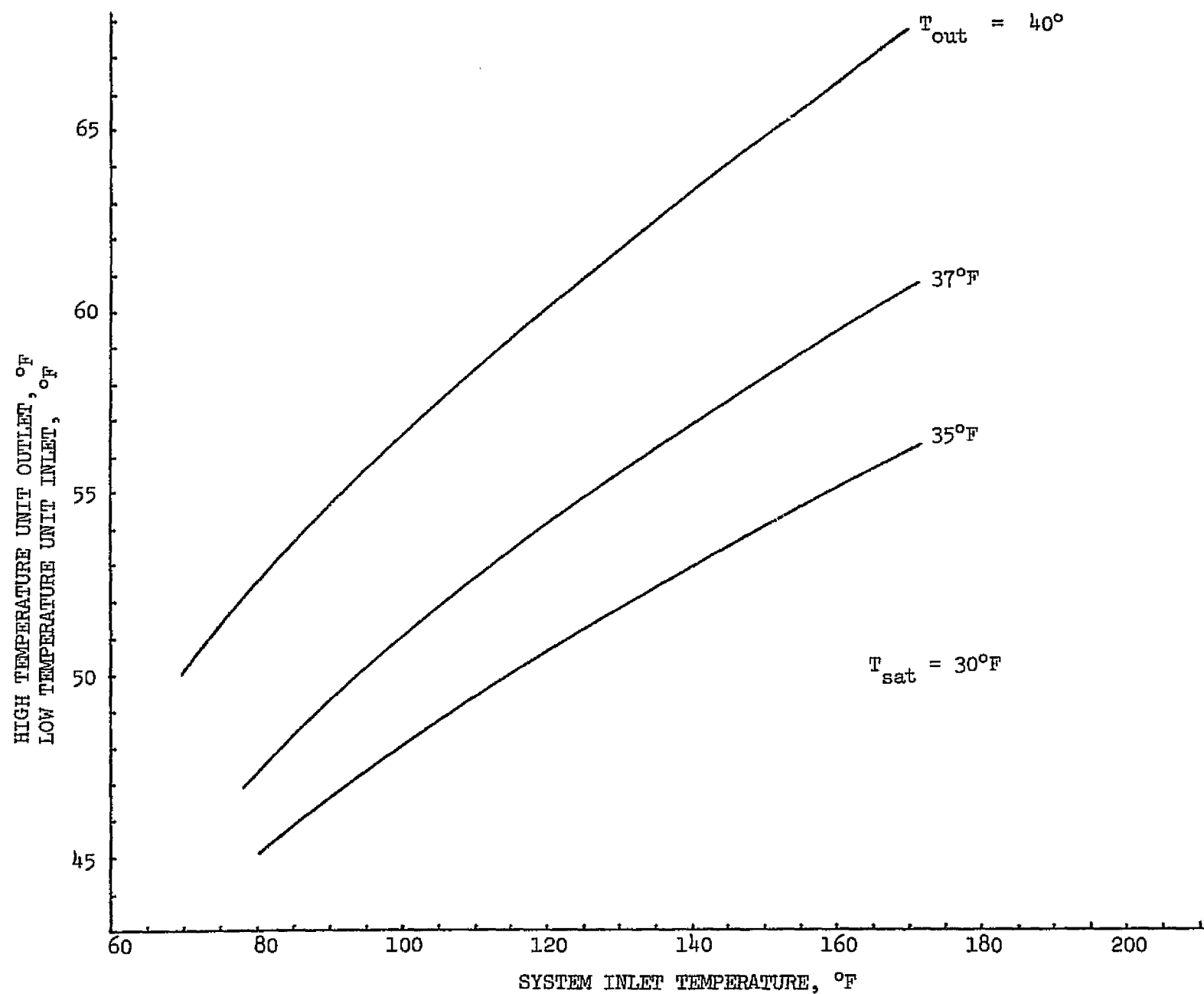
FIGURE 4-4   OPTIMUM TEMPERATURE SPLIT BETWEEN HIGH AND LOW TEMP. UNITS
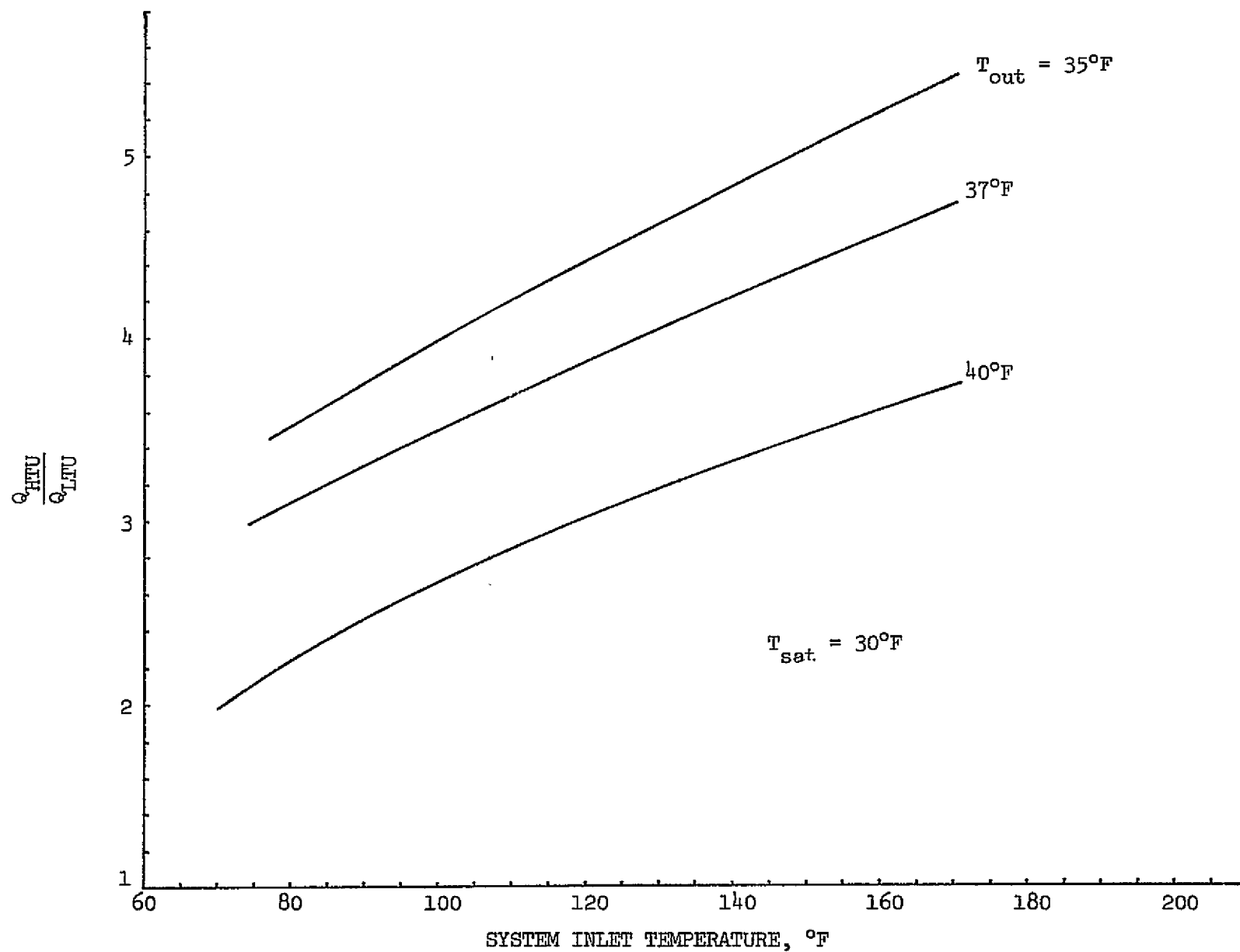
FIGURE 4-5   HEAT LOAD RATIO FOR OPTIMUM TEMPERATURE SPLIT

4-7

4.3   Design Trade Studies

Design trade off studies were performed for the Prototype 2 and 3
flash evaporators in order to evolve optimized units consistent with weight,
cost, and availability of materials. The design variables considered for
this design study and selection rationale are listed in Table 4-1. Included
on Table 4-1 in the comment column are the factors which affect the design
selection. The study variables consisted of: core configuration, unit shape,
core redundancy, spray deposition rate, and nozzle configuration.

Because the Shuttle flash evaporator system performance and configura-
tion requirements were not firm at the time of the Prototype 2 and 3 design,
it was decided that the resulting designs should possess "building block"
flexibility so that any number of configurations and design variables could
be evaluated in the test program. The criteria for selecting the various design
choices reflect this approach.

The heat transfer surfaces considered for selection included: the wound
tube approach used in the Prototype I unit; rectangular and triangular fin compact
heat exchanger core; and pin fin heat exchanger core. The wound tube heat transfer
surface was discarded due to its high weight and the state-of-the-art of brazing the
wound tubes as described in Appendix F. The feasibility of using compact heat exchanger
core was analyzed in Ref. 2 and proven in the tests described in Section 3.4.
Of the heat exchanger cores considered, the availability of the Kays and London
(Ref. 11) and the Shah and London (Ref. 12) cores with structurally sound fins of
aluminum to withstand the 380 psi Shuttle Freon system operating pressures was un-
certain. After discussion with various heat exchanger vendors, the 18.5 fins per inch
rectangular core was selected due to its good performance, availability, optimum
weight and manufacturing lead time. This heat exchanger underwent a series of
element tests to verify performance with the results reported in Section 3.5.

The various shapes that the flash evaporator unit could take included:
rectangular, octagonal, and cylindrical (or round). The cylindrical unit was
selected due to the inherent low weight and volume, and due to the flow path
flexibility in the event multipasses were needed in the core.

The dual loop operation of the Shuttle Freon coolant loop provided the
flash evaporator system opportunity to operate with either single or two core
layer. With a single layer core design, the two Freon loops would flow through

4-8

4-9

TABLE 4-1 TRADE STUDY VARIABLES AND SELECTION

VARIABLE	SELECTION POSSIBILITIES	COMMENTS	SELECTION	RATIONALE
Core	18.5R-.1/.1-1/8(L)-.005	+ Available, off-the-shelf + Performance of inner layer with low $\Delta P/\ell$ - Redundant (outer layer) operation not feasible - Wt/ft^2(wet)≈2.0 lb/ft^2(dry)=1.0 lb/ft^2(2 layer core) + Fluxless braze S.O.A. + Available in Al and Ni/SS	Yes	Good performance, Availability, cost, and schedule
	Kays & London 46.45T - .1 - .002	+ Performance of inner layer with $\Delta P/\ell$ + Fluxless braze S.O.A. + Wt/ft^2(dry) .85 lb/ft^2 (2 layer core) - availability uncertain - Al & Ni/SS availability uncertain - Redundant (outler layer) operation not feasible	No	
	Shah & London 36.85R-.026-.001	Same as Kays & London except: + Wt/ft^2(dry) .4 lb/ft^2(2 layer), .75 wet + Operation with redundant core possible	No	
	Pin Fin	+ Available off-the-shelf	No	
	Wound Tube	+ Operation with Redundant core same as primary + Available (Stock in hand) - Wt.(dry) 4.0 lb/ft^2, (wet)(5.0 lb/ft^2) - Can't be fluxless brazed - Braze separation of flow passages	No	
F.E. Shape	Rectangular	+ Cost + Tooling time - Volume, area, weight - Less flexible for flow split (2,4 flow paths)	No	Lowest weight and volume units
	Octagonal	- Cost - Tooling time + Lower volume, area, weight - Less flexible for flow split (2,4,8 flow paths)	No	

- = Disadvantage
+ = Advantage

TABLE 4-1 (Cont'd)

VARIABLE	SELECTION POSSIBILITIES	COMMENTS	SELECTION	RATIONALE
F.E. Shape (Cont'd)	Cylindrical	− Cost + Lowest volume, area, weight + Most flexibility of # of flow paths	Yes	
Core Redundancy	2 Layer core F-21 F.O. In Single Device	. Spray across, core sized for Q_t either loop at 1 loop flow; nozzles spray 1/2 time at full load for $Q_t/2$ capability + F.O. capability for Q_t in single loop − Larger volume & weight since only 1/2 capability of core used	No	Minimum weight since redundancy not needed
	1 Layer core need 2 Devices for Operation, F.S.	. Spray from 1 side, sized for $Q_t/2$ for each loop, nozzle spray full time; $Q_t/2$ F.S. load + 1/2 weight, .7 volume of 2 layer − F.S. capability of $Q_t/2$ − More vapor ducting required . Same # valves/nozzles as 2 layer	Yes	
Spray Deposition Design	Even, Single Unit	+ Proven ability to control outlet temperature − Larger device (area, weight, volume) + Single fluid temperature sensor for control + Proven controller design + Simple core geometry and flow path selection	No	Load partitioning is lighter weight, evaluation of even and uneven spray with effect on control.
	Even, Multiple Units Load Partitioning	. Same comments as for even single nozzle + Smaller volume, less area	Yes	
	Uneven, Single Unit	+ Smaller device (area, weight, volume) (increase Q/A eff by 50% for 2:1 ratio) − Have not demonstrated with controller − Core geometry flowpath selection becomes important/intricate	No	
	Uneven, Multiple Units Load Partitioning	. Same comments as for Uneven, Single Nozzle − Multiple nozzles/valves cost more	Yes	

TABLE 4-1 (Cont'd)

VARIABLE	SELECTION POSSIBILITIES	COMMENTS	SELECTION	RATIONALE
Nozzle	Hollow Cone	+ Same spray deposition at high & low flowrates + Applicable to top-off & re-entry designs - Larger volume flash evaporator	Yes	Desirable to build device using any nozzle for performance comparison
	Solid Cone	+ Smaller volume flash evaporator - Available for low flowrates only - Applicable to top-off design only	Yes	
	1/2H - 1/2S	+ Smaller volume F.E. hollow cone - Available for low flowrates only - Applicable to Top-off design only	Yes	

separate devices as shown in the schematic of Figure 4-3. This provides
for maximum separation of the two Freon loops and results in half the total heat
sink capability in the event of failure of one loop. For a two layer core design,
the heat from the outer loop must be transferred through the inner core layer
to the area of spray contact. The Freon leaving the unit from the outer loop
will tend to be warmer than the inner loop, and therefore, control of the
spray nozzle may be complicated due to this temperature difference. The heat
exchanger surface would also have to be larger than an individual single layer
core unit because of the lower conductance from the outer loop core. The single
loop, single layer core concept was selected because redundancy was not needed,
it is resistant to system failure due to metering valve failure (ice build up
on active core area), and it would result in a simpler outlet temperature control.

The choices of spray deposition design include load partitioning and
non-load partitioning, and even and uneven spray deposition. Load partitioning
was selected based on lower weight as described in Section 4.2. Even spray
deposition was successfully utilized in the Prototype I unit. The use of an
uneven spray deposition postulates putting the higher spray in the areas with
higher fluid/wall temperatures to take advantage of the greater evaporation
potential. (This can be seen in Figure 3-3). The use of uneven spray can re-
sult in less heat transfer area and thus provide a unit with less volume and
weight. The Prototype 2 and 3 designs evaluated the effects both even and
uneven spray concepts on controller operation.

The nozzles evaluated during the program development (see Section 3.1
and Appendix A) included solid, hollow, and 1/2 solid 1/2 hollow cone designs.
The use of a particular nozzle depends on the exhaust duct configuration and
spray deposition approach. The hollow cone nozzles can be used in units where
the exhaust is opposite to the spray nozzle with either even or uneven spray
deposition. The solid cone nozzles are applicable to units with the exhaust
at the same end of the device as the nozzles, with even or uneven spray deposi-
tion. Both types of nozzles were selected consistent with the building block
approach to the device design mentioned earlier.

Using the above selected variables of an 18.5 fins per inch
rectangular-lanced fin core in a single layer, cylindrical (or round) configura-
tion compatible with even or uneven spray deposition and load partitioning, con-
ceptual designs of the flash evaporators were generated for the baseline and

alternate system performance requirements of Figures 4-1 and 4-2. These 12 conceptual designs, presented in Figures 4-6 and 4-7 respectively, were configured using core performance data of Section 3.5, the nozzle performance data of Appendix A, and the evaporation data of Figure 3-3. Figures 4-6 and 4-7 compare the volume, and detailed weight estimates for each of the concepts considered with each meeting the pressure drop design requirement of 4.5 psi at 2400 lb/hr Freon flow.

The six designs in Figure 4-6 for the baseline performance requirements resulted in units which vary from 380 to 600 mm (15 to 26 in.) in diameter with weights from 7.25 to 15.5 Kg (16 to 32 lbs). Four units of each identical core design were required for the system installation of Figure 4-3. The six designs in Figure 4-7 for the alternate performance requirements had units that varied from 280 to 457 mm (11 to 18 in.) in diameter with weights of from 5.9 to 12.7 Kg (13 to 28 lbs).

4.4   Design Configuration Selections and Prototype Description

Although for Shuttle application the four evaporator units (two high temperature, two low temperature) would have identical heat exchanger core configurations, it was decided to build two different configurations to obtain performance comparison data. Using the building block philosophy and the design variables selection of the previous section, two configurations were selected for the Prototype 2 and 3 flash evaporators.

A 380 mm (15 in.) diameter, cylindrical unit was selected for both evaporators since it closely (or exactly) approximated 6 of the 12 concepts on Figures 4-6 and 4-7. In addition, a sidewall core height of 216 mm (8-1/2 in.) in conjunction with a moveable backplate with valve/nozzle mounting provisions was selected so that the nozzle height could be varied to evaluate these 6 design concepts.

Both prototype evaporators employ the single layer of 18.5 fins per inch, rectangular, lanced fin heat exchanger core with the flow running axially in the cylindrical sidewalls. Structural analyses (reported in Appendix E) of the evaporators were performed to determine the maximum safe operating pressure, the optimum mounting system and various thermal effects on the structural integrity.

The Prototype 2 evaporator, shown in Figures 4-8 and 4-9, was designed for a hollow cone spray nozzle with the exhaust aperture opposite of the

4-13

REQUIREMENTS:	2 LOOPS NOMINAL	1 LOOP ABORT
TOP OFF		
Q BTU/HR	12,500	24,500*
ṁ lb/hr/loop	1800	2,600
T_{in} °F	53.8°	78°
T_{out} °F	40°	40°
RE-ENTRY		
Q BTU/HR	24,500	24,500
ṁ lb/hr/loop	400	600
T_{in} °F	163°	203°
T_{out} °F	40°	40°

ΔP max = 4.5 @ 2600 lb/hr

* Not thru S.S. Nozzle
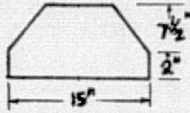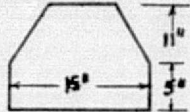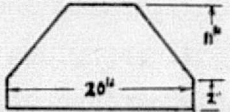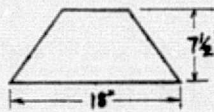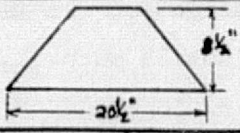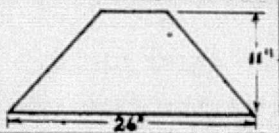
CONFIGURATION	NUMBER OF UNITS	VOL. ft³	TOTAL WT. LBS.	CORE AREA PER UNIT	CORE WEIGHT LBS	MANIFOLD WT. LBS.	CLOSE-OUT WT. LBS.	SPRAY DEPOSITION	SPRAY RATIO (MAX/AVG.)
7½", 2", 15"	4	2.1	16.1	1.88	9.06	5.0	2.0	Uneven – Re-entry Even – at Top-Off	2.4
11", 15", 5"	4	3.1	22.0	2.9	13.6	6.3	2.1	Even	
11", 20", 2"	4	4.25	29.6	3.5	16.3	6.6	3.7	Even	
7½", 18"	4	2.4	18.0	1.77	8.88	6.04	3.04	Uneven – Re-entry Even – at Top-OFF	2.3
8½", 20½"	4	3.2	24.6	2.3	11.2	7.1	4.3	Even	
11", 26"	4	6.1	32.0	3.7	17.3	8.4	6.3	Even	

FIGURE 4-6   EVAPORATOR CONCEPTS FOR BASELINE PERFORMANCE REQUIREMENTS

	REQUIREMENTS:	2 LOOPS NOMINAL	1 LOOP ABORT
TOP-OFF			
Q BTU/HR		12,500	-
$\dot{m}$ lb/hr/loop		1800	2400
T_{in} °F		53.8	-
T_{out} °F		40°	-
RE-ENTRY			
Q BTU/HR		92,000	92,000
$\dot{m}$ lb/hr/loop		1800	2400
T_{in} °F		148°	193°
T_{out} °F		40°	40°

$\Delta P = 4.5$ @ 2400 lb/hr
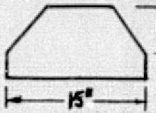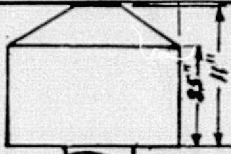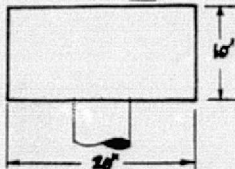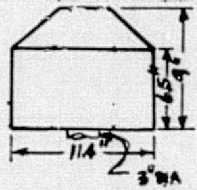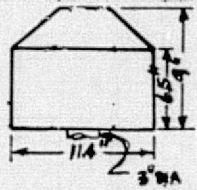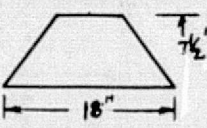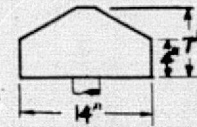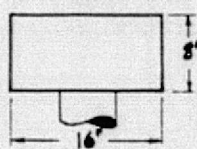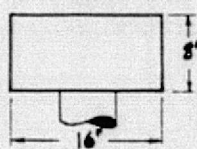
CONFIGURATION	NUMBER OF UNITS	VOL. ft³	TOTAL WT. LBS.	CORE AREA PER UNIT	CORE WEIGHT LBS	MANIFOLD WT. LBS.	CLOSE-OUT WT. LBS.	SPRAY DEPOSITION	SPRAY RATIO (MAX./AVG.)
	6	3.2	24.1	1.88	13.6	7.5	3.0	Even	
	4	4.	27.3	3.8	19.	5.3	3.0	Uneven	3.5
	(2)	(1.50)	(9.45)	3.11	6.76	1.72	0.97	Even	2.05
	(2)	(4.02)	(18.45)	6.91	15.04	1.96	1.45	Uneven	3.03
	4	5.5	27.9						
	4	1.23	13.08	2.27	8.28	3.2	1.6	Uneven	3.5
	6	3.6	26.9	1.77	13.3	9.1	4.5	Even	
	(2)	(1.02)	(5.59)	2.38	3.24	1.60	0.75	Even	2.05
	(2)	(2.05)	(8.84)	4.3	5.85	2.06	0.93	Uneven	2.97
	4	3.1	14.4						

FIGURE 4-7 EVAPORATOR CONCEPTS FOR ALTERNATE PERFORMANCE REQUIREMENTS
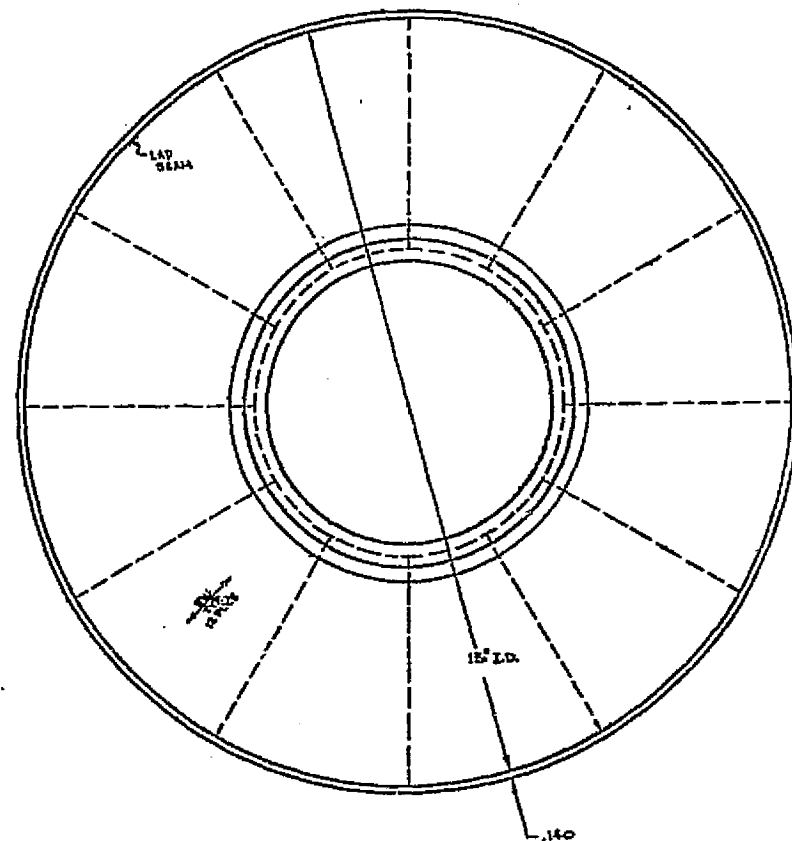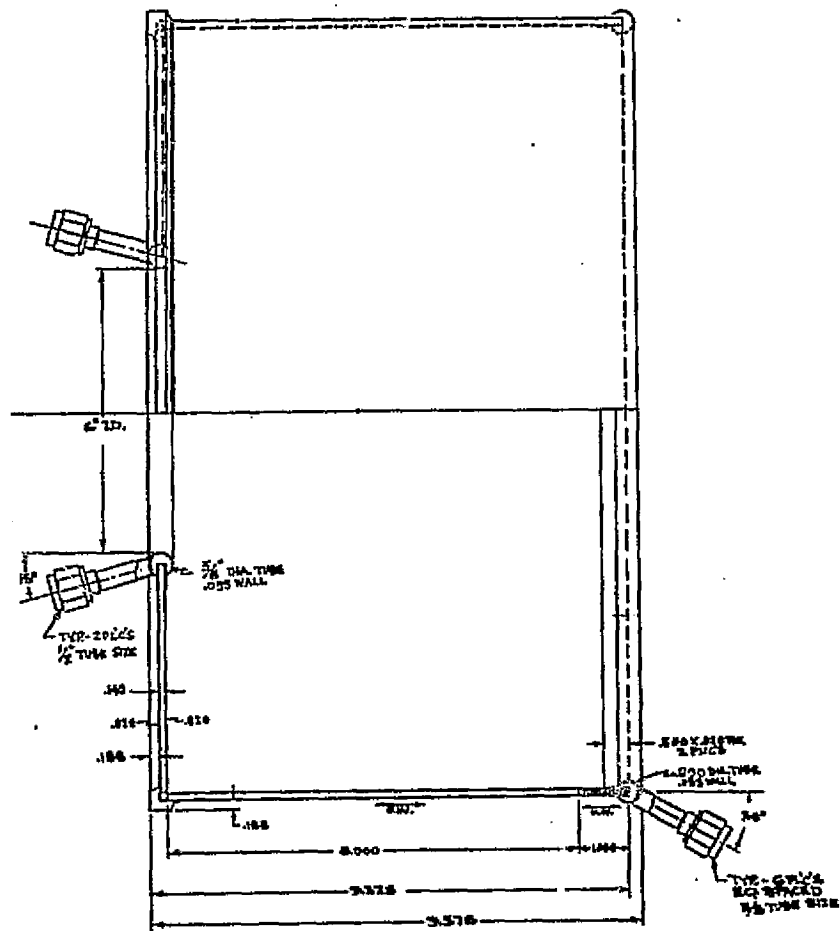
FIGURE 4-8   PROTOTYPE 2 DESIGN
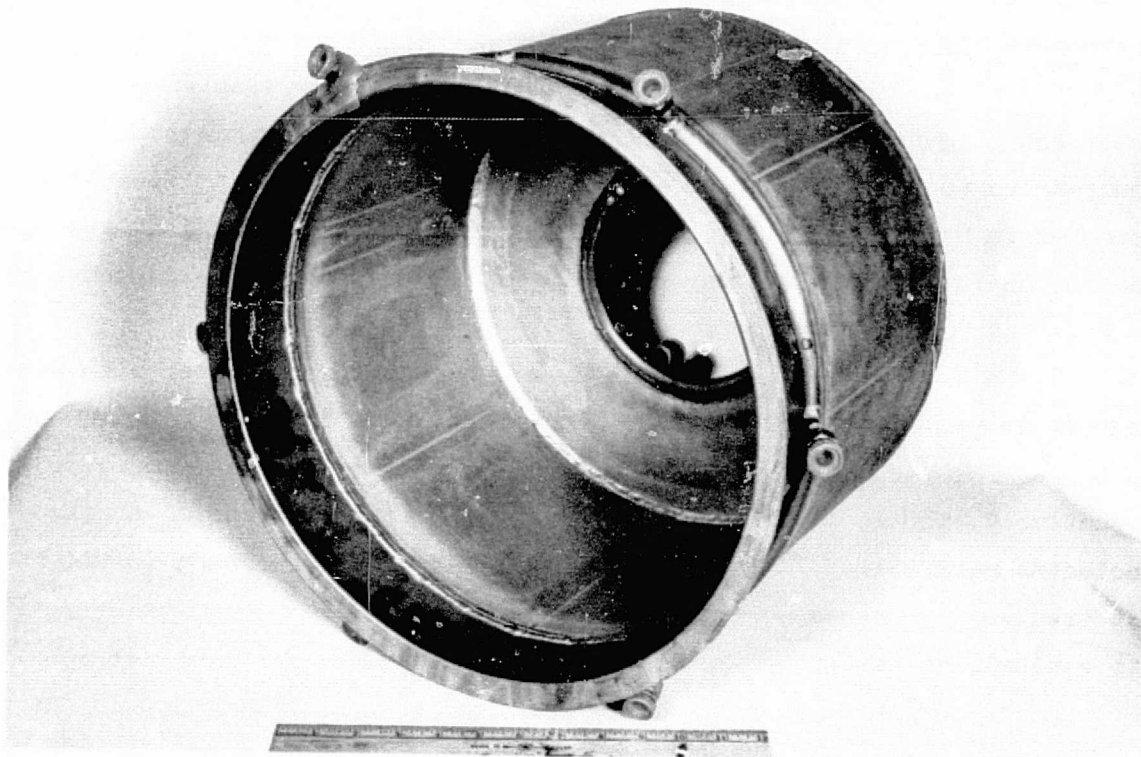
FIGURE 4—9 PROTOTYPE 2 FLASH EVAPORATOR

spray nozzle. This is the same approach used in the Prototype I evaporator. The 127 mm (5 in.) diameter exhaust hole in the bottomplate is of sufficient size to permit passage of exhaust steam in either the high or low temperature configuration.

The Prototype 3 unit, shown in Figures 4-10 and 4-11, was designed for use with either a solid or hollow cone nozzle. The steam exhaust exits the unit in the same plane as the nozzle with the duct entrance accommodated in the backcone (or backplate). The solid bottomplate permits the use of the solid cone nozzle. The evolution of the Prototype 3 device to a flight configuration is shown in Figure 4-12 to demonstrate its applicability for the Space Shuttle.

Although the appearance of the Prototypes 2 and 3 bottomplates were different, the core material was identical in type and in installation approach. The core material was cut in circular sectors with the "easyway" direction bisecting each circular sector as can be seen in Figures 4-8 and 4-10. This arrangement directed the flow in the bottomplate in a radial direction along the sector centerlines which was also the path of least resistance. (The core sector design generated areas of inherent stagnation along the sector radii resulting in poor heat transfer along each sector splice joint as will be discussed in Section 5.3.) The sidewall designs of the two units were identical with 790 mm (7-1/2 in.) easyway and 25.4 mm (1 in.) hardway core running in the axial direction from the bottom.

The Prototype 2 and 3 flash evaporators were fabricated with 3003 aluminum using a salt bath process, according to the drawings in Figures 4-8 and 4-10. The two units weighed 2.064 Kg (4.55 lbs) and 2.195 Kg (4.85 lbs) respectively, for approximately .371 m^2 (4 ft^2) of heat transfer surface (including manifolding). This is approximately a 4:1 reduction in weight per unit area when compared to the Prototype 1 device. The two units were fitted with a plexiglas backplate which incorporated moveable valve/nozzle mounting plate and exhaust port provisions for test. The backplate design is described in Section 5.1.

In addition to the evaporator configuration, detailed design was performed to integrate the valve/nozzle combination to reduce the holdup volume from 0.5 cc in the Prototype 1 unit to 0.10 cc. An off-the-shelf, light weight,
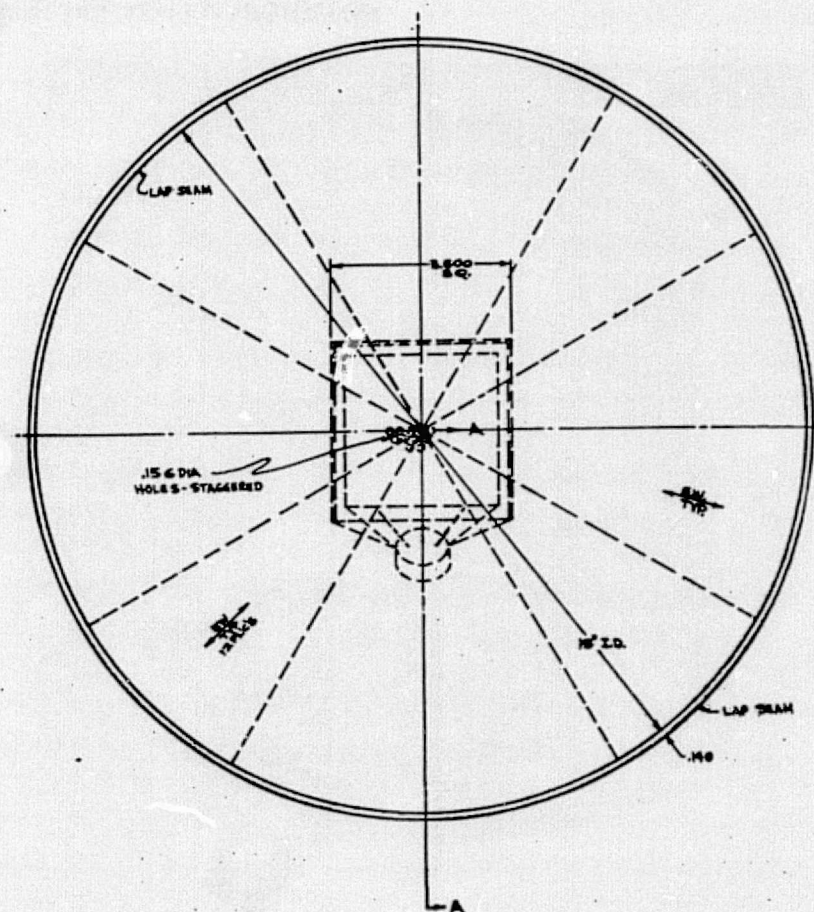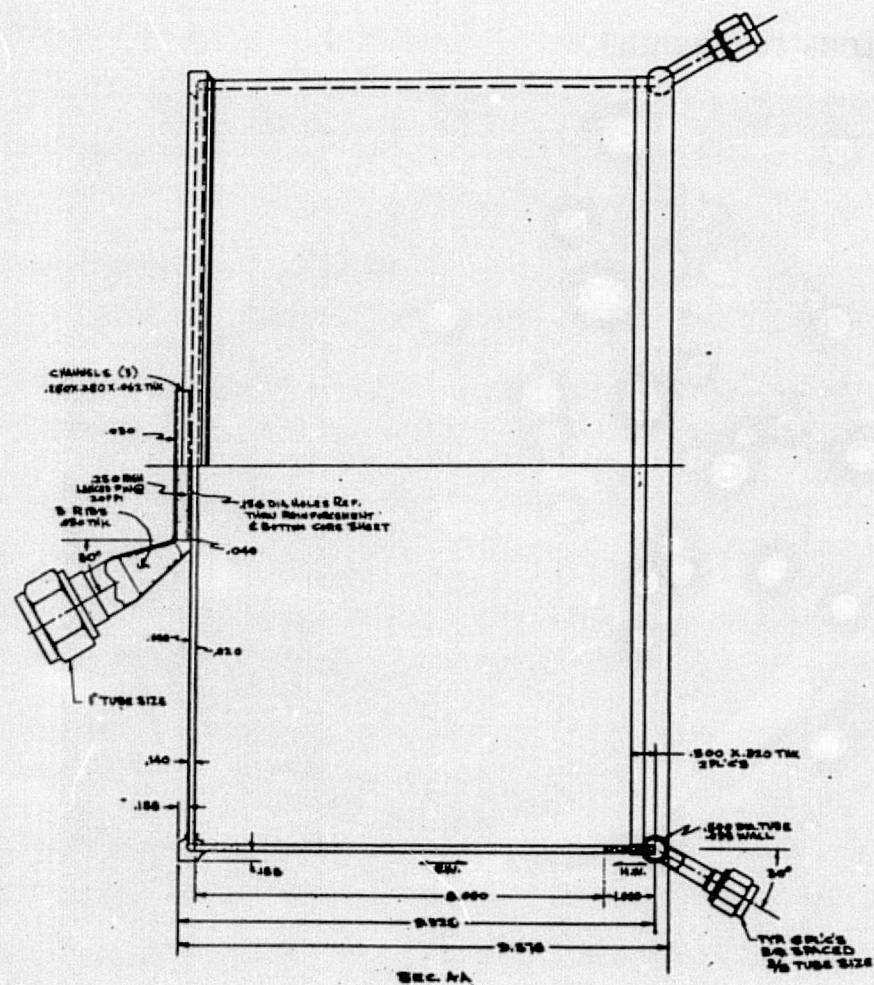
FIGURE 4-10. PROTOTYPE 3 DESIGN
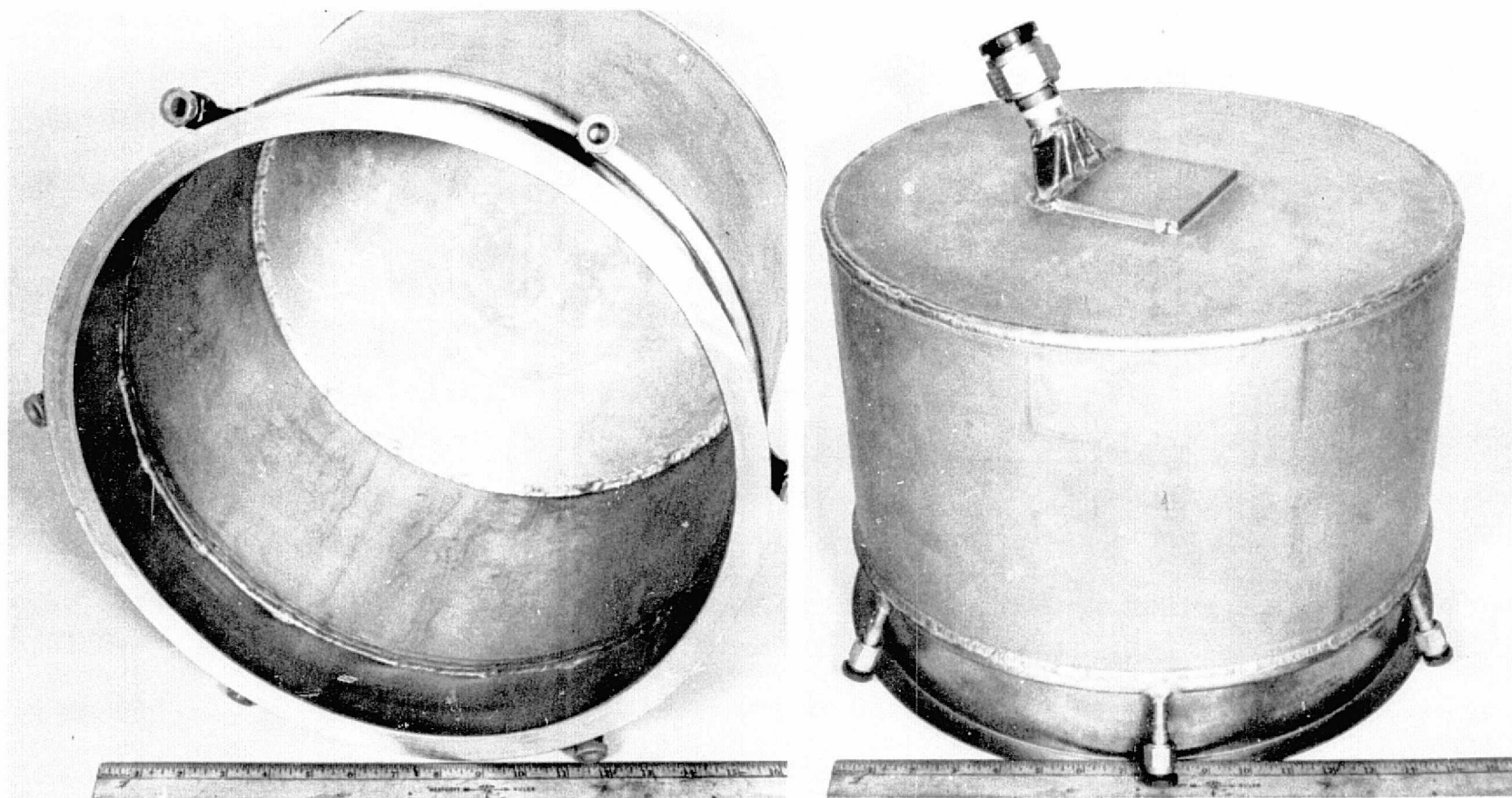
FIGURE 4—11 PROTOTYPE 3 FLASH EVAPORATOR

EXHAUST PORT ————

FREON OUTLET

FREON INLET
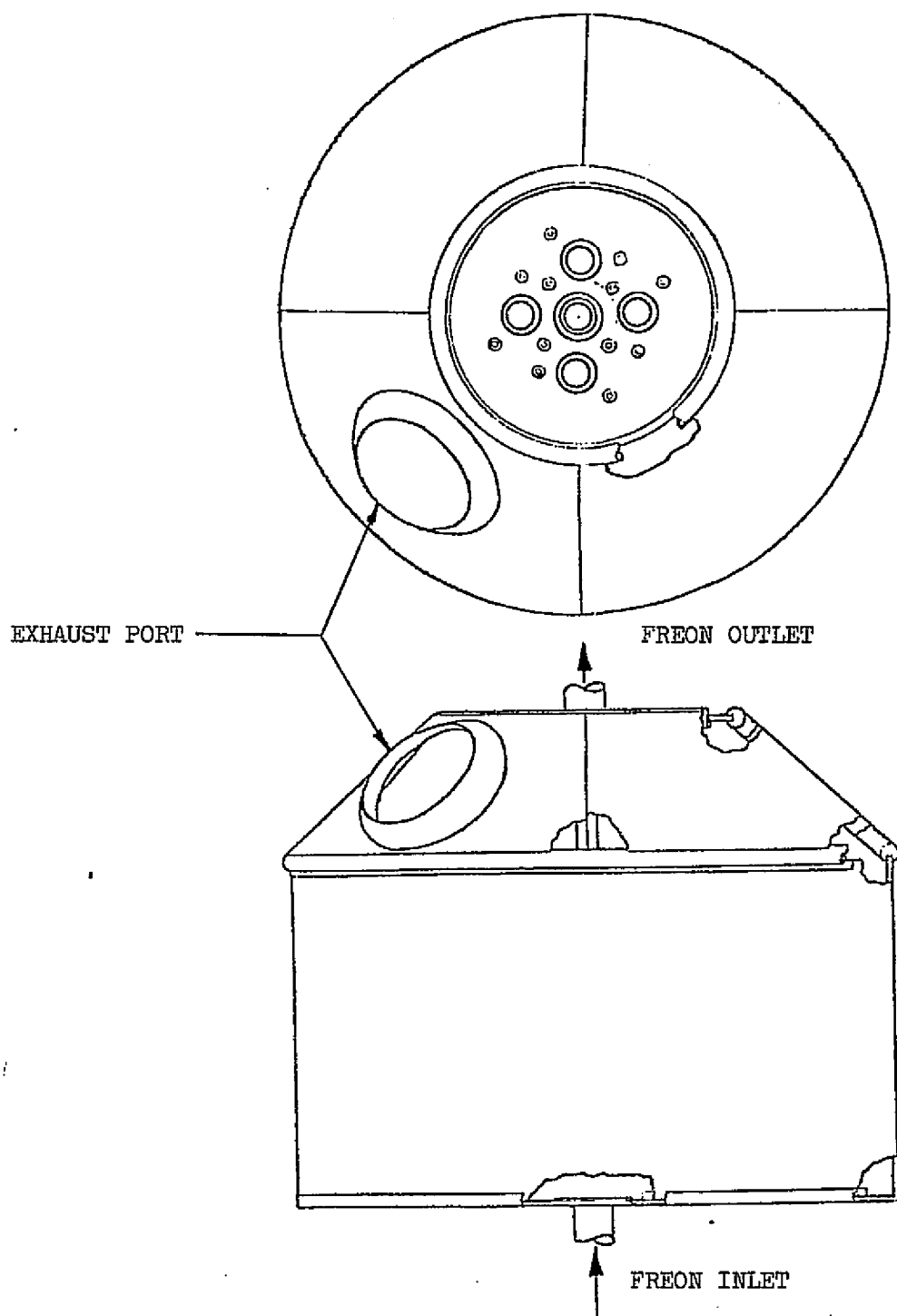
FIGURE 4-12

PROJECTED PROTOTYPE EVAPORATOR INSTALLATION CONFIGURATION

Parker Hannifin propellant valve was selected and integrated with the class
of nozzles used with the Prototype designs selected above. The resulting
design, shown in Figure 4-12, was selected from many integration concepts
and achieved a liquid holdup volume of 0.15 cc.

The Prototype 2 and 3 flash evaporators described above underwent
an extensive test program to verify the design. This is reported in the next
section.
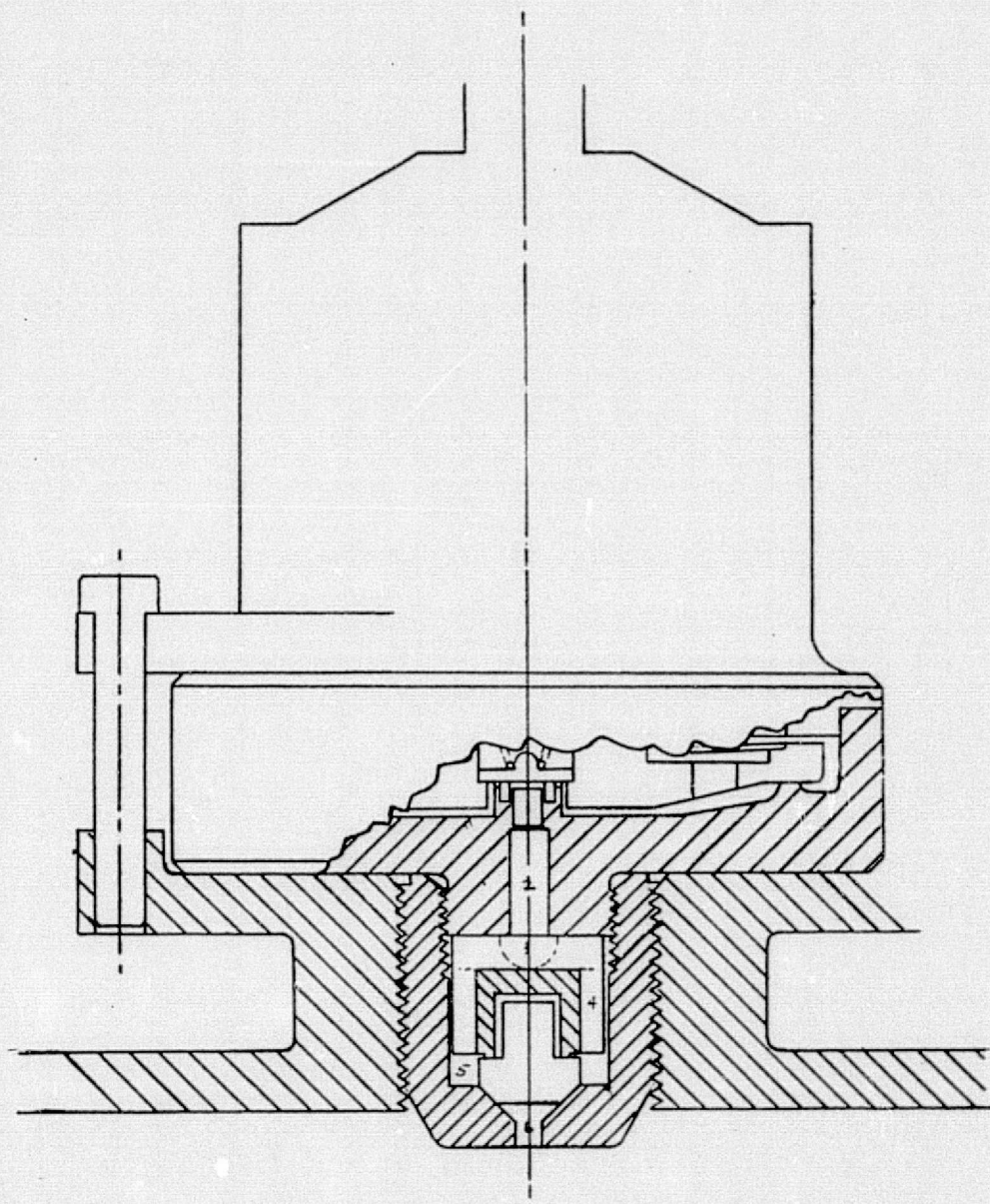
FIGURE 4-13 VALVE NOZZLE INTEGRATION

5.0   SYSTEM TESTING

Prototype 2 and 3 evaporators were tested independently for extended periods in a vacuum environment. The purpose of these tests were to verify the design approach in the use of heat exchanger core as the evaporation surface; to verify the concept of partitioning the heat load between two evaporators (high/low temperature units); and to verify the design approach for hollow and solid spray cone evaporators. The test program plan included demonstration of capability to me.. the Shuttle baseline performance requirements in the area of orbital operation, on-orbit water dumping, and re-entry payload cooling.

Overall test objectives to determine the successful operation of the system included:

1. Determination of efficiency of evaporant utilization
2. Determination of exact evaporant spray distribution
3. Demonstration of valve/nozzle freedom from freezing
4. Verification of controller design approach for partial loads

5.1   System Test Equipment

5.1.1   Test Article Description

The evaporator as a system included prototype heat exchanger assemblies, backcone, solenoid valve/nozzle, electronic controller and associated fluid manifolding. The Prototype 2 flash evaporator heat exchanger was designed for a hollow cone spray nozzle. This hollow cone spray design had the exhaust port on the evaporator centerline in the bottom heat exchanger plate as shown in Figure 5-1. Fluid manifolding to the heat exchanger was made through two tube-ring manifolds. The bottom plate manifold is around the exhaust port and has two manifold spools. The cylindrical sidewall manifold has six manifold spools to assure uniform flow distribution in the sidewall.

The Prototype 3 flash evaporator heat exchanger was designed for a solid cone spray nozzle. This design has the exhaust port located in the backcone and the bottom heat exchanger plate as also shown in Figure 5-1 is closed-out solid. Proto 3 had a sidewall manifold identical to that of Proto 2; however, the bottom plate manifold is a collection chamber outside the evaporator accessed through a single manifold spool.

An evaporator backcone was constructed of 6.4 mm (1/4 inch) thick plexiglas which allowed observation of the spray impacting the heat exchanger surface. The
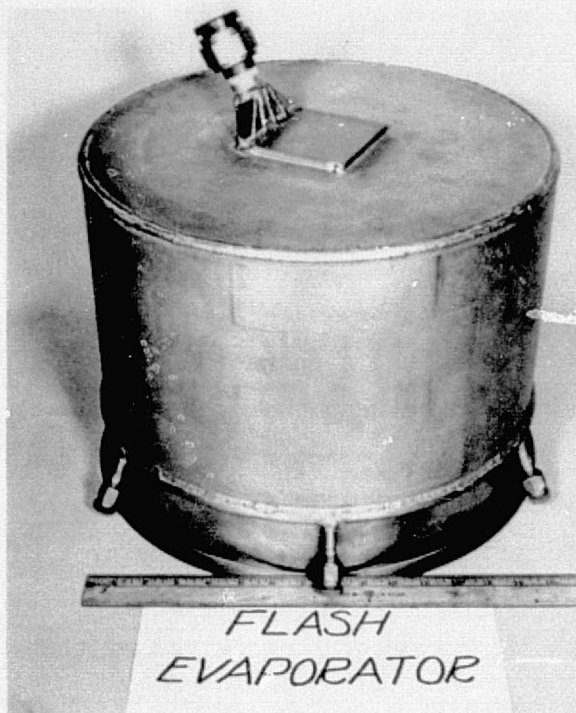
PROTOTYPE 3
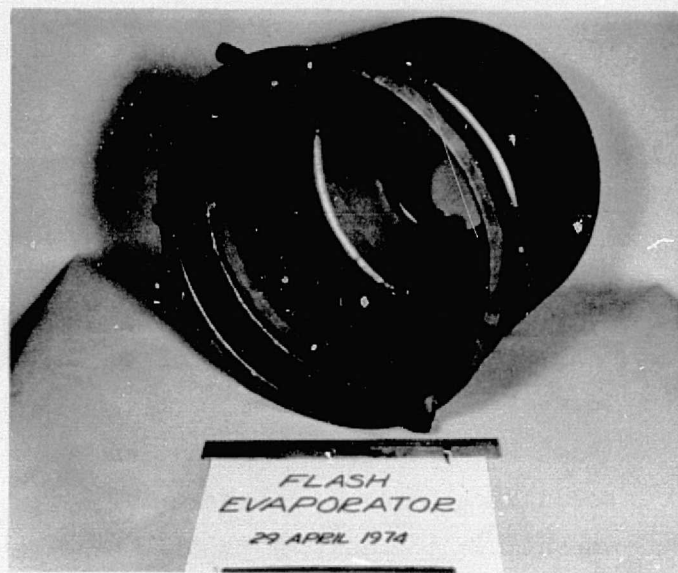
PROTOTYPE 2

FIGURE 5—1 FLASH EVAPORATOR PROTOTYPES 2 & 3
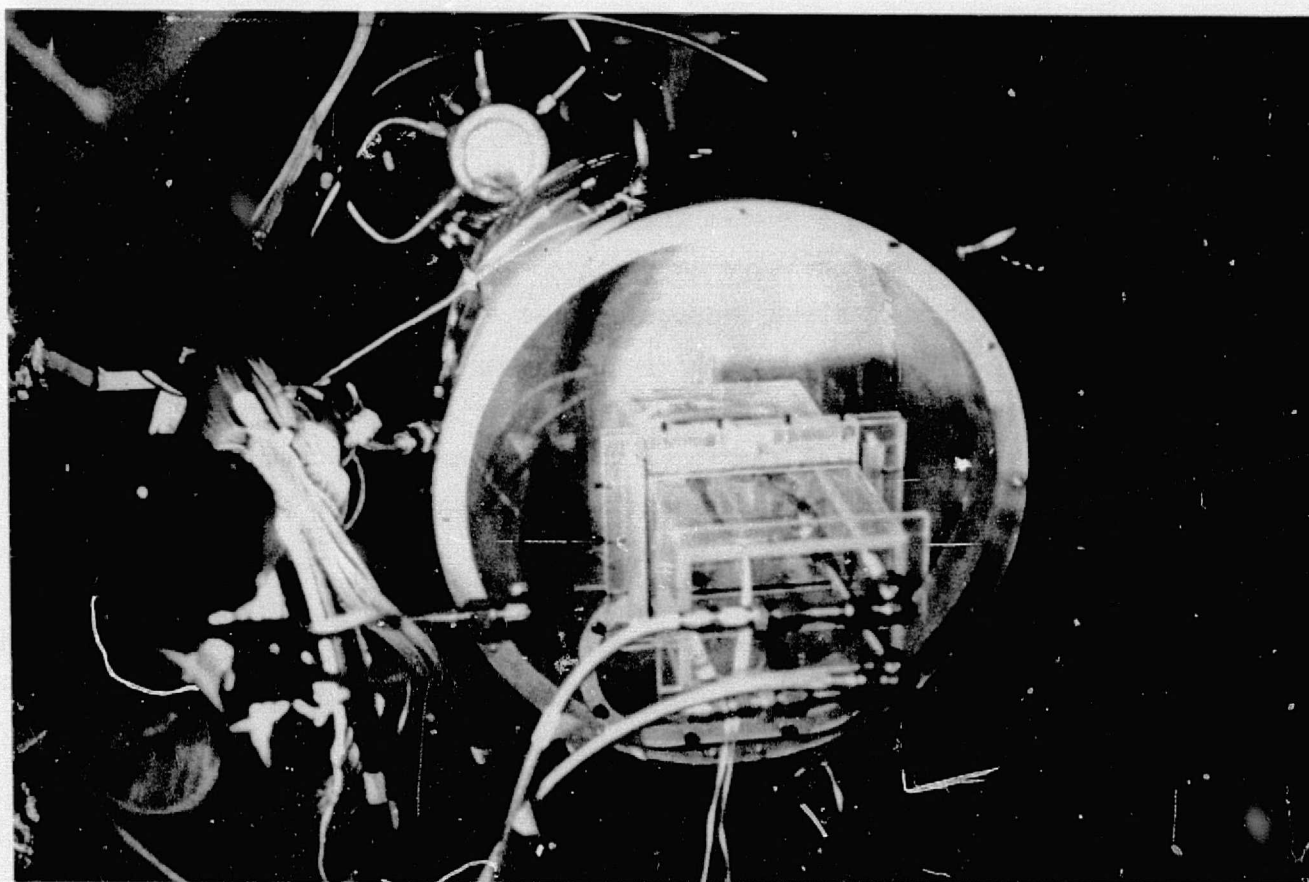
FIGURE 5—2 VARIABLE LOCATION NOZZLE TESTS

backcone was fabricated to permit interchangeability between the Prototype evaporators. Figure 5-2 shows the plexiglas backcone with the variable valve/nozzle holder (box) which permitted evaluation of the evaporator/nozzle at various nozzle heights. The exhaust port shown in Figure 5-2 below the nozzle box was varied, depending on the evaporant spray rate being sprayed, to maintain a evaporator chamber pressure of approximately 3.8 mmHg.

5.1.2   Test Setup

The evaporators were instrumented to monitor the thermodynamic conditions pertinent to evaluating the evaporator performance. Figure 5-3 illustrates the fluid connections to the evaporators and the various fluid parameters which were monitored. Figure 5-4 shows the external thermocouple locations which were placed in four arrays along the cylindrical sidewall and converging to the center of the bottomplate.

Data acquisition was made with an automated system which converted all the measurements to customary U.S. engineering units and displayed these on closed-circuit television monitors to the test director. Printed data in the format shown in Figure 5-5 provided a permanent record of the tests. Data channels 20 through 84 were external evaporator thermocouples which were used to infer spray pattern uniformity and/or transport fluid sidewall flow distribution. Table 5-1 defines instrumentation, data channels 1-19 (see Figure 5-5), and accuracy attained during testing.

Both evaporators were tested in a small vacuum chamber (1.22 meter, 4' dia.) with a 6.4 cm thick plexiglas door which allowed continuous observation of the test article in operation.
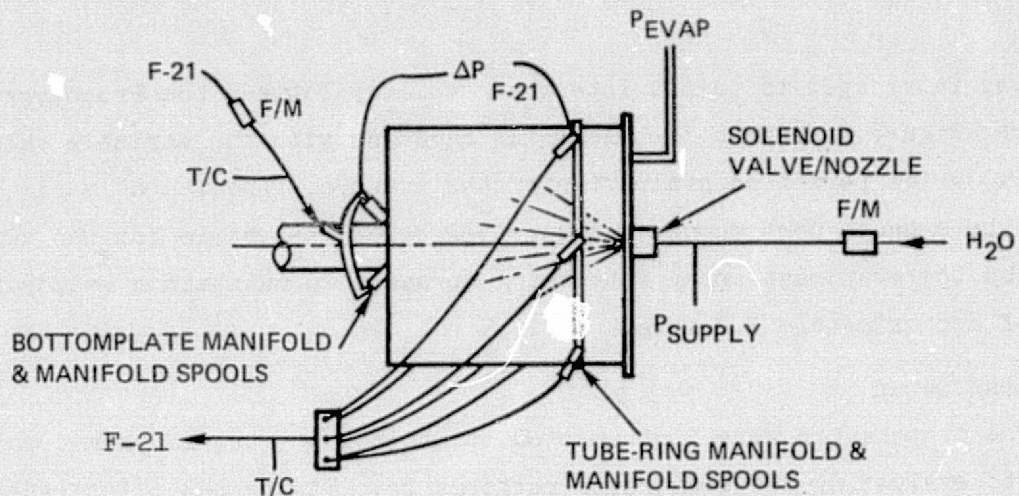
PROTOTYPE 2 (HOLLOW CONE)
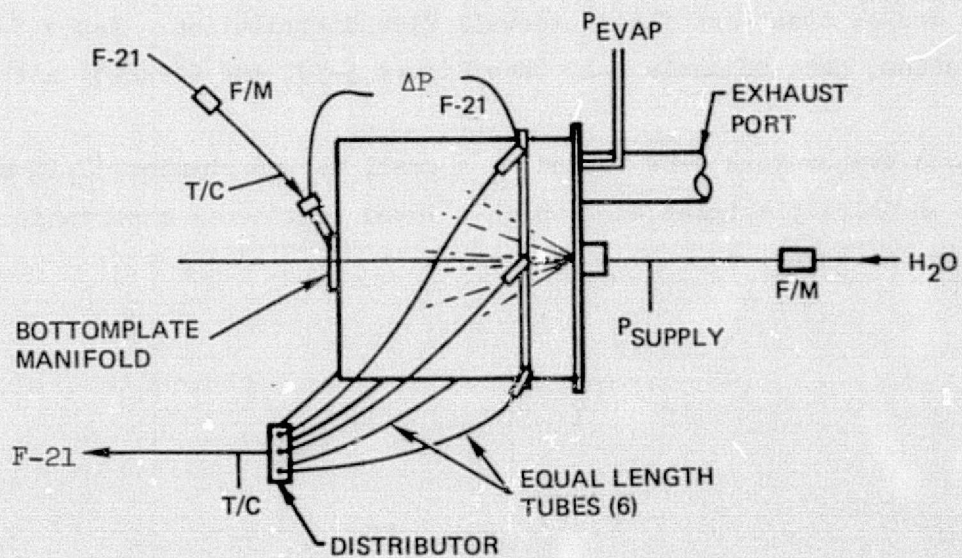
PROTOTYPE 3 (SOLID CONE)

FIGURE 5-3 TEST ARTICLE SET-UP
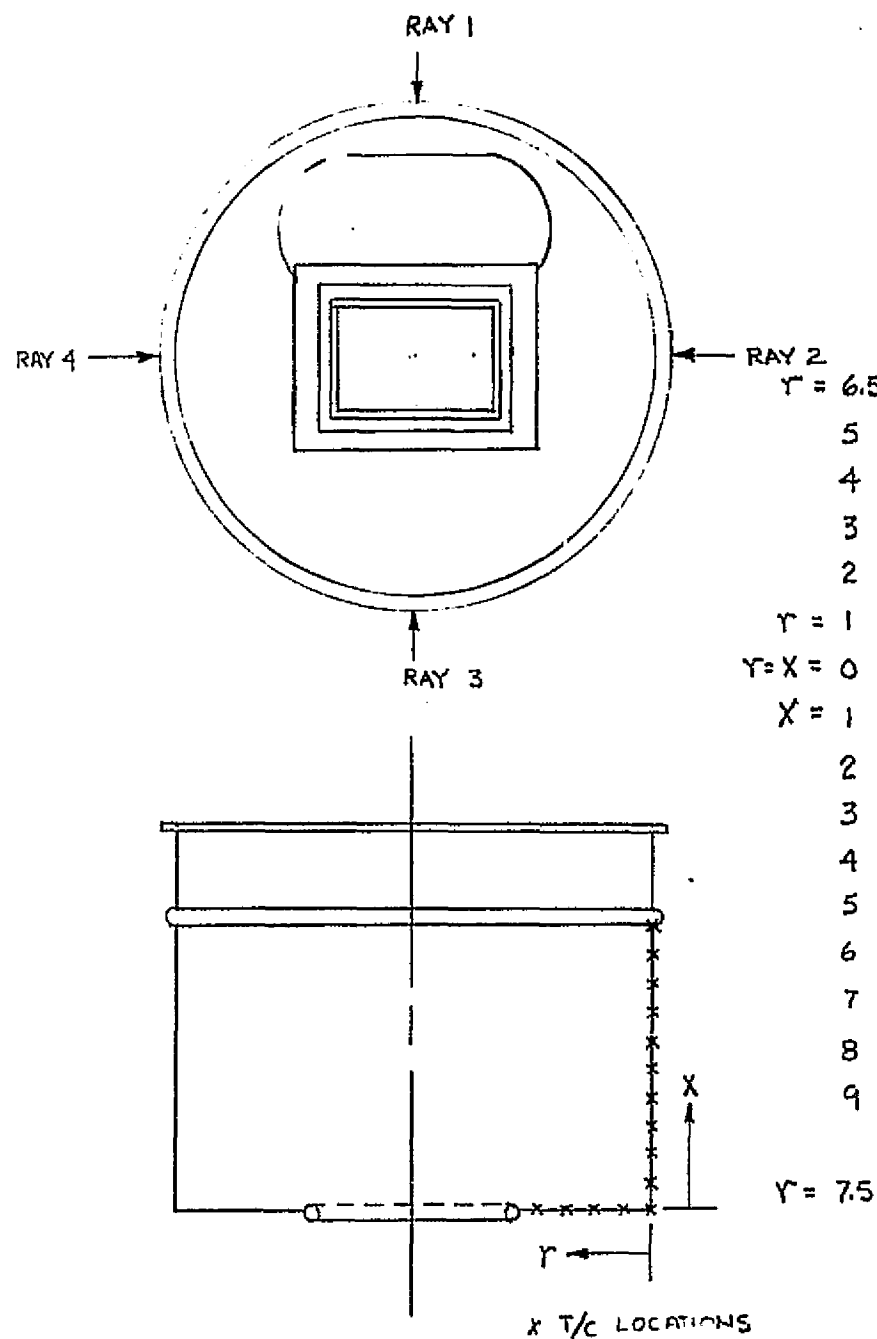
EVAPORATOR THERMOCOUPLE LOCATION DEFINITION

	SOLID BOTTOM				HOLLOW BOTTOM			
	RAY 1	RAY 2	RAY 3	RAY 4	RAY 1	RAY 2	RAY 3	RAY 4
$Y = 6.5$	76	92	108	124	—	—	—	—
5	77	93	109	125	—	—	—	—
4	78	94	110	126	20	34	48	62
3	79	95	111	127	21	35	49	63
2	80	96	112	128	22	36	50	64
$Y = 1$	81	97	113	129	23	37	51	65
$Y = X = 0$	82	98	114	130	24	38	52	66
$X = 1$	83	99	115	131	25	39	53	67
2	84	100	116	132	26	40	54	68
3	85	101	117	133	27	41	55	69
4	86	102	118	134	28	42	56	70
5	87	103	119	135	29	43	57	71
6	88	104	120	136	30	44	58	72
7	89	105	121	137	31	45	59	73
8	90	106	122	138	32	46	60	74
9	91	107	123	139	33	47	61	75
$Y = 7.5$	—	—	—	140	—	—	—	—

x T/C LOCATIONS

FIGURE 5-4 EVAPORATOR THERMOCOUPLE INSTALLATION

```
FLASH  EVAPORATOR  TEST
TIME    14:54:00    DAY    017    RECORD    0199
CH   1 +     0 1 #/HR   F21 LO     CH   2 + 2709 9 #/HR   F21 HI
CH   3 +     0 0 #/HR   H20 LO     CH   4 +    0 1 #/HR   H20 MED    CH   5 +     0 1 #/HR   H20 HI
CH   6 +     6 3 PSID   EVAP #1    CH   7 +    0 0 PSID   EVAP #2
CH   8 +     4 0 MMHG   CHAMBER    CH   9 -    12 2 PSIG   H20 SYS    CH  10 -    51 4 LBS    H20 TANK
TEMPERATURES - DEGF
CH  11 +   150 0 F21 IN #1     CH  12 +   150 0 F21 OUT #1/IN #2     CH  13 +    81 9 F21 OUT #2
CH  14 +   150 0 F21 IN #1     CH  15 +   150 0 F21 OUT #1/IN #2     CH  16  ********  F21 OUT #2
CH  17 +   146 3 NOZZLE #1     CH  18  ********  NOZZLE #2            CH  19 +    85 5 FLOW BENCH
FLASH EVAPORATOR - DEGF
CH  20 +   149 2      CH  21 +   149 6      CH  22 +   149 2      CH  23 +   149 2      CH  24 +   149 6
CH  25 +   149 2      CH  26 +   150 0      CH  27 +   149 6      CH  28 +   149 2      CH  29 +   149 6
CH  30 +   149 6      CH  31 +   149 6      CH  32 +   149 6      CH  33  ********      CH  34 +   150 0
CH  35 +   150 0      CH  36 +   149 6      CH  37 +   149 6      CH  38 +   150 0      CH  39 +   149 2
CH  40 +   149 6      CH  41 +   149 6      CH  42 +   149 2      CH  43 +   149 6      CH  44 +   150 0
CH  45 +   149 6      CH  46 +   149 6      CH  47 +   149 6      CH  48  ********      CH  49 +   150 0
CH  50 +   150 0      CH  51 +   149 6      CH  52 +   149 6      CH  53 +   150 0      CH  54 +   150 0
CH  55 +   150 0      CH  56 +   150 0      CH  57 +   150 0      CH  58 +   150 0      CH  59 +   149 6
CH  60 +   150 0      CH  61 +   150 0      CH  62 +   150 0      CH  63 +   150 0      CH  64 +   150 0
CH  65 +   150 0      CH  66 +   150 0      CH  67 +   150 0      CH  68 +   150 0      CH  69 +   150 0
CH  70 +   149 6      CH  71 +   150 0      CH  72 +   149 6      CH  73 +   150 0      CH  74 +   150 0
CH  75 +   150 0      CH  76 +   150 0      CH  77 +   150 0      CH  78 +   150 0      CH  79 +   150 0
CH  80 +   150 0      CH  81 +   150 0      CH  82 +   150 0      CH  83 +   150 0      CH  84 +   149 6
```

FIGURE 5-5 DATA OUTPUT FORMAT

TABLE 5-1   PROTOTYPE 2 & 3 EVAPORATOR TEST INSTRUMENTATION

DATA CHANNEL	MEASUREMENT	RANGE (ACCURACY)	INSTRUMENT
1	R21 Flowrate	50-520 LB/HR ($\pm$ 10 LB/HR)	LF6-2 SN3259
2	R21 Flowrate	200-3000 LB/HR ($\pm$ 10 LB/HR)	AN-8 SN8434
3	H_2O Flowrate	0-25 LB/HR ($\pm$ .5 LB/HR)	Cox SN 8501278
4	H_2O Flowrate	5-50 LB/HR ($\pm$ .5 LB/HR)	Cox SN 8501281
5	H_2O Flowrate	50-100 LB/HR ($\pm$ .5 LB/HR)	Cox AN8-45
6	R21 Press. Drop Evap. #1	0-30 psi (0.1%)	Bell & Howell SN6944
7	R21 Press. Drop Evap. #2	0-30 psi (0.1%)	Bell & Howell SN6990
8	Chamber Pressure	0-10 mmHg (1%)	MKS Baratron 6978
9	H_2O Supply Pressure	0-50 psig ($\pm$ 5 psi)	Teledyne S/G SN2160
10	Evaporant H_2O Weight	0-300 lbs ($\pm$ .3 lbs)	SN-129 0-500 lb Load Cell
11	Evap. #1 R21 Inlet Temp	+40-+180°F ($\pm$ .5°F)	Thermistor
12	Evap. #1 R21 Outlet Temp	+40-+60°F ($\pm$ .5°F)	"
13	Evap. #2 R21 Outlet Temp	=+40°F ($\pm$ .5°F)	"
14	Redundant (Channel #11)		"
15	" (" #12)		"
16	" (" #13)		"
17	Evap. #1 Nozzle Plate Temp	($\pm$ .5°F)	Thermocouple
18	" #2 " " "	($\pm$ .5°F)	"
19	Flow Bench Temp	($\pm$ .5°F)	"

5.2   Initial Prototype Testing

An extensive four week test program was conducted in August and
September 1974 with the purpose of verifying evaporator design and performance
as mentioned previously. Execution of the test sequence started with valve/
nozzle verification and proceeded through nozzle spray location optimization.
During this testing, however, problems with achieving the desired performance
without forming small amounts of frost on evaporator heat transfer surfaces
were encountered. The results of these tests are presented in this Section

The Prototype 3 unit was installed horizontally in the chamber with
the previously described test set-up with the low temperature unit configuration.
The baseline Shuttle re-entry design conditions, 2.83 kg/hr (6.25 lb/hr) evaporant
flow with 181 kg/hr (400 lb/hr) Freon flow were established. The data presented
in Figure 5-6, the baseline nozzle, indicated a severe flow maldistribution in
the core due to the wide variation in ray thermocouple data with localized frost
formation along this ray. It was suspected, and verified by analyses and further
testing, that the flow maldistribution was caused by gravity which stagnated the
flow along ray 1. The Freon flow rate was increased to 272 kg/hr (600 lb/hr),
the Shuttle re-entry abort condition, with the same overall flow maldistribution
and local frost formation results prevailing as before.

The Freon flow was reversed in the Prototype 3 to ascertain whether the
gravity effects would be as severe. As seen in Figure 5-7, the ray temperature
data diverges although not as severely as noted previously. This was due to the
larger amounts of cooling occurring in the floor of the device which is vertical
within the chamber. Again localized frost formation along the low temperature
rays was obtained.

The gravity effects on the performance of the evaporator at 181 kg/hr
(400 lb/hr) Freon flow conditions would have serious implications for Shuttle
application since the evaporator would have to be aligned with gravity forces
in an installation for both ascent and re-entry. Subsequent to this testing,
however, the Shuttle baseline configuration changed so that the alternate per-
formance requirements became the baseline with a minimum Freon flow rate of
815 Kg/hr (1800 lb/hr). This increased flow virtually eliminates flow
stagnation problems due to gravity.

FIGURE 5-6

PROTOTYPE 3 EVAPORATOR TEMPERATURE DISTRIBUTION

RUN A1   8-5-74
NOZZLE #1   2.0-W-90°
P_e = 2.5 mmHg
$\dot{m}_{H_2O}$ =   5.9 lb/hr
$\dot{m}_{R-21}$ =   400 lb/hr
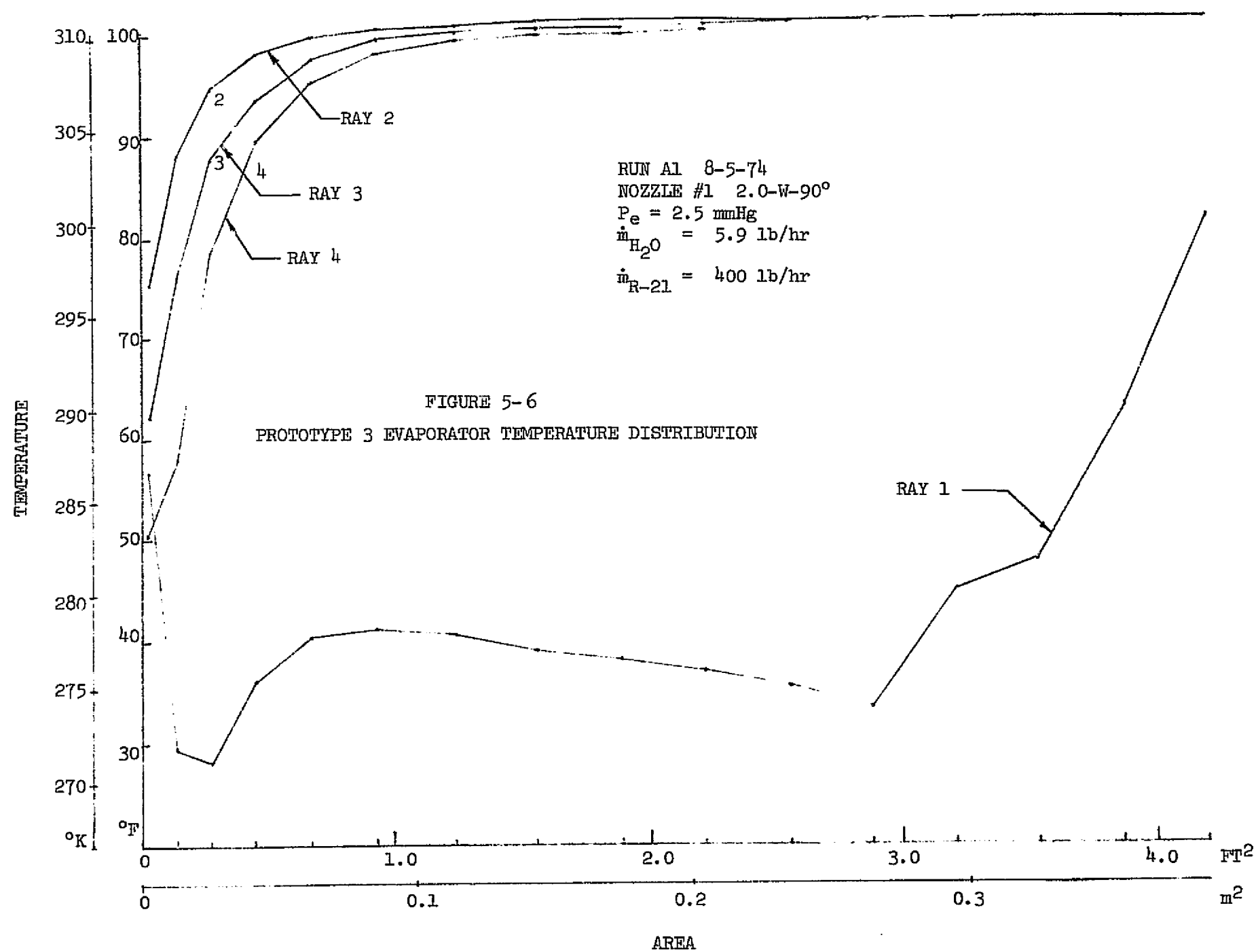
FIGURE 5-7

PROTOTYPE 3 EVAPORATOR WITH REVERSE FLOW

RUN A22   8-8-74
NOZZLE #1   2-W-90°
P_e = 3.9 mmHg
$\dot{m}_{H_2O}$ = 6.2 lb/hr

$\dot{m}_{R-21}$ = 593 lb/hr

RAY 1

RAY 2

RAY 3

RAY 1

RAY 4

TEMPERATURE

AREA

°K °F

5-10
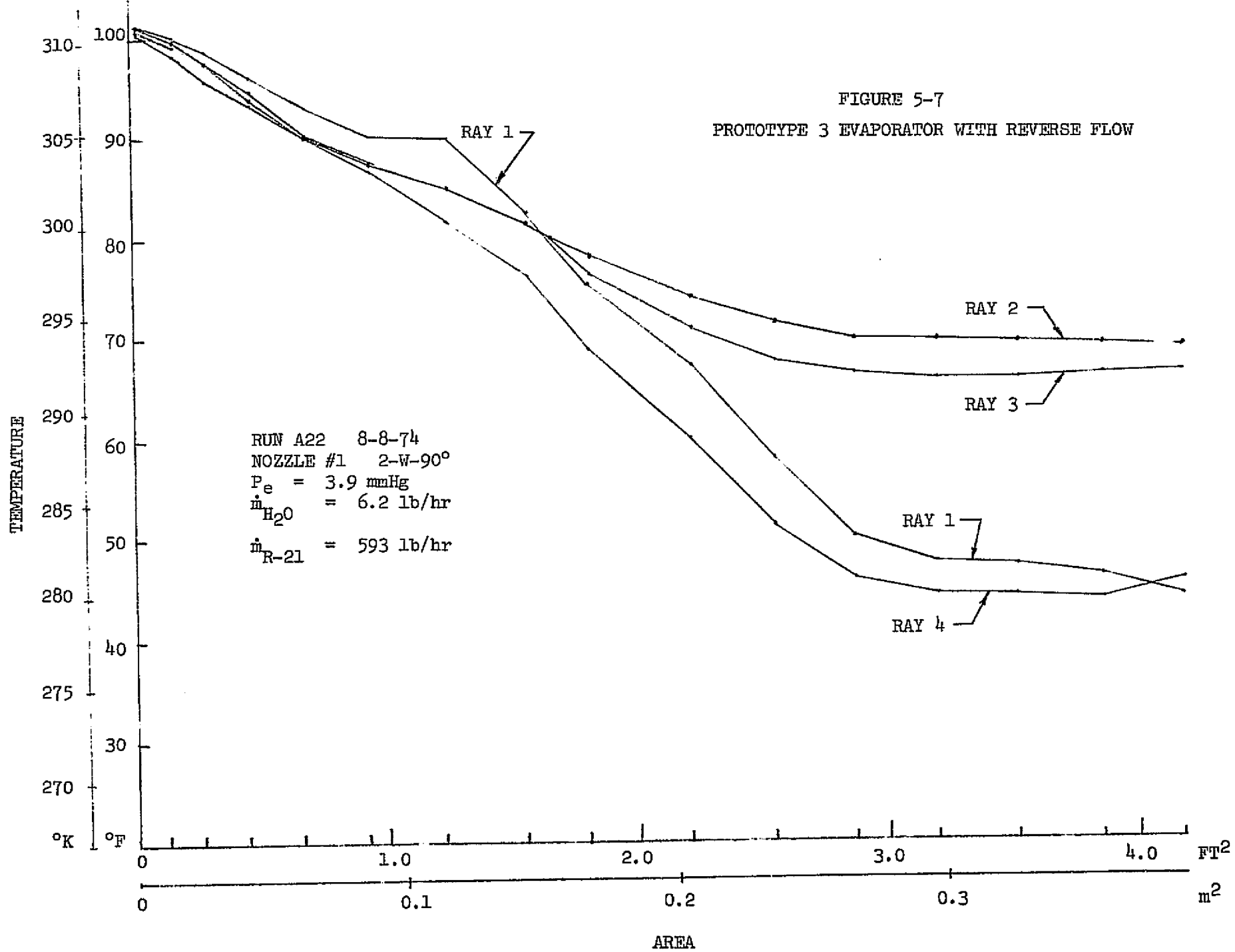
The new Shuttle baseline design conditions of 815 Kg/hr (1800 lb/hr) Freon flow and 7.26 Kg/hr (16 lb/hr) evaporant flow were then tested in the Prototype 3 evaporator. The data, shown in Figure 5-8, still showed wide variation in ray temperature with frost formation on the sidewalls of the device. Lowering the evaporant flow rate to 6.3 kg/hr (14 lb/hr) caused the spray cone to collapse slightly, as desired, and to spread the spray over a larger part of the evaporator area as seen in Figure 5-9. However, the increased spray on the bottom of the device resulted in ice "fingers" forming over the core splice joints in the bottom. These ice fingers are shown in Figure 5-10. Apparently the Freon flow stagnates when the easy way core ends in a core splice, thus causing uneven flow distribution in the bottom. Seven other nozzles were selected and tested for these flow conditions with the same results: at the design evaporant flow rate, frost formed on the device sidewalls; at lower evaporant flow rates, frost fingers form on the device bottom. Using larger capacity nozzles, frost formed on the bottom.

The Prototype 2 unit was then installed in the chamber, in the same manner as the Prototype 3, and tested to see if the bottom flow stagnation at the core splices would be less severe. The large exhaust hole in the bottom resulted in less core splice area encountered by the Freon where flow stagnation could occur. At the high temperature design conditions of 34 kg/hr (75 lb/hr), the unit formed a frost band on the device sidewalls. The evaporant flow was reduced to 27 kg/hr (60 lb/hr) to obtain stab. e operating conditions with no frost formation. The performance data, presenced in Figure 5-11, again shows divergence in ray temperature data as was obtained for the Prototype 3 device. The potential causes of this ray temperature divergence were postulated as due to gravity induced flow maldistribution, heat exchanger core induced flow maldistribution (due to either design and/or fabrication), manifold induced flow maldistribution, or uneven spray distribution. A series of tests were then performed to isolate each of the aforementioned postulations to determine the exact cause.

Analyses indicated that no gravity effects were expected for the high Freon flow rates of 1000 Kg/hr (2250 lb/hr), however, tests were conducted to verify the analyses. The Prototype 2 unit was rotated about its centerline

FIGURE 5-8

PROTOTYPE 3 EVAPORATOR WITH 7.26 kg/hr EVAPORANT FLOW

RUN A64   8-20-74
NOZZLE #2   4.5-W-90°
P_e = 3.0 mmHg
$\dot{m}_{H_2O}$ =   16 lb/hr

$\dot{m}_{R-21}$ =   1812 lb/hr

RAY 3

RAY 1

RAY 4

RAY 2

RAY 1

TEMPERATURE

°K   °F

AREA

80
295   70
290   60
285   50
280   40
275   30
270

0   1.0   2.0   3.0   4.0   FT²
0   0.1   0.2   0.3   m²
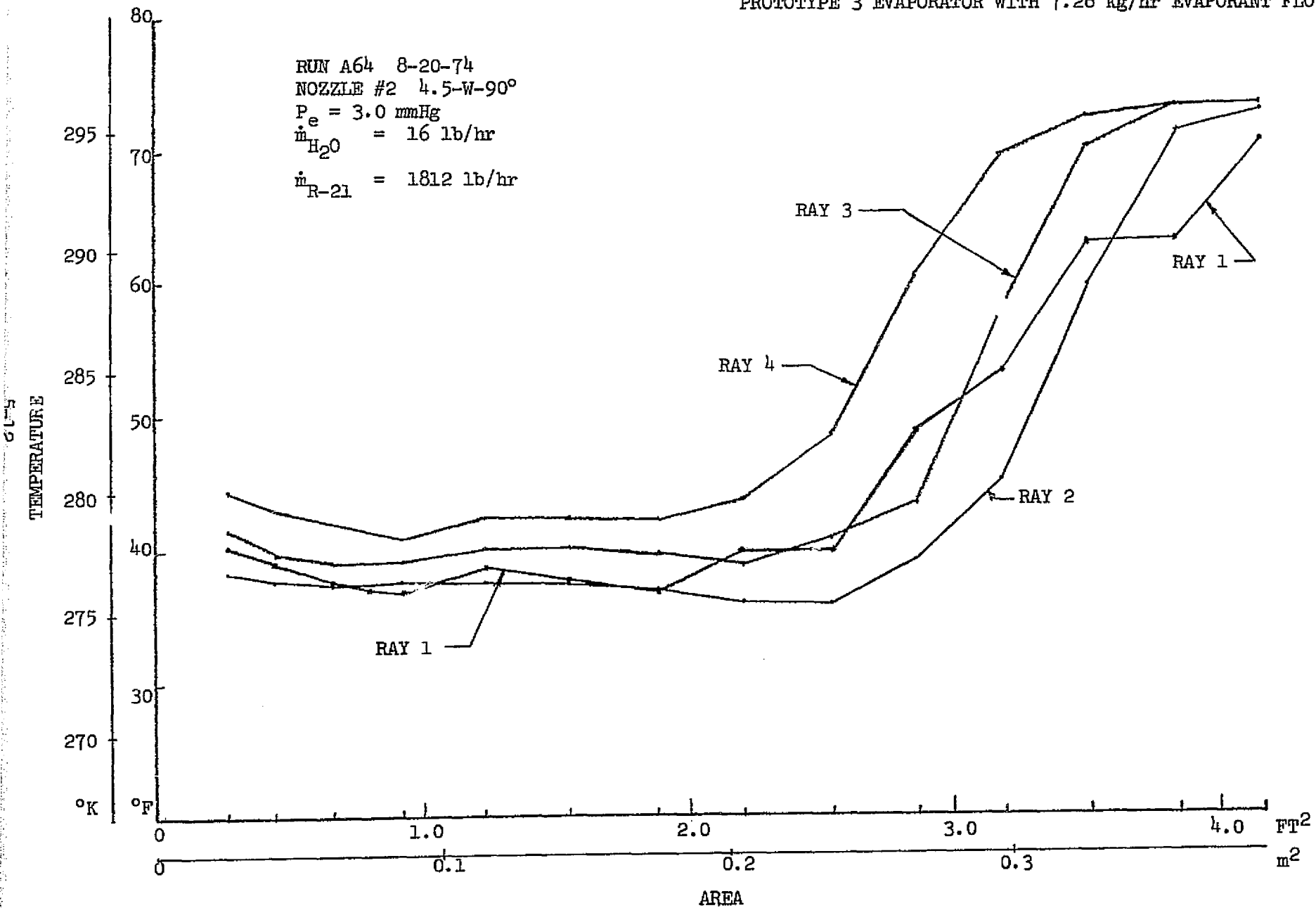
FIGURE 5-9

PROTOTYPE 3 EVAPORATOR WITH 6.3 kg/hr EVAPORANT FLOW

RUN A66   8-20-74
NOZZLE #2   4.5-W-70°
P_e = 3.5 mmHg
$\dot{m}_{H_2O}$ = 13.9 lb/hr
$\dot{m}_{R-21}$ = 1809 lb/hr

RAY 4
RAY 3
RAY 1
RAY 2

TEMPERATURE

5-13
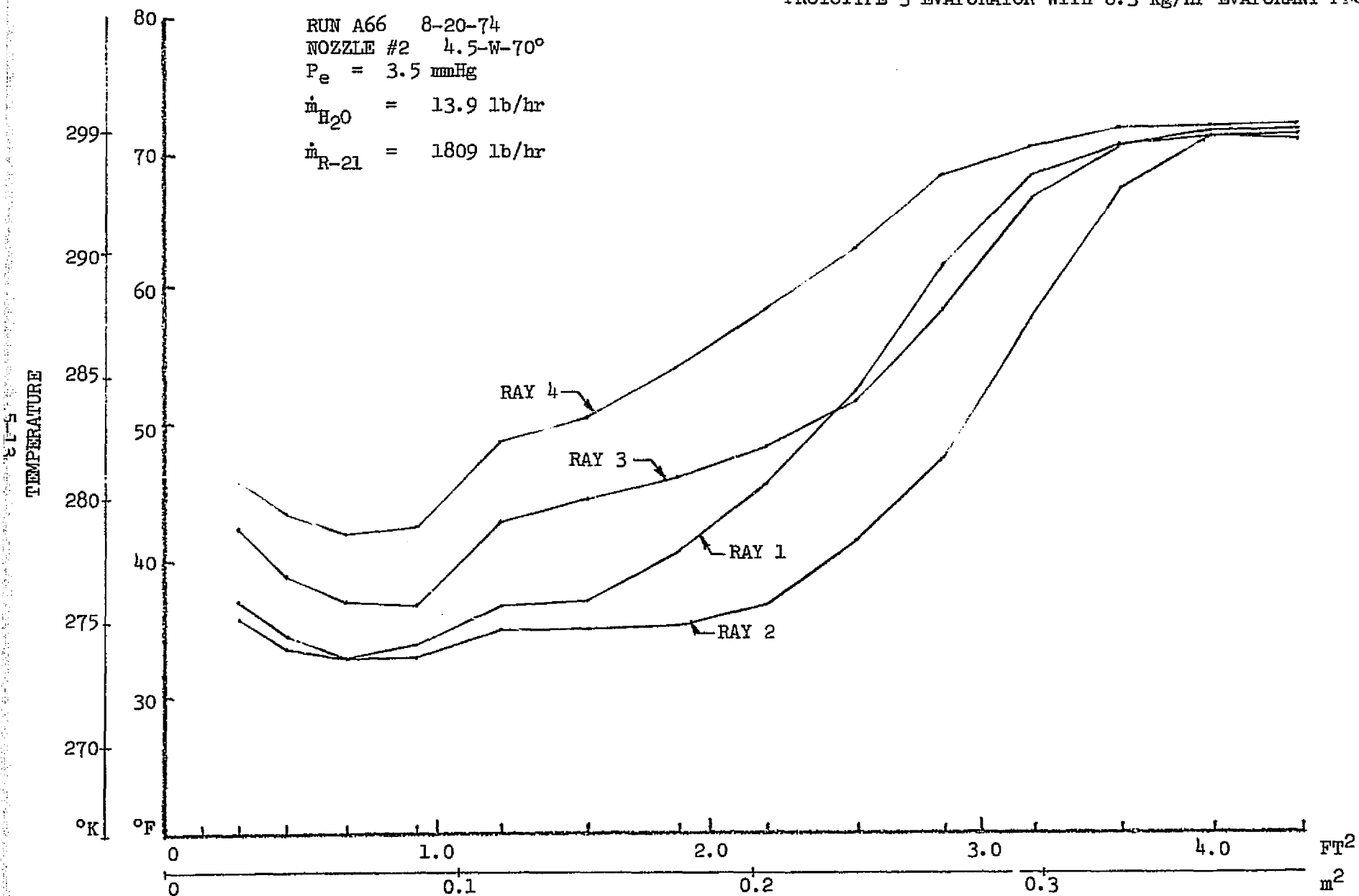
M_{H_2O} = 6.3 Kg/hr (13.9 lb/hr)
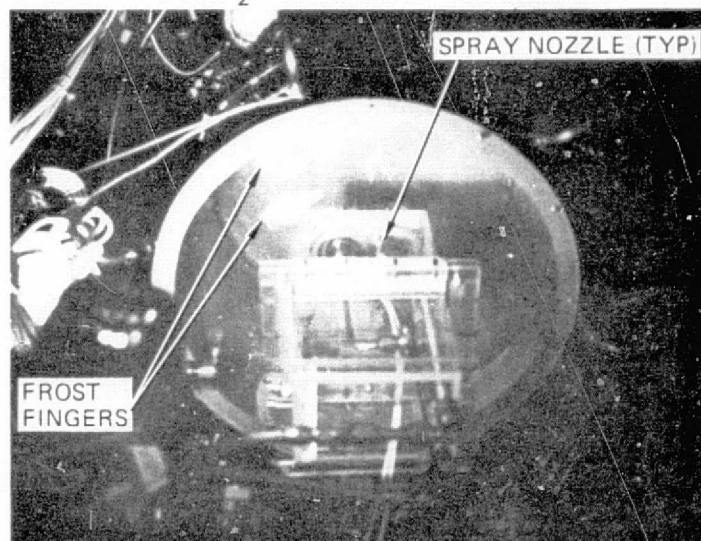
FIGURE 5—10   PROTOTYPE 3 EVAPORATOR WITH
FROST FINGERS

FIGURE 5-11

PROTOTYPE 2 EVAPORATOR WITH 27 kg/hr EVAPORANT FLOW

RUN B3   9-7-74
NOZZLE 22-B-90° on ℄
P_e = 3.7 mmHg
$\dot{m}_{H_2O}$ = 60 lb/hr
$\dot{m}_{R-21}$ = 2268 lb/hr
hfg = 995 BTU/lb

5-15
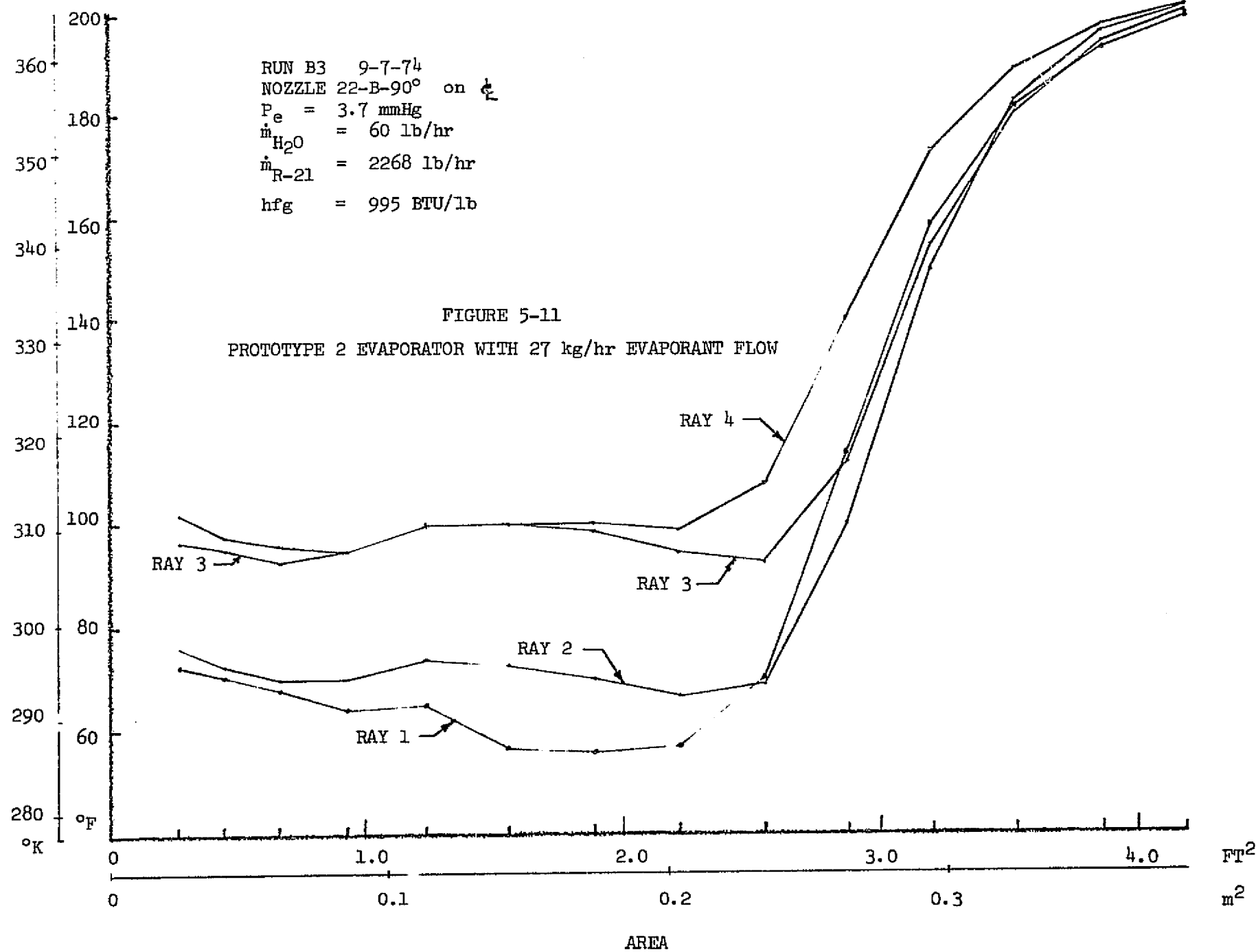
by 90° and 180° and data recorded. As expected the data showed no significant change in the ray temperatures. Rays 1 and 2 were lower than rays 3 and 4, indicating higher temperatures as observed in the previous data in Figure 5-11. This ruled out gravity as the reason for the large ray temperature differences.

Tests were then conducted to determine if the uneven nozzle spray pattern caused the temperature maldistribution. The nozzle was rotated by 180° and a second, as received (not modified for low hold up volume), nozzle was tested in the Prototype 2 unit. Again, the ray temperature data showed the same types of differences between rays 1, 2 and 3, 4 as previously shown in Figure 5-11. Therefore, the nozzle was discarded as the cause of the temperature maldistribution.

The manifold tubing connecting the distributor evaporator tube ring manifold was disconnected, rotated 180°, reconnected and the unit tested to determine whether or not the distribution of flow was affected by the manifold design approach. Figure 5-12 presents the data for this test with the Prototype 2 unit rotated 180°, with an as received nozzle; and the manifold tubing remained rotated 180° relative to the unit. Again, the ray temperature data shows the same types of temperature differences between the rays as was noted in Figure 5-11.

The Prototype 2 unit was then tested in the low temperature configuration to determine if flow stagnation at the core splice intersection occurred as it had for the Prototype 3 device with spray deposition on the floor. As with the Prototype 3 unit, with 7.26 kg/hr (16 lb/hr) evaporant flow rate, frost formation was obtained on the side walls. By reducing the flow rate to 5.4 kg/hr (12 lb/hr), the spray cone collapsed and ice fingers formed on the floor as it had also done previously. The data for this run is shown in Figure 5-13.

Based on the above test results for the Prototype 2 and 3 evaporators, it was concluded that: gravity, manifolding, and uneven spray deposition did not cause the wide variation in ray temperature data, but was due to flow maldistribution caused by core design and fabrication anomalies. The flow maldistribution could be attributed, at least in part, to flow stagnation at core splice intersections in the bottom of the device and that fabrication anomalies more than likely caused the flow maldistribution in the device sidewalls. Since the evaporators performance was considerably below the design conditions, further testing of the evaporators was cancelled in lieu of additional investigation of the flow distribution.

FIGURE 5-12

PROTOTYPE 2 WITH UNIT AND MANIFOLD ROTATED
OFF-THE-SHELF NOZZLE

RUN B-23   9-6-74
NOZZLE   22-B-90 on ⊄
$\dot{m}_{H_2O}$ =   60.3 pph
$\dot{m}_{R-21}$ =   2236 pph
hfg   =   1020 BTU/lb
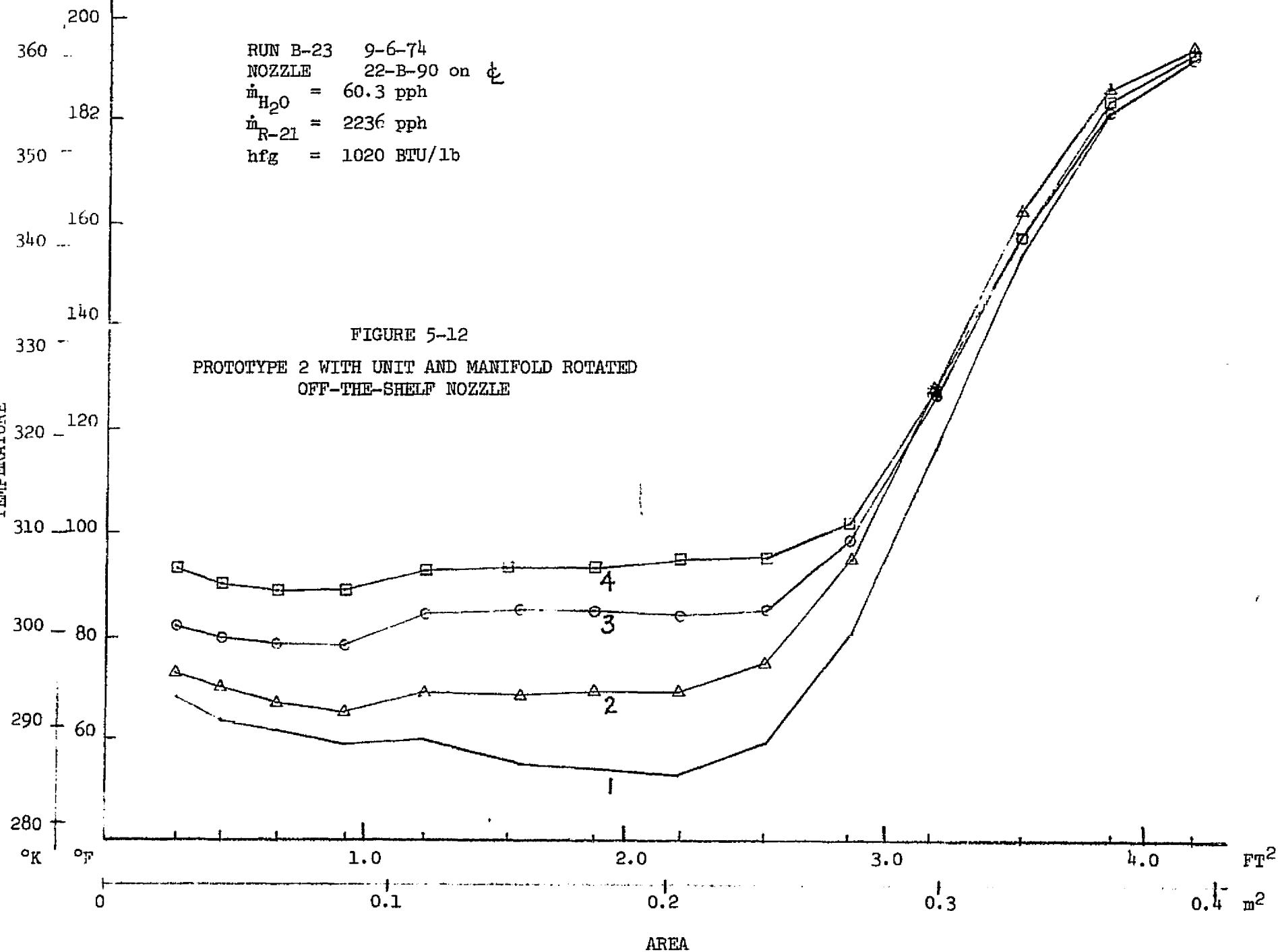
RUN B49   9-11-74
NOZZLE 3-W-90 on ₵
P_e = 3.5 mmHg
$\dot{m}_{H_2O}$ = 11.9 lb/hr
$\dot{m}_{R-21}$ = 2259 lb/hr
hfg = 990 BTU/lb

FIGURE 5-13

PROTOTYPE 2 EVAPORATOR WITH 5.4 Kg/Hr EVAPORANT FLOW

RAY 3

RAY 4

RAY 2

RAY 1

TEMPERATURE

°F

AREA

5-18
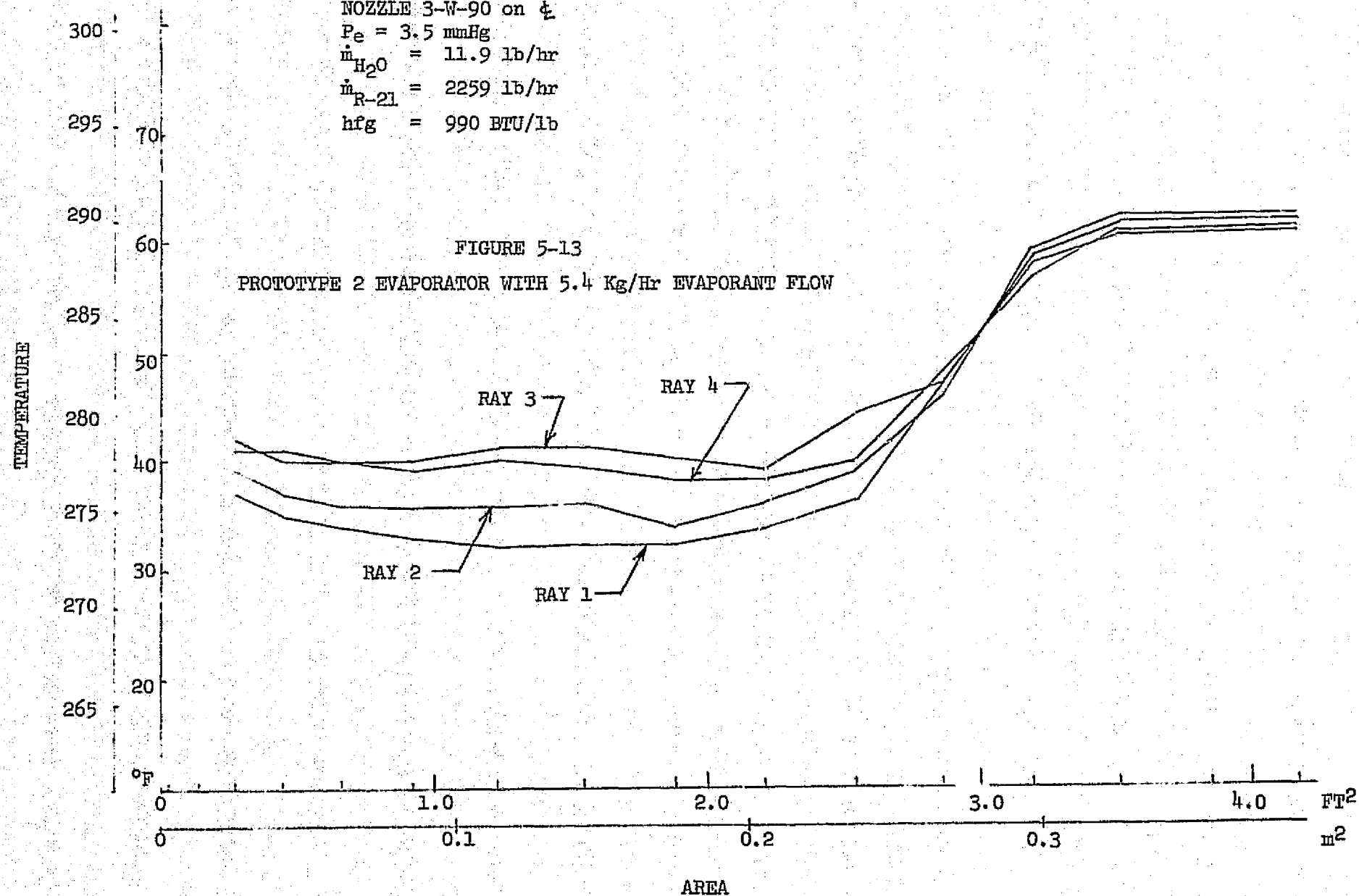
5.3   Core Flow Distribution Determination

To resolve the poor core flow distribution, the two prototype evaporators were disassembled into their component sidewall and bottomplate components, and a series of flow tests were performed to obtain exact flow distribution data. This data was used to reconfigure the evaporator core configuration as reported in the next section. The test data and experimental techniques are described in the paragraphs that follow.

The bottomplate of the Prototype 2 flash evaporator was disconnected from the sidewalls and the flow distribution in each section was determined by flowing water in through the inlet or outlet manifolds and out through the perimeter of the sidewall or bottomplate. The water flowing through the two sections were collected in glass beakers as shown in Figure 5-14. For the sidewall, water was collected in eight beakers positioned at even spacing around the perimeter of the sidewall. The relative flowrate at the eight positions were obtained by comparing the weight of the water in the individual beakers to the average weight of water collected. Data for four runs were recorded to establish the consistency of the measurements. The manifold was filled with water prior to each run and the beakers were positioned accurately to insure repeatability. The unit was maintained in a level position with the water flowing vertically downward throughout the test. The results showed the flow distribution in the sidewall to be fairly uniform. Figure 5-15 shows that low flows were observed in two sections near the locations of thermocouple rays 1 and 2, and a region of high flow was observed between rays 2 and 3.

The flow in the bottomplate was found to be very nonuniform. The edge regions of the pie sections carried almost no flow so that there were gaps approximately 51 mm (2 inches) wide in which very little flow was collected in the beakers. To obtain meaningful data it was necessary to place the beakers at the centers of the pie sections. Therefore 12 beakers would have been required to collect the water from each pie section simultaneously. However, only six of the beakers could be positioned around the bottomplate at one time so that two runs were required to map the flow around the entire perimeter. Data from four runs were recorded to check the consistency of the measurements. The results given in Figure 5-16 show that most of the sections carry approximately the same amount of flow. The maximum deviation from the average is

INLET MANIFOLD

WATER
IN

EVAPORATOR
SIDEWALL

WATER OUT

GLASS BEAKERS

EVAPORATOR
BOTTOM PLATE

WATER IN

OUTLET MANIFOLD

WATER OUT

GLASS BEAKER
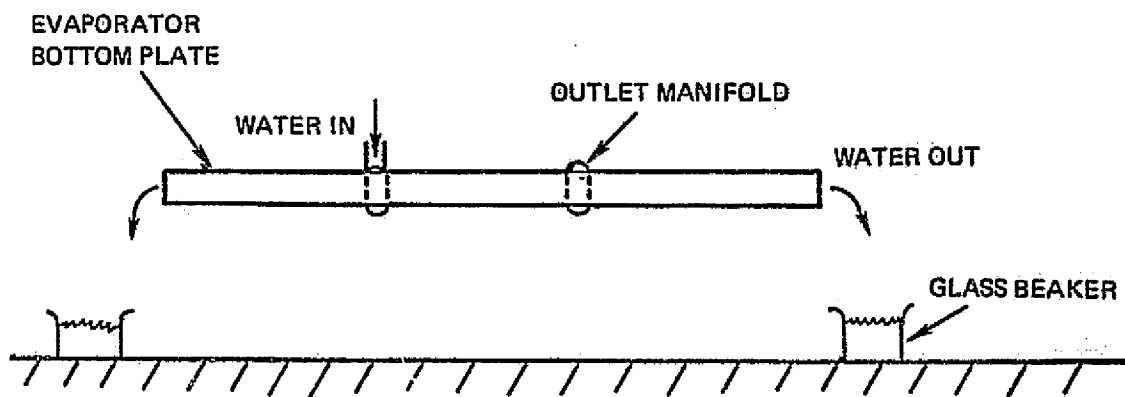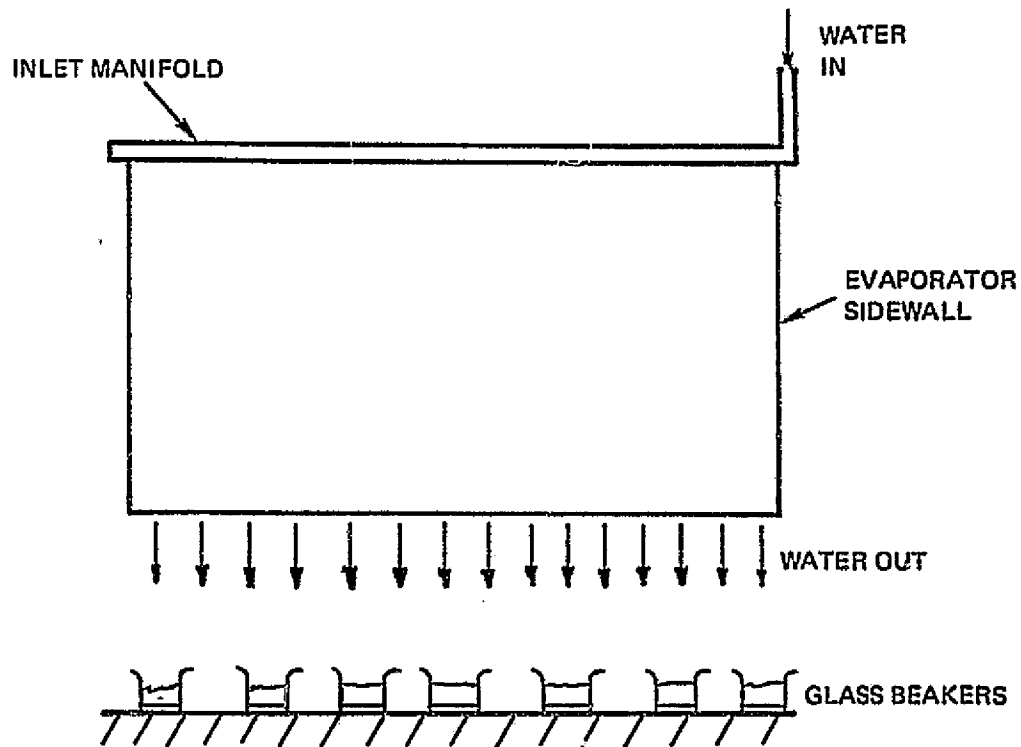
FIGURE 5-14 CORE FLOW DISTRIBUTION TEST APPARATUS

$\boxed{X}$ THERMOCOUPLE RAY LOCATION

FRACTION OF AVG. FLOWRATE

0.85 ①

.1.06   1.02

0.94 ④   ② 0.86

1.00   1.28

③
1.00
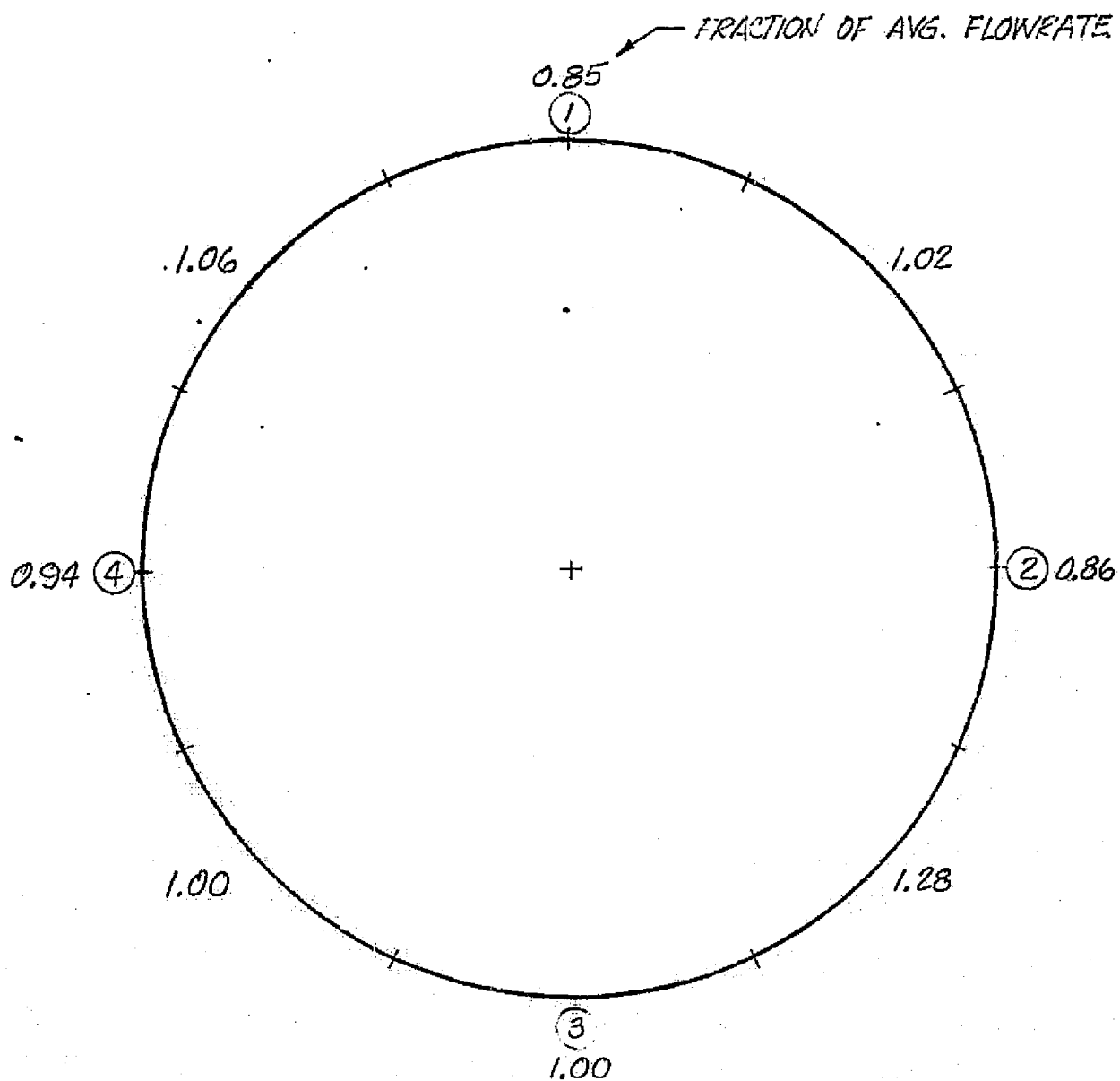
FIGURE 5-15 PROTOTYPE 2 SIDEWALL RELATIVE FLOWRATES
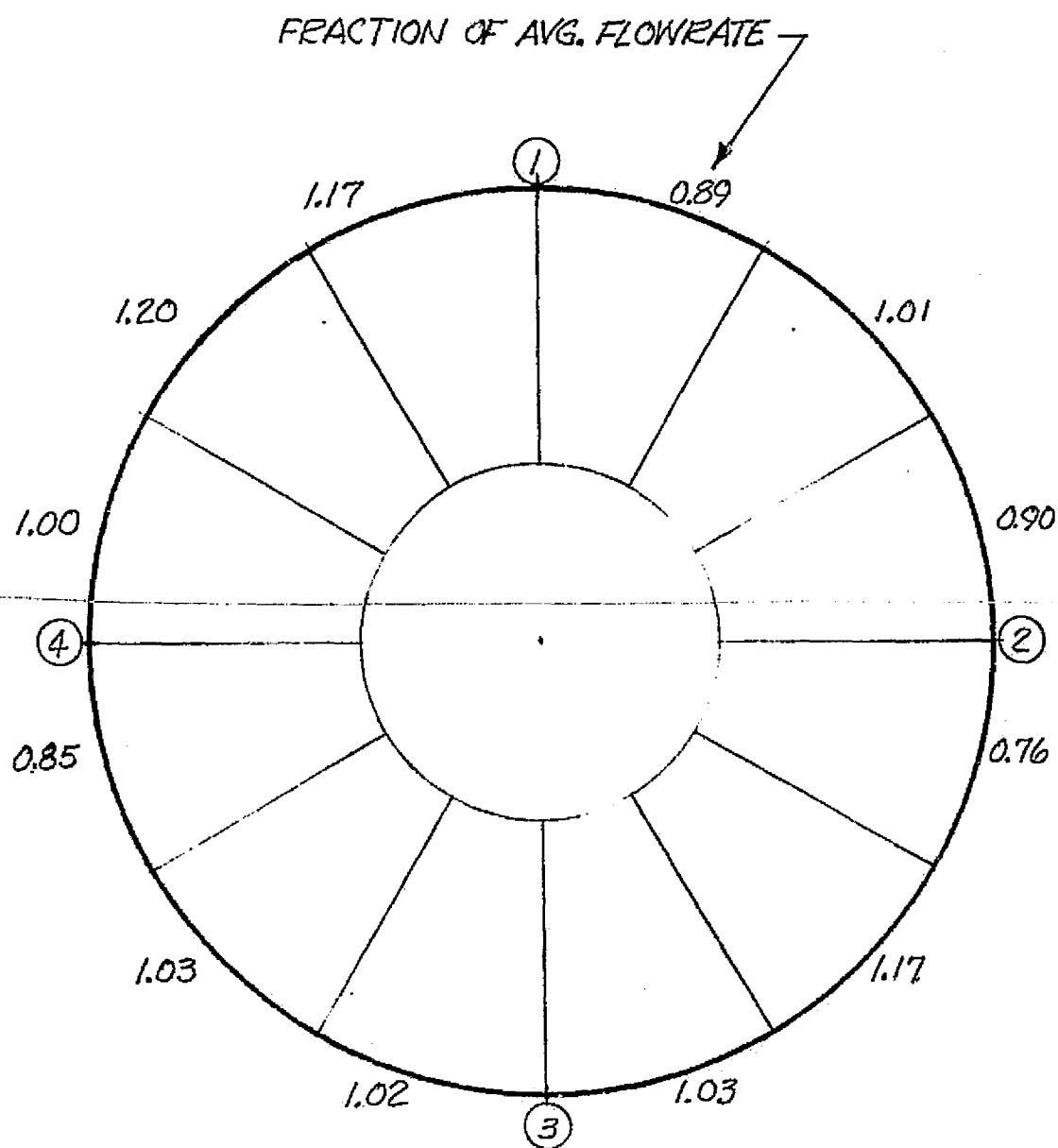
FIGURE 5-16 PROTOTYPE 2 BOTTOMPLATE RELATIVE FLOWRATES

about 24%. The sections near ray 2 carry less flow than the average so that the higher flow resistance in the floor near this ray could add to the flow resistance in the sidewall. If the manifold ring connecting the floor and sidewall were blocked this would cause the flow near ray 2 to be lower than average. Also, a high flow region could appear between rays 2 and 3. Definite conclusions cannot be made because the core fins in the floor were damaged when the evaporator was disassembled. The fins were straightened but could not be completely restored to the original condition. Also the actual flow resistance in the manifold ring could not be measured.

The flow distribution measurements show the bottomplate ice fingers coincide with flow stagnation areas and; further, that some of the localized icing which occurred on the evaporator sidewall in the Prototype 2 vacuum chamber performance test could have been caused by uneven Freon flow distributions. However, the flow maldistributions measured herein do not account for all of the discrepancy in the individual ray thermocouple recordings of the vacuum chamber test. This indicates that there were additional variables such as the nozzle spray pattern and the nozzle orientation which had as great an effect on the evaporator performance as the Freon flow distribution.

The flow distribution measured would result in the nonuniformity of the Freon outlet temperatures around the perimeter of the evaporator. Assuming that the spray is entirely on the sidewalls the outlet temperatures for a 288.71°K (60°F) inlet temperature and 277.59°K (40°F) average outlet temperature would vary from 275.37°K (36°F) to 279.82°K (44°F) for the measured flow distribution. This variation could be significant for cases where the saturation temperature is near 275.37°K (36°F).

The flow distribution in the Prototype 3 unit was determined using the measurement techniques described above. The flow in the Prototype 3 sidewall was found to be fairly uniform. There were no large areas in which the flow stagnated. However, small areas of stagnant flow (of the order of 12.7 mm (1/2 inch) in width) would not have been detected with the techniques applied because surface tension effects caused the water flowing through the sidewall to collect in small streams as it left the evaporator. Figure 5-17 shows the relative flowrates at various positions around the perimeter of the sidewall obtained by collecting the water streaming from the evaporator in glass beakers.
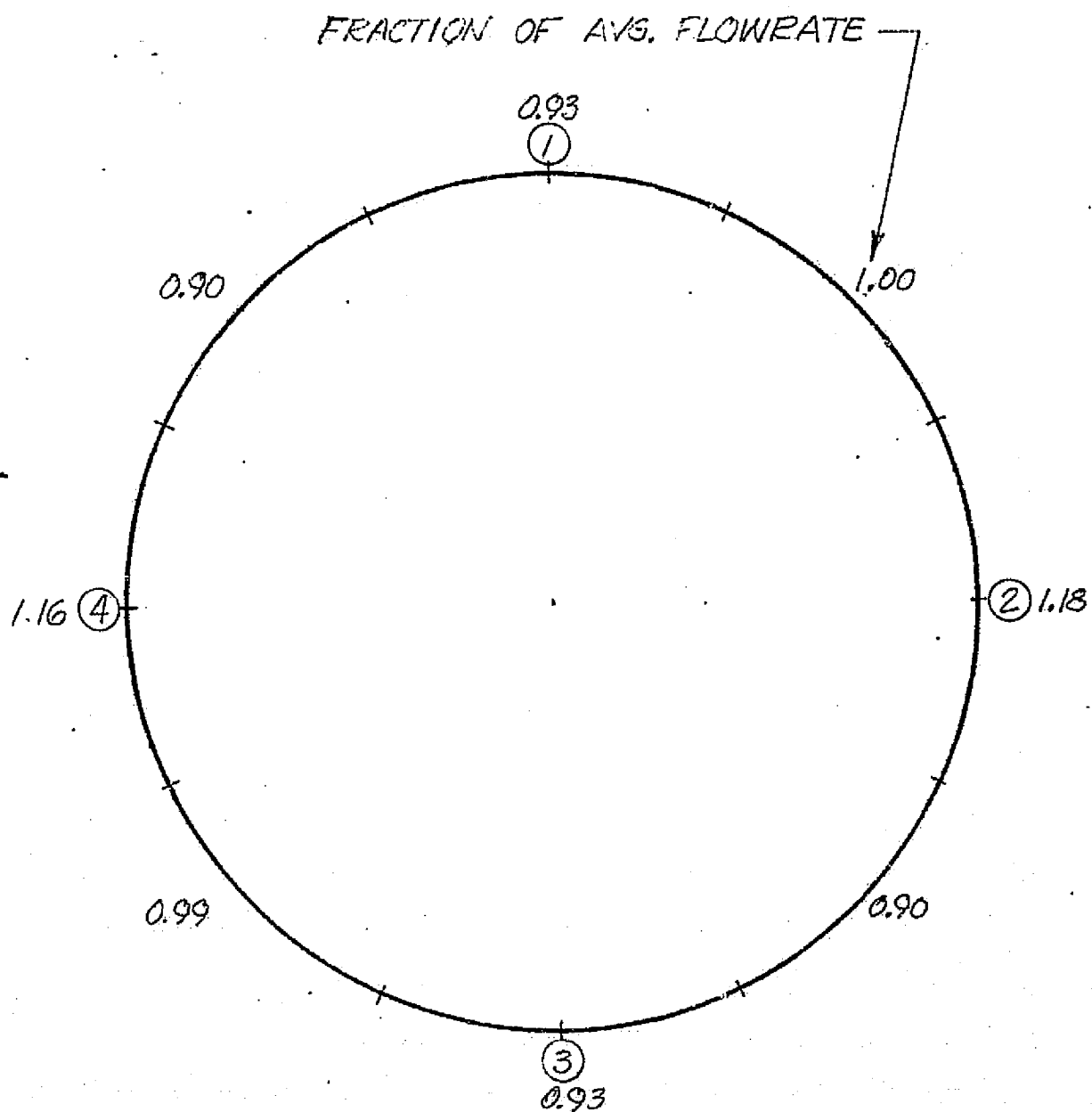
FIGURE 5-17 PROTOTYPE 3 SIDEWALL RELATIVE FLOWRATES

The flow in the Prototype 3 bottomplate had relatively large gaps at the edges of the pie sections as expected. The relative flowrates measured for the twelve pie sections are shown in Figure 5-18.

Based on the results of the flow distribution tests, a redesign of the Prototype 2 and 3 flash evaporators was considered desirable. The flow maldistribution in the bottom plate appeared to warrant a different design approach for distributing flow. The flow maldistribution in the sidewalls was not considered to be a design problem but rather a fabrication/tooling technique problem.

VSD had in existence an on going in-house R&D program for Evaporative Heat Sink Development for Space Applications. The flow distribution in the flash evaporator bottom plates was of concern because VSD was contemplating a proposal to Rockwell International as a potential subcontractor for a flash evaporator heat sink for the Space Shuttle. VSD therefore undertook to evaluate the significance of the flow maldistribution and methods for improvement as part of its IR&D projects number 80 in 1974 and number 107 in 1975. The VSD study revealed that a solid bottom plate for a flash evaporator appeared to be most compatible for a minimum volume and weight Shuttle application. A design was conceived which eliminated flow stagnation areas while retaining high lanced fin rectangular core performance. The flow distribution obtained with this design was checked using the aforementioned techniques and is shown in Figure 5-19. Next, the bottomplate was tested with spray impingement (a temporary manifold being positioned on its periphery) to determine whether any flow stagnation areas could be identified. The bottom plate was placed horizontally in the small vacuum chamber with a solid cone spray nozzle positioned 228mm (9 inches) from the plate. At an evaporant flow of 6.8 kg/hr (15 lb/hr), no frost formation was observed.

Based on the improved flow distribution design and the successful spray testing it was decided to adapt the design to the Prototype 2 and Prototype 3 flash evaporators fabricated under contract to NASA. Therefore, the improved bottomplates were fabricated and retrofitted to the Prototype 2 and 3 sidewalls and the testing of the resultant system continued under the contract.

⊗ THERMOCOUPLE RAY LOCATION

FRACTION OF AVG. FLOWRATE
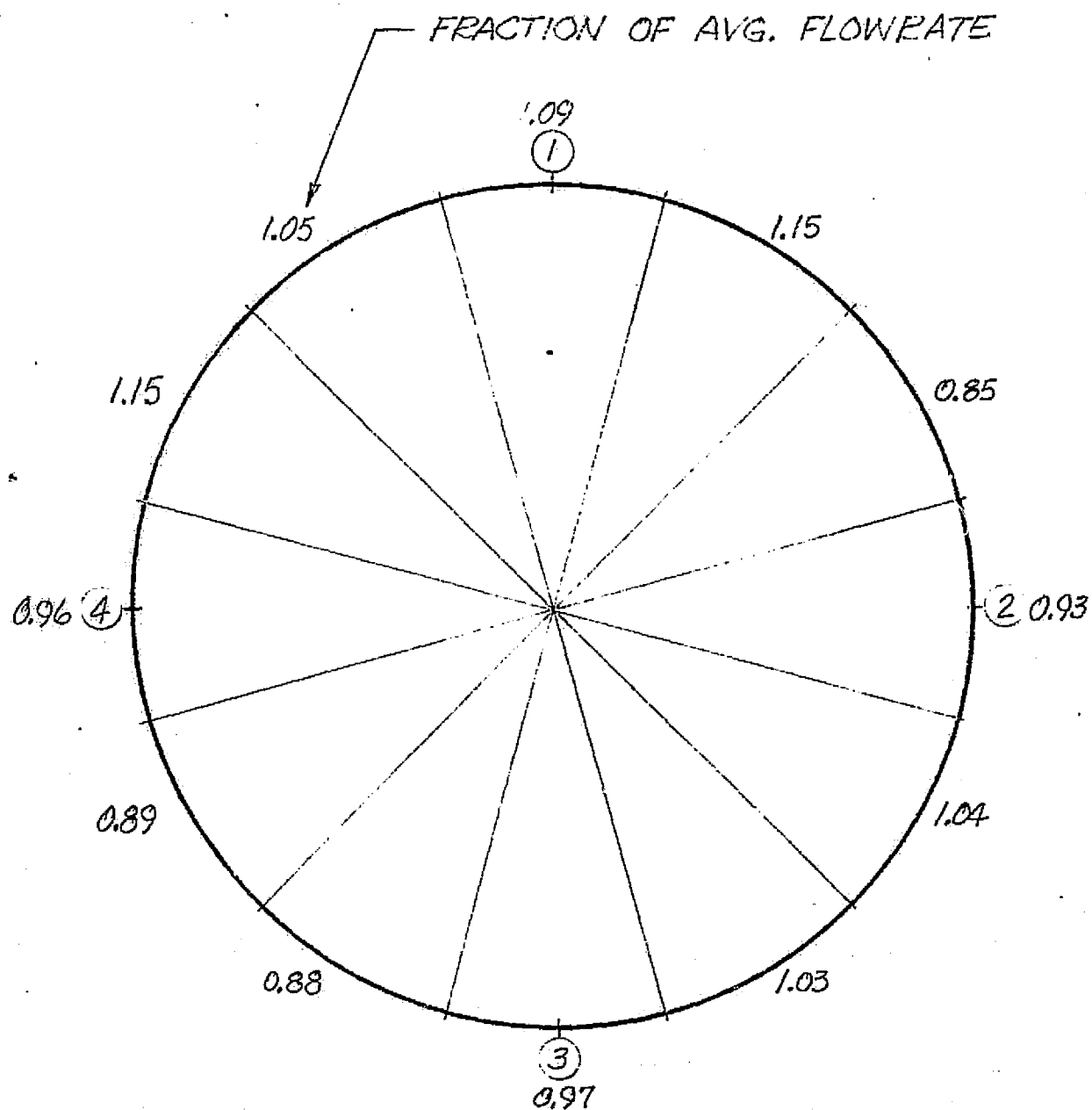
FIGURE 5-18 PROTOTYPE 3 BOTTOMPLATE RELATIVE FLOWRATES

FRACTION OF AVG. FLOWRATES

0.92

0.92   0.95

1.05   0.86

0.98   1.03

1.08   0.98

1.06   1.05

1.11
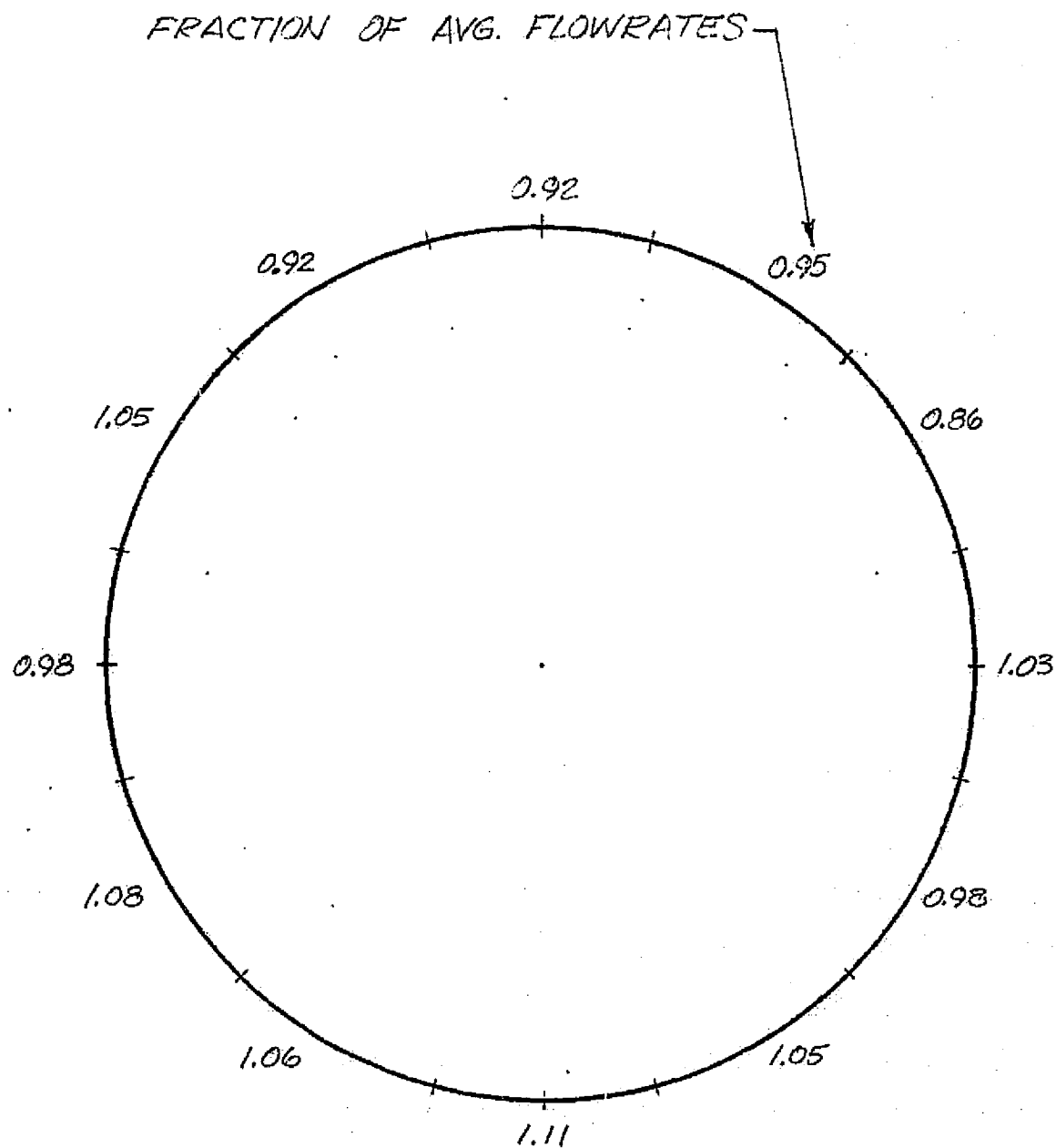
FIGURE 5-19 PROTOTYPE 3 MODIFIED BOTTOMPLATE
RELATIVE FLOWRATES

5.4 Modified Prototype Evaporator Testing

The modified Prototype flash evaporators were tested to determine whether the design and performance of the units could meet the aforementioned test objectives. The testing, conducted in December 1974 and January 1975, was performed using the following heat rejection requirements:

	Top-Off	Re-entry
T_{inlet}, °K (°F)	310.8 (64)	329.7 (134)
T_{outlet}, °K (°F)	297.4 (40)	297.4 (40)
Freon Flow, Kg/hr (pph)	1000 (2500)	1250 (2750)
Heat Rejection, KW (KBTU/HR)	4.4 (15)	19 (65)

Nozzle location optimization tests were conducted to find the nearest location of the nozzle to the evaporator bottom plate at which all the spray is vaporized. The evaporators, first in a low temperature unit (LTU) and then in a high temperature unit (HTU) configuration, were operated in a full on condition and the nozzle height above the bottom plate adjusted to find the minimum volume configuration. In order to achieve the low outlet temperatures and maximize the capacity of the evaporator, it was found during these tests that the Freon transport fluid had to flow in through the bottom plate and then out through the sidewalls of the device. Solid cone nozzles were used for both the HTU and LTU evaporators.

The temperature distribution in the evaporator for the LTU optimum (minimum volume) location of the nozzle is shown in Figure 5-20. For this condition, the nozzle is 203 mm (8.0 in.) from the evaporator floor. This configuration would require a sidewall height of 140 mm (5.5 in.) in order to intercept all the spray leaving the nozzle. Thus the optimization reduced the volume by 30% over the "as fabricated" volume. Evaporation efficiencies of 97% were obtained for the LTU configuration. The HTU optimum nozzle location temperature distribution and performance is shown in Figure 5-21. The HTU nozzle was a Delavan nozzle modified to provide a solid cone. This was done by providing additional slots to obtain an added axial component to the exit water velocity. The evaporation efficiency for this HTU configuration was 98%. For this configuration the nozzle was 140 mm (5.5 in.) above the evaporator floor. A sidewall height of 89 mm

NOZZLE #15
12 Feb 1975
$\dot{m}_{H_2O}$ = 15.0 lbm/hr
$\dot{m}_{F-21}$ = 2500 lbm/hr
hfg = 1020 BTU/lb

FIGURE 5-20

LOW TEMPERATURE UNIT TEMPERATURE DISTRIBUTION

Ray 1
Ray 2
Ray 4
Ray 3

TEMPERATURE

AREA

FIGURE 5-21

HIGH TEMPERATURE UNIT TEMPERATURE DISTRIBUTION
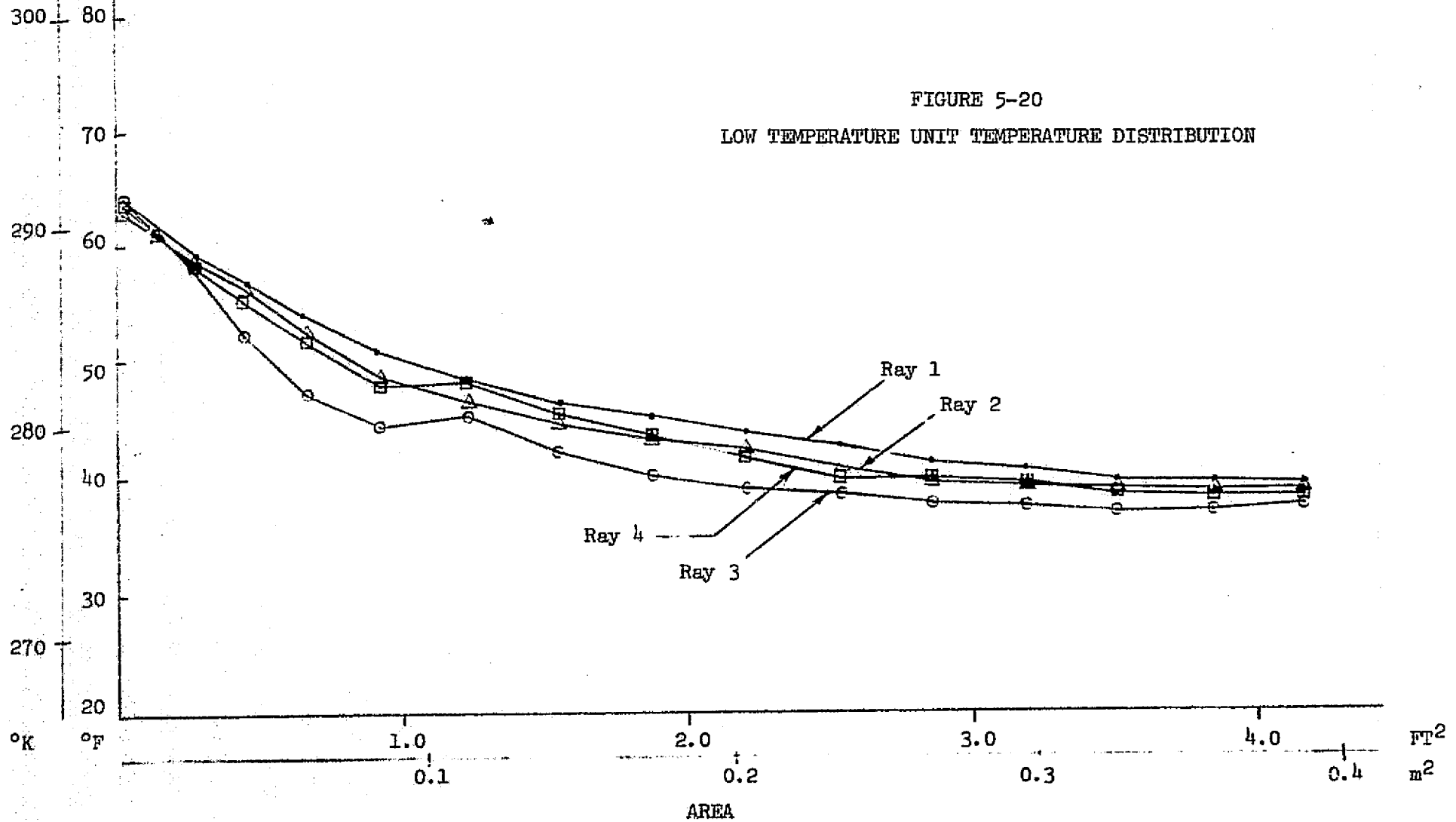
NOZZLE #M
22 Feb 1975
$\dot{m}_{H_2O}$ = 50.6 lbm/hr
$\dot{m}_{F-21}$ = 2756 lbm/hr
hfg = 1020 BTU/lb

Ray 1
Ray 2
Ray 3
Ray 4

TEMPERATURE

AREA
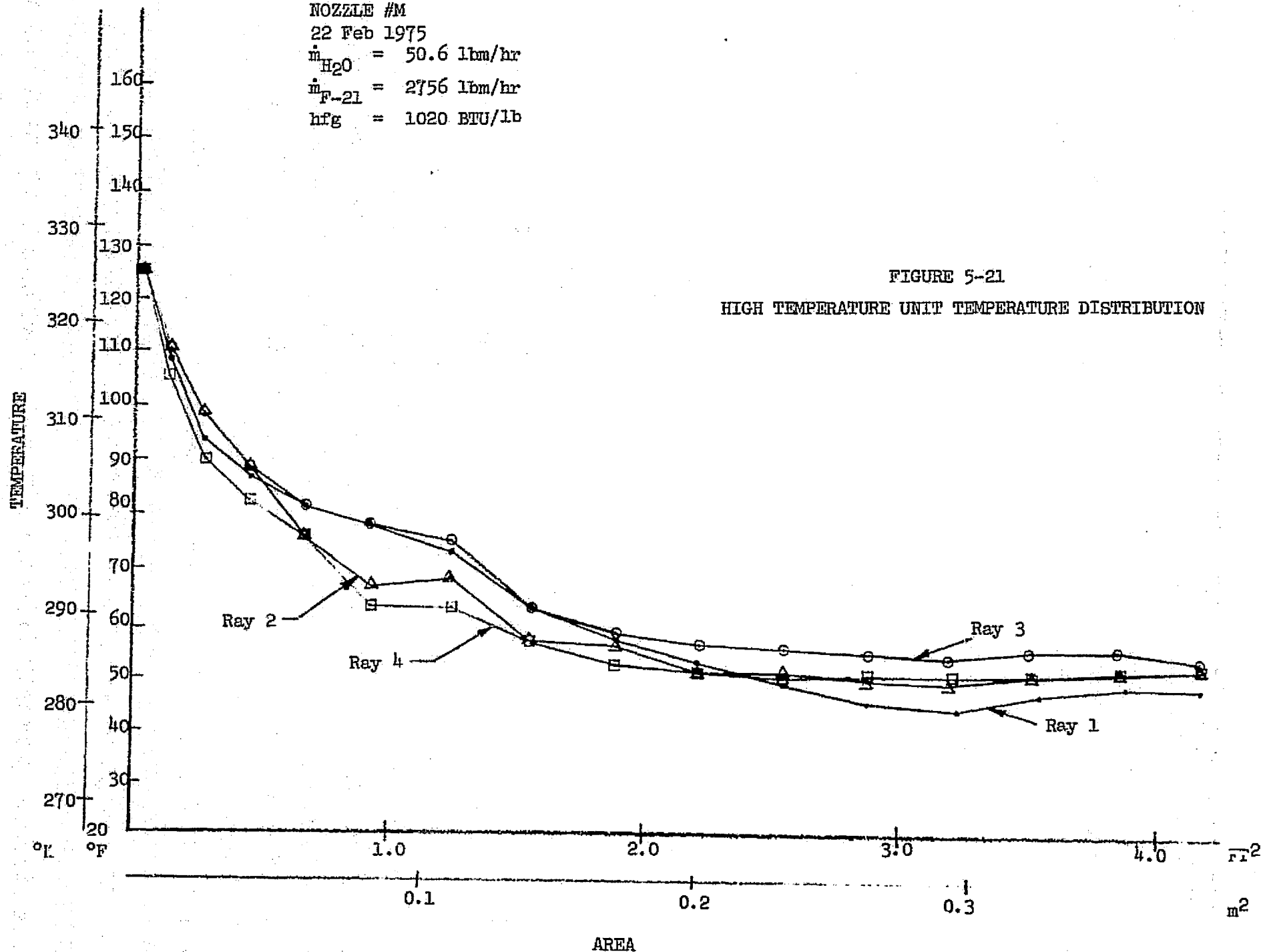
(3.5 in.) would intercept all the spray leaving the nozzle. In addition to demonstrating efficient operation, these tests verified the design approach of using heat exchanger core for evaporation surfaces and the concept of load partitioning the heat load between evaporators.

In addition to determining the optimum nozzle location and flow direction, these initial tests indicated that the exhaust duct port influenced the spray distribution slightly. It was found that this influence could be offset by moving the nozzle off centerline by 3/8" from the exhaust port. It was also demonstrated that the redundant nozzles could be operated with the nozzles 3/4" off centerline. The nozzles had to be inclined at an angle such that the nozzle centerline was pointed towards the evaporator floor centerline.

An on/off controller with integrator circuits using the evaporator sensed outlet temperature was designed and constructed to regulate operation of (pulse) the water solenoid valve. The controller was constructed to accommodate 0.6 °K/min (1°F/min) inlet temperature transients. The full load capability tests were repeated with the electronic controller operating the water solenoid valve. These were followed by steady state partial loads and inlet temperature transients to checkout the controller capability to maintain the desired outlet temperature. A series of tests were run to determine the optimum control system configuration of cycle time and transient response. Cycle times widths of 4 to 10 seconds were tested to control the valve during partial loads to the LTU outlet temperature of 277.4 $\pm$ 1.1°K (40 $\pm$ 2°F). A six second pulse width proved to be the optimum pulse to control the outlet temperature during steady operation, produce a minimum of nozzle ice chips (due to hold up volume) and respond to changes in the inlet temperature.

Faster inlet temperature transients than the design 0.6°K/min (1°F/min) transient rate were run to identify the ultimate capability of the controller/evaporator to meet heat load control. Figure 5-22 shows the LTU test results of the controller cycle/transient optimization. The results were obtained for a 6 second cycle and transient inlet temperature of 1.6°K/min (2.8°F/min). As seen by the data, the outlet temperature remained within the desired $\pm$ 1.1°K ($\pm$ 2°F) control band. These tests verified the on/off controller concept with integrator circuits with sensed temperature as input. Additionally, the verification of the Prototype 2 and 3 flash evaporators to meet the Shuttle on-orbit water dumping requirements was also demonstrated.
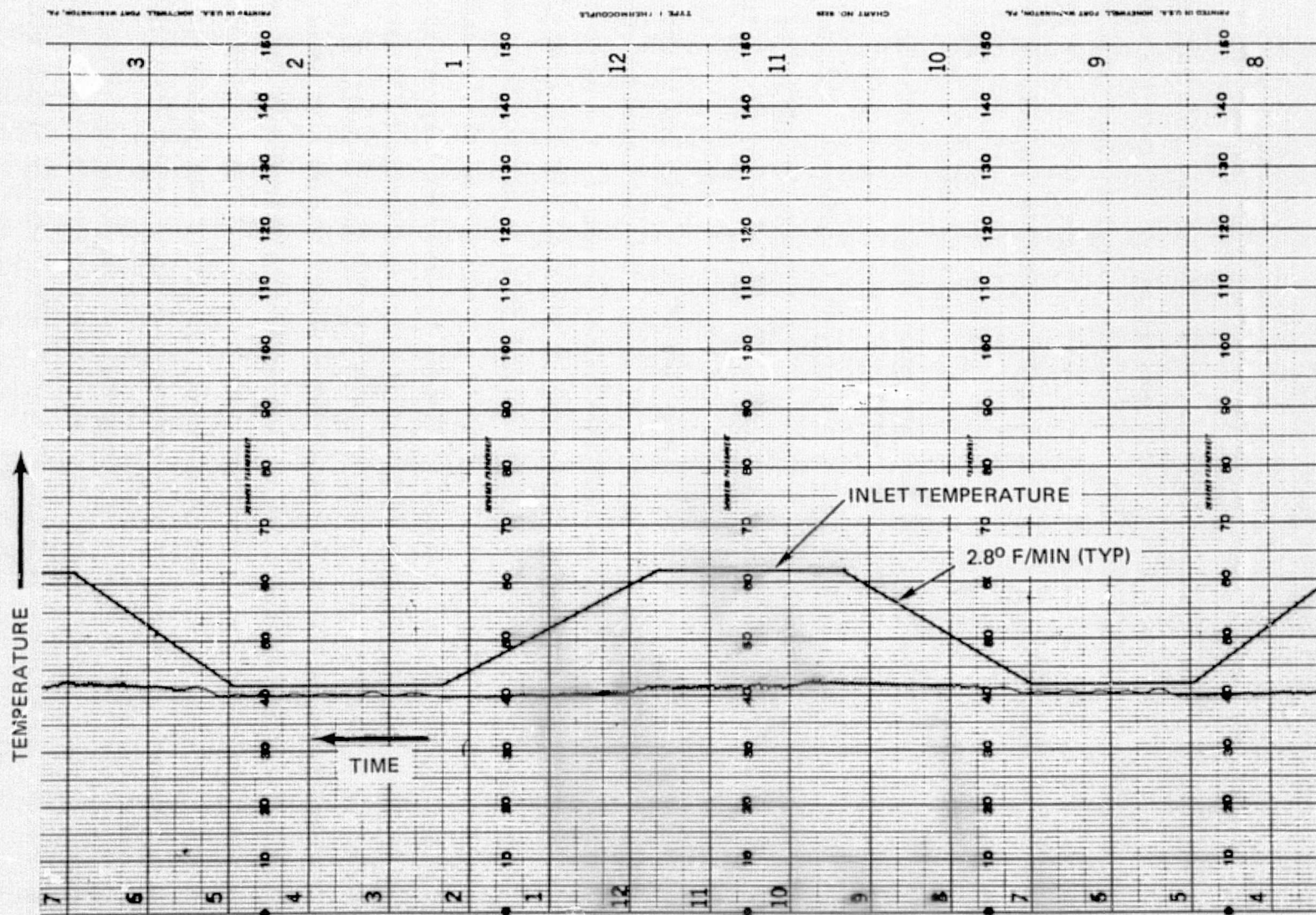
FIGURE 5–22   WATER DUMP FLASH EVAPORATOR CONFIGURATION
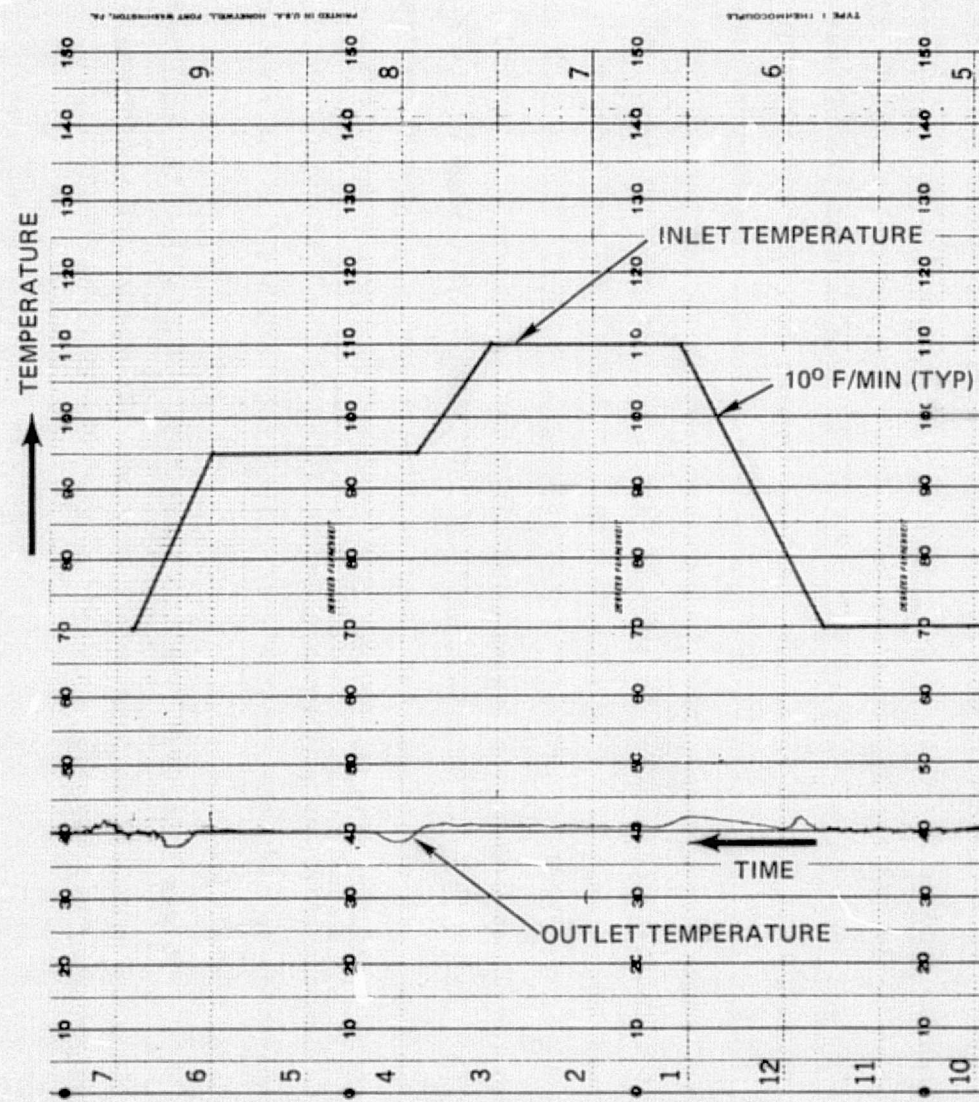
FIGURE 5-23   REENTRY FLASH EVAPORATOR CONFIGURATION

FIGURE 5-24   REENTRY FLASH EVAPORATOR CONFIGURATION

5-35

6.0   FAILURE MODE AND EFFECT ANALYSIS

This section presents the results of a failure mode and effect analysis of a proposed Shuttle Orbiter Flash Evaporator Subsystem. The analysis was performed to identify equipment failure modes, and to determine corresponding effects on the proposed subsystem performance and mission success. The primary objectives in performing the analysis were to detect critical failure areas, and determine an effective means of reducing susceptibility to such failures. It is anticipated that the results of this analysis will be considered as part of detailed design improvement efforts; design reviews, and test/checkout procedure preparation and review.

The required reliability for the Flash Evaporator Subsystem was assumed to be fail-safe based on the required reliability for the Shuttle Orbiter Radiator Subsystem. The requirement is defined as the capability of the Flash Evaporator Subsystem to sustain a single failure in either Freon loop and still maintain a level of performance sufficient for the safe return of personnel and payload. In compliance with the requirement, multiple failures were not included in the analysis, only single failures and their effects were evaluated.

The results of the Failure Mode and Effects Analysis revealed no single failure modes in the Evaporator Subsystem design which would result in a condition that does not meet the fail-safe reliability criteria.

6.1   Equipment Description

The proposed Flash Evaporator Subsystem consists of two identical parallel active coolant loops. Each loop consists of identical downstream and upstream configurations, each consisting of a Control Module and an Evaporator Module. The function of the subsystem is to dissipate waste heat from the two orbiter Freon coolant loops to the deep space environment.

6.1.1   Subsystem Description

Each loop of the Flash Evaporator Subsystem consists of a downstream and an upstream evaporator configuration. Each configuration is made up of a Control Module and an Evaporator Module. A functional block diagram of one loop is presented by Figure 6-1.

The Control Module includes the Electronic Controller and the Failure Detector. The Evaporator Module includes the Evaporator Core, the Primary and

Secondary water metering valves, the primary and secondary isolation valves, and the temperature sensor. This arrangement features physical separation of electronic components and Freon/H_2O components which simplifies packaging and plumbing requirements, and enhances on-line and shop maintenance.

The downstream and upstream evaporator modules are identical. The downstream and upstream control modules are identical also with the exception of the functional difference that the setpoint control temperature for the downstream controller is 277.5°K (40°F), and is 291°K (64°F) for the upstream controller.

6.1.2   Component Description

The components, and functions, of the control and evaporator modules are discussed in the following paragraphs. The modules have been preliminarily classified as LRU's (Line Replaceable Units).

Control Module

The Control Module incorporates electronic control and failure detection components only.

The controller is an on/off type which employs solid-state logic and switching devices. A temperature control signal is supplied to the controller by the temperature sensor. The controller output signal drives the logic and output drive circuitry of the failure detector which, in turn, drives the appropriate water metering valve. Single-sided printed circuit board packaging is utilized for the controller.

The failure detector incorporates the logic, switching, and output drive circuitry for determining proper performance of an evaporator configuration, and driving the appropriate water metering valve. The failure detector compares the pressure switch output signal with the output from the controller. If a fault condition is detected, the failure detector switches the control signal from the primary water metering valve to the secondary water metering valve. The failure detector is housed within the control module enclosure, and utilizes printed circuit board packaging.

Evaporator Module

The Evaporator is a heat transfer component which accommodates an evaporative process for dissipating waste heat from FCL coolant loops. The internal surface of the evaporator is heated by the coolant (Freon 21). Water contacting the surface is transformed to steam and expelled to free space from the evaporator via a duct and supersonic nozzle.

C-2

Sec. H₂O

Pri. H₂O

Pri.
Isol.
Valve
12 Up

Sec.
Isol.
Valve
12US

Sec.
Metering
Valve
11US

Pri.
Metering
Valve
11 Up

Failure
Detector
23U

Controller
22U

Sensor
291°K
21U

Pri.
Isol.
Valve
12DP

Sec.
Isol.
Valve
12DS

Sec.
Metering
Valve
12DS

Pri.
Metering
Valve
12DP

Failure
Detector
23D

Controller
22D

Sensor
277.5°K
21D

Freon

Evaporator
01U

Evaporator
01D

Exhaust
Duct/Nozzle

Pressure
Switch
13U

Exhaust
Duct/Nozzle

Pressure
Switch
13D

FIGURE 6-1   EVAPORATOR SUBSYSTEM FUNCTIONAL BLOCK DIAGRAM (ONE LOOP SHOWN)

The Evaporator Core/Vessel incorporates compact heat exchanger core and an internal evaporative surface. It also serves as the mounting structure for the installation of external components (valves and pressure switch) and incorporates a well in the coolant outlet for temperature sensor installation. It is constructed of an aluminum alloy and weighs approximately 22 Newtons (5 pounds).

Two water metering valves are applied in each evaporator module, a prime valve and a secondary valve. The valve is a solenoid driven on-off type with an integral spray nozzle. In the normal operating mode, the primary metering valve is driven by the failure detector. In the event of failure of the primary valve, the failure detector detects the failure, and subsequently disables the primary metering valve and enables the secondary metering valve.

The primary and secondary valves are installed in ports on the top surface of the evaporator. The valves are driven by a 28 Vdc source and weigh less than 2.22 Newtons (0.5 pounds) each.

The Isolation Valve is a solenoid driven on-off component which is applied for isolating and activating appropriate water metering valves. There are two isolation valves applied for switching primary and secondary water loops with each evaporator module. In the normal mode, the primary isolation valve is enabled. If a failure occurs in the primary water loop, the failed condition is sensed by the failure detector which, in turn, automatically switches off the primary isolation valve and activates the secondary isolation valve.

The primary and secondary isolation valves physically interface with the primary and secondary metering valves respectively and with primary and secondary water plumbing connected to isolation valve inlets. The isolation valves operate on 28 Vdc and weigh less than 2.22 Newtons (0.5 pounds).

The Sensor is a thermistor probe device which is installed at the loop temperature control point in each evaporator outlet. A three element (thermistor) majority voter configuration is proposed for the Evaporator Subsystem to provide a highly reliable control temperature signal source. In addition, the majority voter sensor would provide protection against a degradation type of failure, which would otherwise be difficult to detect with a single element or dual element sensor. With the majority voter configuration, an error due to a sensor failure would be detectable by comparison of the three thermistor outputs. Two of the three outputs would constitute a majority which would be processed as the correct temperature input signal to the controller.

The temperature sensor is installed in a well in the evaporator Freon outlet. It requires a 5.0 Vdc bias voltage.

The Pressure Switch is actuated by steam pressure which is produced by the evaporative process within the evaporator. The switch output signal is applied as a failure detection signal and water metering valve command must, after an instantaneous delay, be accompanied by an output signal from the switch, and vice versa. A variation from this would result in the failure detector switching to the secondary water loop.

The pressure switch is installed in the evaporator steam expulsion outlet. It requires a bias voltage of 5.0 Vdc and weighs approximately 0.25 pounds.

6.2 Analysis

The Failure Mode and Effect Analysis procedure was formulated based on the requirements of Rockwell International PDRD (Procurement Data Requirement Description) RA05A. A reliability block diagram of the evaporator subsystem is presented by Figure 6-2. Each functional item was alpha-numerically coded for correlating components with elements of the analysis. The results of the analysis are presented in Table 1. Major elements covered in the analysis are discussed in the following subsections.

6.2.1 Failure Mode Identification

This element of the analysis required the identification of all single failure modes which could result in loss of function or the inadvertent/transient output from a given component. Failure modes which could result in loss of capability of failure detection and instrumentation circuitry were also considered. The cause and effects of functional failure modes which may result in loss of function, i.e., failure to operate at a prescribed time, failure to stop operation at a prescribed time, and failure during operation were examined in detail.

Failure modes of redundant elements were not evaluated beyond the first failure. Redundant components of the evaporator subsystem include the temperature sensor, and the water metering valves. The sensor is a three-element majority voter, and in order for a component failure to be incurred, two out of the three elements must fail. The primary water metering valve for each evaporator has a secondary back-up valve which is switched to the active mode in the event of failure of the primary unit.
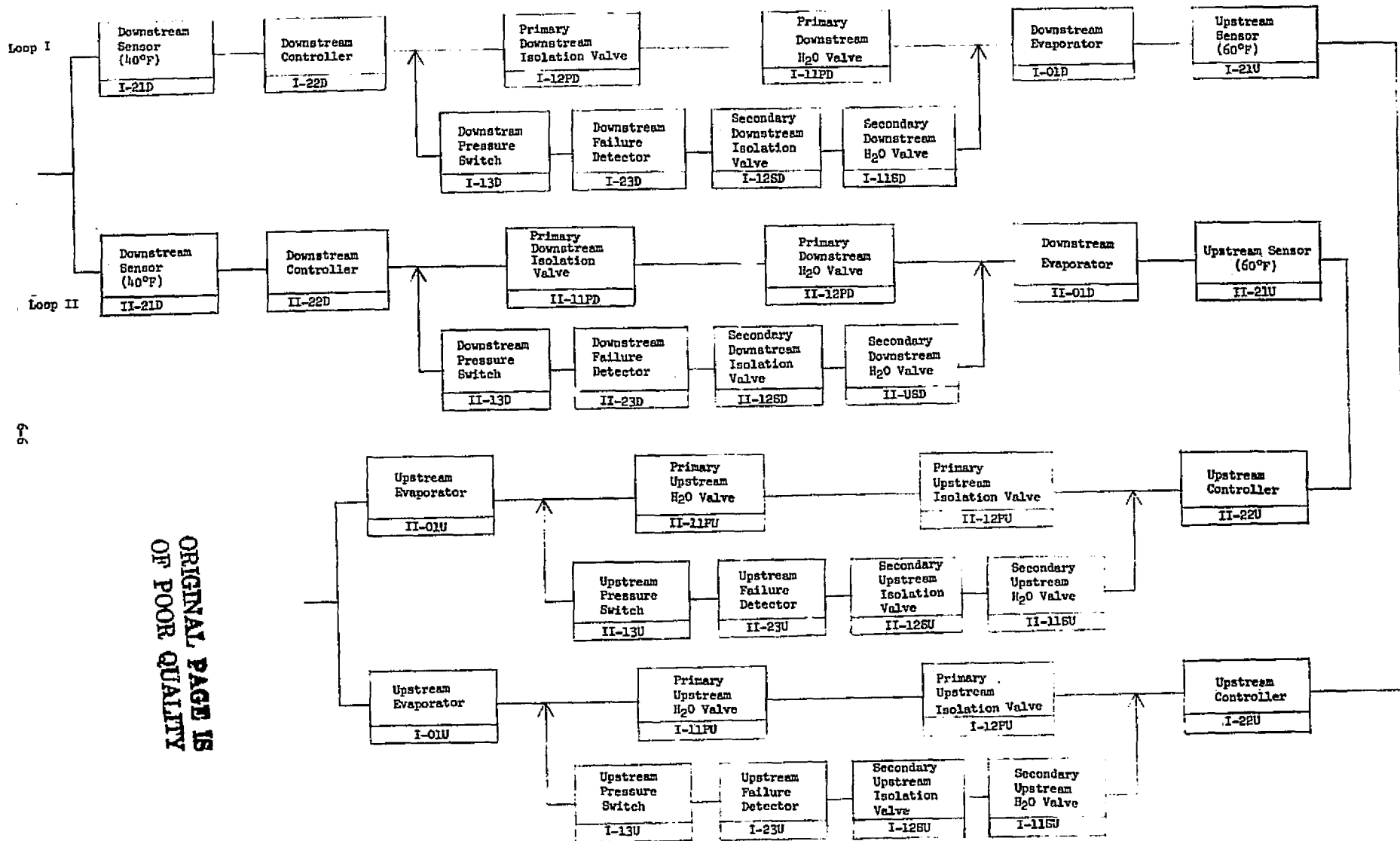
FIGURE 6-2   EVAPORATOR SUBSYSTEM RELIABILITY BLOCK DIAGRAM

Failure modes which were identified for each component are listed in the appropriate column of the Failure Mode and Effects tabulation.

6.2.2   Mission Phase

The mission phase element identifies the mission time interval during which the failure could occur, e.g., prelaunch checkout, launch, orbit, re-entry, horizontal flight, and landing. In the case of the evaporator subsystem, the failure modes which were identified could occur at any time during which subsystem equipment is operating. The effects of each mode would vary with mission phase; e.g., failure and loss of a given upstream evaporator would be more critical during the launch and re-entry phase than it would during the orbit phase. This is primarily due to the fact that both the upstream and downstream evaporators of each loop are active during the launch and re-entry intervals, and only the downstream evaporator is operational during the orbit phase. These functional conditions generally exist, however, both the upstream and the downstream evaporators of each loop are continuously on line throughout the mission, and their operational status is automatically controlled based on outlet control temperature. It was for this reason that identified failure modes were concluded to be able to occur during all mission phases.

6.2.3   Failure Effects

The failure effects of each identified failure mode on evaporator subsystem and interface hardware performance were determined and discussed in the appropriate column of Table 6-1. Those failure effects which were determined to require reliability design improvement action were identified, and are discussed with recommended corrections in Section 6.3.

6.2.4   Failure Detection

The functional or displayed failure indication method was identified and discussed for each failure mode identified in Table 6-1. This equipment consists primarily of circuitry and components which are applied in the subsystem for the detection, isolation and/or correction of failures.

There is one component used in the subsystem for the direct detection of an evaporator failure. This component incorporates the required logic and switching circuitry for detecting a failed condition. After detection the Failure Detection activates stand-by equipment. The Failure Detection mointors evaporator performance by comparing the controller output and a pressure switch signal from the evaporator expulsion duct. Variations from prescribed performance conditions results in automatic switching to secondary equipment.

Another source of failure detection for the subsystem is the evaporator

outlet temperature instrumentation and display. A failed condition of a given
evaporator may be detected by monitoring the displayed temperature indication.

6.2.5   Correcting Action

Automatic failure correction is employed in the Evaporator Subsystem
to correct water metering valve failures. This correction function is performed by
the failure detector. If a primary metering valve malfunctions, it would be detected
by the failure detector. The failure detector would then disable the failed valve
and activate the stand-by valve. If a secondary water metering valve fails, the
failure detector would switch it off, thus fully disabling the affected evaporator.
The correction of this failure would be instantaneous.

6.2.6   Redundancy Evaluation

The redundancy employed in the subsystem was evaluated with regard to
failure detection, redundancy verification, separation of redundant components,
and the isolation of non-critical equipment from critical subsystem equipment.

6.3   FMEA Conclusion and Recommendations

The results of the Failure Mode and Effects Analysis indicate that there
are no single failure modes which would result in a condition that does not meet
the fail-safe reliability criteria. Reliability improvement areas which should re-
ceive further consideration are discussed with associated recommendations as follows:

  a)   The Failure Detector incorporates failure detection and correction
       equipment. It does not, however, incorporate instrumentation for
       indicating that a failure has occurred and the resultant status.
       It is recommended that the capability for displaying a fault condi-
       tion and the resulting corrective status be incorporated.

  b)   A means of verifying the functional condition of back-up equipment
       should be incorporated in the design. This capability would serve
       to verify the condition of redundant equipment during checkout as
       well as during a mission flight interval.

  c)   The incorporation of Freon leak detection capability in each loop
       of the evaporator subsystem or in the interfacing Freon Coolant Loop
       (FCL) is recommended. This detection capability should alert operator
       personnel of leak condition, and should facilitate instantaneous
       automatic detection and isolation of a leak.

ORIGINAL PAGE IS OF POOR QUALITY

6-9

CODE	ELEMENT	QUANTITY	FUNCTION	FAILURE MODE	MISSION PHASE	FAILURE EFFECT	FAILURE DETECTION METHOD	BACK-UP/ALTERNATE	CORRECTING ACTION	REDUNDANCY EVALUATION	COMMENTS
11PD 11PU	Primary Downstream H_2O Valve and Primary Upstream H_2O Valve	One each per loop	On/Off solenoid valve which allows or stops the flow of H_2O to the evaporator core. Normally closed.	1. Open Solenoid or valve mechanically failed in closed position	all	Valve would remain in closed condition. Normal operation would be maintained by failure detection and back-up equipment.	Pressure switch would not be activated. Failure Detector Module would sense this fault.	Secondary H_2O Valve	Failure Detector would deactivate primary isolation valve and activate secondary isolation valve thus enabling secondary H_2O Valve.	Satisfactory	Fault condition should be instrumented for display.
				2. Shorted solenoid or valve mechanically failed in open position.	all	Valve would remain in open condition. Normal operation would be maintained by failure detection and back-up equipment.	Pressure switch would remain continuously activated without command from controller. Failure Detector would sense this and deactivate failed valve.	Secondary H_2O Valve	Failure Detector would deactivate primary isolation valve and activate secondary isolation valve thus enabling secondary H_2O valve and disabling primary H_2O valve.	Satisfactory	Failure Detection Module should include capability to switch power off to shorted valve
				3. Intermittent Operation	all	No effect on subsystem performance. Intermittent failure would be detected and back-up equipment enabled.	Pressure switch would sense pressure or lack of pressure. This would result in Failure Detector disabling the corresponding Isolation Valve.	Secondary H_2O Valve	Primary H_2O Valve would be disabled and secondary H_2O Valve would be enabled through back-up redundant switching of Isolation Valves.	Satisfactory	

SUBSYSTEM: FLASH EVAPORATOR

ASSEMBLY: _____

TABLE 6-1
FAILURE MODE AND EFFECTS ANALYSIS

PAGE __2__ OF __15__ SUPERSEDED _____

DATE __8-5-74__

6-10

CODE	ELEMENT	QUANTITY	FUNCTION	FAILURE MODE	MISSION PHASE	FAILURE EFFECT	FAILURE DETECTION METHOD	BACK-UP/ ALTERNATE	CORRECTING ACTION	REDUNDANCY EVALUATION	COMMENTS
11PD 11PU	Primary Downstream H_2O Valve and Primary Upstream H_2O Valve Continued:			4. Internal Leakage	all	An internal leak of the valve would not affect subsystem performance. A leak of sufficient magnitude would activate Failure Detector which would switch to back-up valve.	Pressure switch would sense pressure at an un-programmed time This would initiate the Failure Detector to switch to back-up valve.	Secondary H_2O Valve	Primary H_2O valve would be disabled and Secondary H_2O Valve enabled.	Satisfactory	A low rate of internal leakage would not be detected and would not constitue a problem.
				5. Degraded Operation (Valve partially open when activated).	all	This mode would not affect subsystem performance. Degraded valve performance of sufficient magnitude would result in activation of back-up redundant valve.	Pressure switch would sense insufficient pressure during a programmed time. This would initiate switching to redundant valve.	Secondary H_2O Valve	Primary H_2O Valve disabled - Secondary H_2O Valve enabled.	Satisfactory	Trip pressure of Pressure Switch should be selected such that insufficient flow of H_2O will activate pressure switch.
11SD 11SU	Secondary Downstream H_2O Valve and Secondary Upstream H_2O Valve	One each per loop.	On/Off solenoid valve which allows or stops the flow of H_2O the downstream evaporator core. Normally closed.	1. Open solenoid or valve mechanically failed in closed position.	all	No effect on subsystem performance; Valve would remain in closed position. Would result in loss of back-up for the affected evaporator.	During checkout this mode would be detected during redundancy verification. During flight, it would not be detectable until the valve is required.	None	When and if the valve is required the Failure Detector would sense the failed condition and disable the failed valve.	Meets single failure failsafe requirement. Redundant back-up for affected evaporator would be lost.	Instrumentation should be included in design which indicates failed condition of back-up equipment.

i

SUBSYSTEM: FLASH EVAPORATOR

ASSEMBLY: _____

TABLE 6-1
FAILURE MODE AND EFFECTS ANALYSIS

PAGE __3__ OF __15__ SUPERSEDED _____

DATE __8-5-74__

CODE	ELEMENT	QUANTITY	FUNCTION	FAILURE MODE	MISSION PHASE	FAILURE EFFECT	FAILURE DETECTION METHOD	BACK-UP/ ALTERNATE	CORRECTING ACTION	REDUNDANCY EVALUATION	COMMENTS
115D	Secondary Downstream H₂O Valve and			2. Shorted solenoid or valve mechanically failed in open position.	all	Valve would remain in open condition. Normal operation would be restored by failure detection and back-up equipment. Would result in loss of redundant back-up for affected evaporator.	Continuous output signal from pressure switch would cause Failure Detector to disable the failed valve.	None. Upstream evaporator would remain operable and operation of alternate FCL loop would be unaffected.	Failure Detector would sense the failed condition and would activate the corresponding Isolation Valve.	Redundant back-up for affected evaporator would be lost.	Instrumentation should be included which indicates failed condition of back-up equipment.
115U	Secondary Upstream H₂O Valve Continued:			3. Intermittent Operation	all	Un-commanded intermittent operation would be detected and the valve disabled.	Erroneous output signal from pressure switch would be sensed by Failure Detector which would disable corresponding Isolation valve.	None. Upstream evaporator would remain operable and operation of alternate FCL loop would be unaffected.	Failure Detector would sense the failed condition of the valve and would activate the corresponding Isolation Valve.	Redundant back-up for affected evaporator would be lost.	"
				4. Internal Leakage	all	A leak of sufficient magnitude would be detected and the leaking valve isolated.	Pressure switch would sense pressure at an unprogrammed time. This would result in a signal to the Failure Detector to activate the corresponding Isolation valve.	None. Upstream evaporator would remain operable and operation of alternate FCL loop would be unaffected.	Failed valve would be isolated as a result of the activation of corresponding Isolation valve.	Redundant back-up for affected evaporator would be lost.	"

6-11

SUBSYSTEM: FLASH EVAPORATOR

ASSEMBLY: _____

TABLE 6-1

FAILURE MODE AND EFFECTS ANALYSIS

PAGE ___4___ OF ___15___ SUPERSEDED _____

DATE ___8-5-74___

CODE	ELEMENT	QUANTITY	FUNCTION	FAILURE MODE	MISSION PHASE	FAILURE EFFECT	FAILURE DETECTION METHOD	BACK-UP/ ALTERNATE	CORRECTING ACTION	REDUNDANCY EVALUATION	COMMENTS
12PD 12PU	Primary Downstream Isolation Valve and Primary Upstream Isolation Valve	One each per loop	Latching solenoid controlled valve. Normally open. Valve closes on command from Failure Detector	1. Open Solenoid or valve mechanically failed in open position.	all	No effect on subsystem performance. Normal operation would be restored by failure detection and redundant back-up equipment.	Pressure switch would not be activated when Controller Commands H₂0 Valve. Failure Detector would sense this and activate Secondary Isolation Valve.	Secondary Isolation Valve	Failure Detector would deactivate Primary Isolation Valve and activate Secondary Isolation Valve, thus enabling secondary H₂0 Valve.	Satisfactory	
				2. Shorted solenoid or valve mechanically failed in closed position.	all	No effect on performance. Normal operation would be restored and maintained by failure detection and secondary back-up equipment.	Pressure switch would remain continuously activated without command from controller. Failure Detector would sense this and deactivate failed Isolation Valve.	Secondary Isolation Valve	Failure Detector would deactivate Primary Isolation Valve and activate Secondary Isolation Valve, thus enabling secondary H₂0 Valve.	Satisfactory	
				3. Internal Leakage	all	An internal leak of the valve would not affect subsystem performance. The Primary H₂0 Valve controls the flow of H₂0 and would be unaffected by a leaking Isolation valve.	A leak condition of a primary isolation valve would not be detectable until a command to deactivate it was initiated.	None	None Required.		A series application of two isolation valves in each primary H₂0 loop with manual control capability for one is recommended.

CODE	ELEMENT	QUANTITY	FUNCTION	FAILURE MODE	MISSION PHASE	FAILURE EFFECT	FAILURE DETECTION METHOD	BACK-UP/ ALTERNATE	CORRECTING ACTION	REDUNDANCY EVALUATION	COMMENTS
12PD 12PU	Primary Downstream Isolation Valve and Primary Upstream Isolation Valve Continued:			4. Intermittent Operation	all	No effect on subsystem performance. An intermittent off condition of an isolation valve would be detected and back-up equipment enabled.	Pressure switch would sense lack of pressure. This would result in Failure Detector disabling the failed valve and enabling the secondary isolation valve.	Secondary Isolation Valve	Primary H_2O Valve would be disabled and Secondary H_2O Valve enabled through back-up redundant switching of isolation valves.	Satisfactory	
				5. Degraded Operation (Valve partially closes when activated)	all	No effect on subsystem performance. Degraded performance of sufficient magnitude would result in activation of back-up equipment.	Pressure switch would sense lack of pressure during a demand interval. This would initiate switching to secondary valve.	Secondary Isolation valve	Primary H_2O Valve disabled- Secondary H_2O Valve enabled through primary/ secondary isolation valve switching.	Satisfactory	
12CD 12CU	Secondary Downstream Isolation Valve and Secondary Upstream Isolation Valve	One each per loop One each per loop	Latching solenoid controlled valve. Normally closed. Valve opens on command from Failure Detector.	1. Open solenoid coil or valve mechanically failed in closed position.	all	No effect on subsystem performance. Valve would remain in closed position. Would result in loss of back-up for affected evaporator.	During checkout this mode would be detected during redundancy verification. During flight it would not be detectable until the secondary equipment is required.	None	When the valve is activated, the Failure Detector would sense the failed condition and disable the failed valve.	Meets single failure, fail-safe criteria. Redundant back-up for affected evaporator would be lost.	

| SUBSYSTEM: FLASH EVAPORATOR | | |
| ASSEMBLY: | | |

TABLE 6-1
FAILURE MODE AND EFFECTS ANALYSIS

PAGE 6 OF 15 SUPERSEDED ____
DATE 8-5-74

CODE	ELEMENT	QUANTITY	FUNCTION	FAILURE MODE	MISSION PHASE	FAILURE EFFECT	FAILURE DETECTION METHOD	BACK-UP/ ALTERNATE	CORRECTING ACTION	REDUNDANCY EVALUATION	COMMENTS
12SD	Secondary Downstream Isolation Valve and			2. Shorted solenoid coil or valve mechanically failed in open position.	all	An electrical short of the solenoid coil would be correctd by Failure Detector switching. A mechanical failure may not be correctable. This failure may only constitute a problem if it occurred during a non-demand period for the secondary isolation valve.	During a non-programmed interval for the valve, failure sensing and switching circuitry would detect and isolate the problem. During a programmed interval for the valve, the condition would not be detectable and would effect subsystem performance.	None	During a non-programmed interval for the value the Failure Detector would disable the failed valve. During a programmed interval no correction would be necessary.	If this problem occurs during a non-programmed period for the valve, redundant back-up for the affectd evaporator would be lost.	A mechanical failure(open) of the valve during a non-demand period would constitute a serious problem in that a continuous flow of H_2O to the affected evaporator would be experienced. A series configuration of isolation valves in each secondary H_2O loop with manual override is recommended. "
12SU	Secondary Upstream Isolation Valve Continued:			3. Internal Leakage	all	Would adversely affect subsystem performance during a non-programmed interval for the valve, H_2O from both the primary and secondary H_2O loops would be delivered to the affected evaporator.	During a non-programmed interval for the valve, a leaking valve would be detected by the Failure Detector. This condition would not be correctable without another isolation valve and manual.	None			

6-14

							FAILURE DETECTION	BACK-UP/	CORRECTING	REDUNDANCY	
CODE	ELEMENT	QUANTITY	FUNCTION	FAILURE MODE	MISSION PHASE	FAILURE EFFECT	METHOD	ALTERNATE	ACTION	EVALUATION	COMMENTS
125D	Secondary Downstream Isolation Valve and			3. Internal Leakage		at the same time. This would result in excessive cooling of freon in the affected FCL loop and possible loss of the loop. During a programmed interval for the valve there would be no effects on subsystem performance.	override to isolate the leaking valve. During a programmed interval leakage of the valve would not be detectable nor would its detection be required.				
125U	Secondary Upstream Isolation Valve Continued:			4. Intermittent Operation	all	During a non-programmed interval for the valve, an intermittent on-condition would be detected and corrected with no effect on subsystem performance. This would result in the loss of back up capability for the primary isolation valve. During a programmed interval this problem would be detected and	During non-programmed interval, Pressure switch would sense pressure. The Failure Detector would then disable the valve. During programmed interval, pressure switch would sense lack of pressure. Failure Detector would the disable	None	Failed condition of would be detected and the valve disabled.	During demand period for secondary valve and intermittent failure would result in loss of the affected evaporator. During a non-demand period for secondary valve, an intermittent failure would result in loss of back-up capability for	

ORIGINAL PAGE IS OF POOR QUALITY

6-16

CODE	ELEMENT	QUANTITY	FUNCTION	FAILURE MODE	MISSION PHASE	FAILURE EFFECT	FAILURE DETECTION METHOD	BACK-UP/ ALTERNATE	CORRECTING ACTION	REDUNDANCY EVALUATION	COMMENTS
123D 12SU	Secondary Downstream Isolation Valve and Secondary Upstream Isolation Valve Continued:			4. Intermittent Operation continued: 5. Degraded Operation (Valve partially opens when activated)	all	the secondary valve disabled. This would result in the loss of the affected evapora- If valve only partially opens when commanded, would result in degraded performance and possible loss of affected evaporator.	the valve. No detection method incorporated.	None	None. Partially open valve would allow at least degraded operation of secondary H2O loop for affected evaporator.	Primary Loop Meets single failure fail-safe criteria. Degraded performance from this condition would result only after the incurrence of two failures.	*
O1D	Downstream Evaporator Core	One per loop	Reject waste heat from Freon loop.	1. Freon leak	all	Would result in loss of the affected FCL loop and abort of mission.	No detection method incorporated.	Alternate FCL loop	Leaking freon loop would be disabled. Waste heat rejection would be performed by remaining FCL loop.	The failure would result in a fail-safe condition. The alternate freon loop would provide sufficient heat rejection capability to allow safe return of crew and payload.	
				2. Structural Failure.	all	Would result in loss of affected evaporator and degraded heat rejection capability of the affected FCL loop. This failure would also result in H2O contamination of cargo area and possible degradation of susceptible payload elements.	Loss of ability to control to 40°F outlet temperature would be indicated by instrumentation and display.	None	H2O to affected evaporator would be cut off. The evaporator Subsystem would continue to operate with upstream evaporator active in one FCL loop and full capability in the alternate loop.	Meets single failure fail-safe criteria. Subsystem capability following the incurrence of this failure would be sufficient for safe return of crew and payload.	Manual isolation of primary and secondary H2O loops for each evaporator should be possible.

SUBSYSTEM: __FLASH EVAPORATOR__

ASSEMBLY: _____

TABLE 6-1
FAILURE MODE AND EFFECTS ANALYSIS

PAGE __9__ OF __15__ SUPERSEDED _____

DATE __8-5-74__

6-17

ORIGINAL PAGE IS
OF POOR QUALITY

CODE	ELEMENT	QUANTITY	FUNCTION	FAILURE MODE	MISSION PHASE	FAILURE EFFECT	FAILURE DETECTION METHOD	BACK-UP/ ALTERNATE	CORRECTING ACTION	REDUNDANCY EVALUATION	COMMENTS
01U	Upstream Evaporator Core	One per Loop	Reject waste heat from Freon loop	1. Freon Leak	All	Would result in loss of affected FCL loop and abort of mission	None	Alternate FCL Loop	Leaking freon loop would be disabled. Waste heat rejection would be performed by alternate FCL loop.	The failure would result in a fail safe condition. The alternate freon loop would provide suffi- cient heat re- jection capa- bility to allow safe return of crew and payload.	The design should incor- porate suffi- cient separa- tion of tubing of each FCL loop or protec- tion to ensure that damage & subsequent leak- age of one freon path will not impair the per- formance of the alternate loop. The incorpora- tion of freon leak detection capability is recommended to alert crew of a leak condition.
				2. Structural Failure	All (most critical effect during launch & re-entry)	Would result in loss of affected evapora- tor & loss of ability to control evaporator subsystem outlet tem- perature to 40°F. This would result in degraded heat rejec- tion capability of the affected FCL loop during launch & re- entry intervals. This failure would also re- sult in H2O contamina- tion of cargo area & possible degradation of susceptible payload elements.	None. Loss of capability to con- trol to 40°F out- let temperature would be indicated by instrumentation & display equip- ment.	None	H2O affected evaporator would be cut-off. The evaporator sub- system would con- tinue to operate with downstream evaporator in 1 loop & full capability in the alternate FCL loop.	Meets single fail- ure fail-safe cri- teria. Subsystem capability fol- lowing the incur- rence of this failure would be sufficient for safe return of crew & payload.	Capability for manual isola- tion of pri- mary & second- ary H2O loops for each evap- orator should be possible.

SUBSYSTEM: FLASH EVAPORATOR

ASSEMBLY: _____

TABLE 6-1
FAILURE MODE AND EFFECTS ANALYSIS

PAGE 10 OF 15 SUPERSEDED _____

DATE 8-5-74

6-18

CODE	ELEMENT	QUANTITY	FUNCTION	FAILURE MODE	MISSION PHASE	FAILURE EFFECT	FAILURE DETECTION METHOD	BACK-UP/ ALTERNATE	CORRECTING ACTION	REDUNDANCY EVALUATION	COMMENTS
13D 13U	Downstream Pressure Switch & Upstream Pressure Switch	One each loop	Provides signal to failure detector for verification of proper evaporator operation.	1. Shorted contacts or contacts mechanically failed in closed position.	All	Would result in continuous output signal to Failure Detector. If this occurs at a time when primary H2O valve has not been commanded, the Failure Detector will deactivate primary isolation valve and activate secondary isolation valve. The failure detector would again sense the fault and de-activate the secondary isolation valve. The ultimate effect would be the loss of the affected evaporator & subsequent reduced heat rejection capability of the evaporator subsystem	The problem would be detected as a result of the affected evaporator's inability to control to the required outlet temperature.	There is no back up alternate pressure switch.	None. The remaining evaporator & the alternate FCL loop would continue to provide heat rejection capability.	This mode involves a limitation of failure detection equipment in that evaporator subsystem capability would be reduced due to the failure of a failure detection element. The use of established hi-rel pressure switches is recommended for evaporator applications.	
				2. Open Contacts or contacts mechanically failed in open position	All	Would result in no output signal to failure detector which would constitute an erroneous failure indication. The failure detector would deactivate the primary isolation valve and activate the secondary isolation valve. The fault would be sensed again in the secondary mode and the secondary isolation valve deactivated. The ultimate effect would be the loss of the affected evaporator & subsequent reduced heat rejection capability of the Evaporator subsystem.	None. The pressure switch is a failure detection element. The failure would be detected as a result of the evaporators inability to control to the required outlet temperature.	None	None. The remaining evaporator and the alternate FCL loop would continue to provide heat rejection capability.	Redundant pressure switch applications are not recommended. The use of established hi-rel pressure switches is recommended for evaporator applications.	

CODE	ELEMENT	QUANTITY	FUNCTION	FAILURE MODE	MISSION PHASE	FAILURE EFFECT	FAILURE DETECTION METHOD	BACK-UP/ ALTERNATE	CORRECTING ACTION	REDUNDANCY EVALUATION	COMMENTS
13D 13U	Downstream Pressure Switch & Upstream Pressure Switch Continued:			3. Leakage	All	This failure mode would result in loss of the affected evaporator & subsequent degraded heat rejection capability of the affected FCL loop. It would also result in H₂O contamination of cargo area & possible degradation of susceptible payload elements.	The loss of ability of the affected loop to control to a 40°F outlet temperature would be indicated by instrumentation and display.	None	The pri. & sec. H₂O to the affected evaporator would be cut off. The evaporator subsystem would continue to operate with the remaining evaporator active in one FCL loop and full capability in the alternate loop.	Meets single failure fail-safe criteria. Subsystem capability following the incurrence of this failure would be sufficient for safe return of crew and payload.	
				4. Intermittent/ Degraded Output	All	This failure would be detected by the Failure Detector which would then switch to secondary H₂O. If the intermittent condition continued, the failure detector would then switch off the sec. H₂O. If the intermittent failure occurred with the affected evaporator already on sec. H₂O, the Failure detector would switch the secondary H₂O off. The ultimate effect would be the loss of the affected evaporator.	Instrumentation & display equipment would indicate the affected evaporator's inability to control to the required outlet temperature.	None	The pri. & sec. H₂O to the affected evaporator would be successively cut off disabling the evaporator. The evaporator subsystem would continue to operate with the remaining evaporator active in one FCL loop & full capability in the alternate loop.	Meets single failure fail-safe criteria. Subsystem capability following the incurrence of this failure would be sufficient for safe return of crew and payload.	The selection of established Hi-Rel pressure switches is recommended for evaporator subsystem applications.

6-19

SUBSYSTEM: FLASH EVAPORATOR

ASSEMBLY: _____

TABLE 6-1
FAILURE MODE AND EFFECTS ANALYSIS

PAGE 12 OF 15 SUPERSEDED _____

DATE 8-5-74

CODE	ELEMENT	QUANTITY	FUNCTION	FAILURE MODE	MISSION PHASE	FAILURE EFFECT	FAILURE DETECTION METHOD	BACK-UP/ ALTERNATE	CORRECTING ACTION	REDUNDANCY EVALUATION	COMMENTS
21D 21U	Downstream Temperature Sensor & Upstream Temperature Sensor	One each per loop	Senses coolant temperature and provides corresponding output signal to Controller	1. Short	All	Would result in incorrect output signal to controller which in turn would incorrectly shutoff the evaporant. The affected configuration would attempt to correct an erroneous high temperature condition. The final effect would necessitate shutdown of the affected evaporator.	None. The proposed sensor is a three-element majority voter configuration. The outputs of two-out-of three sensing elements must be incorrect before an incorrect sensor output would be experienced.	The proposed sensor is a three-element majority voter component.	None. The remaining evaporator and the alternate FCL loop would continue to provide heat rejection capability.	Excellent. The three-element parallel redundant (majority voter) will provide an extremely low probability of failure for the sensor. Exceeds fail-safe criteria.	
				2. Open	All	Would result in incorrect temperature output signal to Controller. The affected configuration would attempt to correct an erroneous low temperature condition. The final effect would necessitate shutdown of the affected FCL loop.	None	The sensor is a three-element majority voter configuration.	None	Excellent. Exceeds fail-safe criteria.	The sensor has an extremely low probability of failure as it is a three-element majority voter configuration.
				3. Degraded Output (Out-of-Tolerance)	All	This failure may result in an erroneous high temperature or low temperature output signal. Either condition would result in the affected configuration attempting to correct to the erroneous temperature signal. The failed condition would necessitate shutdown of the affected evaporator.	None required	Sensor is a three-element majority voter	None. If a sensor failure should occur the affected evaporator would be disabled. The subsystem would continue to operate with the remaining evaporator in one loop and the other FCL loop fully operational.	Meets fail-safe criteria. Sensor is majority voter configuration. Exceeds fail-safe criteria.	

SUBSYSTEM: FLASH EVAPORATOR

ASSEMBLY: _____

TABLE 6-1
FAILURE MODE AND EFFECTS ANALYSIS

PAGE __13__ OF __15__ SUPERSEDED _____

DATE __8-5-74__

CODE	ELEMENT	QUANTITY	FUNCTION	FAILURE MODE	MISSION PHASE	FAILURE EFFECT	FAILURE DETECTION METHOD	BACK-UP/ ALTERNATE	CORRECTING ACTION	REDUNDANCY EVALUATION	COMMENTS
22D 22U	Downstream Controller & Upstream Controller	One each per loop	Regulates evaporator freon outlet temperature. Provides on-off signal to H$_2$O valve, via Failure Detector in response to temperature signal from sensor.	1. No Output	All	Would result in loss of the affected evaporator. Performance of remaining evaporator and alternate FCL loop would be unaffected.	The failure detector would detect the no-output condition. The H$_2$O valves are normally closed and with no control signal from the controller will remain in the closed position.	None	None. Subsystem would continue to perform with the remaining evaporator in the affected loop & the alternate FCL loop.	Meet fail-safe criteria. Failed condition would not prohibit safe return of crew & payload.	Instrumentation should be included in the design which indicates this failure condition to operator personnel.
				2. Intermittent Output	All	Would degrade the ability of controller to control the corresponding H$_2$O valve. The extent of the degradation would be dependent on the degree of intermittency. The ultimate effect would be loss of efficiency of the affected evaporator.	The failure would not be readily detectable. The inability of the affected evaporator to maintain the required setpoint temperature would be detected by coolant temperature readout.	None	None. The affected evaporator may continue to operate intermittently without critical effects	"	"
				3. Degraded Output	All	If output control signal is degraded to a point where the corresponding H$_2$O valve drops out, then the effect would be loss of the affected evaporator. This failure would not affect the performance of the remaining evaporator and the alternate FCL loop.	The inability of the affected evaporator to maintain the required setpoint temperature would be detected by coolant temperature readout.	None	None. The subsystem would continue to operate with the remaining evaporator and the alternate FCL loop.	Meets failsafe criteria. Failed condition would not prohibit safe return of crew and payload.	Instrumentation should be included in design which indicates the status of pri. & sec. H$_2$O valves for each evaporator.

SUBSYSTEM: _____

ASSEMBLY: _____

TABLE 6-1

FAILURE MODE AND EFFECTS ANALYSIS

CODE	ELEMENT	QUANTITY	FUNCTION	FAILURE MODE	MISSION PHASE	FAILURE EFFECT	FAILURE DETECTION METHOD	BACK-UP/ ALTERNATE	CORRECTING ACTION	REDUNDANCY EVALUATION	COMMENTS
23D 23U	Downstream Failure Detector & Upstream Failure Detector	one each per loop	Provides signal to de-activate primary H_2O valve and activate sec. H_2O valve in the event of pri. H_2O valve failure	1. No output	All	A no-output condition for a given failure detector would result in loss of the affected evaporator. The controller output signals to the H_2O valve(s) are routed through the Failure Detector. The loss of the output signals would result in the appropriate H_2O valve not being actuated.	None. The failed component is a failure detection element. The failure would be detected through coolant temperature instrumentation and display.	None.	None. The subsystem would continue to operate with the remaining evaporator and the alternate FCL loop.	Meets failsafe criteria. Failed condition would not prohibit safe return of crew and payload.	Instrumentation should be included which provides direct and rapid indication of H_2O valve status for each evaporator.
				2. Logic and/or Switching Failure	All	The following effects could be experienced: (1) Failure to detect a failed condition. (2) Failure to switch to sec. H_2O valve when required. The ultimate effect would be loss of the affected evaporator.	The failure would be detected by coolant temperature instrumentation and display.	None. The subsystem would continue to perform with the remaining evaporator in one loop and the alternate FCL loop.	Would require disabling the affected evaporator	Meets single failure failsafe criteria	Capability to manually isolate all pri. and sec H_2O loops should be incorporated.
				3. Intermittent Output	All	The ability of the affected controller to control the active H_2O valve would be degraded. This would subsequently result in degraded performance of the affected evaporator.	This failure would not be readily detectable unless the degree of intermittency is extreme. The inability of the affected evaporator to maintain the required coolant set point temperature would be detected by coolant temp. instrumentation.	None	None. The affected evaporator may continue to operate intermittently without critical effects.	"	

CODE	ELEMENT	QUANTITY	FUNCTION	FAILURE MODE	MISSION PHASE	FAILURE EFFECT	FAILURE DETECTION METHOD	BACK-UP/ ALTERNATE	CORRECTING ACTION	REDUNDANCY EVALUATION	COMMENTS
23D	Downstream Failure Detector & Upstream Failure Detector Continued:			4. Degraded Output	All	Degradation of Failure Detector to a level below drive threshold of H₂0 valve would result in some failure effects as a no-output condition. The ability to command corresponding pri. and sec. H₂0 valves would be lost. The ultimate effect would be loss of the affected evaporator.	The failure would be detected by temperature instrumentation and display	None	None. The evaporator subsystem would continue to operate with remaining evaporator in one loop and the alternate FCL loop.	Meets single failure failsafe criteria.	

ORIGINAL PAGE IS
OF POOR QUALITY

6-23

7.0   REFERENCES

1.   Gaddis, J. L., "Feasibility Demonstration of A Spraying Flash Evaporator", NASA CR114913, 7 May 1971

2.   Gaddis, J. L., "Laboratory Prototype Flash Evaporator", NASA-MSC-07098, October 1972

3.   Gaddis, J. L., "Development of A Prototype Spraying Flash Evaporator", ASME Paper 72-ENAv-28, August 1972

4.   Scheps, P. B., "Integrated Radiator/Expendable Cooling System Tests", LTV Aerospace Corporation, Report T169-28, Volume V, 15 April 1974

5.   McGinnis, F. K., and Summerhays, R. M., "Water Ejector Plume Tests", LTV Aerospace Corporation, Report T169-28, Volume VI, 16 November 1973

6.   Fleming, M. L., et.al., "Shuttle Active Thermal Control System Development Testing", ASME Paper 74-ENAs-43, August 1974

7.   Bagwell, P. R., "Cold Plate Flash Evaporator Feasibility Demonstration", T157-29, 24 October 1973

8.   Schneider, P. J., Temperature Response Charts, John Wiley and Sons, New York, 1963.

9.   Holman, J. P., Heat Transfer, McGraw-Hill, New York, 1968.

10. Rizza, J. J., "A Droplet Impact and Evaporation Study Using High Speed Photography", Report to NASA, 1973.

11. W. M. Kays and A. L. London, Compact Heat Exchangers, McGraw-Hill Book Co., New York, N.Y.

12. Shah, R. K, and A. L. London, "The Influence of Brazing on Very Compact Heat Exchanger", Technical Report No. 73, Contract Nonr 225(91) (NR-090-342) for Office of Naval Research, November 1970

APPENDIX A
NOZZLE DEVELOPMENT TESTING

1.0   SUMMARY

The spray nozzle has been demonstrated to be a critical factor in the evaporator design. Nozzle configurations have been observed to produce a combined droplet size, distribution, and supply rate such that local accumulations of frost result independent of surface temperature. Additionally, non-uniform spray patterns, spray adherence to the nozzle face, and evaporant supply pressure limitations can plague the evaporator operation. During the development of the Prototype 2 and 3 flash evaporators and the Prototype I modification program, extensive nozzle testing was performed to find an acceptable combination of nozzle spray characteristics with various configurations of evaporator heat transfer geometry.

The various nozzle configurations selected for evaluation during the program (shown in Figure 3-1) encompassed a wide range of capacities, spray patterns, and flow geometries. Nozzles with water flow capacities from 7.3 to 45 kg/hr (16 to 100 lbs/hr) consistent with expected spacecraft supply pressures were tested. In addition to hollow cone spray patterns tested previously in the Prototype I program, nozzles with solid cone were evaluated in conjunction with six different potential heat exchanger core configurations. Two techniques were used in evaluating spray pattern/droplet distribution: (1) "implied distribution" using the surface temperature profiles of the Prototype I flash evaporator; and (2) direct analyses obtained from optical observations of a nozzle sprayed into an evacuated bell jar.

The data obtained from the nozzle testing was reduced and put into a useful format for the designer having to select a nozzle or nozzles for a particular evaporator heat exchanger core shape. This data is presented in this Appendix.

2.0   INTRODUCTION

In spray nozzles, liquid breakup is usually caused by the collapse of unstable sheets or jets. Centrifugal pressure nozzles impart a swirling motion to the liquid by tangential passages, slots, or cores. The swirling film of liquid then emerges through a circular orifice as a thin hollow sheet. Since

A-1

it is unstable, it immediately collapses into ligaments which break up into small droplets of various size.

Such devices produce tiny droplets of 1 or 2 microns as well as larger droplets that may range up to several hundred microns. No conventional nozzles, however, are capable of spraying droplets of equal size.

In most cases, larger droplets may be expected as nozzle capacity increases. · As metering passages are enlarged to allow greater liquid through-put, larger droplets generally result. Spray angle rating is also a factor, finer droplets being associated with larger angles.

Droplet size may vary within the pattern of a given spray. In hollow cone sprays, for example, there is usually a preponderance of larger droplets at the outside of the pattern.

In order to gain greater insight into spray nozzle operation and to find an acceptable combination of spray characteristics for various evaporator combinations, spray nozzle testing was performed during Prototype 2 and 3 development using two techniques. These are described in the sections that follow.

3.0   IMPLIED SPRAY DISTRIBUTION NOZZLE TESTING

The implied spray distribution testing (using the surface temperature profiles of the Prototype I flash evaporator) was conducted during the early development of the 14.6 kw (50,000 BTU/hr) Prototype 2 evaporator. Twenty hollow cone nozzles were evaluated (including 13 "off-the-shelf" nozzles and 7 "baseline modified" nozzles) to obtain the optimum nozzle/evaporator having the same heat transfer surface shape/configuration as the Prototype I device.

Typical surface temperature data, such as that shown in Figure A-1 for the WDA-14.0-90° nozzle, was taken for each nozzle tested. The data was reduced to provide the spray distribution per unit heat transfer area using the following relationship:

$$\frac{\dot{m}Cp \; (\Delta T_f)}{h_{fg}(\Delta A_{HT})} = \frac{\Delta M_{H_2O}}{\Delta A_{HT}}$$

where: $\dot{m}Cp$ = fluid heat flow capacitance

$$\frac{\Delta T_t}{\Delta A_{HT}} = \text{surface temperature difference per unit area}$$

$$h_{fg} = \text{latent heat of vaporization}$$

Using this approach, the test data taken in Figure A-1 was reduced to provide the implied spray distribution data shown in Figure A-2. This distribution data was compiled for each nozzle tested using the "implied distribution" technique.

The "off-the-shelf" nozzles were tested to obtain comparative data with the WDA-14.0-90° baseline Prototype I nozzle. The seven "baseline modified" nozzles were tested to determine the effects on spray distribution, opening angles, etc. of variation of the WDA-14.0-90° distributor slot geometry and orifice diameter. The "baseline modified" geometry variations tested are compared in Table A-1. A summary of the nozzle spray characteristics and corresponding evaporator performance are presented in Table A-2. These results showed that for a 14.6 kw evaporator, the baseline WDA-14.0-90° Prototype I nozzle produced the best spray distribution, and that the modified baseline nozzles tended to spray in a heavy, narrow band with an uneven spray pattern. No conclusions on the individual distributor geometry modifications on spray pattern could be separated from test results.

Additional spray distribution data was obtained for 12 off-the-shelf nozzles spraying 6.8kg/sec (15 lbs/hr) using the implied distribution technique during modification of the Prototype I evaporator for use as a radiator top-off device. These data are presented in Table A-3.

4.0   OPTICAL SPRAY DISTRIBUTION NOZZLE TESTING

As development of the Prototype 2 and 3 evaporators progressed, the use of the implied distribution technique for testing spray nozzles was not possible due to the larger amounts of water evaporant flow rate expected (up to 45 kg/hr-100 lb/hr). This was due to the Prototype I heat exchanger core and exhaust duct size being limited to spray rates of 22.5 kg/hr (50 lb/hr).

In order to obtain quantative spray pattern data, a visual analysis method was developed for nozzle evaluation. It had been previously observed that the spray into a near vacuum which impacted a bell jar wall formed a band

of frost which corresponded in shape and thickness to the local spray pattern. It was decided to use the effect to obtain quantitative spray pattern information on the spray patterns of the various nozzle candidates at a variety of flow rates/ supply pressures. As seen in Figure A-3, the nozzle/valve assembly was centrally located in the chamber for these tests, so that an unsymmetrical impingement pattern was produced. The spray was maintained for a sufficient period of time to establish a visible frost layer on the bell jar wall. The pertinent geometrical parameters (shown in Figure A-3) were then recorded at each location.

The results of these tests are summarized in Tables A-4 and A-5 in Figure A-4. Computed angles θ_t, θ_b, θ_1, and θ_2 define the outer and inner limits of the spray and heavy spray respectively, while θ_c corresponds to the location of maximum spray intensity. From the data, it was noted that for hollow cone nozzles, the effect of ambient bell jar pressure on the included angle of the spray and the cone width remained at essentially 130° and 25°, respectively, for all nozzles. For solid cone nozzles, it was observed that increasing flow (and supply pressure) caused the nozzles to spray in a hollow cone while decreasing flow caused the included angle to decrease.

5.0 SPRAY NOZZLE/HEAT EXCHANGER CORE DESIGN DATA

The spray nozzle data reported in Sections 3.0 and 4.0 of this appendix for a spray rate of 7.2 kg/hr (16 lb/hr) was compiled into useful design data for six different evaporator configurations for 3.6 kg/ft^2 (8 lb/ft^2) maximum spray densities. Figure A-5 presents the design data for a circular flat plate evaporator configuration. The data for a cylindrical configuration are presented in Figures A-6 thru A-8 for heavy spray on the side, corner, and bottom respectively. Figure A-9 presents cone shape configuration data, while Figure A-10 compares configurations where spray intercepts a cylinder side only. These data were used in evaluating various concepts of Prototype 2 and 3 evaporators.

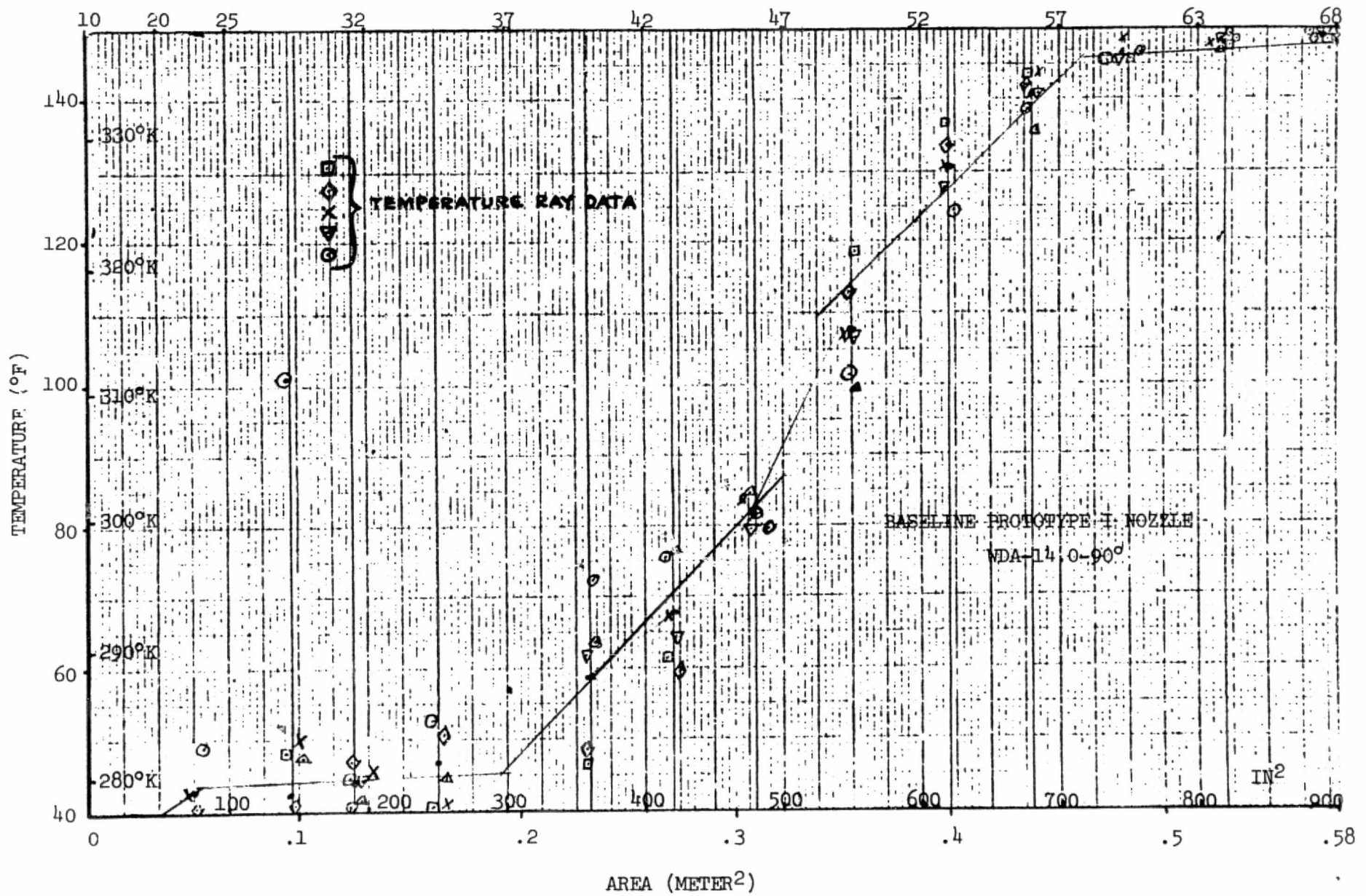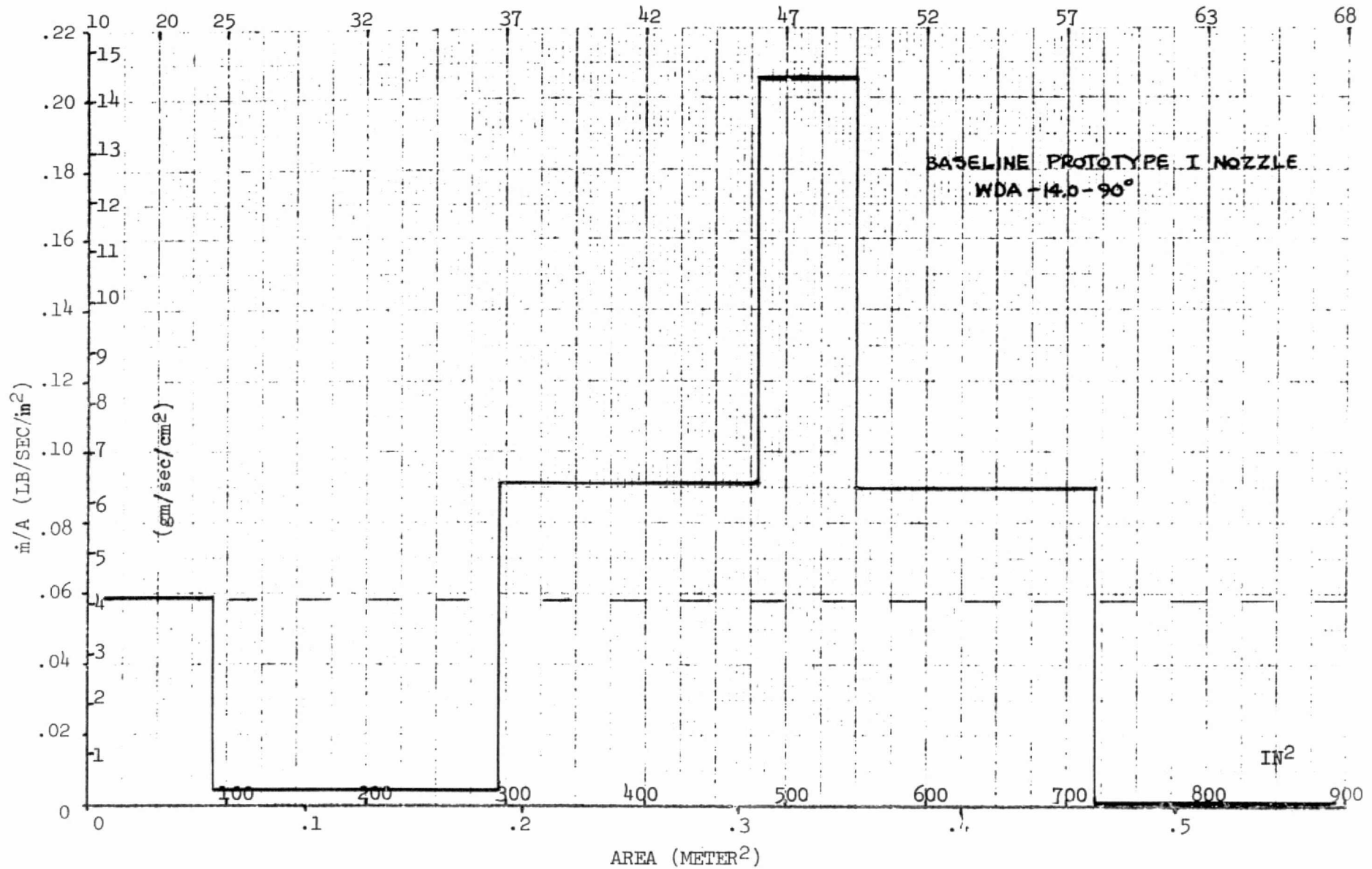FIGURE A-1 PROTOTYPE I EVAPORATOR TEMPERATURE DISTRIBUTION

FIGURE A-2 PROTOTYPE I EVAPORATOR SPRAY DISTRIBUTION

TABLE A-1

COMPARISON OF BASELINE AND MODIFIED NOZZLE

DISTRIBUTOR/ORIFICE CONFIGURATIONS

	NO. SLOTS	SLOT DEPTH	SLOT WIDTH	ORIFICE DIAMETER
Baseline*	6	.018	.018	.040
Mod 6	6	.022	.016	.040
Mod 7	6	.034	.016	.040
Mod 8	6	.041	.016	.040
Mod 9	6	.025	.018	.040
Mod 10	6	.031	.018	.040
Mod 11	6	.037	.018	.040
Mod 13	6	.018	.018	.038
Mod 14	6	.018	.018	.042

*WDA-14.0-90°

TABLE A-2 IMPLIED DISTRIBUTION NOZZLE/EVAPORATOR TEST RESULTS

NOZZLE *	PERFORMANCE				EFFICIENCY η	SPRAY ANGLES		REMARKS
	$Q_e (\frac{BTU}{in})$	$T_{in}(°F)$	$T_{out}(°F)$	$\dot{m}_{H2O}(\frac{LB}{HR})$		BOTTOM DEGREES	TOP DEGREES	
WDA-14-90°	51800	150.3	45.1	50.0	.984	45	65	Proto I Baseline
WDA-12-90°	51800	150	44.4	50.0	.983	48	70	Heavy Spray
WDA-12-90°	53458	150.4	127.6	51.6	.205	53	64	Ice
WDA-12-90°	51904	149.5	44.1	50.1	.976	41	64	Ice
WDA-10-90°	51904	149.6	45.0	50.1	.974	36	70	
WDA-10-90°	52111	149.6	46.1	50.3	.963	10	70	Nozzle Leaks
WDA-8-90°	51696	148.8	46.2	49.9	.960	40	70	
WDA-14-70°	51489	150.4	43.0	49.7	1.003	40	64	
MOD 6	52007	150.1	45.2	50.2	.972	47	70	Nozzle Ice
MOD 7	51800	152.0	46.3	50.0	.983	53	70	
MOD 8	52111	150.3	42.5	50.3	.996	53	70	Ice
MOD 9	52214	150.6	43.2	50.4	.992	40	70	
MOD 10	52111	149.0	43.8	50.3	.973	52	65	Ice
MOD 11	52214	150.8	53.4	50.4	.905	53	64	Ice
MOD 13	52007	151.0	44.0	50.2	.992	43	70	Nozzle Ice
MOD 14	52318	149.9	42.0	50.5	.994	40	70	Nozzle Ice
1/4-NN-4	52111	149.4	46.7	50.3	.973	36	60	Ice
1/4-NN-8	52111	150.6	42.9	50.3	.9995	40	70	Heavy Ice

*
WDA-XX-YY -- Delavan nozzles, XX gph at 125 psig supply
                YY opening angle in atmosphere
MOD   -- Modified WDA-14-90° nozzles
1/4-NN-XX -- Spray Systems Co. nozzles

TABLE A-3

IMPLIED DISTRIBUTION DATA FOR

TOP-OFF EVAPORATOR NOZZLES

NOZZLES *	EVAP FLOWRATE lb/hr	SUPPLY PRESSURE psig	EFFICIENCY η	T_{out} °F	SPRAY ANGLES		REMARKS
					BOTTOM deg	TOP deg	
1/4-NN-2	15.5	18.2	96.4	42.2	10	47	
1/4-NN-2	15.7	11	98.0	42.1	10	45	
1/4-NN-3	15.8	8.1	98.0	42.7	28	45	
WDW-3.5-90	15.6	26.6	100	41.4	35	50	
WDA-4.0-90	15.7	18.5	98.7	40.4	45	70	
WDA-4.0-70	15.7	13.3	100	40.8	40	53	
WDA-3.0-90	16.0	42.7	98.4	41.3	43	60	
WDW-4.0-90	16.1	15.4	99	40.2	36	55	
WDW-4.0-90	16.1	16.6	99	40.0	40	53	
WDW-3.0-90	15.5	38	99.5	41.3	40	57	
WDB-4.0-90	16.1	21	98.4	40.8	10	47	
WDB-4.0-90	15.8	17.1	98	41.5	10	46	

*See notes on Table A-2
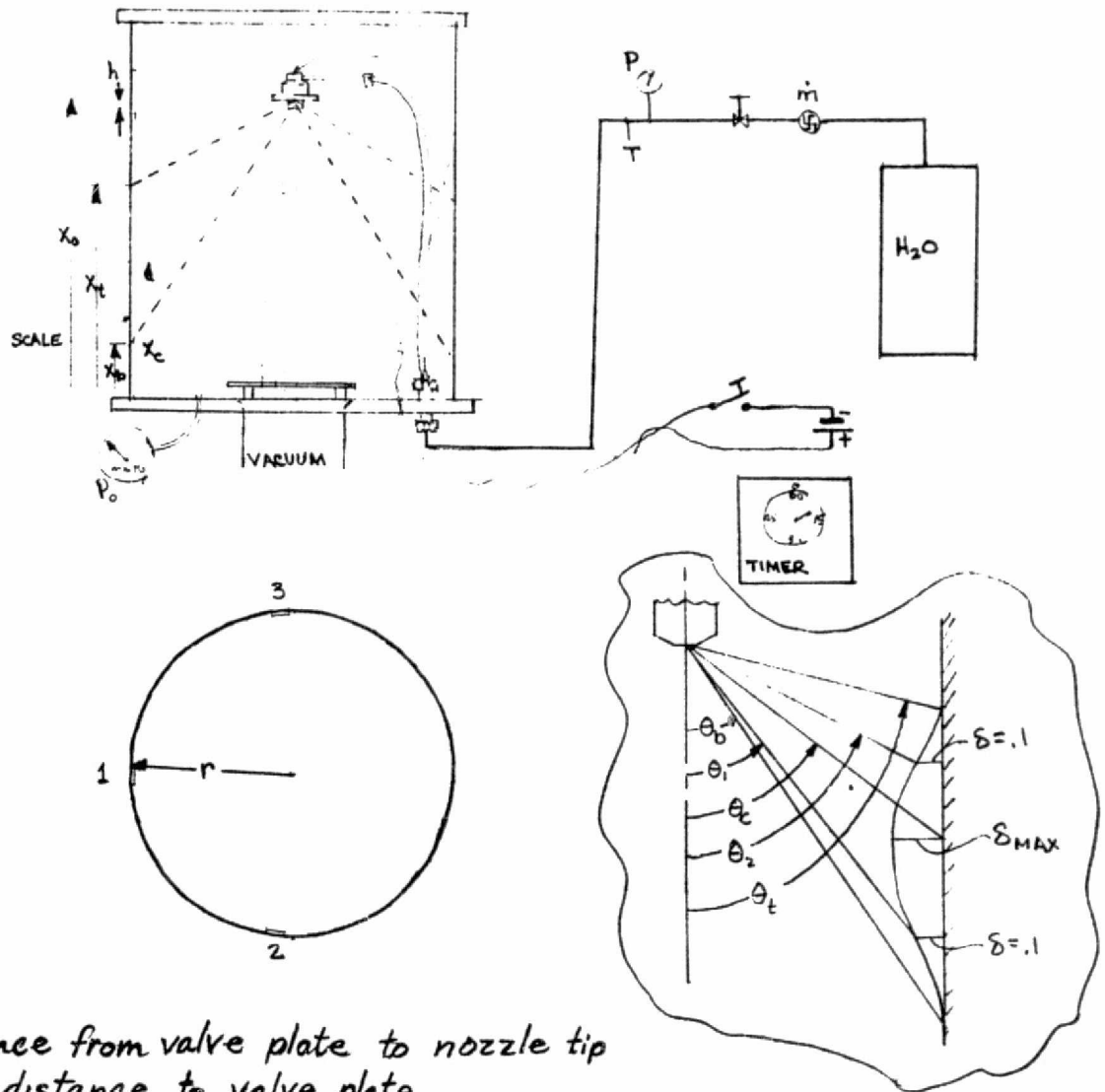
h — distance from valve plate to nozzle tip
X_o — ref. distance to valve plate
X_t — top of spray deposition as est. by experimenter
X_c — center of spray deposition
X_b — bottom of spray deposition
r — distance from nozzle to bell jar at location 1
P_o — bell jar pressure, mm Hg

TABLE A-4

FLASH EVAPORATOR NOZZLE OPTICAL SPRAY DATA

16 lb/hr FLOWRATE

NOZZLE*	θ_b (DEG)	θ_1 (DEG)	θ_c (DEG)	θ_2 (DEG)	θ_t (DEG)	$\dfrac{M_{1-2}}{MT}$
4.5-W-90	30	40	46	59	60	.80
5.0-W-90	37	46	55	65	72	.87
3.5-W-90	25	33	39	46	52	.47
3.5-W-70	27	37	42	50	51	.85
4.5-W-70	30	40	47	5"	60	.774
4.0-B-70	0	–	–	–	45	–
3.5-B-70	30	32	–	36	50	.92
3.5-B-90	33	37	42	48	52	.62
5.0-B-90	0	–	–	–	48	–
4.5-B-70	0	–	–	–	46	–
5.0-B-70	0	–	–	–	45	–
5.0-A-70	30	32	40	53	56	.70
4.5-A-70	25	44	54	60	66	.72
1/4-NN-2	23	33	39	47	53	.65
4.0-B-90	0	–	–	–	47	–
4.0-B-90	0	–	–	–	46	–
4.0-A-90	41	48	54	59	71	.53
4.0-W-70	0	25	28	31	44	.18
4.0-A-70	30	38	43	48	54	.38
4.0-A-45	–	–	–	–	48	–
4.0-W-45	–	24	27	30	45	–
3.5-A-90	40	44	51	58	67	.60

*Delevan Nozzles
XX-YY-ZZ

        XX – flow gph at 125 psi supply
        YY – A – hollow
             B – solid   spray cone in atmosphere
             W – 1/2 and 6
        ZZ – Cone opening angle in atmosphere

TABLE A-5

FLASH EVAPORATOR NOZZLE OPTICAL SPRAY DATA
75 lb/hr FLOWRATE

NOZZLE *	θ_b (DEG)	θ_1 (DEG)	θ_c (DEG)	θ_2 (DEG)	θ_t (DEG)	$\frac{M_{1-2}}{M_T}$
35.0-B-90	40	46	51	56	67	.584
32.0-B-90	42	47	52	57	67	.545
30.0-B-90	43	48	54	59	69	.556
28.0-B-90	40	46.5	55	63	70	.598
26.0-B-90	41	50	57	60	74	.461
32.0-B-70	27	40	46	55	60	.765
28.0-B-70	37	42	47	58	63	.705
32.0-A-70	27	41	47	59	70	.646
28.0-A-90	23	46	52	61.5	77	.470
35.0-A-70	28	41	44	57	68	.695
26.0-B-70	28	36	45	50	62	.791
35.0-A-90	27	46	51	60	70	.589
32.0-A-90	24	45	53	68	84	.740
30.0-A-90	28	47	55	67	75	.715
24.0-B-90	28	46	56	67	80	.502
22.0-B-90	28	42	58	60	74	.519
20.0-B-90	32	49	53	63	70	.723
18.0-B-90	39	47	51	60	68	.710
22.0-B-80	28	40	44	58	74	.502
22.0-B-70	28	40	46	57	70	.621
24.0-A-90	40	49	56	68	72	.552
26.0-A-90	29	47	53	65	72	.552

*SEE NOTES ON TABLE A-4

FIGURE A-4
NOZZLE SPRAY DEPOSITION DATA

* SEE NOTES ON TABLE A-4
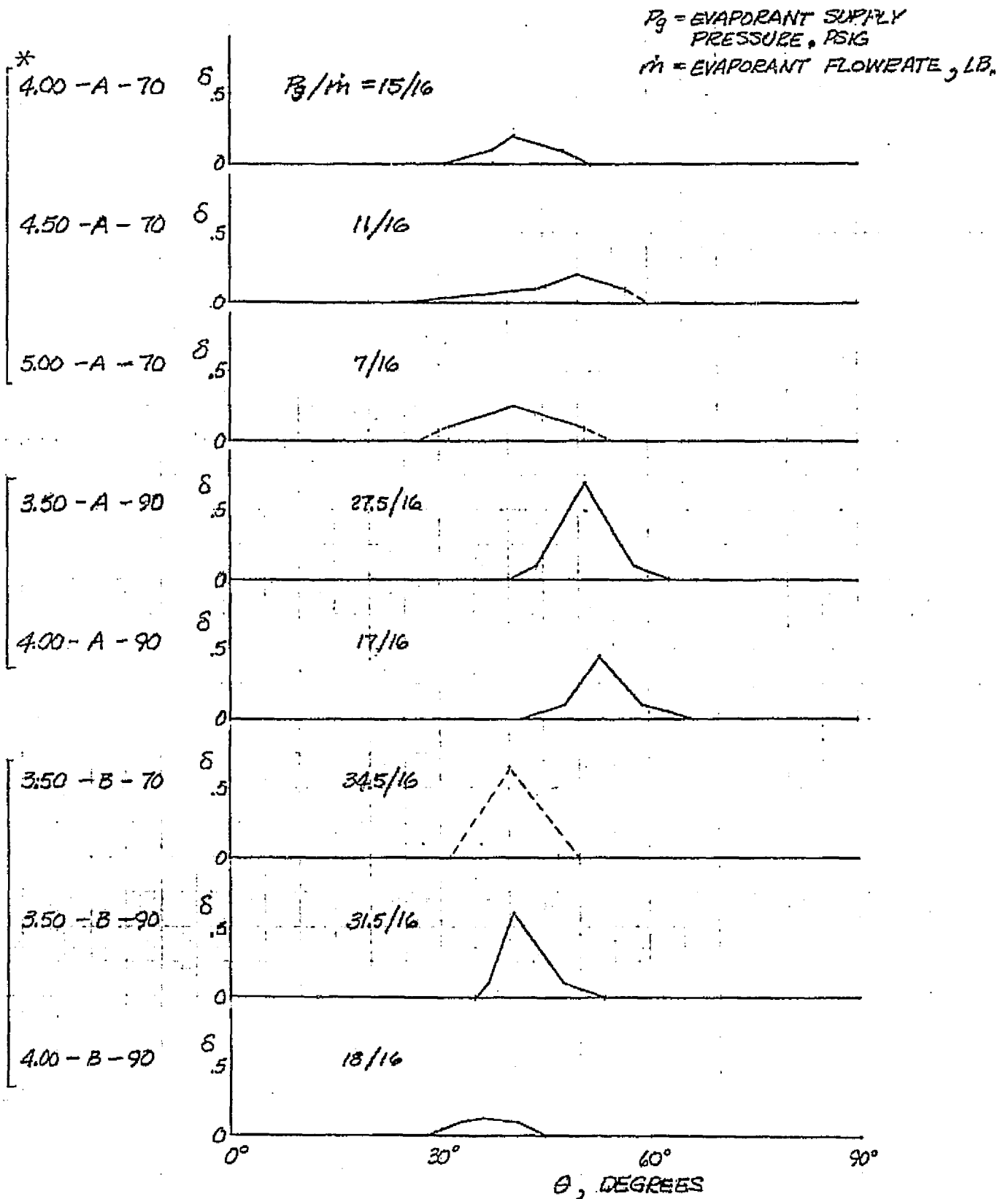
P_g = EVAPORANT SUPPLY PRESSURE, PSIG

$\dot{m}$ = EVAPORANT FLOWRATE, LB.

* 4.00 - A - 70	δ .5 / 0	$P_g/\dot{m}$ = 15/16
4.50 - A - 70	δ .5 / 0	11/16
5.00 - A - 70	δ .5 / 0	7/16
3.50 - A - 90	δ .5 / 0	27.5/16
4.00 - A - 90	δ .5 / 0	17/16
3.50 - B - 70	δ .5 / 0	34.5/16
3.50 - B - 90	δ .5 / 0	31.5/16
4.00 - B - 90	δ .5 / 0	18/16

θ, DEGREES

0°   30°   60°   90°

FIGURE A-4 cont'd
NOZZLE SPRAY DEPOSITION DATA

P_g = EVAPORANT SUPPLY PRESSURE, PSIG

$\dot{m}$ = EVAPORANT FLOWRATE, LB_m

3.50-W-70 $P_g/\dot{m}$ = 31/16
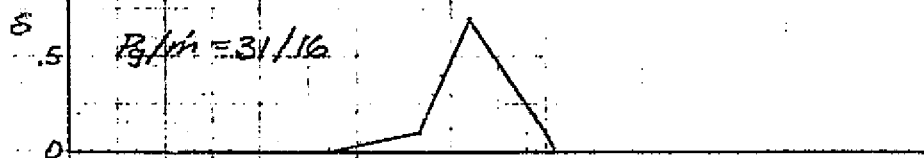
4.00-W-70   17.7/16

4.50-W-70   12.5/16
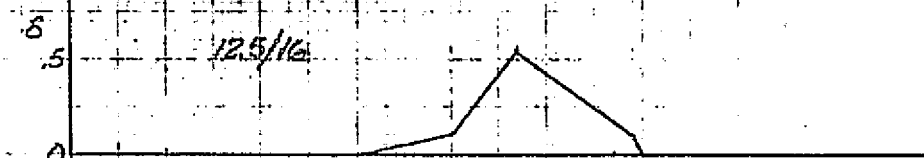
3.50-W-90   23.5/16
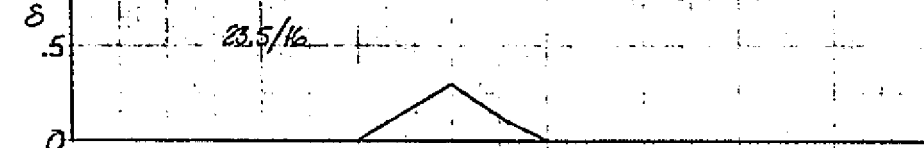
4.50-W-90   14.5/16
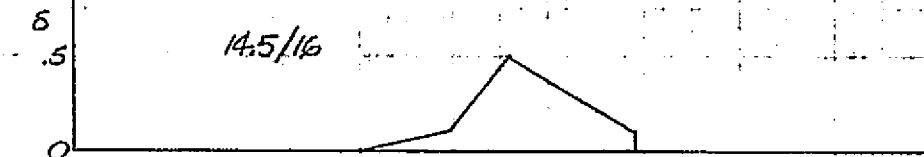
5.00-W-90   10.5/16

θ, DEGREES

FIGURE A-4 cont'd
NOZZLE SPRAY DEPOSITION DATA

P_g = EVAPORANT SUPPLY
PRESSURE PSIG
$\dot{m}$ = EVAPORANT FLOWRATE, LB_n

12.00-A-90 δ $P_g/\dot{m} = 34.5/50$

14.00-A-90 δ 24/50

16.00-A-90 δ 19/50

θ, DEGREES

50 LB/HR.

A-15

FIGURE A-4 cont'd
NOZZLE SPRAY DEPOSITION DATA

P_g = EVAPORANT SUPPLY PRESSURE PSIG
$\dot{m}$ = EVAPORANT FLOWRATE, LB_m

18.00-B-90 δ .5 $P_g/\dot{m}$ = 51/75

20.00-B-90 δ .5   44/75

22.00-B-90 δ .5   39/75

24.00-B-90 δ .5   35/75

26.00-B-90 δ .5   32.5/75

28.00-B-90 δ .5   31/75

30.00-B-90 δ .5   29.5/75

32.00-B-90 δ .5   29/75

35.00-B-90 δ .5   27/75

$0°$ $30°$ $60°$ $90°$
θ, DEGREES

75 LB/HR

A-16

FIGURE A-4 cont'd
NOZZLE SPRAY DEPOSITION DATA

P_g = EVAPORANT SUPPLY PRESSURE, PSIG
$\dot{m}$ = EVAPORANT FLOWRA LB$_m$

18.00-A-90 $P_g/\dot{m} = 50.4/75$

19.00-A-90   425/75

22.00-A-90   40/75

24.00-A-90   36.5/75

26.00-A-90   35.5/75

28.00-A-90   31/75

30.00-A-90   30/75

32.00-A-90   25/75

35.00-A-90   25/75

θ, DEGREES

75 lb/HR

FIGURE A-4 cont'd
NOZZLE SPRAY DEPOSITION DATA

P_g = EVAPORANT SUPPLY
PRESSURE, PSIG

$\dot{m}$ = EVAPORANT FLOWRATE, Lb_m

26.00 - A - 70   .5 $P_g/\dot{m}$ = 27/75

30.00 - A - 70   .5   23/75

32.00 - A - 70   .5   27.5/75

35.00 - A - 70   δ .5   26.5/75

26.00 - B - 70   δ .5   32.5/75

28.00 - B - 70   δ .5   30/75

30.00 - B - 70   δ .5   27.5/75 (18/64)

32.00 - B - 70   δ .5   25/75

35.00 - B - 70   δ .5   22.5/75

$0 \qquad 30° \qquad 60° \qquad 90°$

θ, DEGREES

75 $^{1b}/_{hr}$

A-18

FIGURE A-4 cont'd
NOZZLE SPRAY DEPOSITION DATA

P_g = EVAPORANT SUPPLY PRESS(
PSIG

$\dot{m}$ = EVAPORANT FLOWRATE, LB_m

22.00 - B - 80 δ .5 $P_g/\dot{m}$ = 39.5/75

24.00 - B - 80 δ .5   34.5/75

22.00 - B - 70 δ .5   37.5/75

26.00 - A - 70 δ .5   .27/75

30.00 - A - 70 δ .5   23/75

32.00 - A - 70 δ .5   27.5/75

35.00 - A - 70 δ .5   26.5/75

0   30°   60°   90°

θ, DEGREES

75 LB/HR

A-19

FIGURE A-5   COMPARISON OF EVAPORATOR DIMENSIONS FOR 16 lb/hr NOZZLES
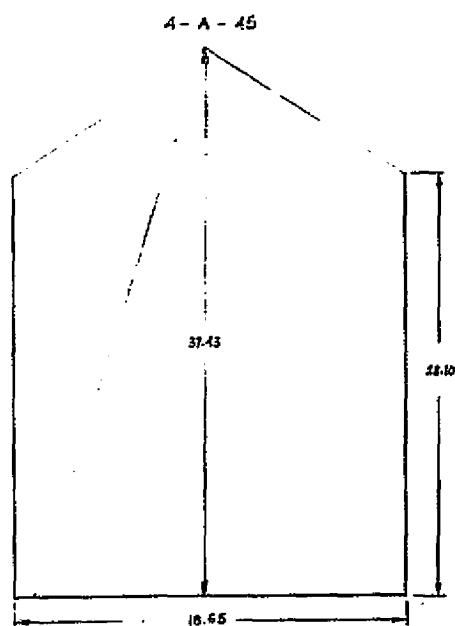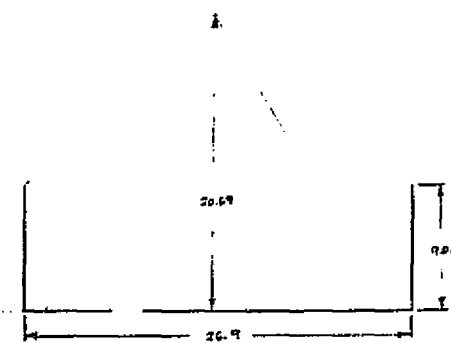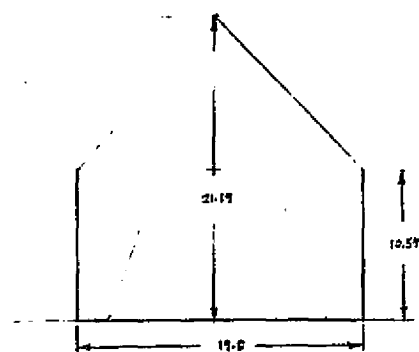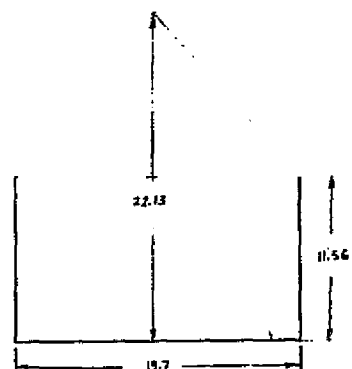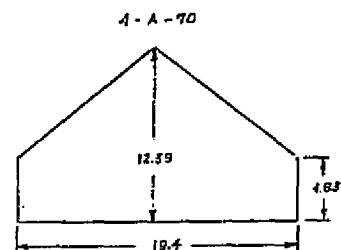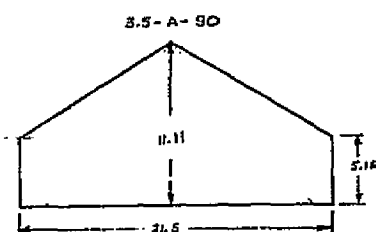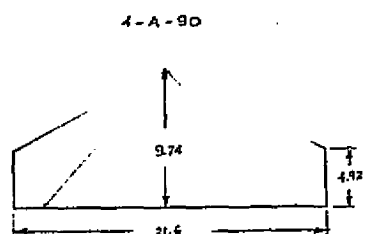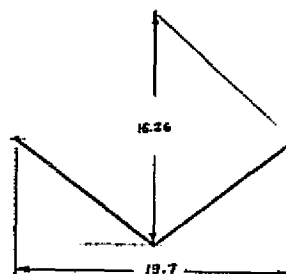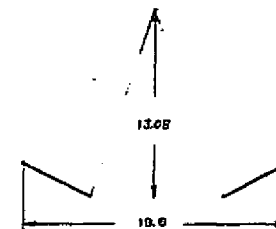
CONFIGURATION No. 1

4-A-90

3.5-A-90

4-A-70

4-A-45

4-B-90-1
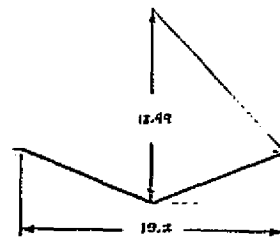
4-B-90-2
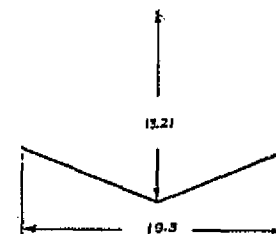
4-B-90-3
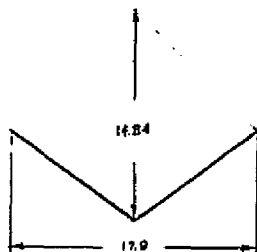
4-B-90-4

4-W-45

4-W-70

3.5-W-90

SCALE: 1" = 6" FOR 8 lb/hr-ft² SPRAY DENSITY

FIGURE A-6 COMPARISON OF EVAPORATOR DIMENSIONS FOR 16 lb/hr NOZZLES

CONFIGURATION No. 2

SCALE: 1" = 6" FOR 8 lb/hr-ft² SPRAY DENSITY

FIGURE A-9 COMPARISON OF EVAPORATOR DIMENSIONS FOR 16 lb/hr NOZZLES
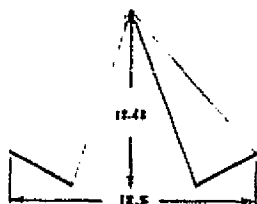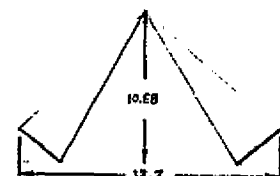
CONFIGURATION No. 5

FIGURE A-10 COMPARISON OF EVAPORATOR DIMENSIONS FOR 16 lb/hr NOZZLES

CONFIGURATION No. 6
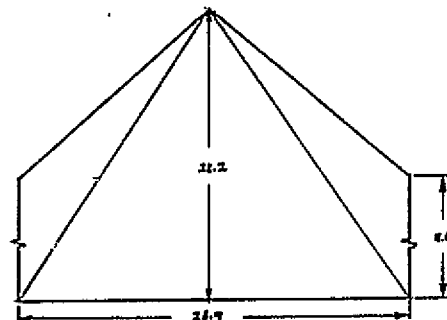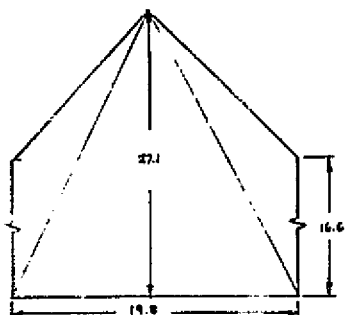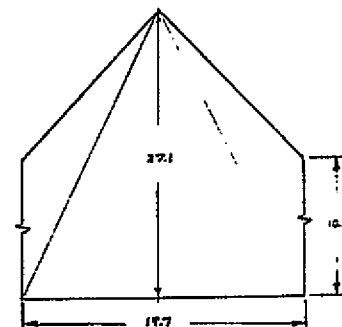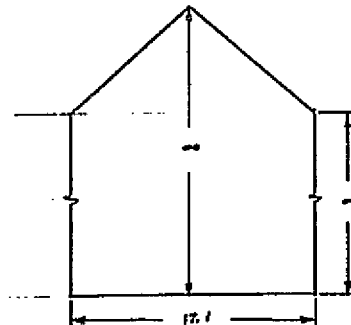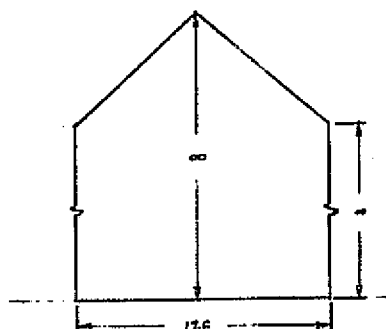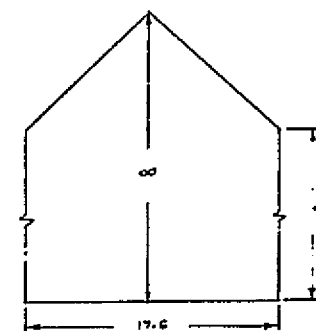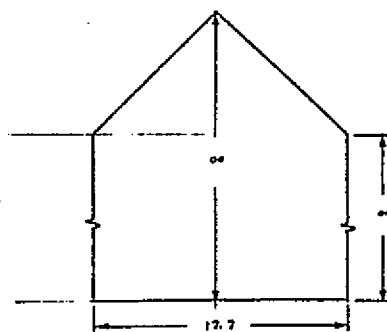
SCALE: 1" = 6" FOR 8 lb/hr-ft² SPRAY DENSITY

APPENDIX B
DROPLET SPRAY IMPACT/VAPORIZATION TESTS

1.0   INTRODUCTION AND SUMMARY

This report documents the droplet spray impact and vaporization tests performed as part of the Prototype 2 Flash Evaporator Program. These tests were performed in two segments: a brief initial series, completed in August of 1972, and a second series, completed in March of 1973. The initial tests were performed at an ambient pressure of 133 N/m^2 (1 mmHg), somewhat lower than the nominal flash evaporator operation pres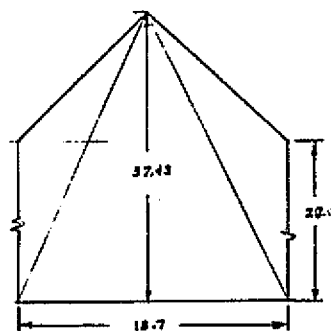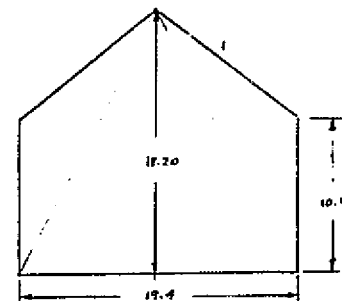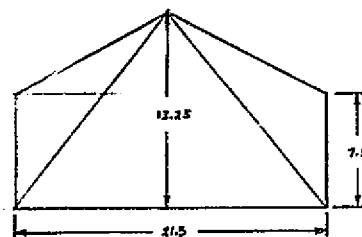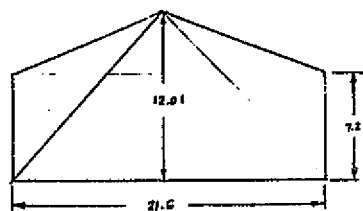sure of 506 n/m^2 (3.8 mmHg). Hence, the additional tests at more representative pressures were deemed necessary. This report deals primarily with the results of the tests comprising the second series.

The specific objectives of these tests were as follows:

o To observe, with the aid of high-speed photography, the impacts of droplets striking a target placed at various locations within the spray pattern produced by typical flash evaporator nozzle.

o To observe, again with the aid of high-speed photography, the subsequent droplet vaporization process.

o To make quantitative measurements of the superficial heat flux produced by the spray impact/vaporization process.

In the pursuit of these objectives, the parameters to be investigated included ambient pressure, surface temperature, spray impact angle, and annular/radial location in the spray. As the tests progressed, it became apparent that spray pattern information would be required for interpretation of the heat transfer results. Thus approximate pattern data were also obtained during the course of this study.

The body of this Appendix describes the experimental equipment and procedures, the test results, and the conclusions reached as a result of this test program. In addition, recommendations for further investigations of a phenomenological nature are presented.

The results of this study are summarized as follows:

o A variety of phenomena are present in the impact/ evaporation process. At any instant, sublimation, nucleate boiling, ice cap ejection, and mass agglomeration may be occuring simultaneously.

o However, the efficiency of the phase change process appears to deviate from 100% only under extreme conditions: i.e., surface temperatures sufficiently high to produce significant droplet bounce and splatter, or surface temperature sufficiently low, and pressure sufficiently high to cause surface flooding.

o Based upon spraying heat flux values inferred from target-transient response, it appears that droplet bounce/splatter becomes significant at surface temperature in excess of 339°K (150°F). A surface flooding boundary is postulated which allows heat fluxes in excess of 63.1 kw/m^2(20000 BTU/ft^2-hr) at a surface temperature of 277.5°K (40°F). Thus the range of 100%-efficient operating condition is quite wide.

o It is recommended that immediate future efforts concentrate on steady-state measurements of spray heat flux values, rather than additional studies of the

properties of the spray itself, such as droplet size and distribution. It is this heat transfer data which will be most useful in the optimization of flash evaporators designed around the current class of spray nozzle.

2.0   EXPERIMENTAL EQUIPMENT AND PROCEDURES

2.1   Apparatus

The test set-up is pictured in Figures B-1 and B-2 and shown
schematically in Figure B-3. As shown in Figure B-4, the target assembly con-
sisted of an instrumented 6061-T6 aluminum slug imbedded in a polycarbonate
body. The base of this slug contained a 100 watt electrical heater, retained
by a phenolic insulator. De-ionized water was supplied to the spray nozzle
at a nominal 30 psia, with flow control provided by a Parker-Hannifin solenoid
valve of the type used in the Prototype 2 Flash Evaporator. The spray nozzle
itself was the proven Delavan WDA-14 for the majority of the tests. Two special
order Delavan nozzles were used exclusively in spray pattern testing. The
target and nozzle/valve assemblies could be moved relative to one another to
vary the impact geometry, which is defined in Figure B-5.

This apparatus was mounted in a bell jar, which was evacuated
by the VSD Space Environment Simulation Chamber (SES) through a large gate
valve. In order to maintain a constant bell jar pressure and to protect
the vacuum system of the larger chamber, a LN_2 cooled cold trap was placed
within the bell jar and used to condense the evaporant gas during the test
runs.

2.2   Instrumentation

The target assembly was instrumented with thermocouples as shown
in Figure B-4. The output of the surface thermocouple, TC#1, was displayed on
an Esterline-Angus Millivolt recorder. In addition, the initial transient
response of TC#1 was recorded for a period of several seconds at the begin-
ning of each run using an X-Y Millivolt recorder. The remaining thermocouple
outputs were displayed on a Brown Multichannel Recorder. Bell jar pressure

B-4

NOZZLE/VALVE ASSEMBLY
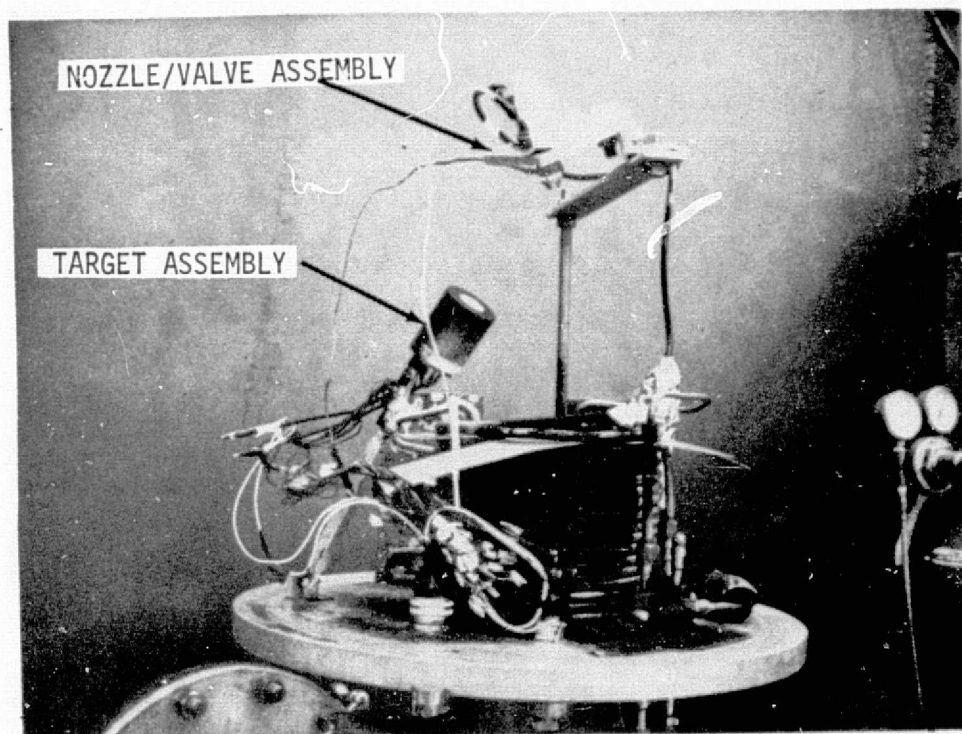
TARGET ASSEMBLY

FIGURE B-1 TEST SETUP

REDLAKE HIGH SPEED CAMERA

COLD TRAP
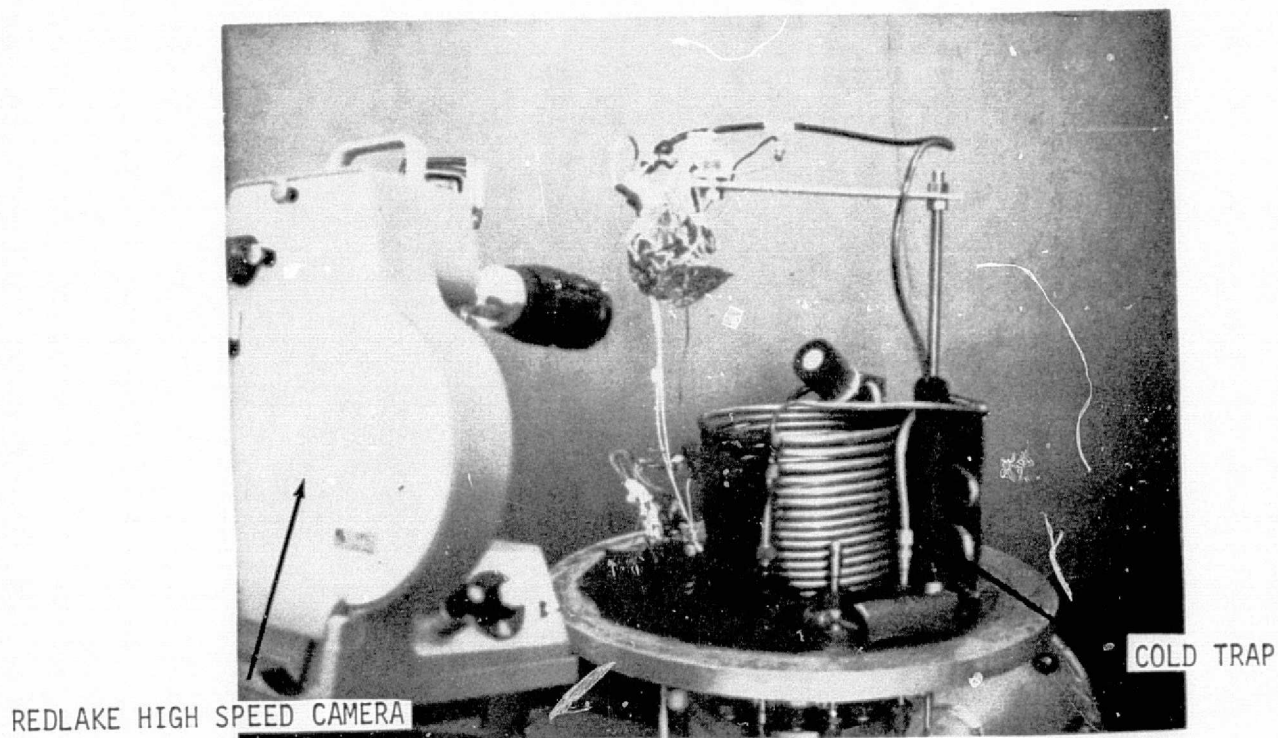
FIGURE B-2 TEST SETUP

ORIGINAL PAGE IS
OF POOR QUALITY

FIGURE B-3
TEST SCHEMATIC

2.0
DIA.

1.0
DIA.

0.125
TYP.

TIC #1

TIC #2

TIC #3

TIC #4

TIC #5

ALUMINUM TARGET

POLYCARBONATE SHIELD

TIC #6

TIC #9

TIC #10

TIC #7

2.0

1.0

100 WATT HEATER

0.5

TIC #8

PHENOLIC INSULATOR
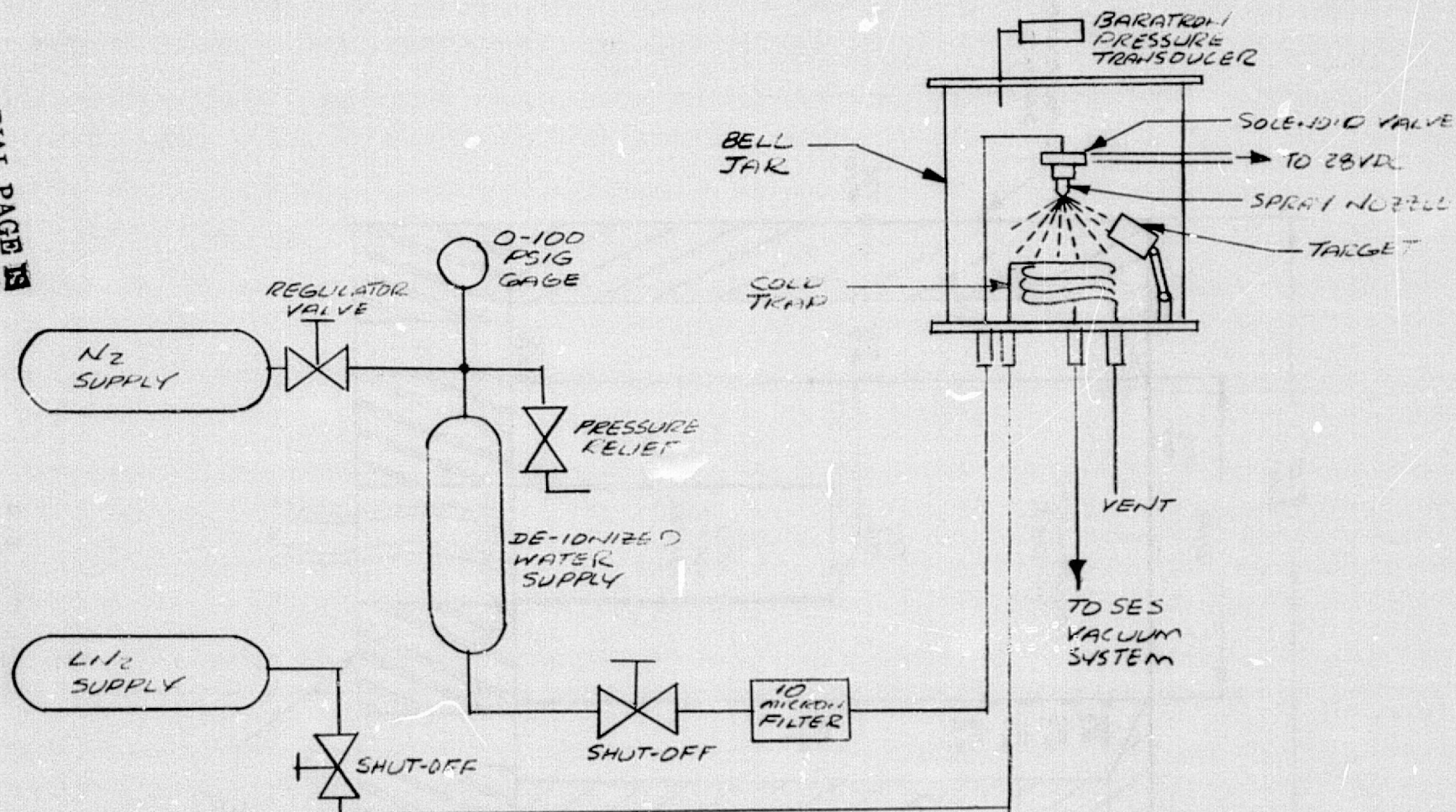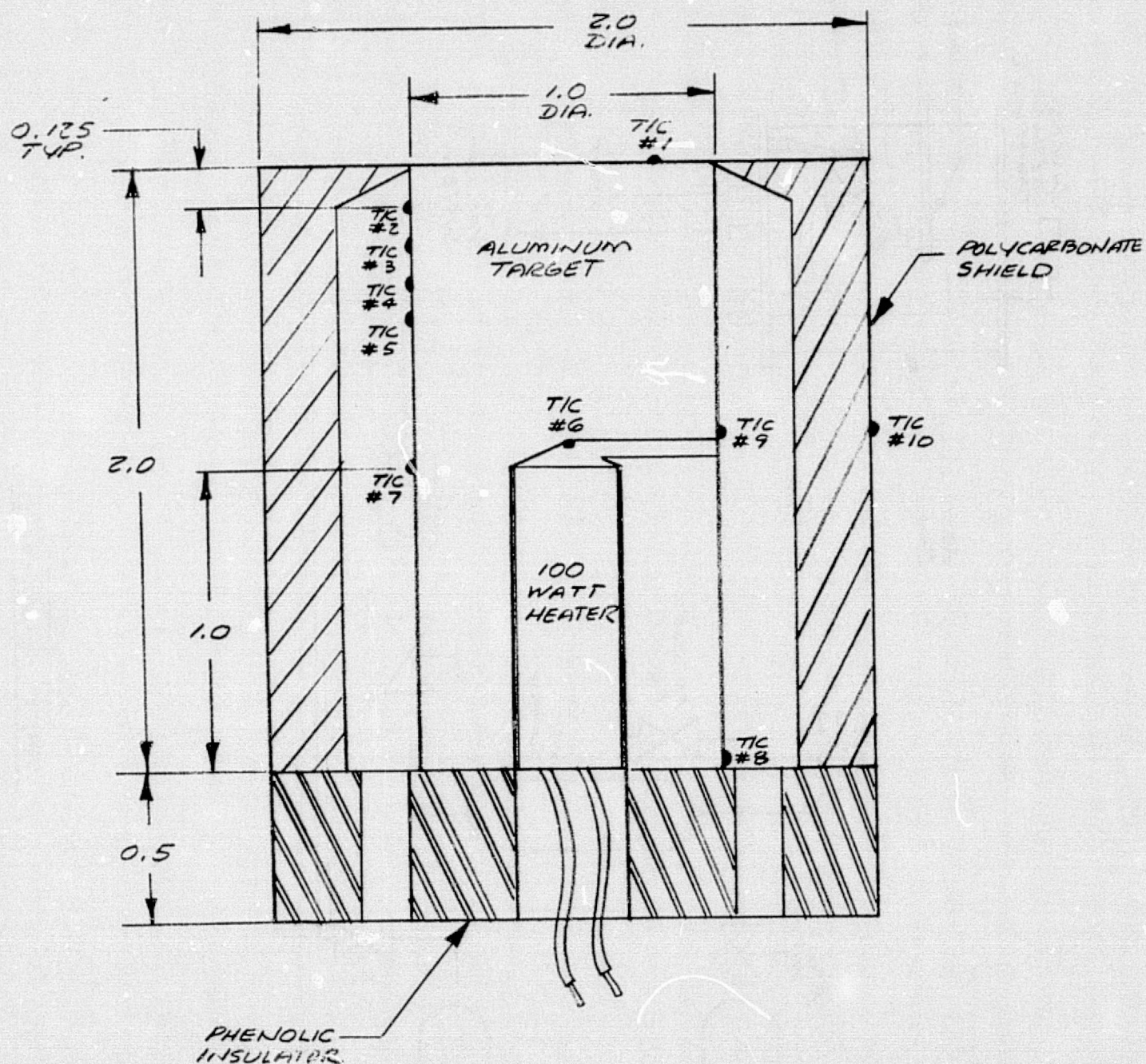
FIGURE B-4
TARGET ASSEMBLY
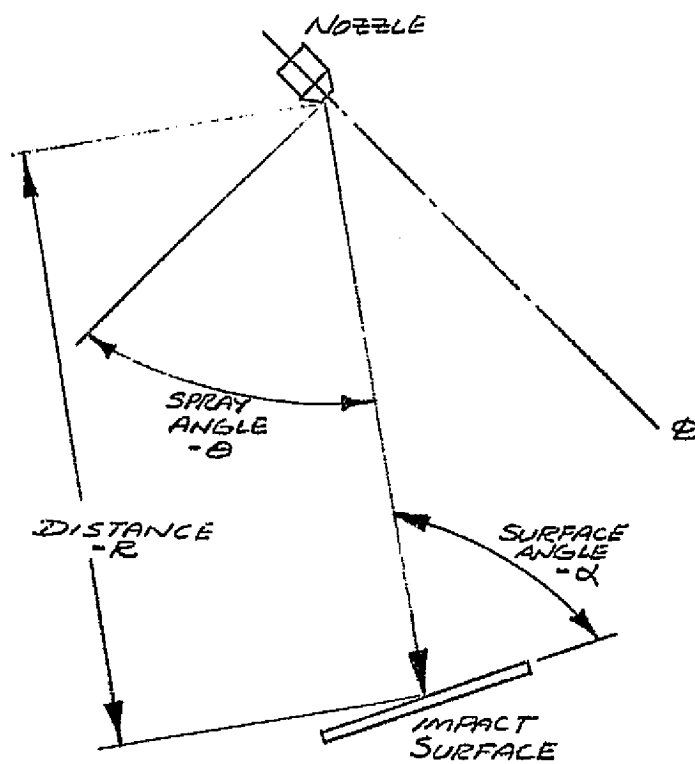
FIGURE B-5

IMPACT GEOMETRY

was measured by means of an MKS Baratron gage. The Baratron output was also recorded on the Esterline-Angus Millivolt Recorder.

High-speed photography was accomplished for selected test conditions using a Redlake Hycam Model 41-0004 camera. Film speeds ranging from 2000 to 10000 frames per second were employed at various times during the experiments. The film used was Kodak Tri-X, in roll lengths of 100, 200, and 400 feet depending on the film speed. Illumination was provided by four 1000 watt lamps, the position of which was refined during the course of the experiments to provide best illumination of the droplet input/vaporization process.

2.3   Procedure

The basic procedure followed for each test condition included these steps:

(1) Set-up desired test configuration, position camera and lights (if required).

(2) If required, shoot a short film leader at 100 frames per second to define scale.

(3) Evacuate bell jar and initiate LN_2 flow to the cold trap.

(4) Stabilize target at desired temperature and adjust bell jar pressure to the required value.

(5) In rapid sequence, initiate spray flow, X-Y recorder, lights, and camera (as required). After five seconds, turn off spray and lights.

(6) Bring bell jar to atmospheric pressure, disassemble and dry test fixture.

As noted, the spray was maintained for only a brief period of a few seconds. Originally, it was planned to spray until a steady-state temperature distribution was established in the target slug, so that the spraying heat flux could be inferred. However, the heat fluxes obtained were so large that a steady condition could not be established with the target/heater configuration utilized. Even with full heater power, the target surface cooled monotonically under all conditions of pressure and geometry and flooding of the surface eventually occurred. Thus a transient technique had to be adapted for purposes of heat flux measurement, and spraying time was limited to the duration required for photography and recording of the initial portion of the temperature transient. As an added benefit, this reduced the quantity of water accumulated in the bell jar and allowed a quicker dry-out between test points.

3.0 RESULTS AND DISCUSSION

The actual test conditions investigated are summarized in Table B-1, along with an indication of the length and nominal speed of the film taken, if any. A "map" of the initial target temperature/bell jar pressure conditions investigated for the WDA-14 nozzle spray is presented in Figure B-6. Results of the high speed photography and the surface temperature response measurements are summarized and discussed in the following paragraphs.

3.1 High-Speed Photography

For approximately half of the test condition, high speed films were obtained. All of these films display two common features: a great deal of droplet impact, rebound, and vaporization activity; and an absence of detail as to the size and shape of the incoming droplets. Because of the shallow depth of field associated with the high-magnification less, only an occasional incoming droplet was in focus. Considerable time and effort was expended in an attempt to improve the quality, but the final films still left much to be desired. The salient features of the various films are summarized in Table B-2, and this table is recommended for use as a guide in selecting films for detail study. Any or all of the film data can be obtained from the writer upon request.

TABLE B-1
SUMMARY OF EXPERIMENTAL CONDITIONS

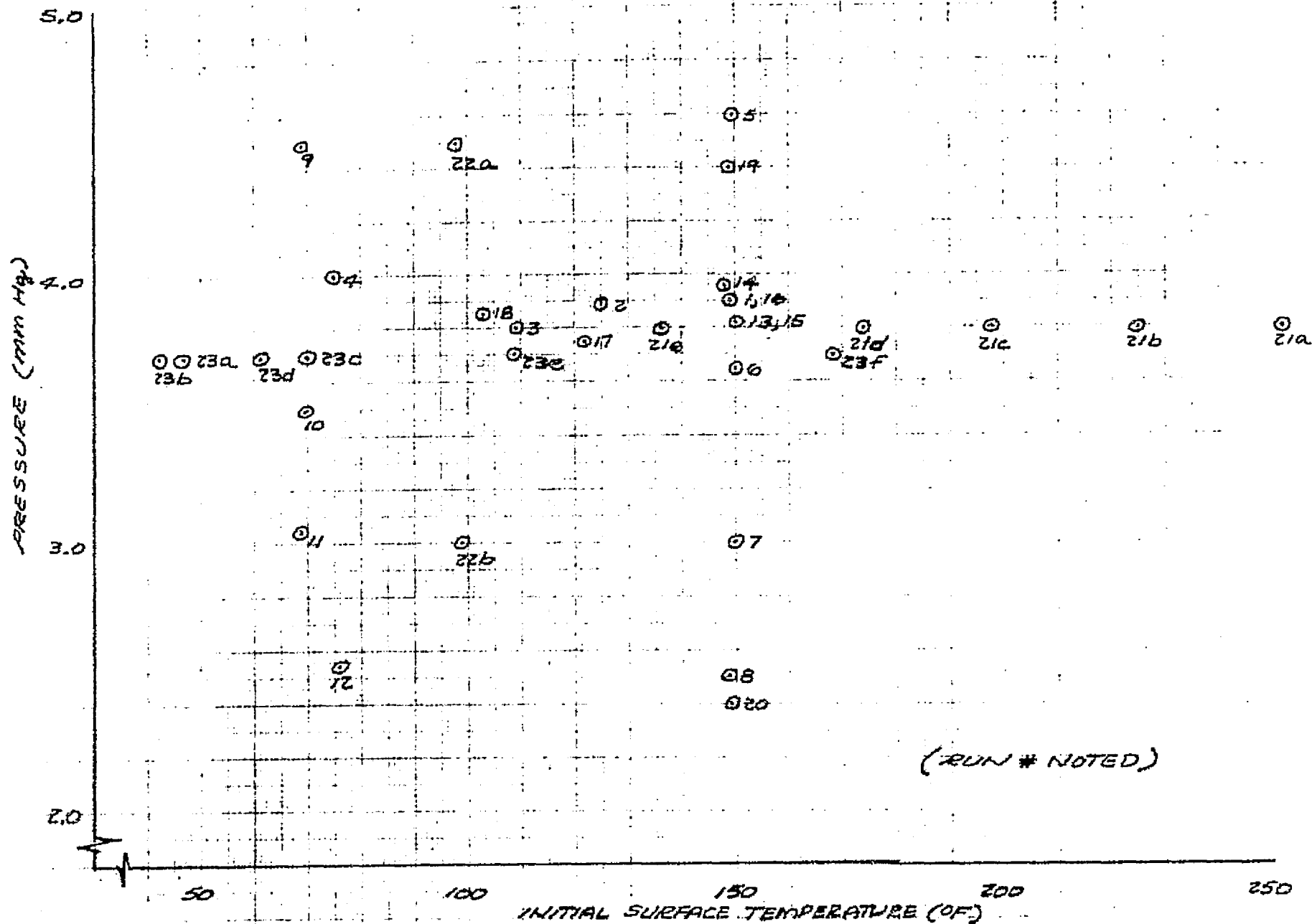| RUN #	PRESSURE (mmHg)	INITIAL TEMP (°F)	DISTANCE (IN.)	SPRAY ANGLE (DEG.)	SURFACE ANGLE (DEG.)	FILM LENGTH (FT.)
1	3.9	149	8.3	45	90	200
2	3.9	124	↑	↑	↑	200
3	3.8	109				100
4	4.0	75				↑
5	4.6	149				
6	3.6	150				
7	3.0	150				
8	2.5	149				
9	4.5	69				
10	3.5	70				
11	3.0	69	↓	↓		
12	2.55	76	8.3	45		
13	3.82	150	10.0	40		
14	3.95	148	10.0	50		
15	3.8	150	4.87	45		
16	3.9	149	9.75	↑		
17	3.75	122	↑			
18	3.85	103				
19	4.4	149	↓			↓
20	2.4	149	9.75			100
21a	3.8	252	8.3			---
21b	↑	225	↑			---
21c		198				---
21d	↓	174				---
21e	3.8	136				---
22a	4.5	98	↓			---
22b	3.0	99	8.3			---
23a	3.7	47	9.75			---
23b	↑	42	↑			---
23c		70				---
23d		61				---
23e		109				---
23f	3.7	168	9.75	45	90	---

FIGURE B-6
PRESSURE/TEMPERATURE CONDITIONS INVESTIGATED

TABLE B-2
SUMMARY OF HIGH SPEED FILM RESULTS

RUN #	ACTUAL FILM SPEED (FRAMES/SEC)	DESCRIPTION
1	4500	Clear impact about half way through roll. Ice cap ejected near end. Clear splattering near end. Good example of high surface temperature phenomena. Slightly underexposed.
2	4600	Exposure better than Run #1. Excellent incoming drop just over half way through. Good impact/splatter results at two-thirds through. Parallel incoming droplets near end.
3	5300	Not much activity. Surface focus poor. Good incoming droplet about half way through. Droplet diameter estimated at 0.005 inches, velocity at 120 ft/sec.
4	5700	Clear ice cap ejection near beginning. Good activity, but less splattering than high temperature cases. Sticking impact about two-thirds through.
5	5400	Condition near triple point. Good exposure, much liquid accumulation, some apparent nucleate boiling.
6	5500	Similar to Run #1, but less overall activity.

RUN #	ACTUAL FILM SPEED (FRAMES/SEC)	DESCRIPTION
7	5500	Much less bounce/splatter than other 150°F runs. Most incoming droplets stick.
8	6000	Mixed splattering/sticking. Good splattering results about two-thirds through. Slightly underexposed.
9	6100	Condition near triple point. Much splashing on impact, Agglomeration of liquid, some post-impact boiling.
10	6000	Underexposed, minimal activity.
11	6300	Poor surface illumination/focus. Generally not much activity. Good incoming droplet about two-thirds through.
12	6000	Good exposure, marginal focus. Ice particle stands on edge, falls over, and sublimes. More ice present than for high temperature case at this pressure (2.5 mm Hg).
13	6000	Spray missed target during film run.

TABLE B-2 (CONTINUED)

RUN #	ACTUAL FILM SPEED (FRAMES/SEC)	DESCRIPTION
14	3800	Switched to larger FOV lens to observe vaporization. Bad positioning, minimal activity, some splattering.
15	3800	Film accidentally exposed.
16	3800	Photography adequate. Some splattering, gyration of impacted droplets observed.
17	3200	Droplets visibly adhering to the surface, occasionally ejected. Good overall view of phenomena.
18	3200	Impacting droplets visible and migrating on surface. Not as clear as Run #17. Agglomeration visible about one-third through.
19	3200	Poor focus. Migration of droplets resembles the Leidenfrost phenomenon (stable film boiling.)
20	3200	Underexposed, poor focus. Not much activity.

3.2   Surface Temperature Response

When the spray is initiated, the short-time response of the target surface is of interest since it reflects the spraying heat flux corresponding to the initial surface temperature. Typical, measured surface temperature time histories are shown in Figure B-7. The initial damped oscillation present in the traces is a characteristic of the instrumentation system, while the small perturbations are interpreted as the response of the thermocouple to droplet "hits" on or near it. The general downward trend in surface temperature represents the overall response of the target front-face to the spray.

The data from Run #17 are presented in Figure B-7(a). For that case, the initial surface temperature was 128^OF and a drop of 36^OF was observed during the initial five seconds of spraying. Results of Run #23d are shown in FigureB-7(b). There, the initial temperature was 70^OF and a drop of 15^OF was experienced during the recording period. Surface response for an initial temperature of 54^OF (Run #23b) is shown in Figure B-7(c).This value was representative of the lowest attainable with the apparatus, and a drop of 7^OF was observed during the observation time. The interpretation of these results in terms of spray heat flux is discussed in detail in Section 4.0 of this Appendix.
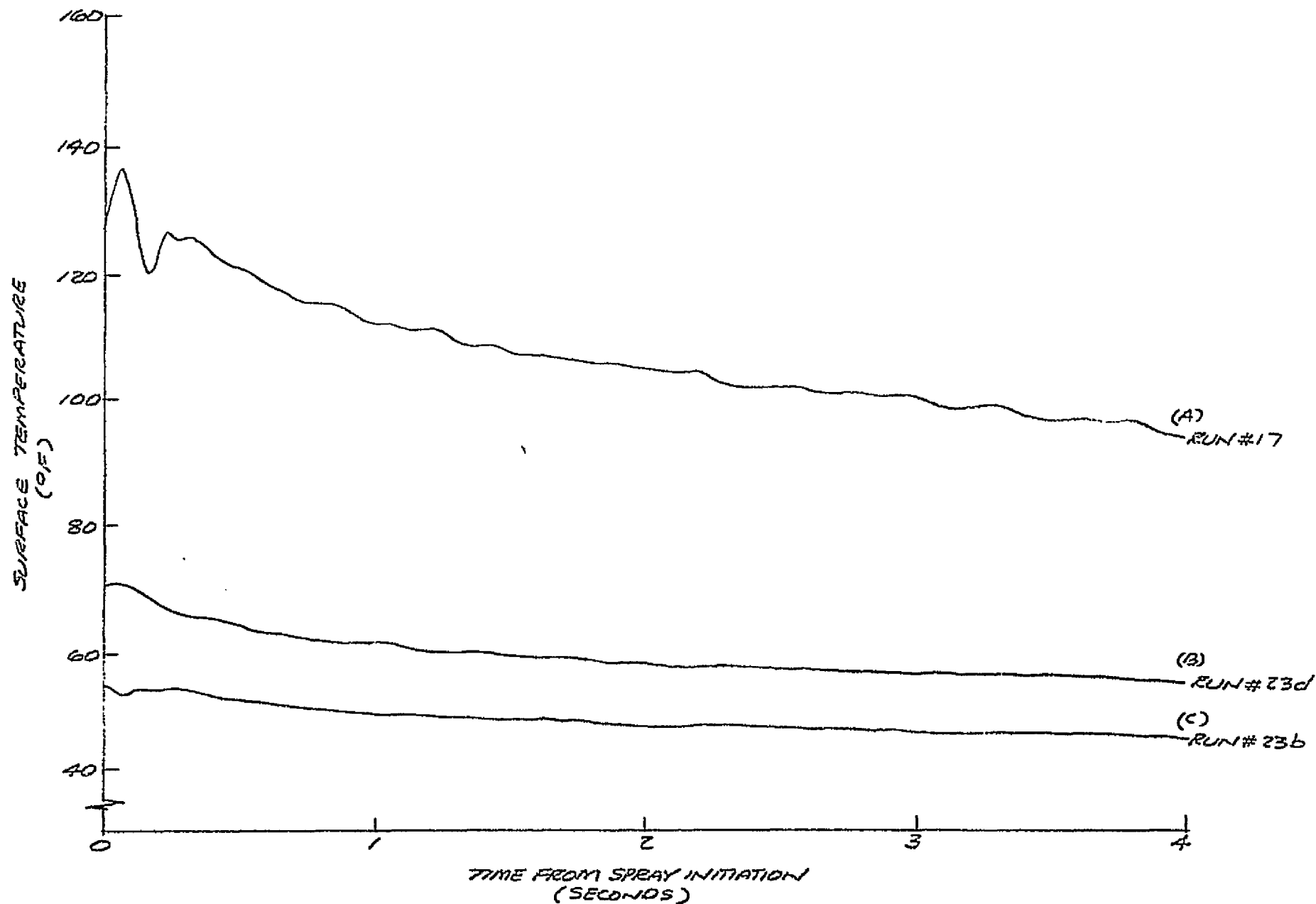
FIGURE B-7

SURFACE TEMPERATURE-TIME HISTORIES

4.0 HEAT TRANSFER DATA ANALYSIS

As mentioned earlier in this report, it was originally intended to infer spraying heat flux values by means of a steady-state energy balance at the target surface. However, the rather large heat flux levels obtained prevented establishment of a steady condition. Thus a transient data analysis technique was employed, and the results are described in the following paragraphs.

4.1 Surface Response Model

The target was a 1" diameter by 2" long slug, and the first inclination is to model the front surface response as that of a semi-infinite solid exposed to a constant heat flux. Schneider (Reference 8) presents the analytical solution and working curves for this problem. The front surface response is given by:

$$\frac{k}{2q\sqrt{\alpha\theta}} \ (T-T_0) = \frac{1}{\sqrt{\pi}}$$

where:

k = material thermal conductivity (BTU/hr-ft-°F)

q = heat flux (BTU/hr-ft^2-°F)

T = instantaneous surface temperature (°F)

T_0 = initial surface temperature (°F)

α = material thermal diffusivity (ft^2/hr)

θ = time from exposure (hr)

Solving for the heat flux:

$$q = \frac{k}{2} \sqrt{\frac{\pi}{\alpha\theta}} \ (T-T_0)$$

For aluminum:

$$k = 102 \text{ BTU/hr-ft-}°\text{F}$$

$$\alpha = 2.33 \text{ Ft}^2/\text{hr}$$

Substituting and manipulating units:

$$q = 3230 \frac{T-T_0}{\sqrt{\theta}} \quad \text{BTU/ft}^2\text{-hr}$$

where θ is in seconds. This is the basic equation used in the computation of the spraying heat flux.

In order to effectively utilize this semi-infinite solid model, it is necessary to define its limitations. Referring again to Schneider (Reference 8), it is found that the front face of a semi-infinite plate (of finite thickness) generally responds as that of a semi-infinite solid (of infinite thickness) for Fourier numbers less than 0.1:

$$Fo = \frac{\alpha\theta}{\ell^2} < 0.1$$

where ℓ is the plate thickness. For the 2" deep aluminum target of these tests:

$$\theta_{Fo = 0.1} = \frac{(0.1)\left(\frac{2}{12}\right)^2 (3600)}{(2.83)} \quad \text{seconds} = 3.53 \text{ seconds}$$

Thus effects of finite slab thickness would be expected to be present in the front face data after three to four seconds. In order to provide some margin against this limitation, data from the first two seconds of spraying were used in the heat flux calculations.

A second source of error is found in three-dimensional effects. The target is actually a cylinder with an insulated side wall, and the imperfection of the insulation will lead to some radial heat loss. However, the

maximum temperature change observed in two seconds was on the order of 30°F, and if it is postulated that the insulation remains at the initial temperature while the slab temperature changes by this amount, the radial conduction loss would be

$$q_{radial} \approx k_{insulator} \frac{\Delta T}{\ell_{insulator}/2}$$

Here:

$$k_{insulator} \quad = \quad 0.1 \text{ BTU/hr-ft-°F}$$

$$\ell_{insulator} \quad = \quad 0.25 \text{ inches}$$

$$q_{radial} \quad = \quad \frac{(0.1)(30)}{\frac{.25}{12}} \quad = \quad 144 \text{ BTU/ft}^2\text{-hr}$$

Since the measured spray heat flux values were on the order of tens of thousands of BTU/ft-hr, this loss is negligible.

Note that the spraying heat flux is directly proportional to the temperature change during the measurement period and hence will have, at the minimum, the uncertainty of that measurement. Based upon the estimated assembly of the thermocouples and recording equipment, it is believed that the temperature measurements had at best ± 1°F accuracy. The corresponding uncertainty is calculated as follows:

$$\Delta q \quad = \quad \frac{3230}{\sqrt{\theta}} \quad \Delta(T-T_0)$$

$$= \quad \frac{3230}{\sqrt{2}} \quad (1)$$

$$\Delta q \quad = \quad 2340 \text{ BTU/ft}^2\text{-hr}$$

As the results of the following paragraphs will illustrate, this absolute uncertainty can represent a 10% to 30% uncertainty in the computed spraying heat flux value.

4.2   Computed Heat Flux Data

Heat flux values computed using the above technique are summarized in Table B-3. The parametric behavior of these data is discussed in the following paragraphs.

The variation of heat flux with mean surface temperature is shown in Figures B-8 and B-9, for a nominal pressure of 3.8 mm Hg. The uncertainty of each data point is indicated along with a curve following the trend of the data. The data of Figure B-8 correspond to a target-to-nozzle distance of 8.3 inches, while the data of Figure B-9 are for a distance of 9.75 inches. The greater spray intensity of the closer location is seen to produce the higher heat flux level expected in the absence of flooding. In both cases, the data are seen to display a downward trend in heat flux as the surface temperature exceeds 100°F. This trend is due to the increased bounce and splattering (decreased efficiency) brought about by vaporization at the droplet/target surface interface. Such film boiling phenomenon would normally be expected at surface-to-saturation temperature excesses on the order of 80°F (Reference 9), so this result is not surprising. Thus some loss in efficiency can be expected in areas where the evaporator surface exceeds 100°F, and this loss increases rapidly with temperature as 150°F is exceeded. The slight low temperature downward trend of the data of Figure B-9 is attributed to the onset of surface flooding, which will be discussed in Section 4.3.

It is interesting to compare the relative magnitudes of the maximum heat flux values shown in Figures B-8 and B-9. At the low temperature

TABLE B-3
COMPUTED SPRAY HEAT FLUX VALUES

| RUN #	PRESSURE (mmHg)	TEMPERATURE (^{0}F)	HEAT FLUX (BTU/FT^2-HR)
1	3.9	149	35500
2	3.9	124	32300
3	3.8	109	38800
4	4.0	74	46800
5	4.6	149	68100
6	3.6	150	42000
7	3.0	150	41100
8	2.5	149	43000
9	4.5	69	35000
10	3.5	70	38800
11	3.0	69	40000
12	2.55	76	42900
13	3.82	150	45200
14	3.95	148	35600
15	3.8	150	116000
16	3.9	149	35600
17	3.75	122	38800
18	3.85	103	38800
19	4.4	149	67000
20	2.4	149	58000
21a	3.8	252	14500
21b		225	17808
21c		198	33900
21d		174	38800
21e	3.8	136	38800
22a	4.5	98	59400
22b	3.0	99	48900
23a	3.7	47	29100
23b		42	29100
23c		70	29100
23d		61	32300
23e		109	32300
23f	3.7	168	13600
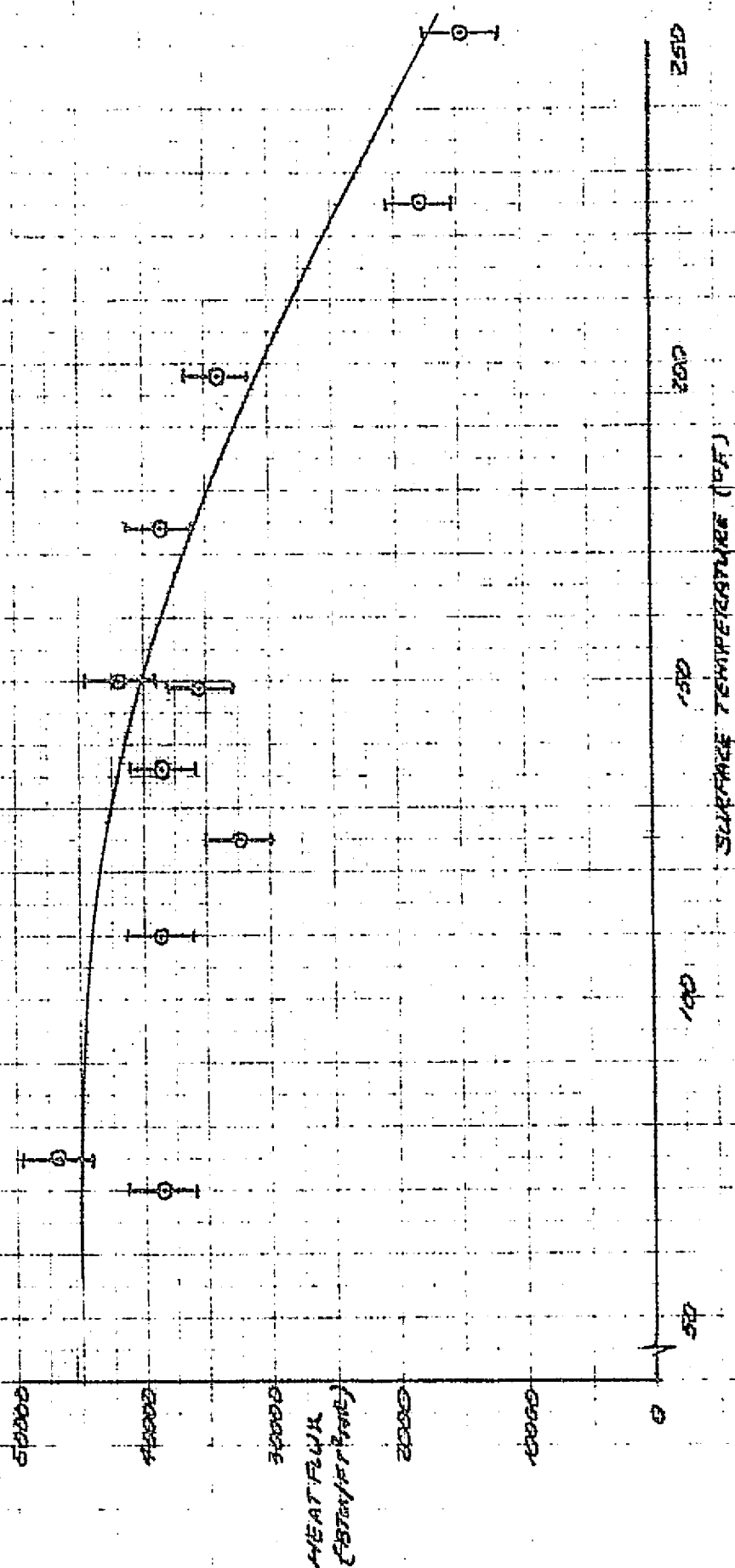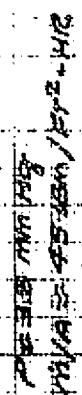
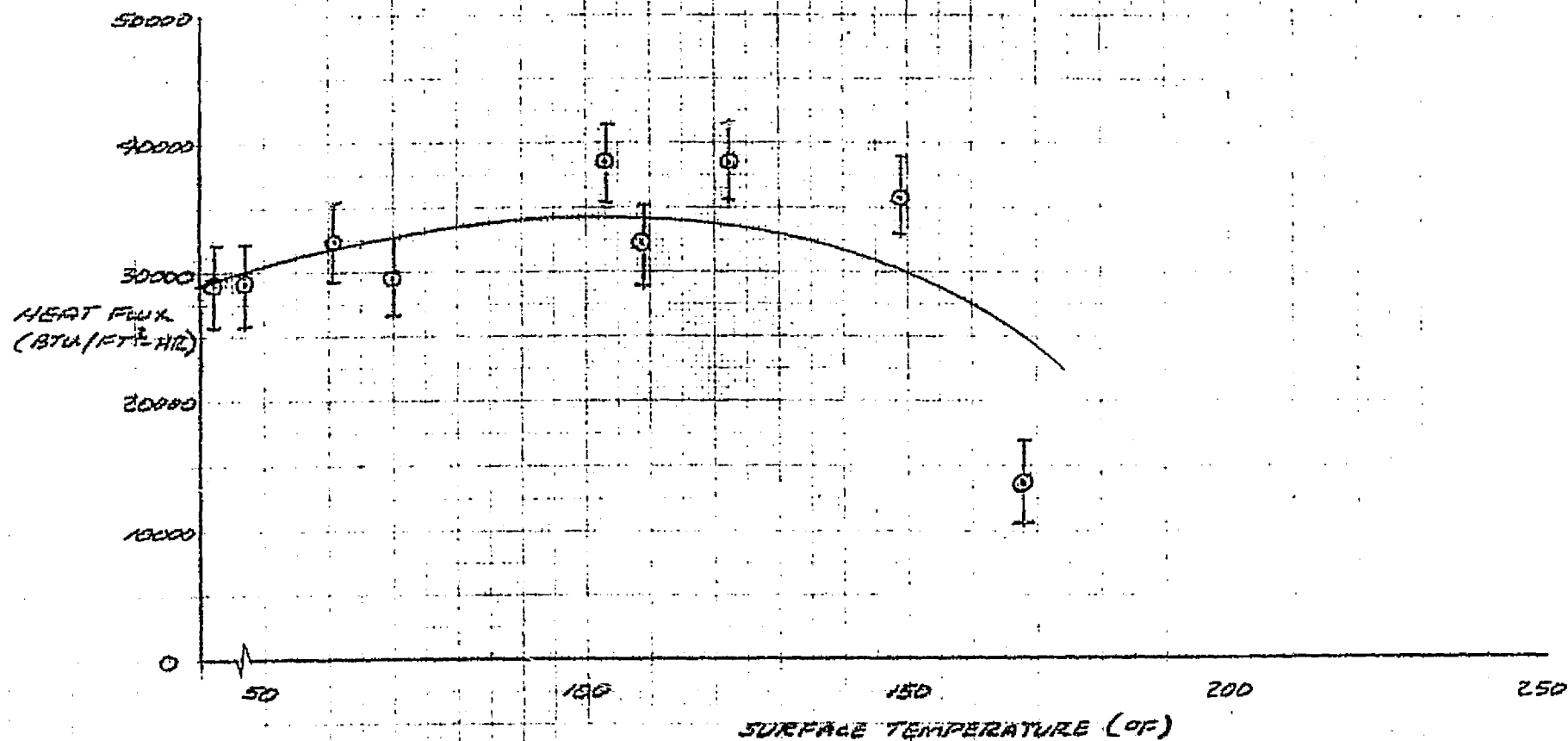FIGURE B-8

SPRAY HEAT FLUX VS SURFACE TEMPERATURE

FIGURE B-9
SPRAY HEAT FLUX VS SURFACE TEMPERATURE

B-26

limit, the Figure B-8 (8.3") data indicate a heat flux of 45,000 BTU/ft^2-hr. while the Figure B-9 (9.75") data indicate a nominal flux of 33,000 BTU/ft^2-hr. Thus the corresponding local mass fluxes (assuming $\sim$ 1000 BTU/lbm) are 45 lbm/ft^2-hr and 33 lbm/ft^2-hr, respectively. Since the mass distribution in the spray cone should be source-like, the ratio of mass fluxes at the same angular position and two different radial positions should have an inverse square dependence on radius:

$$\left.\frac{\dot{m}_1}{\dot{m}_2}\right| = \frac{r_2^{\,2}}{r_1^{\,2}} = \left(\frac{9.75}{8.3}\right)^2 = 1.38$$

THEORETICAL

The measured mass flux/heat flux ratio is:

$$\left.\frac{\dot{m}_1}{\dot{m}_2}\right|_{\text{MEASURED}} = \frac{q_1}{q_2} = \frac{45,000}{33,000} = 1.36$$

so that the source flow behavior of the spray can be considered verified in the light of the uncertainty of the present data.

The effect of pressure on spray heat flux in a fixed geometry is shown in Figure B-10. Data points for various surface temperatures are indicated, along with their associated uncertainty. There appears to be no trend in terms of surface temperature effects, and a slight, downward trend appears as the triple point is approached. It is therefore concluded that the efficiency of the spray heat transfer process is not significantly effected by pressures ranging from 2.5mm to just below the triple point.

The effect of angular position in the spray is illustrated by the results of Runs #13, #14, and #16, as shown in Figure B-11. For all three
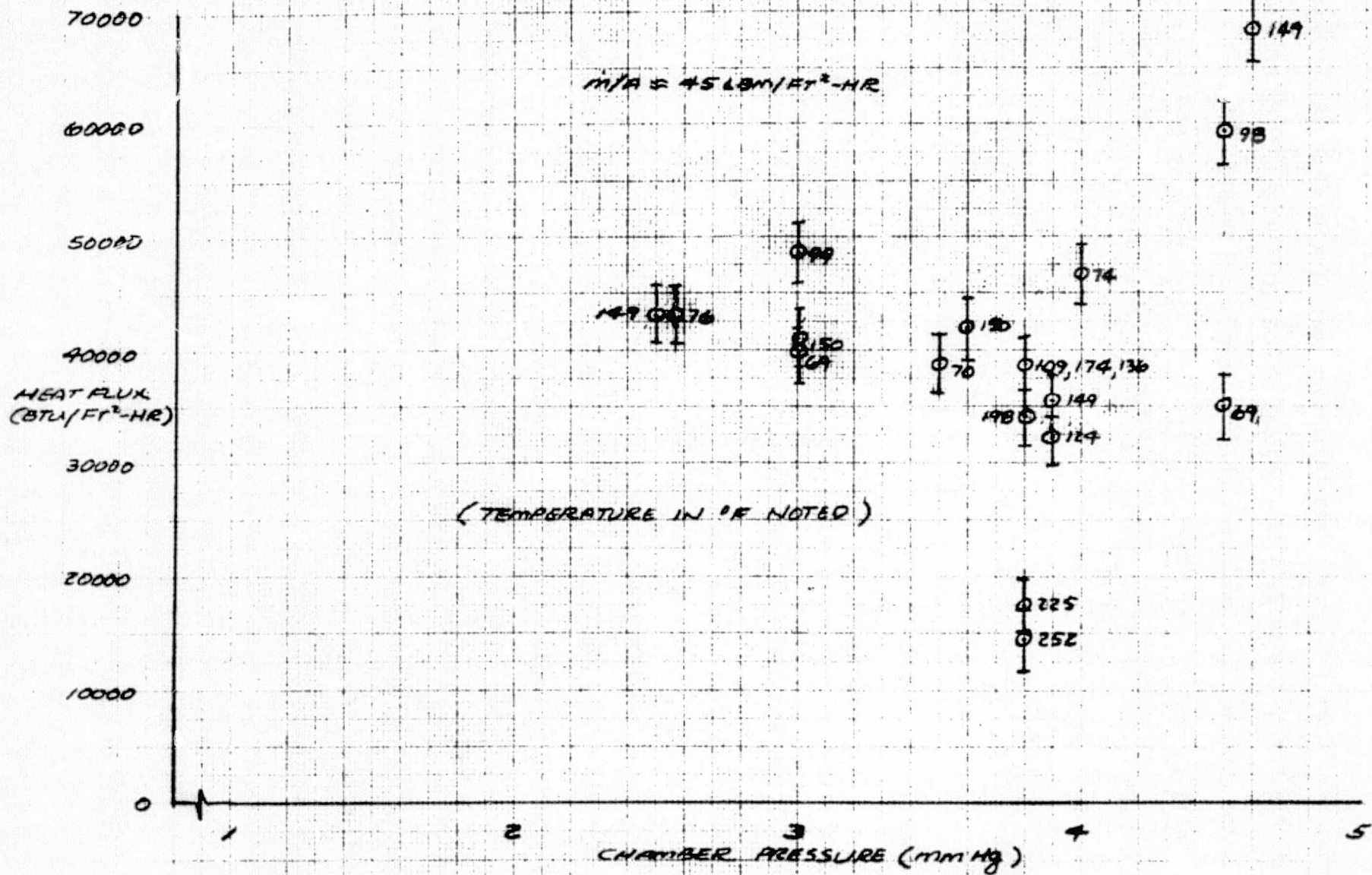
B-27

FIGURE B-10
SPRAY HEAT FLUX VS AMBIENT PRESSURE

$\dot{m}/A \approx 33000$ LBM/FT^2-HR
$T_{SURFACE} \approx 750°F$

MEASURED
SPRAY BAND
(APPENDIX A)

HEAT FLUX
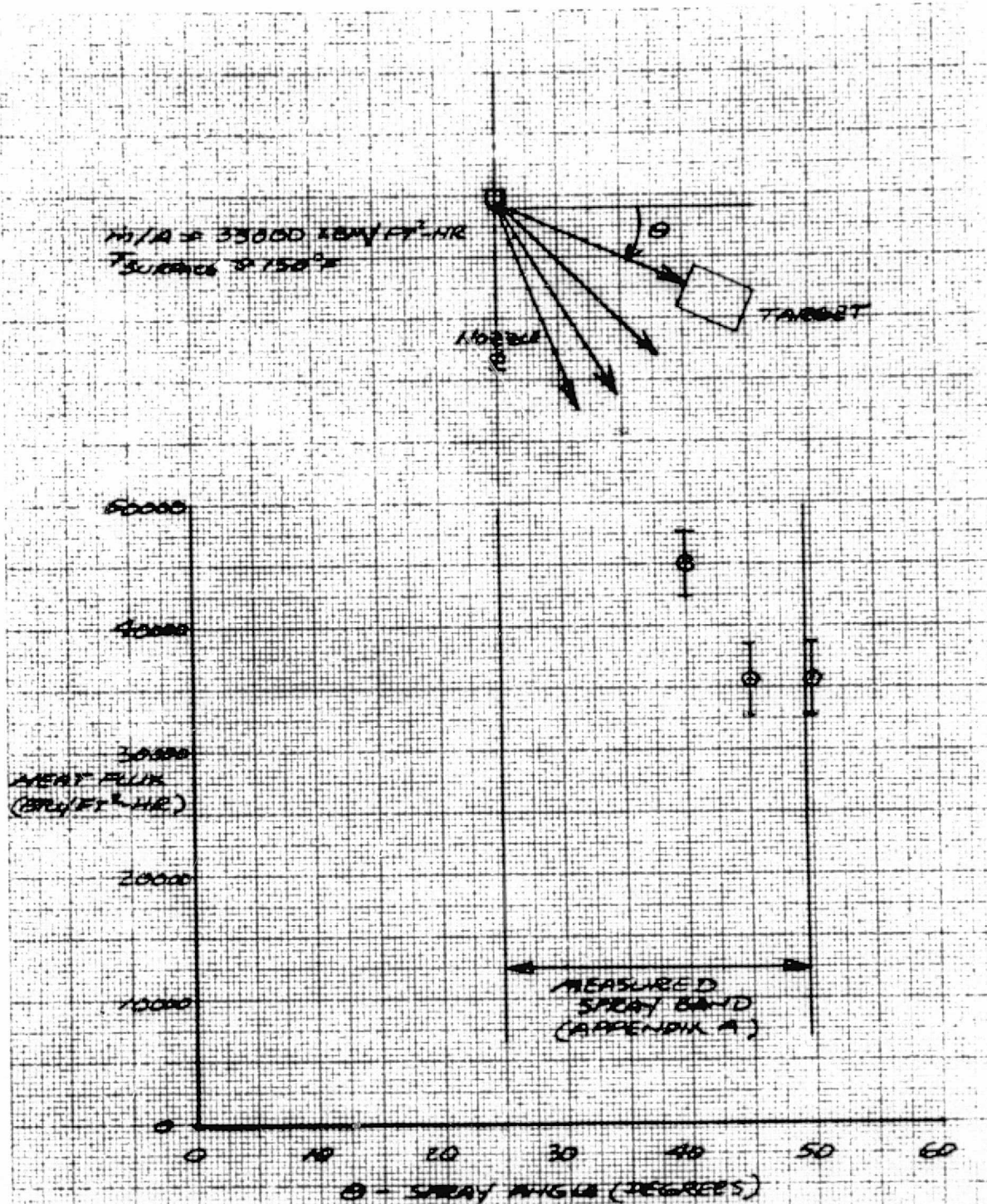(BTU/FT^2-HR)

θ = SPRAY ANGLE (DEGREES)

FIGURE B-11

SPRAY HEAT FLUX VS ANGULAR POSITION

runs, the radial distance was 9.75 inches and the target was normal to the ray. The outer angular location (40°) displayed a somewhat higher heat flux than the 45° and 50° locations. This effect is explained by the spray pattern data of Section 4.0. For the WDA-14 nozzle at a 3.8 mm back pressure, the outer and inner boundaries of the spray were found to be 25° and 50°, while the maximum spray intensity occurred at 37°. Thus the 40° data point corresponds to near-maximum spray intensity, while the 45° and 50° points are toward the inner edge of the spray. It is interesting to note that relatively high fluxes were measured at the very edge of the spray, while in some abortive runs the target was placed just outside the spray and recorded no heat transfer.

4.3   Preliminary Flooding Boundary

Surface flooding is an extremely important constraint in flash evaporator design : if the spray mass flux exceeds a critical value, an incident droplet will fail to evaporate before another strikes the same spot. Water then accumulates and the device efficiency decreases. The heat flux corresponding to this mass flux is then the maximum attainable, and defines the minimum heat exchanger surface area. This flooding phenomenon is obviously surface temperature dependent and occurs even when the heat exchanger core is capable of transferring the equivalent or greater heat fluxes.

Three pieces of information which bear upon the flooding phenomenon were obtained in this study : the data of Figure B-8, which indicate no flooding at a temperature of 50°F and a flux of 45,000 BTU/ft^2-hr; the data of Figure B-9, which indicate incipient flooding at a temperature of 40°F and a flux of 33,000 BTU/ft^2-hr; and the results of Run #15 (R = 4.87 inches), which indicate no flooding at a temperature of 129°F and a flux of 116,000 BTU/ft^2-hr. In addition, it is obvious that flooding will occur at essentially zero heat

flux when the surface temperature is at the saturation value of 29°F (3.8 mm Hg). These data are plotted in Figure B-12, with the uncertainty indicated. If it is assumed that the incipient flooding point and its associated uncertainty define the flooding boundary, the indicated band results. The non-flooding data points do fall outside this boundary, as the results are self consistent. This boundary is preliminary, but use of it should be conservative. Further definition of this boundary should be a major objective of future spray testing and the uncertainty associated with the transient measurement technique strongly recommends adoption of a steady-state technique for such future tests.
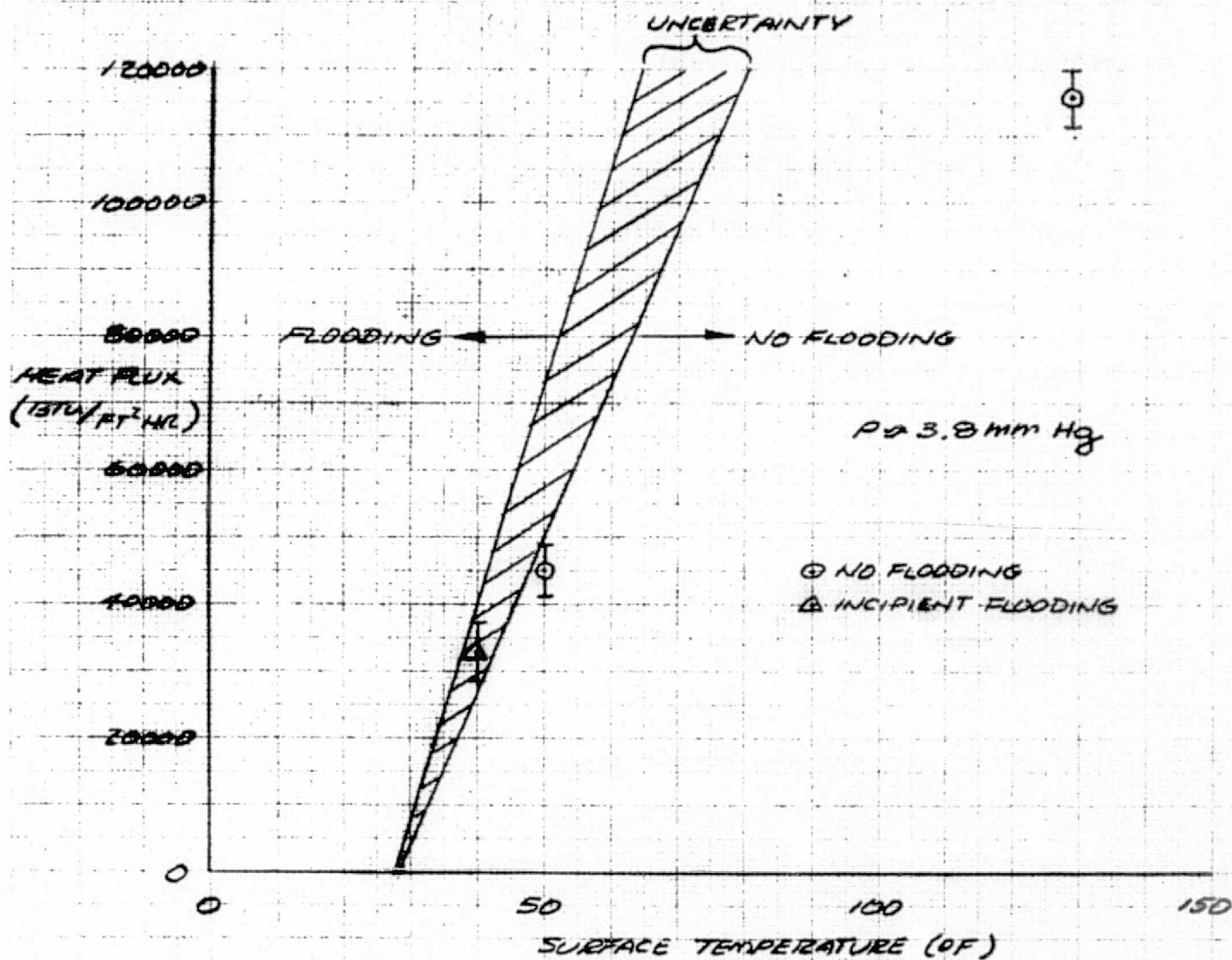
FIGURE B-12

PRELIMINARY FLOODING BOUNDARY

5.0   CONCLUSIONS

Based upon the results of these tests, the following conclusions are drawn:

o A variety of phenomena are present in the impact/
   evaporation process. At any instant, sublimation,
   nucleate boiling, ice cap ejection, and mass ag-
   glomeration may be occuring simultaneously.

o The efficiency of the phase change process appears
   to deviate from 100% only under extreme conditions:
   i.e., surface temperatures sufficiently high to
   produce significant droplet bounce and splatter, or
   surface temperature sufficiently low/pressure suf-
   ficiently high to cause surface flooding.

o Based upon spraying heat flux values inferred from
   target-transient response, it appears that droplet
   bounce/splatter becomes significant at surface tem-
   perature in excess of 150°F. A surface flooding
   boundary is postulated which allows heat fluxes in
   excess of 20,000 BTU/ft^2-hr at a surface temperature
   of 40°F. Thus the range of 100% efficient operating
   condition is quite wide.

6.0   RECOMMENDATIONS

As background information, the various flash evaporator
droplet spray investigations and the types of data obtained or expected from
them are summarized in Table B-4. The two phases (1, 2) of impact and visuali-
zation testing, plus the spray pattern visualization work (3), are complete as
reported herein.   In the Flash Evaporator Prototype 2 Program Plan, additional
droplet size and spatial distribution tests (4) are outlined. These tests,
which would utilize an optical array spectrometer, are currently planned for
the third quarter of 1973. As shown in Table B-4, they would provide quanti-
tative information as to the size and distribution of droplets within the spray.

However, the high speed film results and quantitative data of
the first three test series lead one to conclude that the complex impact/vapori-
zation process is of prime importance in the definition of flash evaporator
performance. Detail information on the spray itself, although interesting, is
not essential so long as the current class of spray nozzle is employed. It is
therefore recommended that additional spray impact/vaporization tests (5) be
substituted for the spatial distribution tests. The primary objective of these
tests would be refinement/completion of the definition of the flooding boundary
discussed in this report. In order to reduce experimental uncertanties, a
steady-state measurement technique would be employed. As shown schematically
in Figure B-3, the impact surface would be a segment of compact heat exchanger
core with Freon 21 as the transport fluid. A steady-state energy balance would
be utilized to infer the spraying heat flux as a function of surface temperature
and pressure.

TABLE B-4

FLASH EVAPORATOR DROPLET SPRAY INVESTIGATION SUMMARY

TEST	STATUS	DATA					
		HEAT TRANSFER		MASS DISTRIBUTION		PARTICLE SIZE AND DISTRIBUTION	
		QUALITATIVE	QUANITATIVE	QUALITATIVE	QUANITATIVE	QUALITATIVE	QUANITATIVE
1. Spray Impact & Vaporization -I	Completed 8/72	X		X		X	
2. Spray Impact & Vaporization -II	Completed 3/73	X	X	X		X	
3. Spray Pattern Visualization	Completed 3/73			X	X		
4. Droplet Size and Spatial Distribution	Planned for 3rd Quarter 1973			X	X	X	X
5. Spray Impact & Vaporization -III	Suggested Alternative To (4)	X	X	X		X	

NOZZLE/VALVE
ASSEMBLY

FREON 21 IN

COMPACT
HEAT EXCHANGER
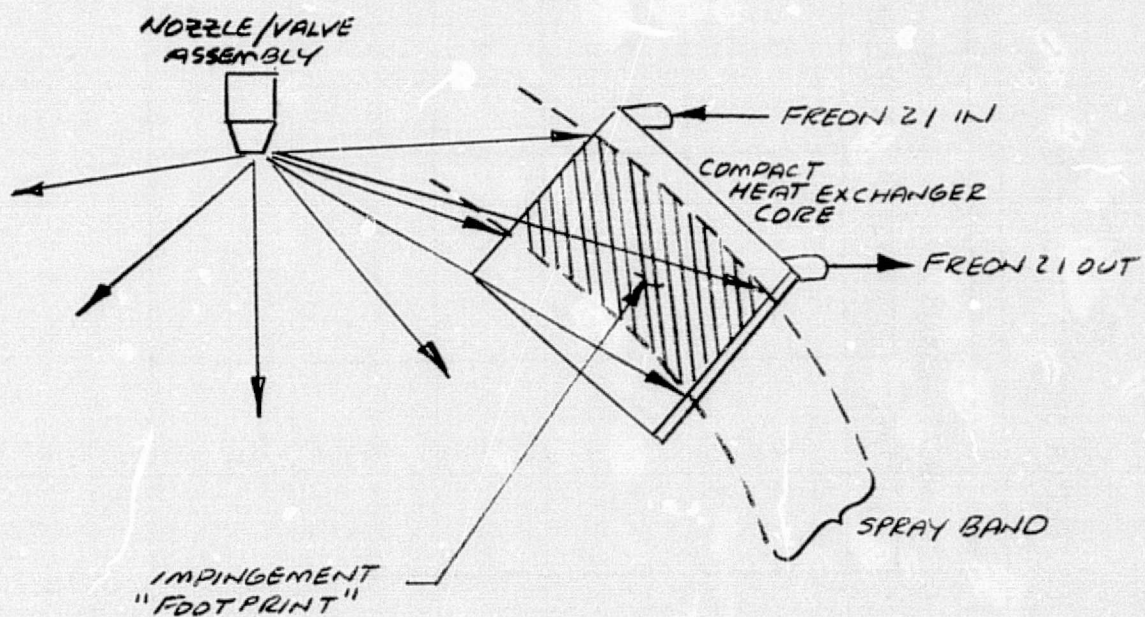CORE

FREON 21 OUT

SPRAY BAND

IMPINGEMENT
"FOOTPRINT"

FIGURE B-13

SKETCH OF STEADY-STATE
SPRAYING HEAT FLUX TEST
SET-UP

APPENDIX C

COLD PLATE EVAPORATOR TESTING

1.0 INTRODUCTION/SUMMARY

Due to the weight and cost penalties incurred in fabricating the wound tube evaporator, an alternate method was sought. One method would be to build the evaporator out of compact heat exchanger core. This would result in a significant reduction in fabrication, cost, weight, and complexity over the original design. Using surplus Lunar Module cold plates, a prototype cold plate evaporator was built and tested during October 1973. The purpose of the test was to determine whether the "cold plate" evaporator approach would function properly at various heat loads without ice or spray buildup on the panels or along seams between panels. In addition, the exhaust duct was to be positioned at various points to determine what influence exhaust duct location had on device operation and evaporator efficiency. Both the ATM controller and a new predictor/corrector controller were used at partial heat load to evaluate the response of the cold plate evaporator/controller combination.

Test result demonstrated that a cold plate evaporator will function quite well at all heat loads and is less prone to ice formation than the original wound tube evaporator. The predictor/corrector controller functioned extremely well at all heat loads above 5500 BTU/hr. Below this point, the nozzle ices badly due to the short cycle time of the controller, and large hold-up volume of the nozzle. Exhaust duct location seems to have little effect on evaporator efficiency or ice formation. Conclusions of the testing are in Section 4.0 of this Appendix.

2.0 TEST ARTICLE DESCRIPTION

The cold plate evaporator was configured as shown in Figures C-1, C-2, and C-3 to meet the following typical radiator "top-off" evaporator performance requirements:
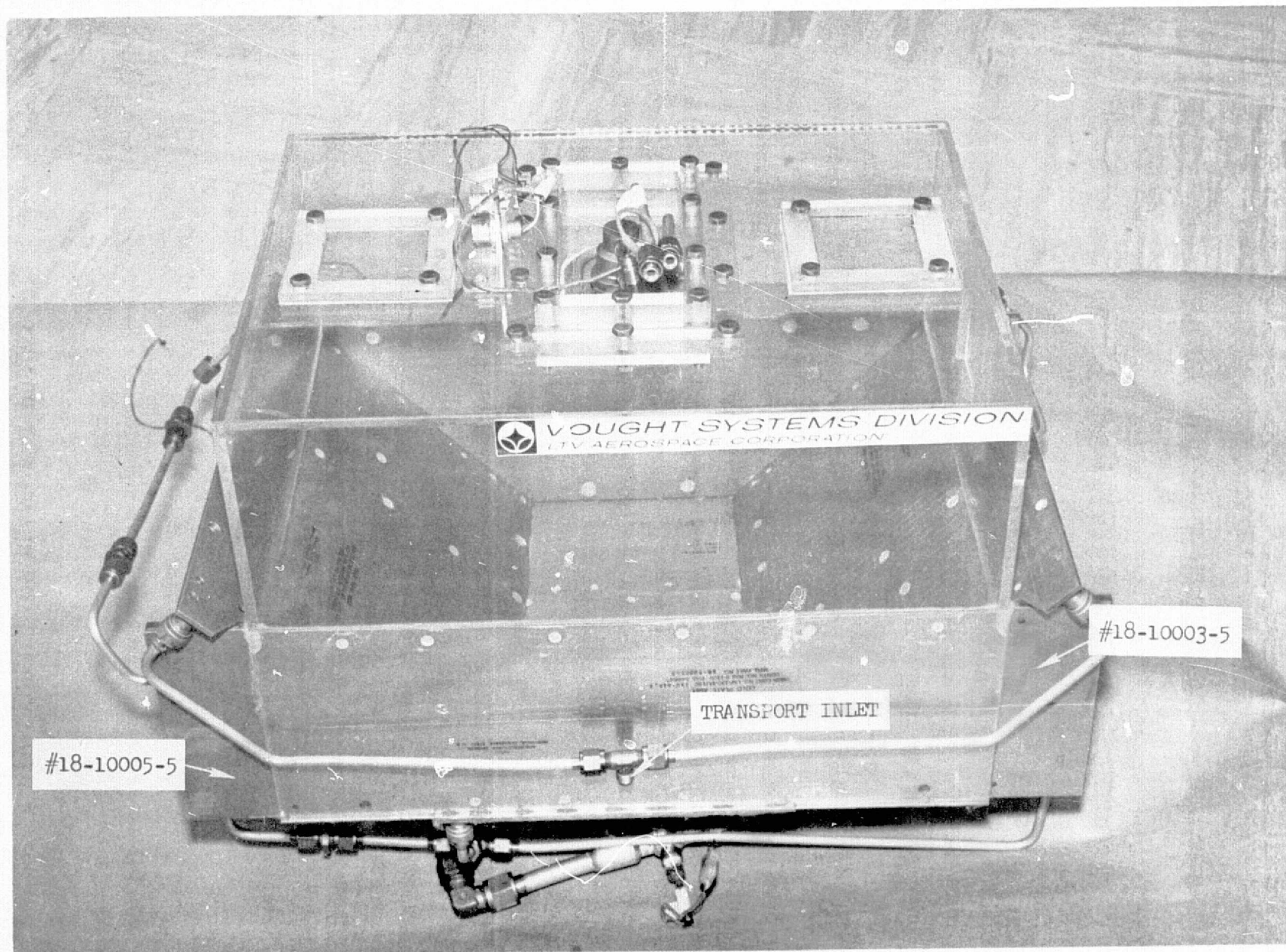
PRECEDING PAGE BLANK NOT FILMED

#18-10003-5

TRANSPORT INLET

#18-10005-5

FIGURE C-1

TOP AND SIDE VIEW OF "COLD PLATE"
EVAPORATOR

TRANSPORT OUTLET

#18-10010-1

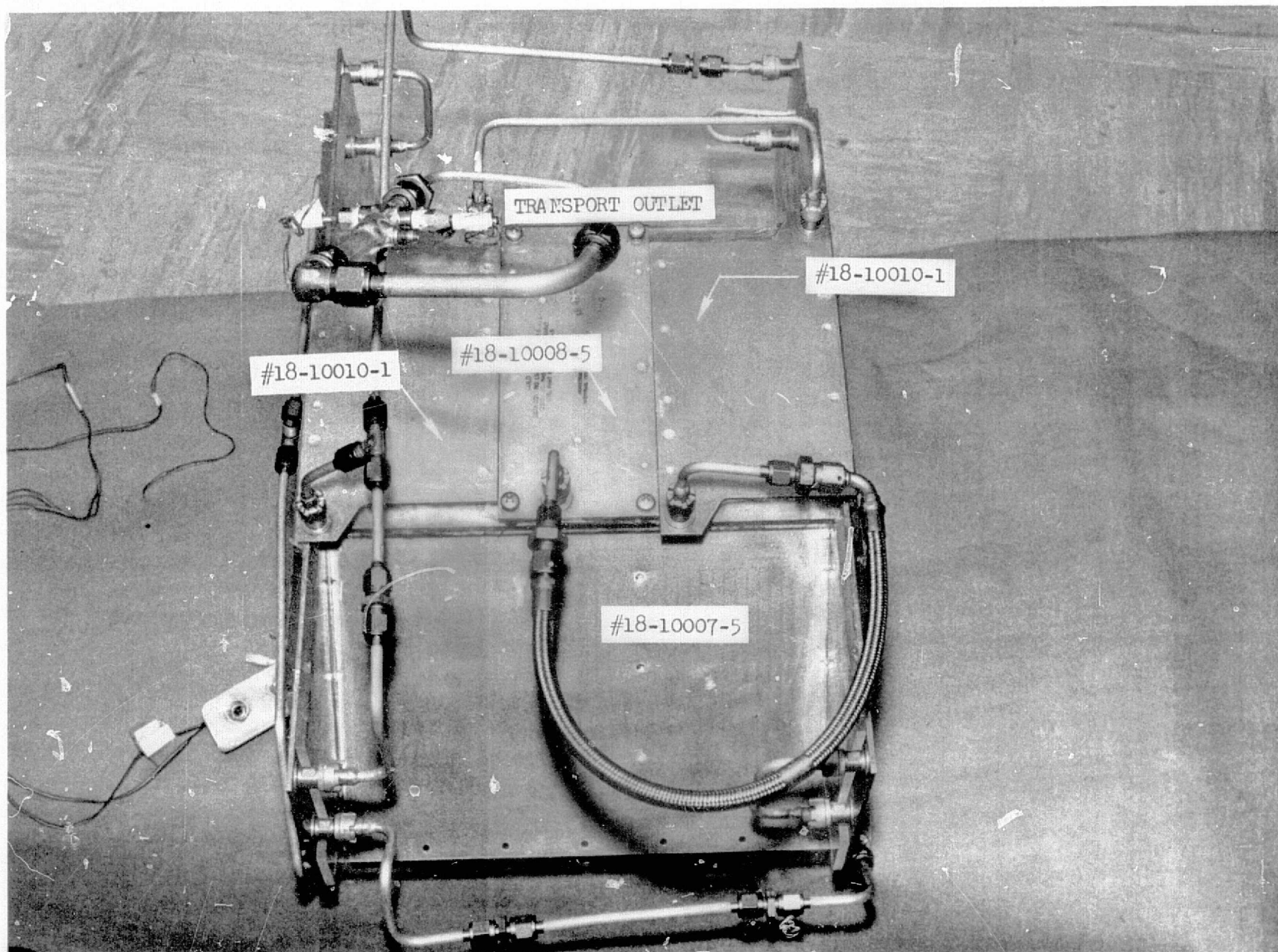#18-10010-1

#18-10008-5

#18-10007-5

FIGURE C-2

END AND BOTTOM VIEW OF "COLD PLATE"
EVAPORATOR
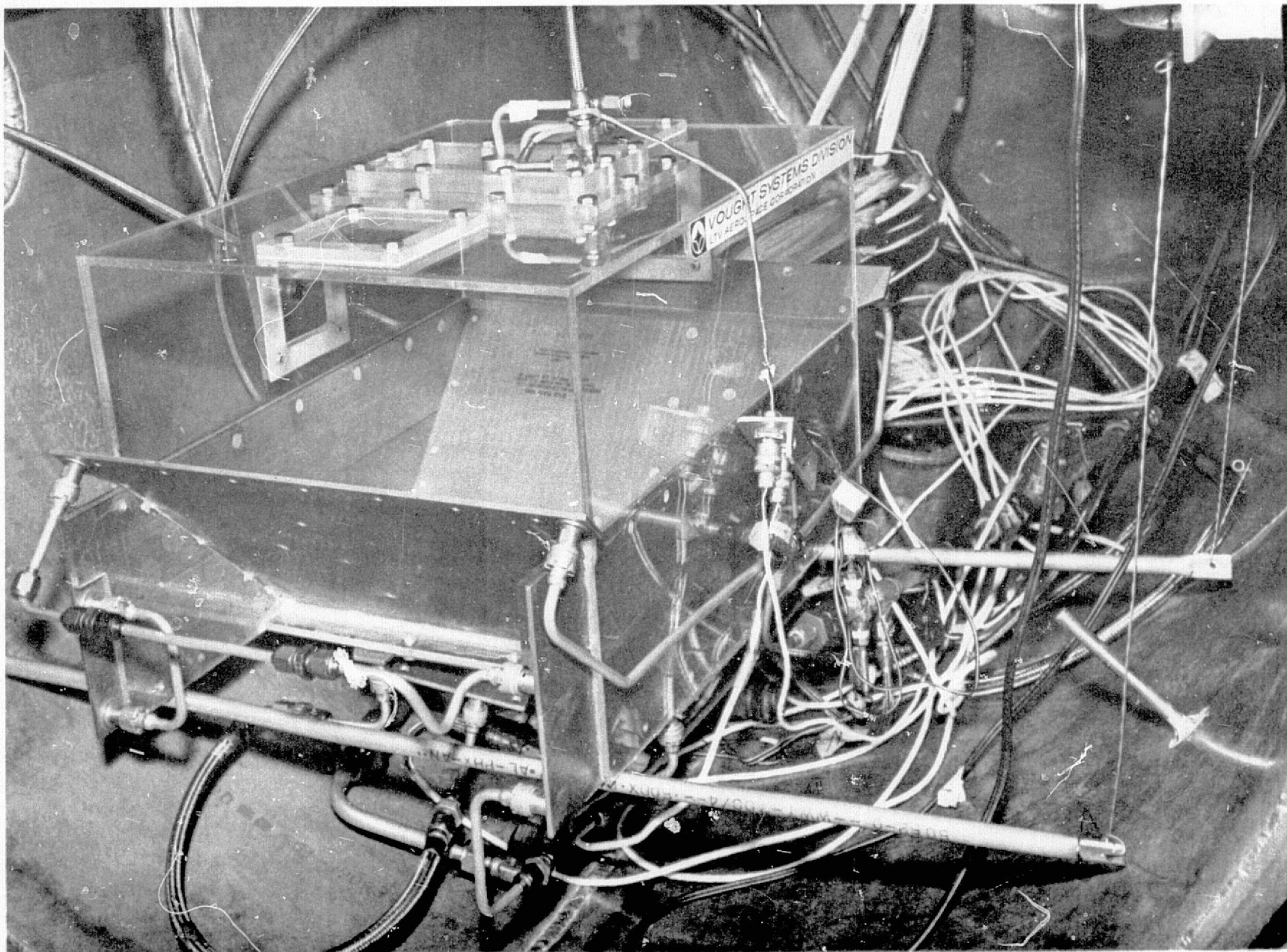
FIGURE C-3

"COLD PLATE" EVAPORATOR INSTALLED IN
THE 4 FT. VACUUM CHAMBER

Evaporant Fluid System

Evaporant	:	Deionized water
Flowrate	:	0 to 16 lb/hr
Supply Pressure	:	0 to 50 psig
Supply Temp.	:	Ambient
Evaporator Pres.	:	3.5 to 4.0 mm

Transport Fluid System

Fluid	:	Freon 21
Flowrate	:	2200 lb/hr
Heat Load Range	:	0 to 16,000 BTU/hr
Inlet Temperature	:	40° to 70°F

The configuration shown optimized surface location for use with either the Delevan hollow cone nozzle (4.0-A-70°) or the solid cone nozzle (4.0-B-90°). The component mounting holes existing on the cold plates were filled with a high conductance silver epoxy to prevent leakage of the evaporant from the CPE. The mating or intersections of the cold plate surfaces were sealed to prevent evaporant leakage.

The plexiglass backcone was used to provide the proper position for either of the 2 nozzles with respect to the cold plates and provide holes at four locations for the evaporant exhaust evaluation. These orifice mounting holes in the backcone were fitted with plexiglas cover plates when not in use. In addition, the bottom center cold plate was removeable such that an orifice plate could be fitted opposite the spray nozzle. Figure C-4 shows the three orifice configurations used in this test. The dual orifice arrangement in the center was installed only in the top two positions on the backcone. The large orifice plate was used to replace the removeable cold plate in the bottom of the evaporator.

The instrumentation used in the test included the following: A Brown multi-point recorder was used to record evaporator inlet and outlet temperatures heater outlet temperature, and transport flowmeter temperature; A Honeywell single point pin recorder was used to record outlet temperature to aid in controller tests; Apollo immersion thermistors were placed in the inlet and outlet lines to serve as control sensors for the predictor/corrector controller; Transport flow rate was measured with a Cox AN-8 flowmeter read on a Flow

SINGLE ORIFICE
(TOP AND SIDES ONLY)

DUAL ORIFICE
(TOP ONLY)

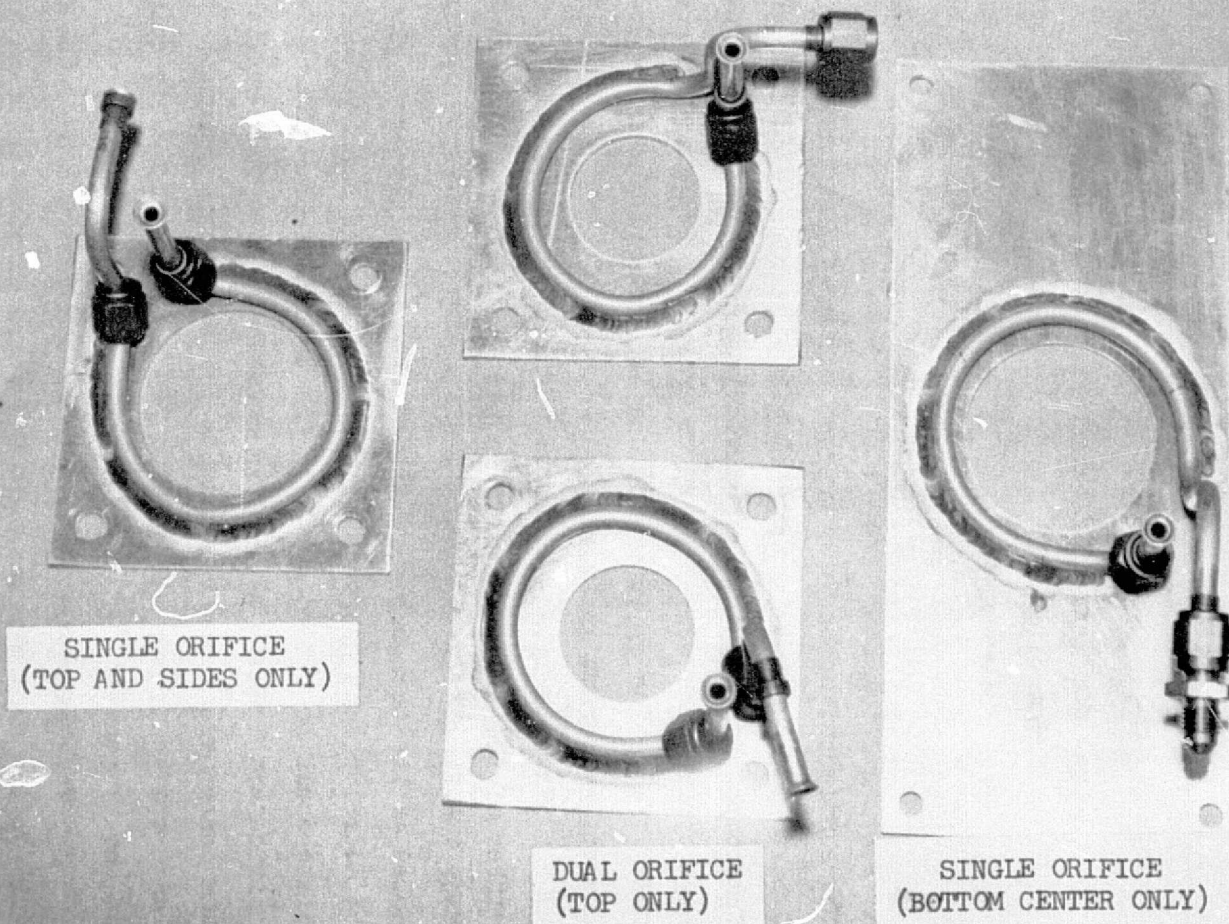SINGLE ORIFICE
(BOTTOM CENTER ONLY)

FIGURE C-4

ORIFICE PLATE CONFIGURATIONS USED
DURING TEST

Technology frequency converter; evaporant flow rate was read out using a
Flow Technologies flowmeter feeding a Foxoboro Model FR-521-1-2-50 frequency
converter.

3.0   RESULTS

3.1   Evaporator Operation

Initial tests on the "cold plate" evaporator were run with all cold
plates and all exhaust orifice plates connected in series. These tests indi-
cated that the pressure drop across the evaporator was too high to establish
a transport flow rate of 2200 pounds per hour. At a maximum obtainable ΔP of
250 pounds, transport flow rate was only 700 pph. The evaporator was removed
and replumbed as shown in Figure C-5 with all orifice plates and the nozzle
plate removed from the circuit. The evaporator was reinstalled and the maximum
flow rate obtainable at 250 pounds ΔP was 1400 pph. It was decided that further
paralleling of the evaporator plates would increase maximum flow rate but only
at the expense of lowering the heat transfer coefficient. As a result, the
evaporator was left in this configuration and the maximum inlet temperature
changed to 85°F to provide the necessary 16,000 BTU/hr heat load and still main-
tain a 40°F outlet.

Typical cold plate evaporator operation is shown in Figure C-6. Twenty
steady state cold plate evaporator conditions were tested during the program
with various configurations of exhaust orifice and spray nozzles. The results
obtained showed that exhaust port location made no difference in operation spray
pattern or efficiency. The device operated with both the hollow and solid cone
nozzle with no apparant effect on efficiency. Efficiencies were calculated to
be between 80% and 85%. This low efficiency is probably due to the non-optimum
design of the core and device configuration, and to spray carryover in the exhaust.
Detailed data from this testing is presented in Appendix A of Reference 7.

3.2   Controller Operation

Outlet temperature control to a 40°F setpoint was attempted with both
the ATM (on-off) type controller and the predictor/corrector (variable pulse rate)
type controller.

The predictor/corrector controller uses two thermistor sensors, one in
both the inlet and the outlet streams. The inlet thermistor determines the pulse
rate and percent "on" time of the spray and the corrector or outlet thermistor
changes these parameters to account for system response changes. During these

18-10003-5

18-10005-5

THERMISTER (ATM)
18-10010-1

18-10008-5

18-10010-1

18-10007-5

18-10007-5

T/c 13
T/c 12

T/c 11
T/c 10

18-10005-5

18-10003-5

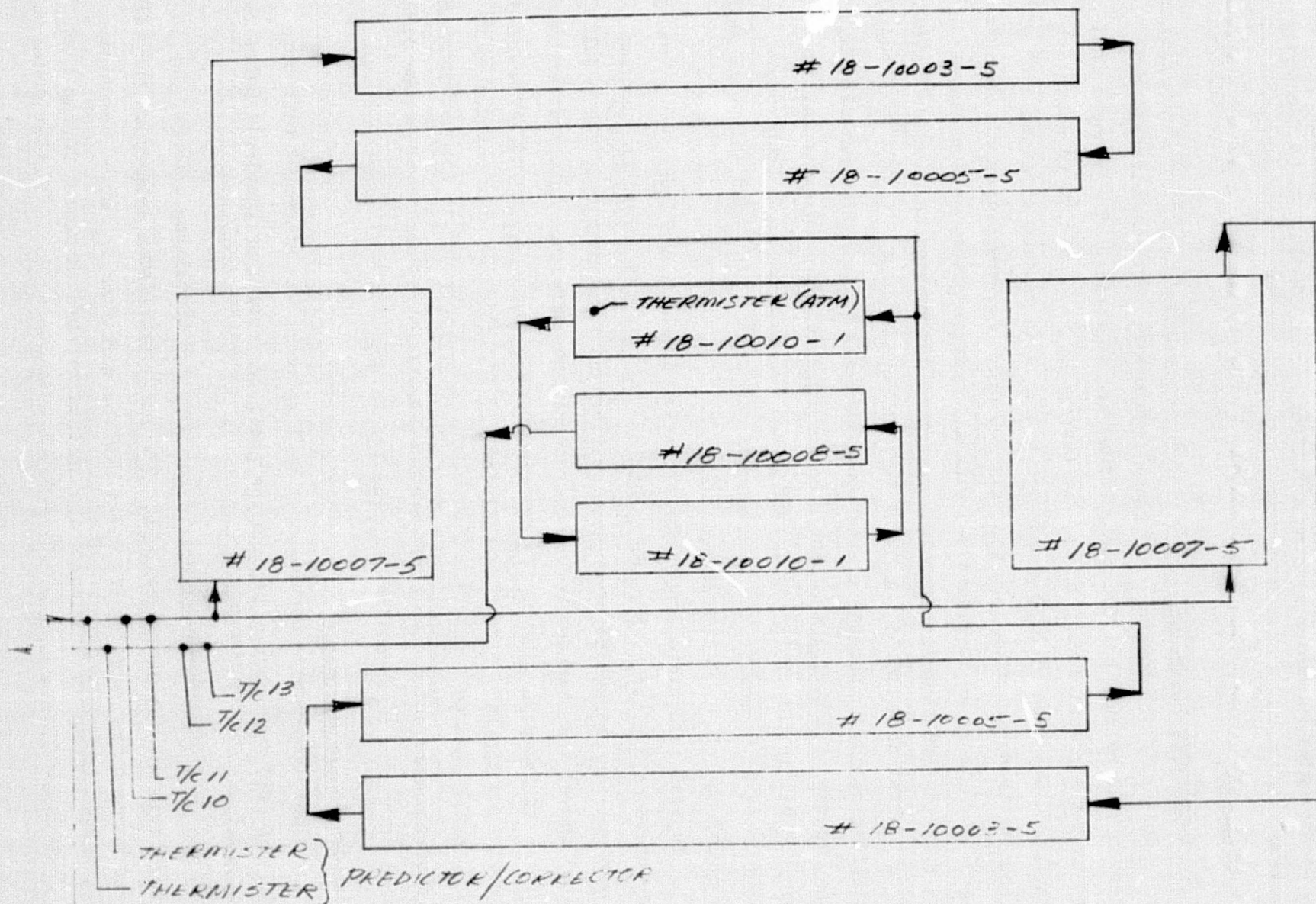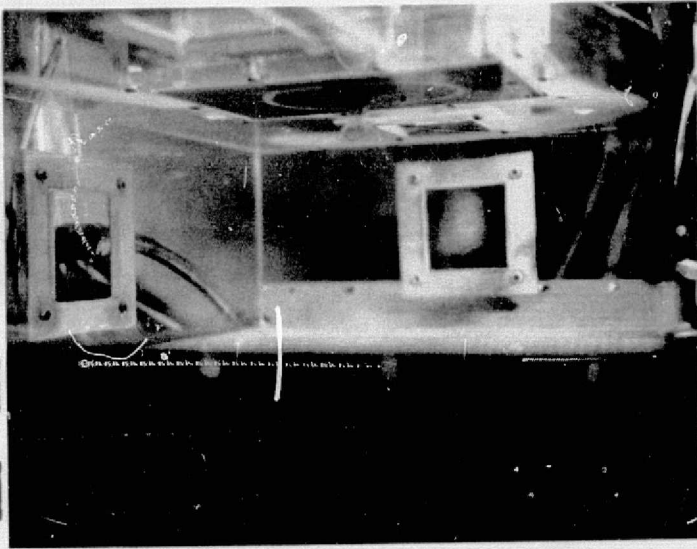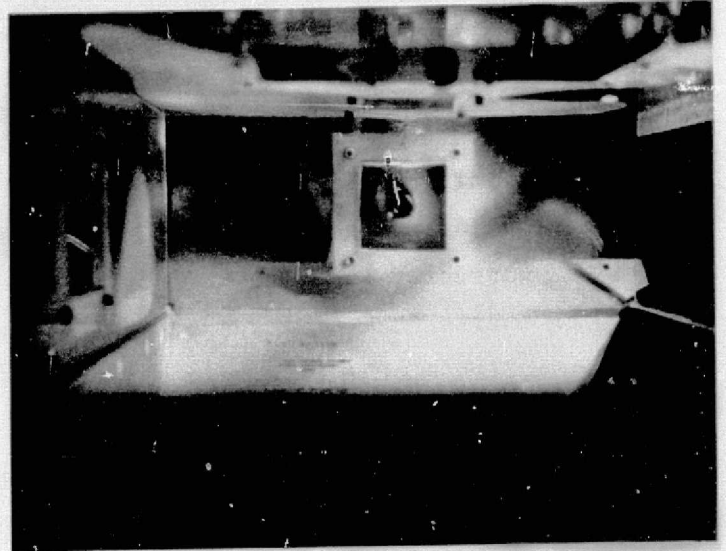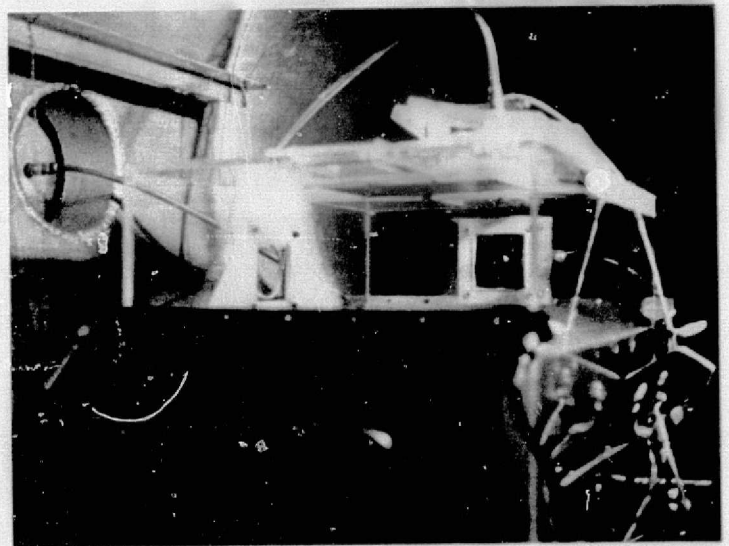THERMISTER
THERMISTER } PREDICTOR/CORRECTOR

FIGURE C-5 FINAL EVAPORATOR FLOW
CONFIGURATION

TYPICAL SPRAY PATTERN

ICE CHIPS FORMED AT NOZZLE
SHUT-OFF

ICE FORMATION ON PLEXIGIAS AROUND EXHAUST ORIFICE

FIGURE C-6

FIGURE C-6 EVAPORATOR OPERATION AND ICING AROUND
EXHAUST ORIFICE

tests, the controller was operated in both the predictor and predictor/corrector modes. For inlet temperatures from 55°F to 75°F, outlet temperature was maintained within 1°F to 40°F operating with the predictor orly. Temperature gradients as high as 150°/hour did not fault the controller operation and the corrector function was not required. Below an inlet temperature of 55°F, the nozzle "on" time was not sufficient to fill the nozzle hold up volume and establish stable flow. As a result, ice chips rather than spray would be produced at random. These missed cycles would result in a run away condition at the outlet and outlet temperature oscillated wildly. With nozzles having very small hold up volume, nozzle cycle times less than 1/2 second could be tolerated and reliable operation could be expected at inlet temperatures approaching 40°F.

The ATM controller uses a thermistor sensor attached to the evaporator wall or immersed in the outlet fluid stream. The controller is then set to turn the valve on or off within some range of temperatures as seen by the sensor. The span adjustment is a function of the response time of the system and the time necessary for cold or hot fluid to reach the sensor. Any change in system response time, such as variations in transport flow rate, affects the temperature swing of the outlet fluid. In the current design, no provision is made for automatic span adjustments to compensate for response changes. Due to physical limitations of the sensor-controller bridge network, the exact response of the "cold plate" evaporator could not be modeled and the minimum outlet swing obtained was ± 5°F. A 10% reduction in transport flow rate with the same controller settings increased the outlet swing to ± 10°F.

4.0 CONCLUSIONS

These preliminary tests indicate that an evaporator constructed of heat exchanger core is entirely feasible. There was no tendency for the cold plates to develop cold spots and ice formation in corners and along seams was not apparent. Efficiency, however, ranged only from 80 to 85%. It is believed that this is due largely to the design of this particular evaporator and the inability to establish proper flow rates and temperatures. The savings in cost, weight, and reliability provided by this type of construction make the approach very desirable. A proper cold plate design needs to be developed specifically for this application and further tests run to determine whether overall system efficiency can be increased.

In addition, the operation of a redundant transport loop needs to be evaluated. The location of the vapor exhaust orifice had no effect on evaporator operation, efficiency, of ice accumulation.

Considering the "make do" nature of the prototype design, controller operation was remarkably good. The predictor/corrector controller operating in only the predictor mode was able to hold outlet temperature to within $1°$ of $40°F$. Control was reliable from maximum heat load all the way down to the point where physical limitation of the valve/nozzle configuration made control erratic. Further tests need to be run using a valve/nozzle arrangement with the smallest hold up volume possible. Only then could a true evaluation of the predictor/corrector be made.

Due to the mismatch between the ATM controller and the sensor which was used, ATM operation was not impressive. At best, the outlet temperature varied by $\pm 5°F$. Proper sensor selection and correct sensor location would probably reduce this swing considerably.

Of the two controllers used, the predictor/corrector seems most desirable. Adjustments are simpler and less critical than those on the ATM controller, making fine tuning of the controller much easier. In addition, the corrector mode makes adjustments to compensate for variations in flow rate, efficiency and system response unnecessary. The electronic package is also much easier to understand and trouble shoot in the event of a malfunction.

The ATM controller, however, is much more difficult to tune. Any change in either set point or span results in a change in outlet temperature, outlet stability, and nozzle operation. A long iterative set up period is required to establish optimum operating conditions. However, any change affecting system response such as transport flow rate can greatly affect system stability necessitating a readjustment of the controller. No provision is made for automatically making these adjustments. During the test, a 10% variation in flow rate caused the outlet temperature swing to double from $\pm 5°F$ to $\pm 10°F$.

APPENDIX D

WASTE WATER EVAPORATOR FEASIBILITY TESTING

1.0   SUMMARY/CONCLUSIONS

A test was conducted on 23 April 1974 to determine if the flash evaporator
can be used to dump waste water and to define those problem areas that need solving
for application of a waste water evaporator in the Space Shuttle. Approximately
27 Kg (60 pounds) per day of waste water is expected to be generated by the Shuttle
occupants and consideration is being given to dumping this waste water through an
evaporator. Advantages of flash evaporator use include elimination of a special
dumping system and/or holding tank system with the subsequent overall weight savings.
The Shuttle waste water has been estimated to be 50 percent urine and 50 percent
waste water.

Spraying of a waste water evaporant composed of 50 percent urine and 50
percent distilled water (collected within 24 hours of test) in the cold plate
evapo? .ur (described in Section 3.4) was performed with the following specific
objectives:

(1) Determine if particulate matter gets into the exhaust stream

(2) Investigate the filtering requirements of a waste water evaporator

(3) Investigate the amount of particulate buildup on the nozzle
     and coldplate surfaces

(4) Determine the effect on performance of particulate buildup on
     evaporator heat transfer surfaces

Approximately 13.5 Kg (30 pounds) of waste water was evaporated by the
cold plate evaporator during 2 hours and 20 minutes of testing. Operating at an
inlet temperature of 308°K (95°F), the transport fluid was cooled to 280°K (45°F)
with evaporation efficiencies between 87 and 92 percent. The impinging spray
caused a froth and left a residue on the heat transfer surfaces but no trend
toward performance degradation was noticed. Further investigation is recommended,
however, to determine if residue does effect performance after extended operation.

The valve/nozzle/filter showed no buildup of solids or malfunctioning as
a result of waste water flow with a 60 µ filter only, a 60 µ and 10 µ in
series or pulsing spray operation. A yellowish brown liquid collected in the
baffle trap and did not freeze or appear to evaporate.

Since the test did not simulate the extended operation of Shuttle usage, the clean-up also did not simulate the actual amount of residue or the time the residue stays on the heat transfer surfaces before clean-up is initiated.

2.0   TEST INSTALLATION AND TIMELINE

The test article, shown installed in Figure D-1, was the LEM coldplate evaporator (CPE) constructed in October 1973 and the fluid hook-up essentially duplicated that used previously and is shown schematically in Figure D-2. A plexiglas baffle chamber 15.25 x 15.25 x 33 cm (6" x 6" x 13") was installed over the orificed exhaust port to trap solid and liquid carryover from the evapora-tor. Two LN_2 cold traps (approximately 9 30 cm^2 (4 ft^2) each) were placed in the satellite vacuum chamber with the evaporator to reduce waste water evaporant carry-over into the large vacuum chamber. The bleed flow valve was opened during the pulsing spray mode to heat the valve mounting plate and remained closed during the continuous spraying mode. The evaporant valve contains a 10 micron filter and it was supplemented by two additional filters of 10 microns and 60 microns upstream of the valve.

Instrumentation consisted of three thermocouples and two flowmeters. The thermocouples measured the evaporator inlet and outlet temperatures and the valve mounting plate temperature. Flowmeters were placed in the transport loop and waste water evaporant loop. The actual amount of evaporant sprayed was monitored con-tinuously by weighing the supply tank and substracting the initial weight. Figure D-3 gives the variation of the supply tank weight throughout the test and the rate of evaporant sprayed.

The satellite vacuum chamber is approximately 1.2 m (4 feet) in diameter and 1.8 m (6 feet) long. One end of the chamber is covered with a thick sheet of plexiglas to allow full viewing of the complete test article in operation. This chamber is connected to a 3 m (10 ft.) diameter vacuum chamber which connects directly to the vacuum pumps. The large chamber can be isolated when the satellite chamber is to be opened.

The urine part of the waste water solution was collected within 24 hours prior to the test. An antifoaming agent (G.E. Antifoam 60) in the amount of two eye-droppers per 16.7 Kg (36.71 lbs.) of urine was added to the urine. The urine was cut with an equal weight of distilled water. The waste water solution was loaded by pulling a vacuum on the supply tank and allowing the vacuum to pull the well mixed solution into the tank. A gaseous nitrogen source forced the waste water evaporant out of the tank through a bottom hose connection.
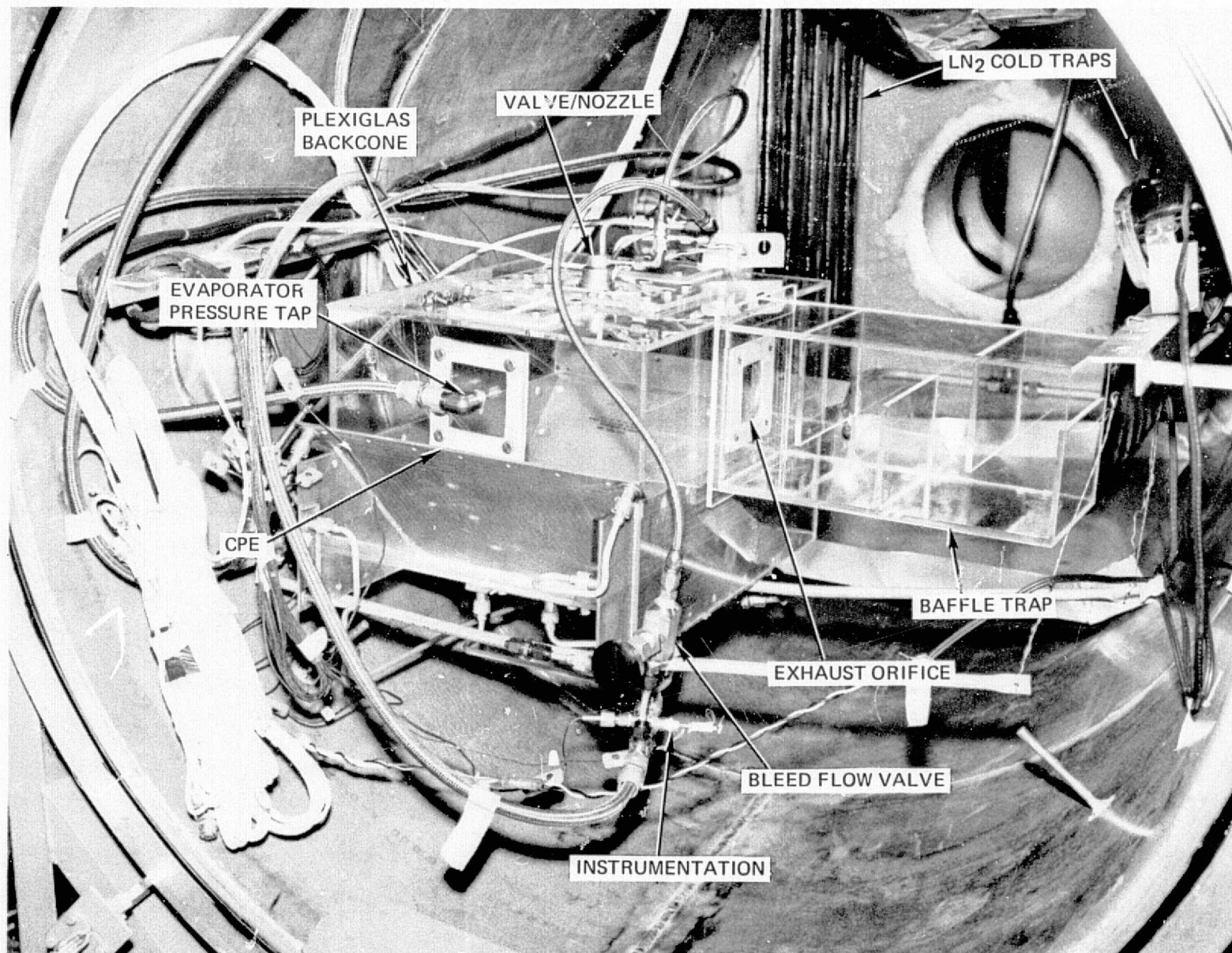
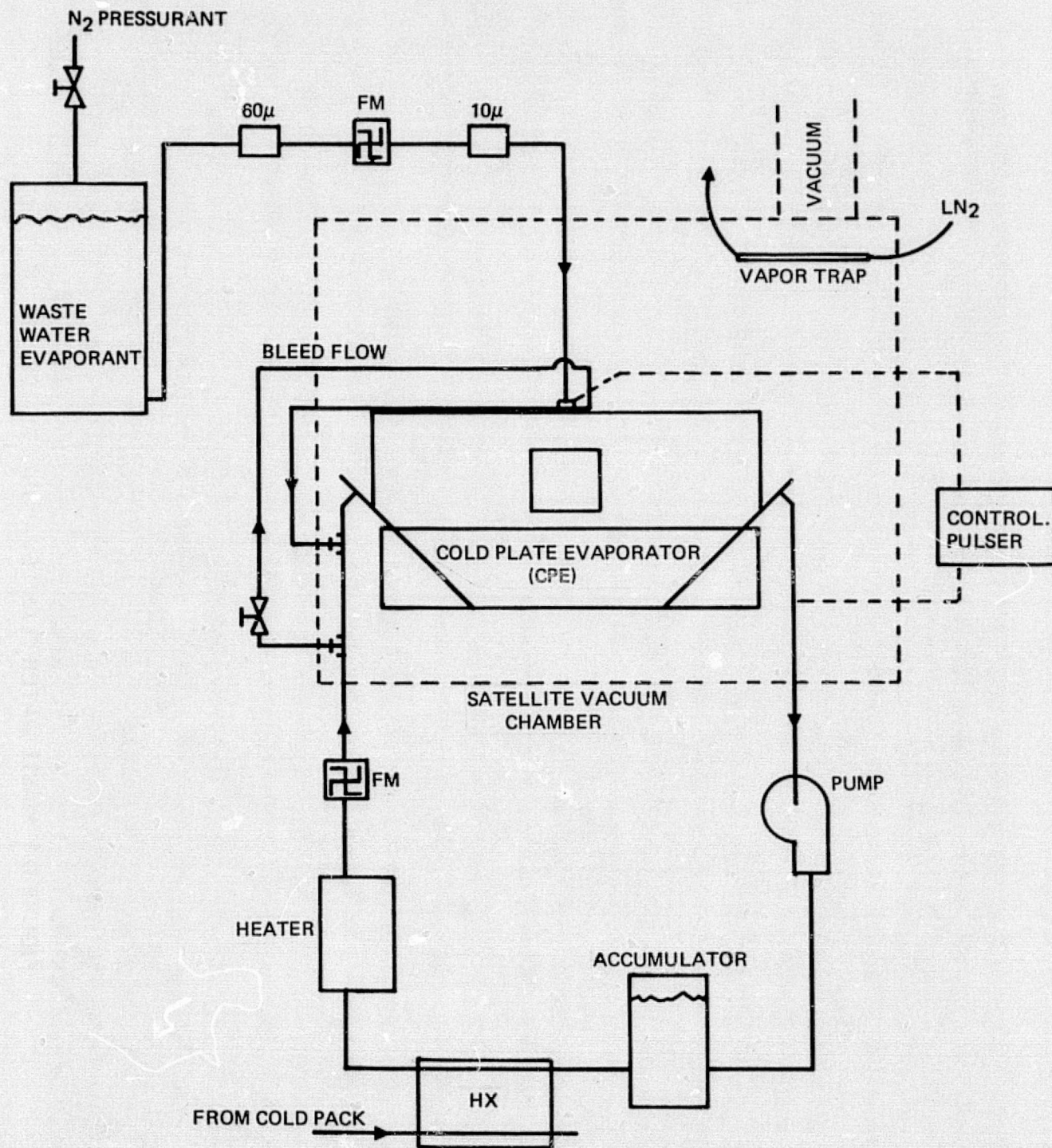FIGURE D-1 WASTE WATER FLASH EVAPORATOR TEST SET-UP (T + 0)

FIGURE D-2 FLOW SYSTEM SCHEMATIC

3.0   EVAPORATOR PERFORMANCE

The total testing time was 2 hours and 20 minutes with the first
hour of testing accomplished in one hour and 32 minutes clock time. The
remaining 1 hour and 20 minutes of testing required 2 hours and 46 minutes
clock time. The chamber was brought up to atmospheric pressure twice to
clean the exhaust port cover to improve visibility: once at 60 minutes elapsed
time and once at 105 minutes. Evaporator performance is recorded in the series
of photographs which follow and will be discussed according to elapsed time.

T + 00:18:30

At this time, 2 Kg(4.53 lbs) of waste water had been sprayed and several trends
are being established. Frothing of the waste water occurred as the spray
impinged on the heat transfer surfaces. The frothing is believed to have con-
tributed to the splattering within the evaporator cavity which speckled the
evaporator plexiglas backcone. Exhaust vapor condensed and froze on the orifice
and an ice cone formed on the first baffle. A small amount of liquid began to
accumulate in the baffle trap with no propensity for solidifying. The downstream
portion of the baffle chamber was clear.

T + 00:30:00

At this time, 3.4 Kg (7.48 lbs) of waste water had been sprayed. The large piece of
ice on the orifice at T + 00:18:30 broke loose and blew into the trap. Ice
can be seen to have reformed on the orifice as was the pattern throughout the
test. The ice cone on the first baffle is shown slipping down the baffle.
Trapped liquid in the baffle chamber was entrained periodically in the flow and
resulted in liquid splattering on the top and sides of the baffle chamber. The
liquid in the trap had a yellowish-brown color. Backcone speckling had made the
plexiglas opaque and the heat transfer surfaces were hidden from view.

T + 01:00:00

At this time, 6.7 Kg (14.73 lbs) of waste water had been sprayed. The ice cone was
on the floor of the baffle trap, setting in a considerable amount of liquid and
partially blocking the flow cross-sectional area. Melting of the ice cone con-
tributed to the trapped liquid which was continually splattering on the baffle
top and sides. The large liquid droplets which hit the sides of the baffle

left visible film patterns on the plexiglas as it ran to the bottom. Liquid droplets adhered to the top of the evaporator backcone and formed the pattern shown. Although the heat transfer surfaces were not visible at this time, there must have been some liquid in the evaporator since leaking occurred at coldplate mating joints. The vacuum chamber was brought up to atmospheric pressure to clean an exhaust port cover and improve evaporation cavity viewing.

T + 01:30:45

At this time, a total of 10 Kg(22.03 lbs) of waste water evaporant has been sprayed. This photo was taken after the evaporator spray was shut off. The liquid in the baffle flash-froze as the pressure fell to about 1 to 2 mmHg. Previously when the spray was stopped, liquid in the trap remained a liquid. It is believed the partial melting of the ice cone diluted the trapped liquid and made it susceptible to freezing as the pressure decreased.

T + 01:30:50

At this time, the chamber has been closed-up and the spray started. The amount of evaporant sprayed has not changed significantly from the last photo. Liquid was re-established in the trap as the pressure in the evaporation cavity increased. All the various aspects concerning operation mentioned previously continued.

T + 02:20:00

At this time the test was terminated and a total of 13.4 Kg(29.53 lbs) of evaporant had been sprayed. The vacuum chamber was isolated and brought up to atmospheric pressure, the plexiglas door opened and the evaporator removed from the chamber. Post-test examination included photographic documentation, visual inspection and weighing the evaporator and baffle chamber. When the valve/nozzle mounting plate was removed the residue on the heat transfer surfaces could be seen to be about 1 to 2 millimeters thick and had a wet appearance. Although the mounting plate did collect a residue, probably from the splattering spray, the nozzle exterior remained clean. Inspection of the internal parts of the nozzle revealed they were likewise clean and showed no effect from the 13.2 Kg (29 lbs) of waste water. The evaporant flow filters appeared clean to the naked eye.

The evaporator has a strong smell of ammonia which was to be expected. Liquid that condensed on the cold traps was clear when it melted but had an odor. This was the case for both the satellite and large vacuum chamber cold traps. Clean-up of the test article and associated equipment was begun immediately and completed within 2 hours of the end of the test. Warm water and paper towels were all that were necessary to clean the residue from the evaporator.

Thermal performance of the evaporator using waste water as the evaporant was similar to the performance obtained when deionized water was the evaporant. Evaporator efficiencies varied between 87 and 92 percent, and did not show a tendency to decrease during the test. A residue built up on the evaporator heat transfer surfaces to a thickness of approximately one-two millimeters and had a very porous appearance.

A weight analysis was performed on the evaporator to determine the weight of the residue deposited due to use of waste water as the evaporant. Table D-1 summarizes the results of the weight analysis. The total weight of solids collected in the evaporator while spraying 13.4 kilograms of 50 percent urine solution was 264 grams. This compares well with the Bioastronautics Data Book which indicates a nominal value of 255 grams of solids in 13.4 kilograms of 50 percent urine solution. The variance of 3.5 percent could be accounted for in the difference in the concentration of solids in the urine solutions. Solids concentrations are known to be a function of the individual and his diet.

TABLE D-1
WASTE WATER FLASH EVAPORATOR TEST WEIGHT ANALYSIS

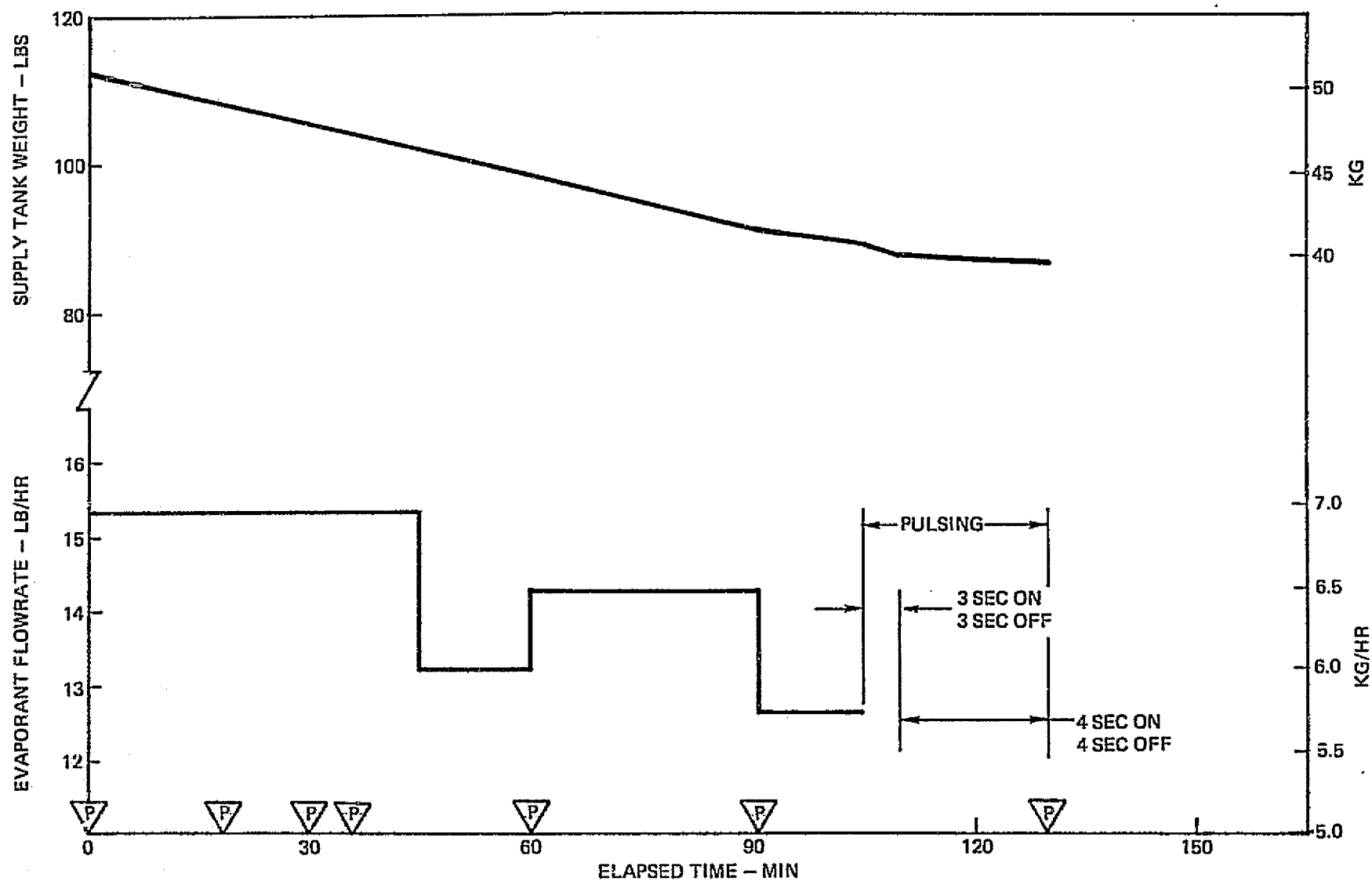|	F/E	TRAP	TOTAL
Weight Delta (Grams)	201	157	358
Weight of Liquid In Trap After Test (Grams)		94	
Weight of Solids Collected (Grams)	201	63	264
Weight of Solids Expected (Grams) (1.9%* x 13.4 Kg = 255g)			255

* Bioastronautics Data Book

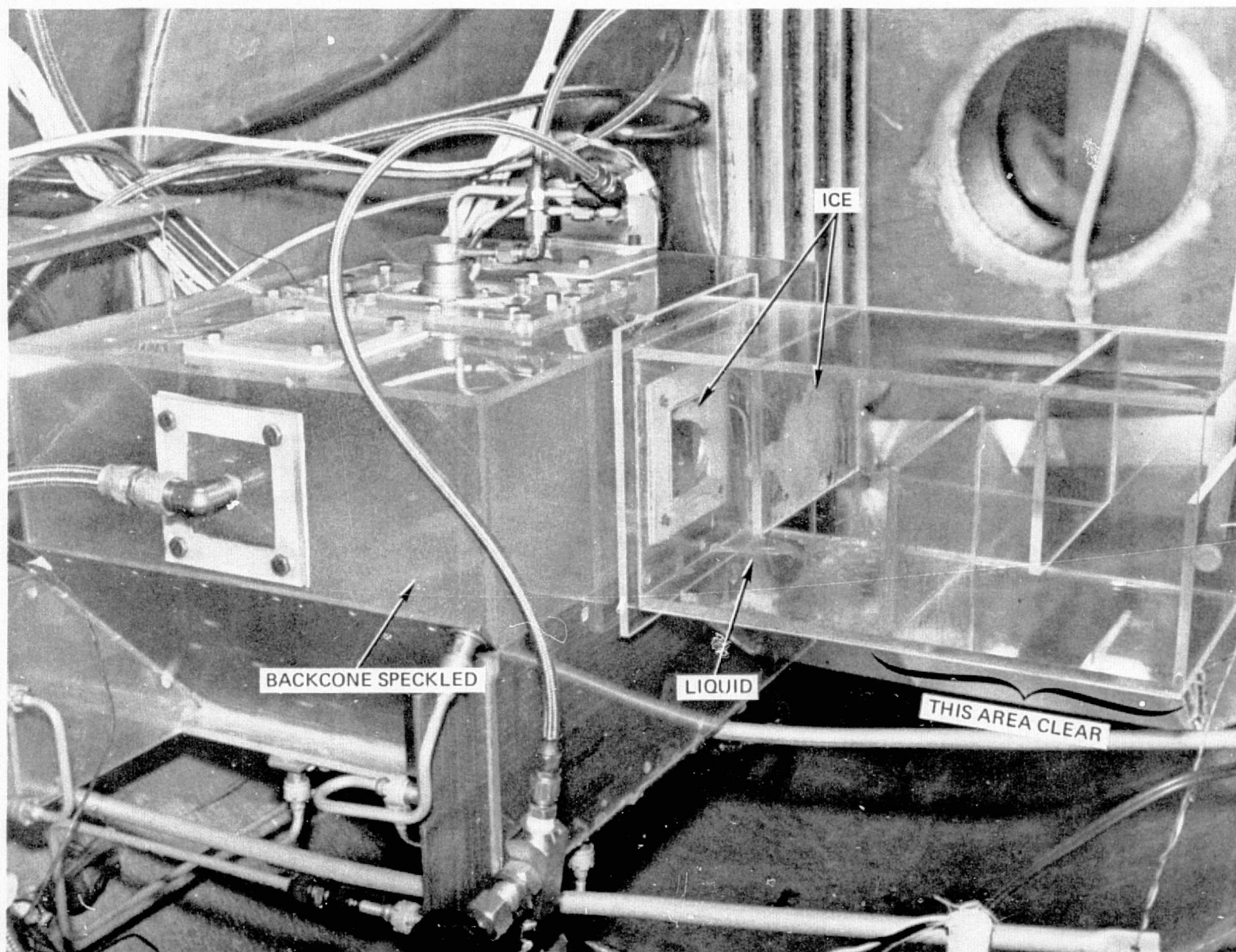FIGURE D-3 WASTE WATER FLASH EVAPORATOR TEST TIMELINE
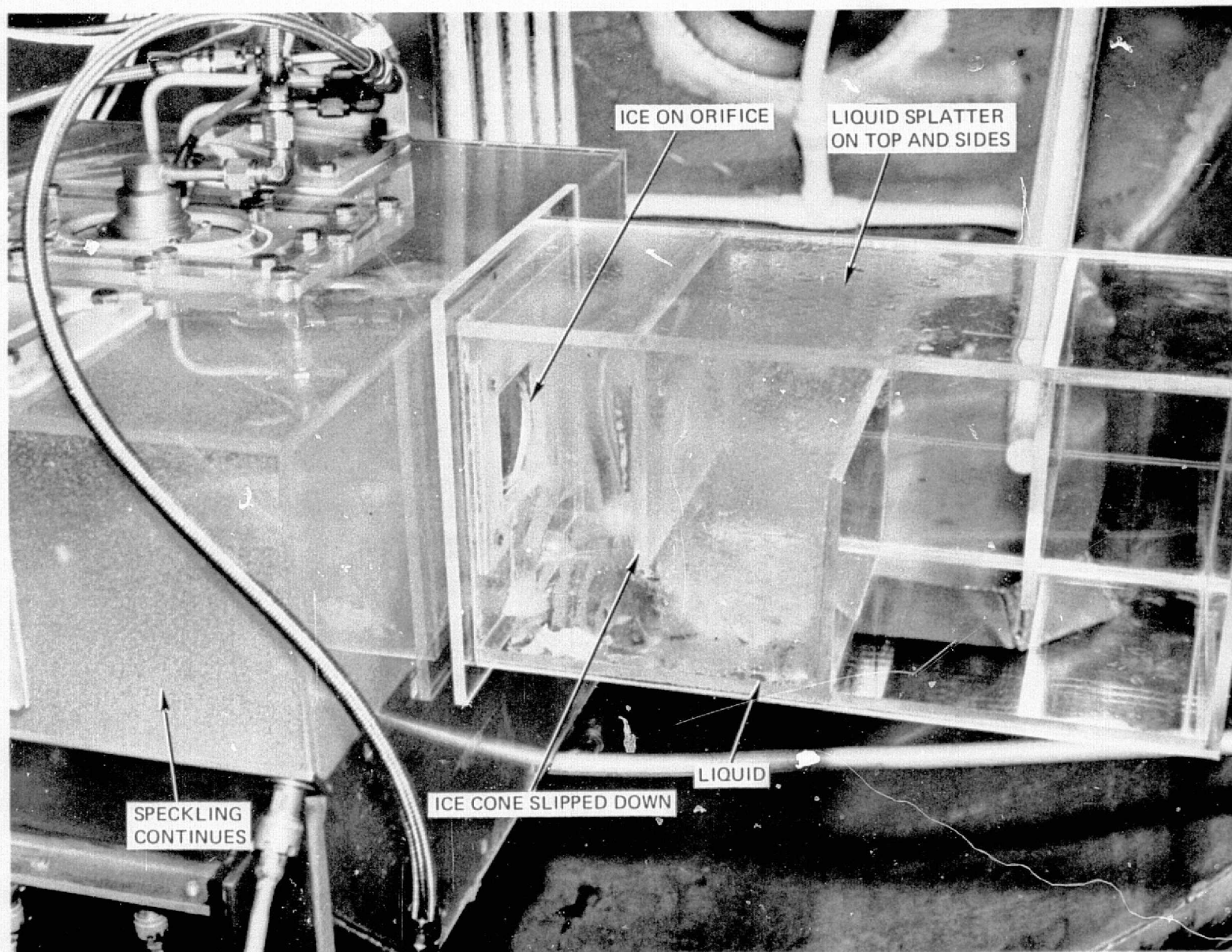
FIGURE D-4   T + 00:18:30 4.53 LBS EVAPORANT SPRAYED

ICE ON ORIFICE

LIQUID SPLATTER ON TOP AND SIDES

SPECKLING CONTINUES

ICE CONE SLIPPED DOWN

LIQUID

FIGURE D-5   T + 00:30:00   7.48 LBS. EVAPORANT SPRAYED
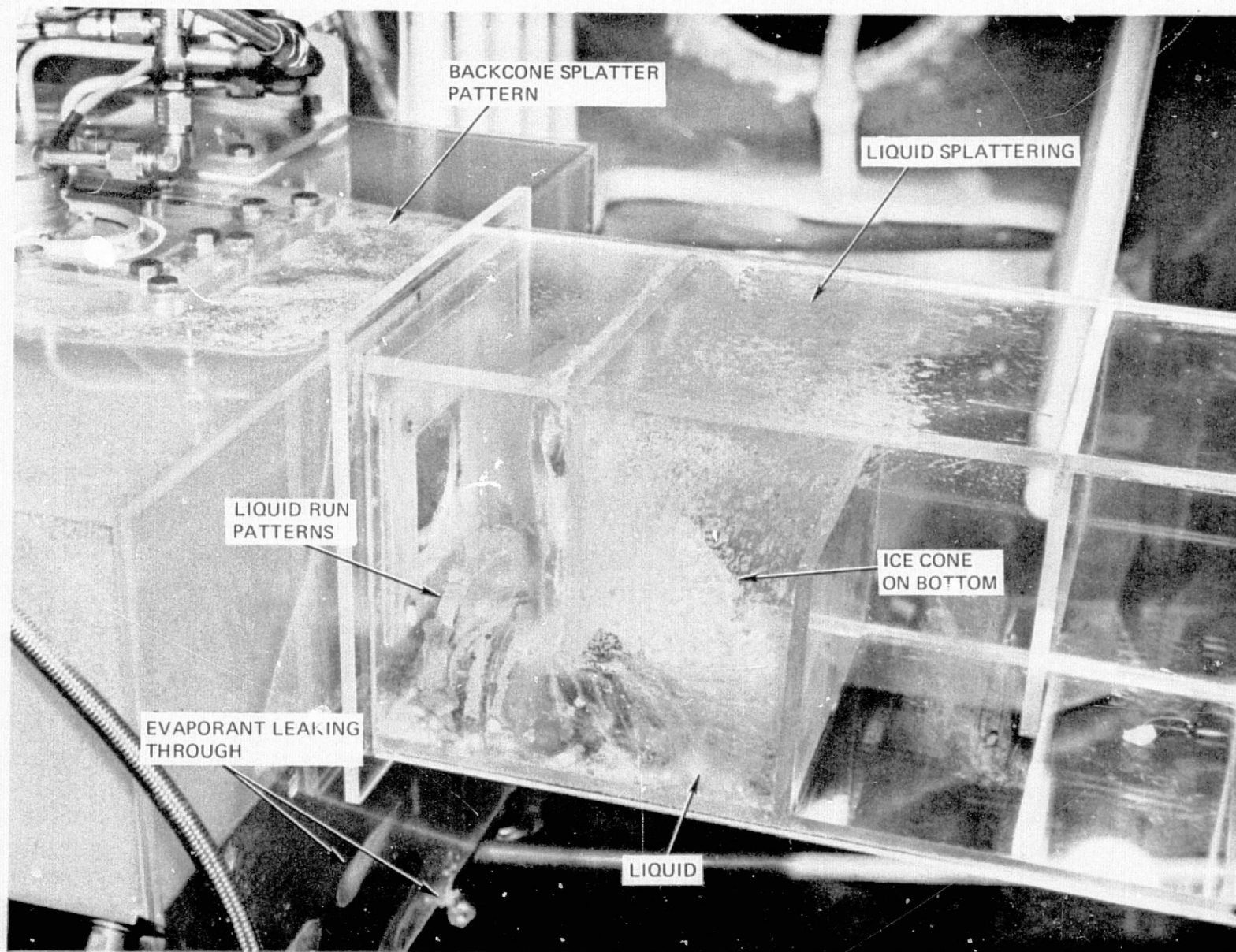
FIGURE D-6   T + 01:00:00   14.73 LBS. EVAPORANT SPRAYED

SPLATTERING ON TOP AND SIDES

DILUTED LIQUID FROZE
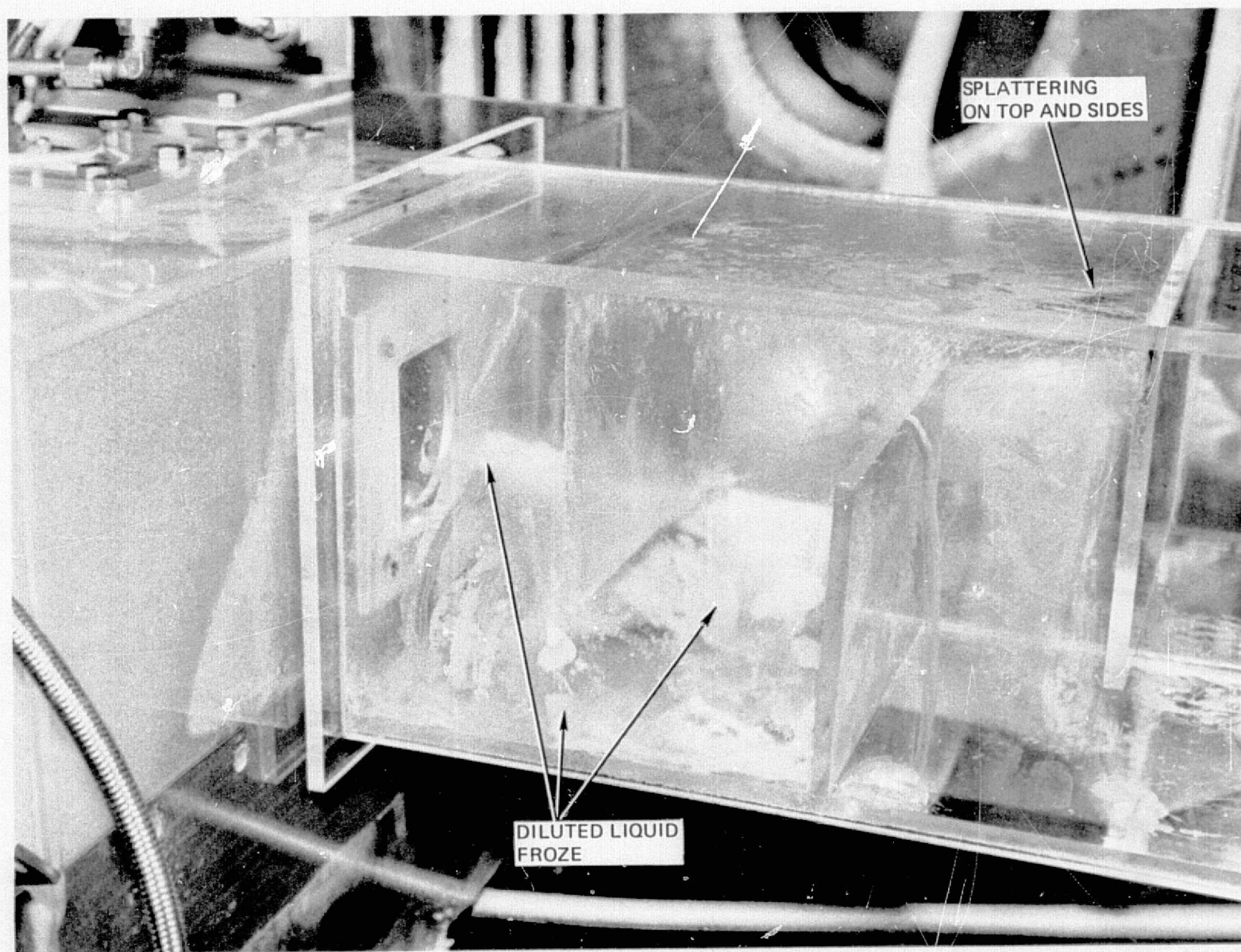
FIGURE D-7 T + 01:30:45 22.03 LBS. EVAPORANT SPRAYED

LIQUID SPLATTERING

LIQUID REESTABLISHED
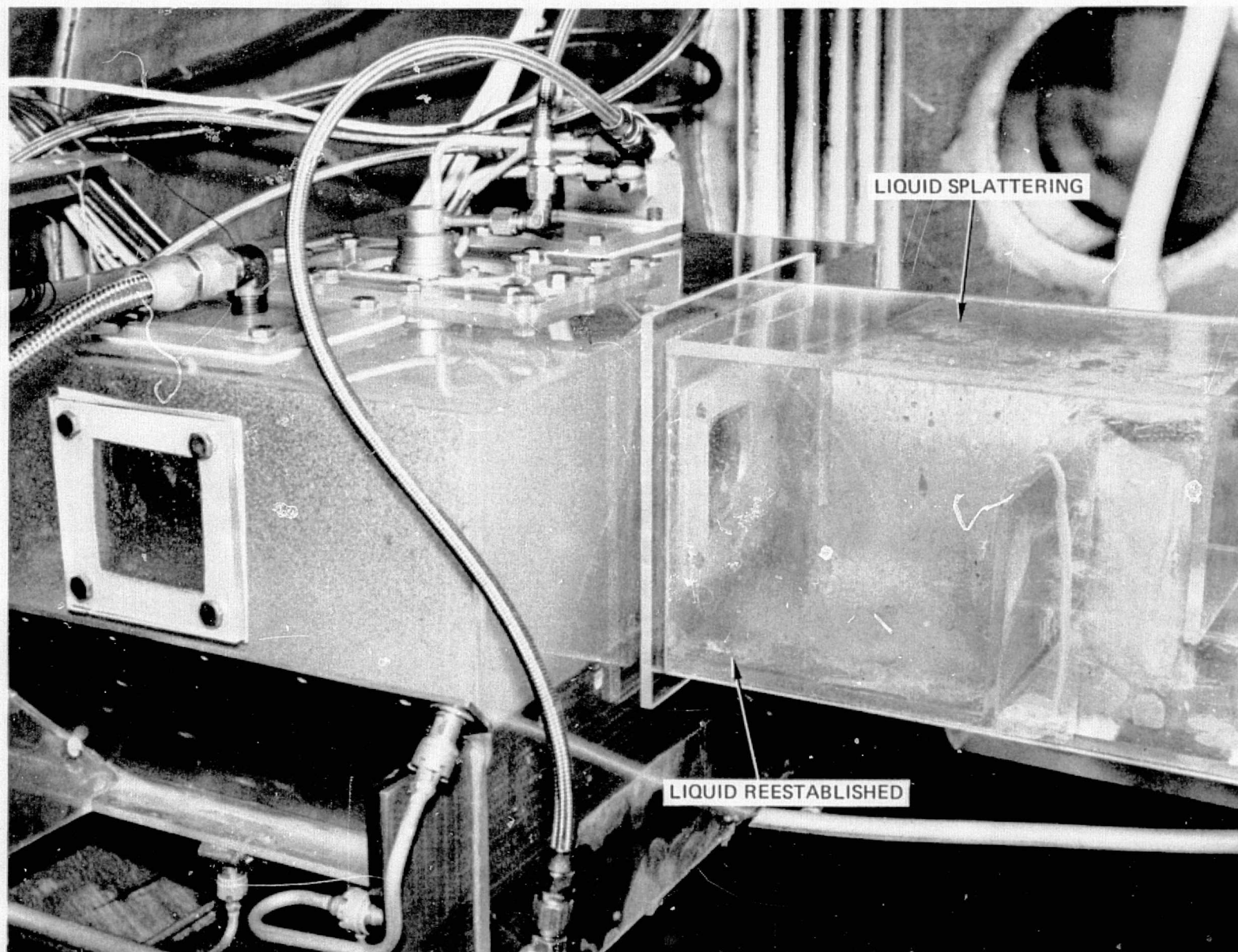
FIGURE D-8   T + 01:30:50   22.03 LBS. EVAPORANT SPRAYED
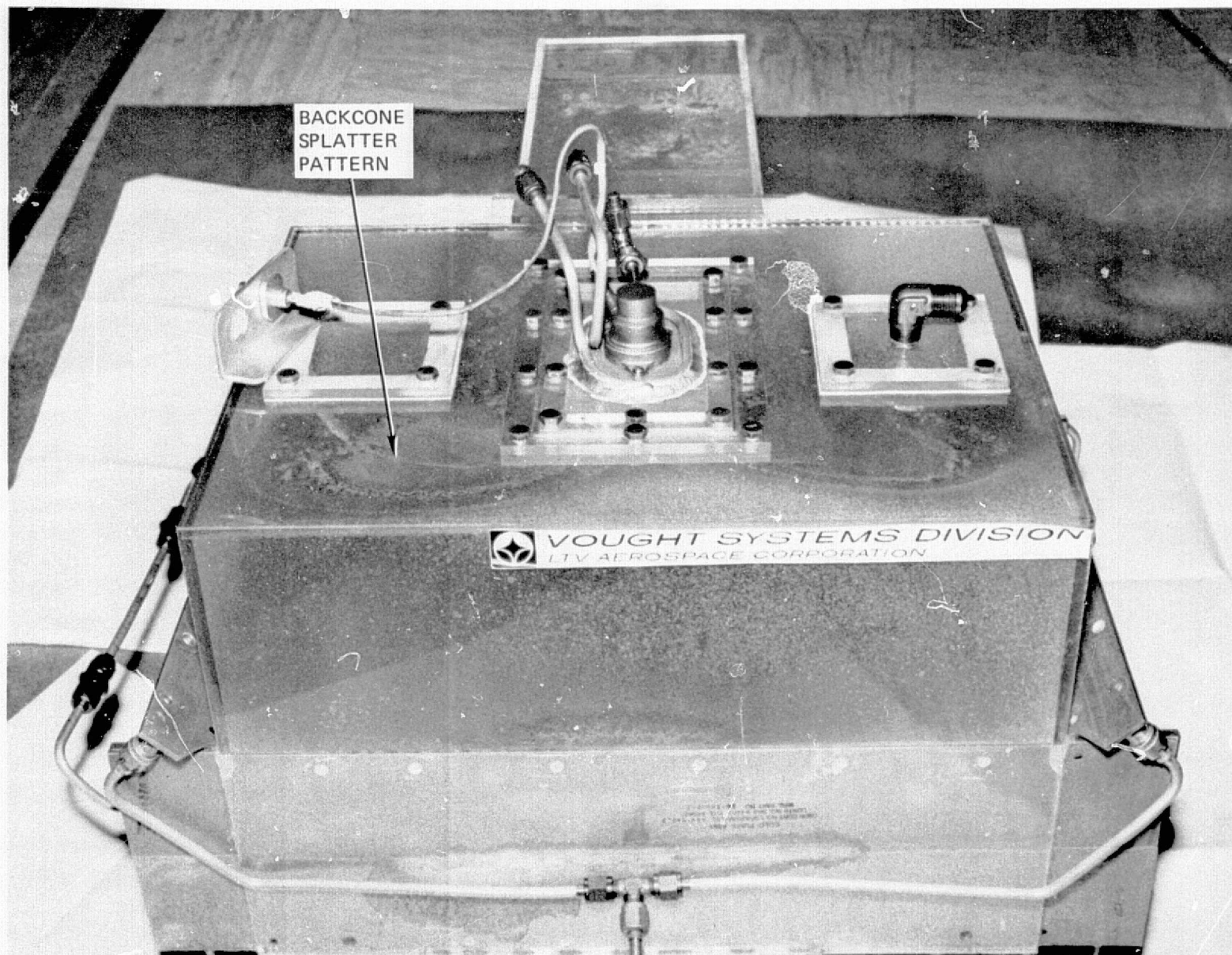
FIGURE D-9   POST-TEST EXAMINATION   29.53 LBS. EVAPORANT SPRAYED

RESIDUE ON
H/T SURFACES
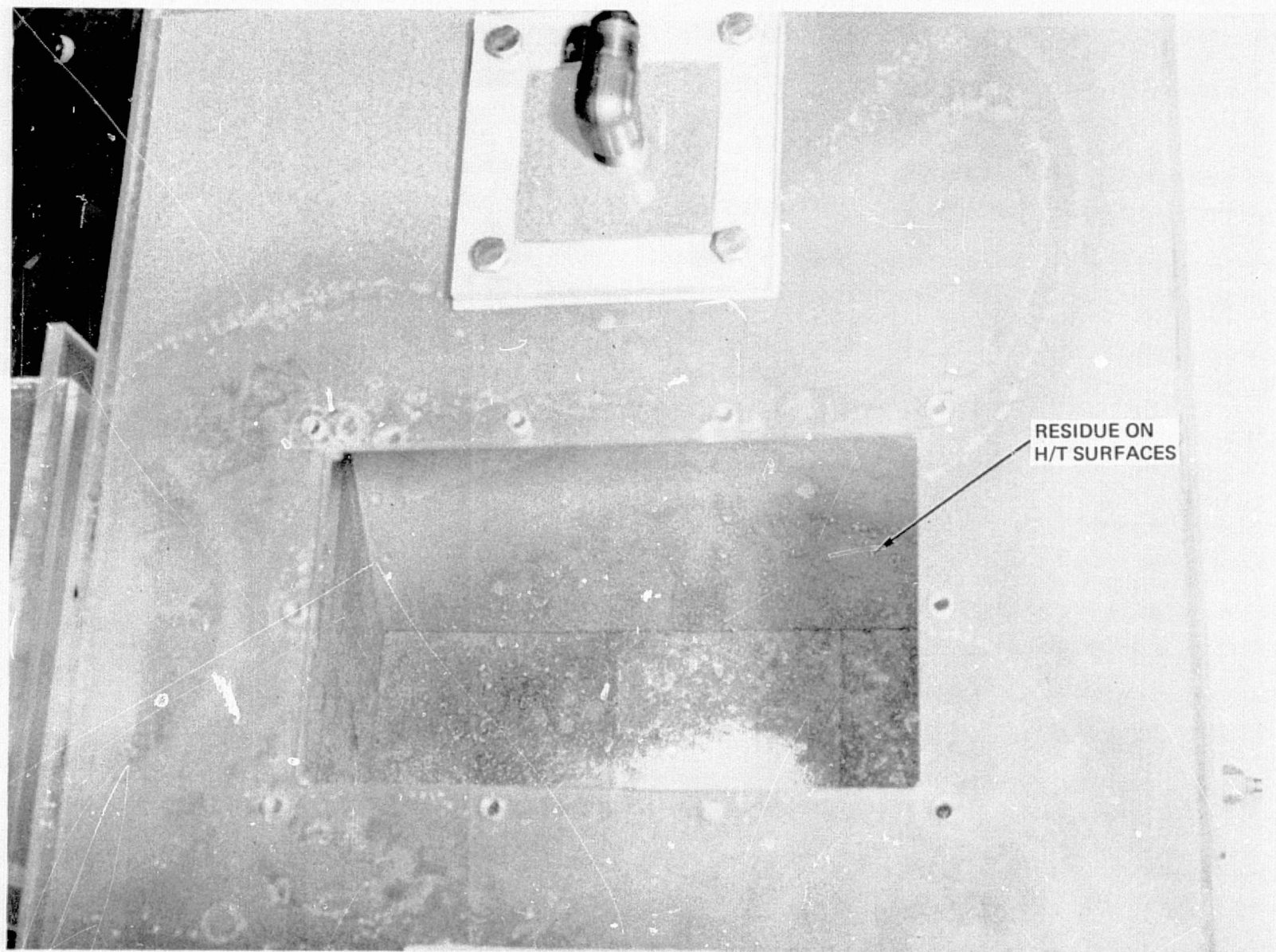
FIGURE D-10 POST-TEST EXAMINATION

RESIDUE ON
H/T SURFACES
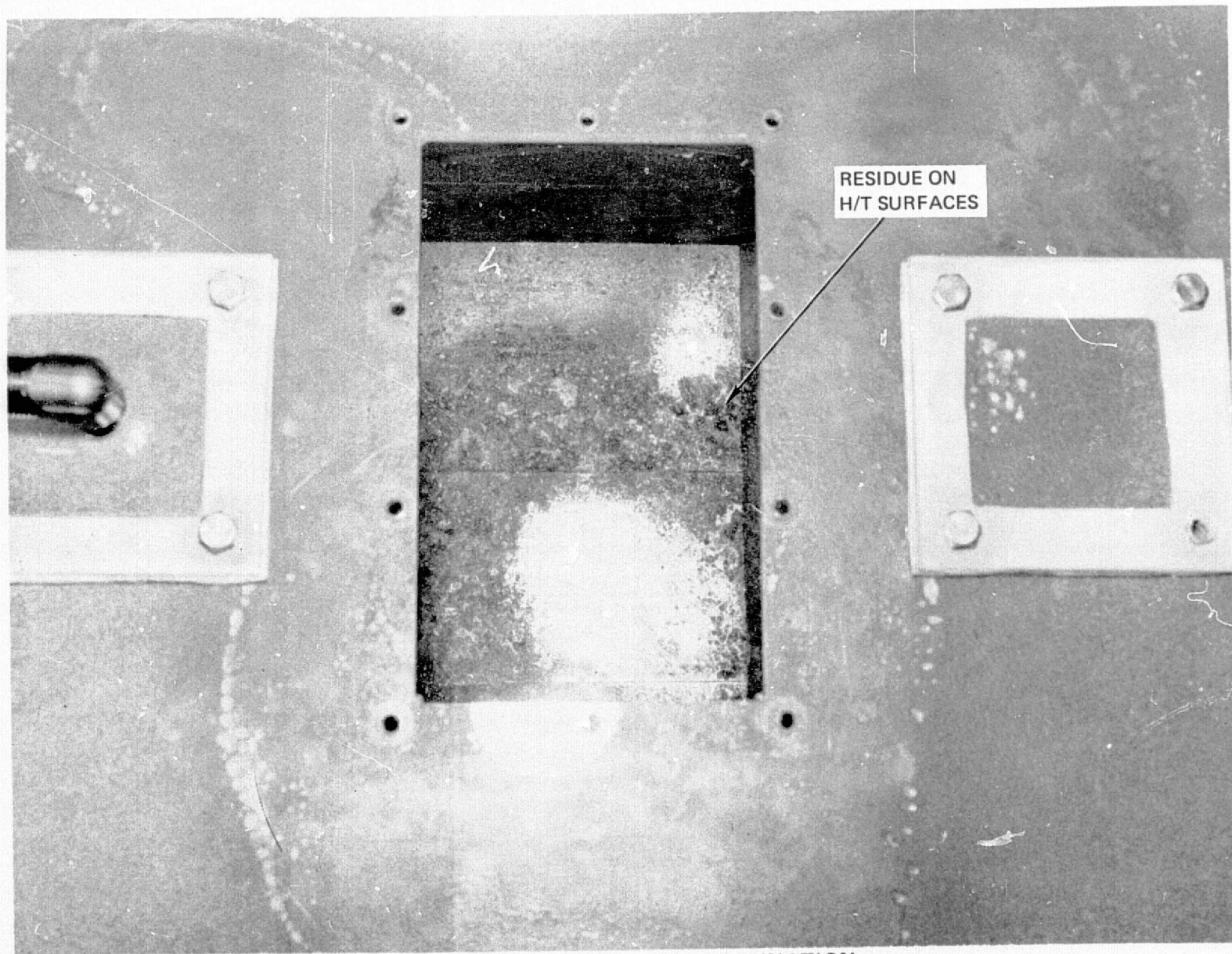
FIGURE D-11 POST TEST EXAMINATION

RESIDUE ON MOUNTING PLATE

NO RESIDUE ON NOZZLE
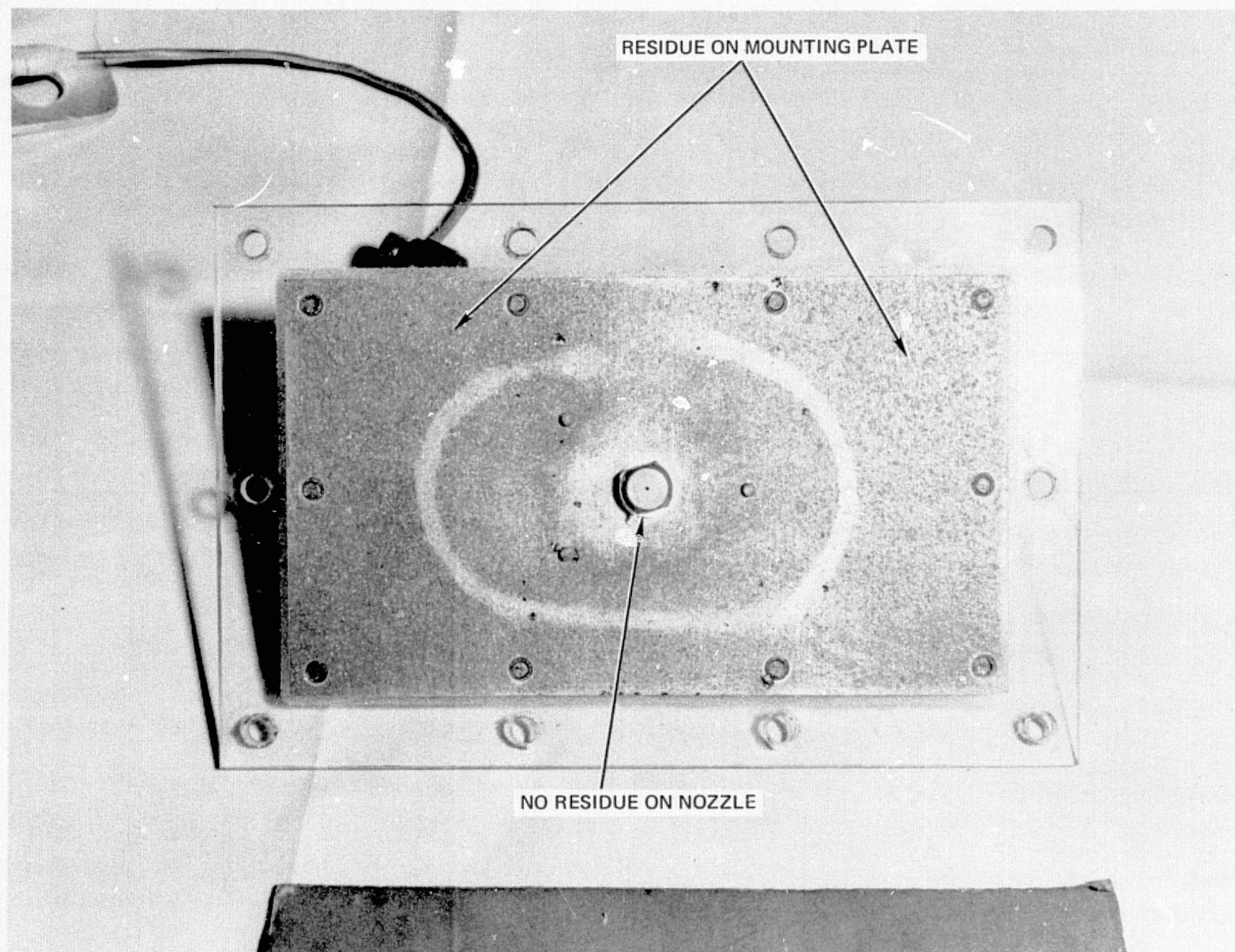
FIGURE D-12   POST-TEST EXAMINATION

APPENDIX E
PRELIMINARY STRUCTURAL ANALYSES OF
THE PROTOTYPE 2 AND 3 FLASH EVAPORATORS

The analyses of the prototype 2 and 3 flash evaporators were performed to determine the maximum safe operating pressure, analyze the mounting system, and analyse the thermal effects. The prototype evaporators will not be subjected to the vibroacoustics, acceleration or shock loading that will be seen on production hardware, and therefore, analyses of these loads were not performed. The results of the analyses are summarized below.

o The maximum allowable operating pressure for the hollow cone prototype is 203 psi, the maximum allowable proof pressure is 305 psi or 1.5 times the operating pressure, and the burst pressure is 1015 psi.

o The thermal gradients and therefore stresses are so low that the analysis is not presented in this report. The inlet temperature is 120° and the exit temperature is 40°. The maximum temperature drop across the core is 20°.

o The prototypes will be supported by a set of straps acting as a cradel. The straps will support the weight of the evaporator plus approximately 25 pounds of equipment. Total estimated weight is 50 pounds, which presents no problem for two straps.

o The maximum allowable operating pressure for the solid cone prototype is 237 psi, the maximum allowable proof pressure is 356 psi or 1.5 times the operating pressure, and the burst pressure is 1000 psi.

o The thermal gradients and support methods for the solid cone prototype are the same as those for the hollow cone prototype.

DISCUSSION:

Factors of Safety - The following factors of safety are applicable to the flash evaporator prototypes to be used for thermal testing at LTV Aerospace. The factors of safety specified are minimum and shall be used in addition to any applicable vibration amplification factors, weld factors, etc.

FACTORS

Element Type	Proof*	Burst
Pressurized lines and fittings	2.0 times max. operating pressure	4 times max. operating pressure
All other pressurized components	1.5 times max. operating pressure	2 times max. operating pressure

*No yielding at proof pressure

All external applied loads shall produce no yielding at limit and no failure at 1.5 times limit.

Design Materials and Allowables - The prototype flash evaporators are constructed of 3003-0 face sheets, core, and tubing. The braze filler material is 4343 and the weld filler material is 4043. The filler material properties are assumed to be higher than those of 3003-0. All welds and brazed joints are assumed to have 75% of the parent material properties along the interface.

	F_{tu} KSI	F_{ty} KSI	E_{LONG} %	F_{cy} KSI	F_{su} KSI	F_{sy} KSI	Endurance Limit KSI
3003-0	14	5	14-23	5	10	3	7

Ref: "Structural Aluminum Design", Reynolds Metals Company, 1967, Pg. 108.

STRUCTURAL ANALYSIS: The structural analyses are shown on pages 5-11.

Two loading conditions have been considered, (a) an overall evaporator burst pressure of .078 #/in^2, and (b) a maximum operating pressure. The maximum safe operating pressure is determined for each prototype design by first determining the maximum allowable proof pressure based on no yield, then taking 2/3 of the proof pressure as the maximum operating pressure. The burst pressure is calculated based on the ultimate allowables for the materials.

CONCLUSIONS: The prototype evaporators are adequate for the currently planned testing to be done at LTV, but changes in material and design will be required for a reliable minimum weight production type evaporator.

The shuttle environment as understood at this time is: an operating pressure of 385 psi, an acceleration loading of ± 5 g's along all axes, a temperature envelope of -100°F to +300°F, and a high shock and vibration loading. To meet these requirements, an increase in the core sheet thickness of 30% or a higher strength core material is required. The exit and intake manifolds should have more continuous load paths, such as a formed tube, shown in Figure 7, or a local thicker core gage under the weld area. Also some provisions for an integral mounting system should be incorporated in the design concept.

PRELIMINARY STRUCTURAL ANALYSIS
FLASH EVAPORATOR
U-408780

INTAKE MANIFOLD

WELD .04 THICK
4043 MATERIAL
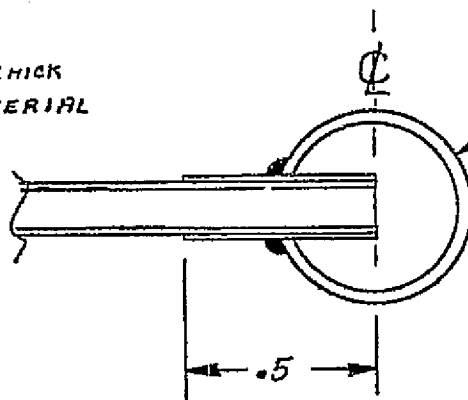
0.5 DIA, .035 THICK WALL TUBE
3003-0 MATERIAL
$F_{tu} = 14,000$ PSI
$F_{ty} = 5,000$ PSI
$F_{sy} = 3,000$ PSI
$F_{su} = 10,000$ PSI

FIGURE E-1

ALLOWABLE PROOF PRESSURE FOR TUBE

Hoop. $P_{A.P.} = \dfrac{F_{ty}\, t}{R_{Avg}} = \dfrac{(5000)(.035)}{.2325} = \underline{\underline{752}}$ PSI

ALLOWABLE PROOF PRESSURE FOR TUBE TO FACE SHEET WELD

Assume WELD EFFICIENCY IS 75%

WELD AREA = .04 IN^2/IN

LOAD PER INCH ON WELD = (% Eff.)(AREA)(F_{sy}^{*}) = (.75)(.04)(3000) = 90 #/IN

$P_{A.P.} = \dfrac{(\% Eff)(A)(F_{sy})}{R} = \dfrac{90}{.2325} = \underline{\underline{387}}$ PSI

* F_{sy} FOR 3003-0 USED AT INTERFACE BETWEEN
   WELD AND PARENT MATERIAL

E-4
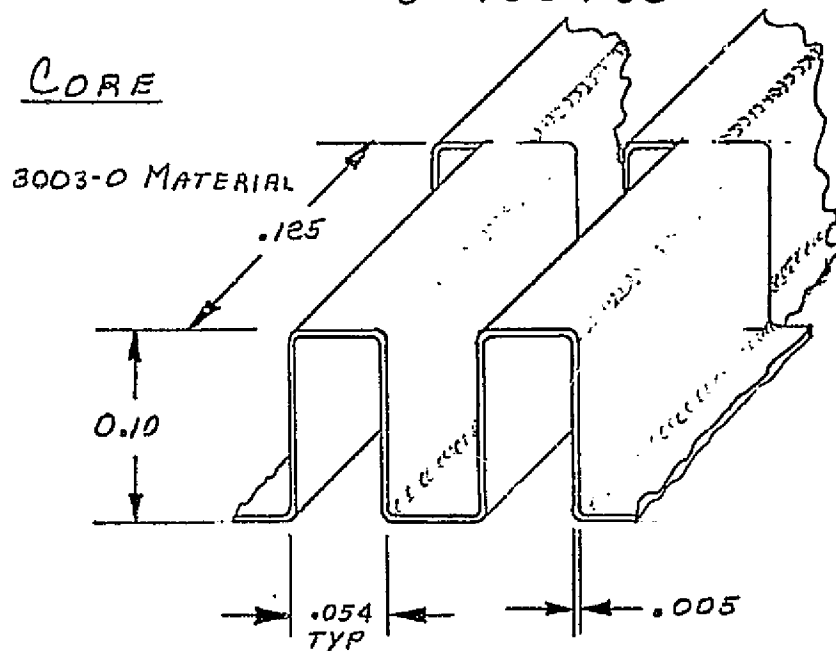
PRELIMINARY STRUCTURAL ANALYSIS
FLASH EVAPORATOR
U-408780

CORE

3003-0 MATERIAL

.125

0.10

.054
TYP

.005

FIGURE E-2

NET TENSION AREA = $(.005)(.125)(18.5)(8) = .0925$ IN^2/IN^2 PANEL

PROOF PRESSURE ALLOWABLE $= (5000)(.0925) = 462.5$ PSI

BURST PRESSURE ALLOWABLE $= (14000)(.0925) = 1295$ PSI

OPERATING PRESSURE ALLOWABLE $= 462.5/1.5 = 308$ PSI

PRELIMINARY STRUCTURAL ANALYSIS
FLASH EVAPORATOR
U-408780

FIGURE E-3
CORE TO FACE SHEET BRAZE
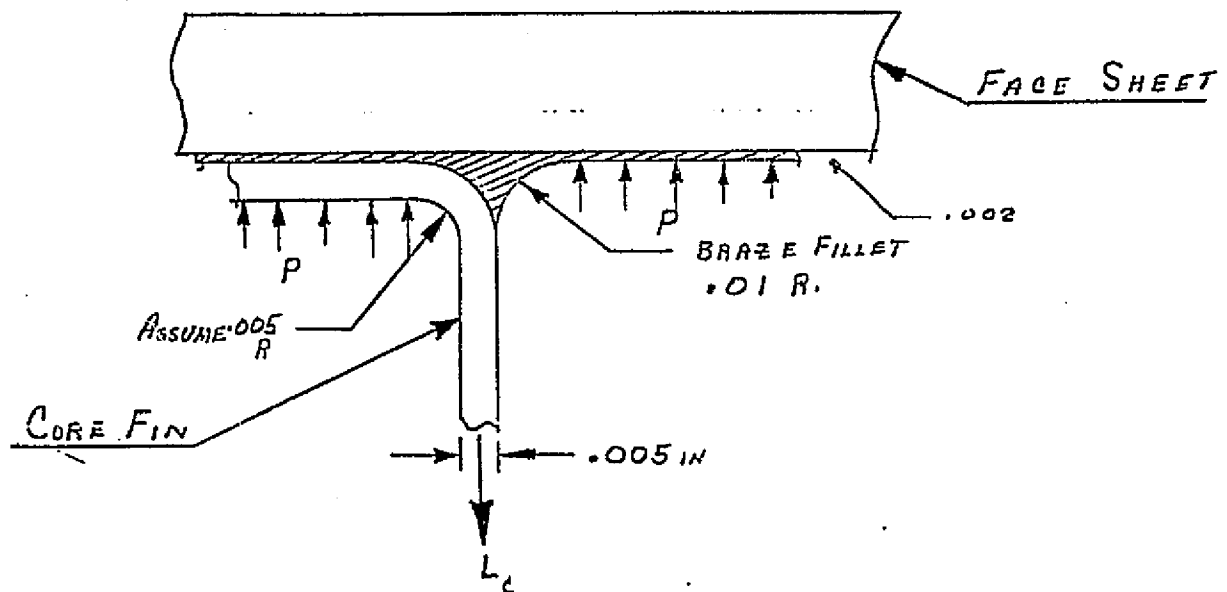
BRAZE FILLER MATERIAL IS 4343

BRAZE WILL CARRY $\frac{1}{2}$ THE LOAD ON EACH FIN.

FILLET AREA PER FIN $= (.125)\left(\frac{(.\pi)(.010)}{2}\right) = .00196$ IN^2

ASSUME 75% EFF. THEN THE PROOF PRESSURE IS

$P_{AP} = (.75)(.00196)(18.5)(8)(3000) = (.217)(3000) = 652$ PSI

BURST PRES. ALLOWABLE $= (.217)(10,000) = 2,170$ PSI

OPPERATING PRESSURE ALLOWABLE $= 652/1.5 = 434$ PSI

PRELIMINARY STRUCTURAL ANALYSIS
FLASH EVAPORATOR
U-408780

EXIT MANIFOLD
    SEE FIGURE 1   Pg —
TUBE DIA = .625 IN   AVG RADIUS = .295
TUBE THICKNESS = .035
3003-0 MATERIAL

HOOP ALLOWABLE ON TUBE FOR PROOF PRESSURE

$$P_{AP} = \frac{F_{ty} \, t}{R_{AVG}} = \frac{(5000)(.035)}{.295} = 596 \text{ PSI}$$

TUBE TO FACE SHEET WELD

ASSUMED WELD BEAD WIDTH = .04
    ASSUMED EFFICIENCY = 75%

PROOF $P_{A.P.} = \frac{(\% EFF)(A)(F_{ty})}{R} = \frac{(.75)(.04)(3000)}{.295} = \underline{305 \text{ PSI}}$

OPPERATING $P_{A.O.} = 305 / 1.5 = \underline{203 \text{ PSI}}$

BURST $P_{A.B.} = \frac{(.75)(.04)(10000)}{.295} = \underline{1015 \text{ PSI}}$

PRELIMINARY STRUCTURAL ANALYSIS
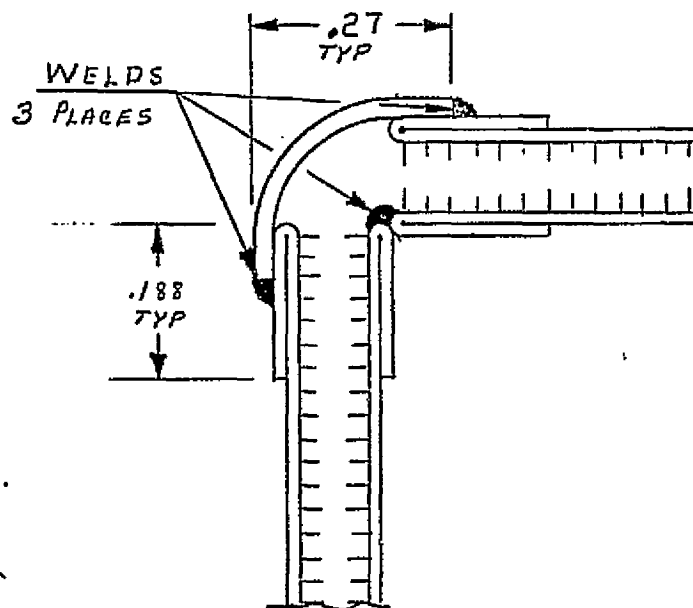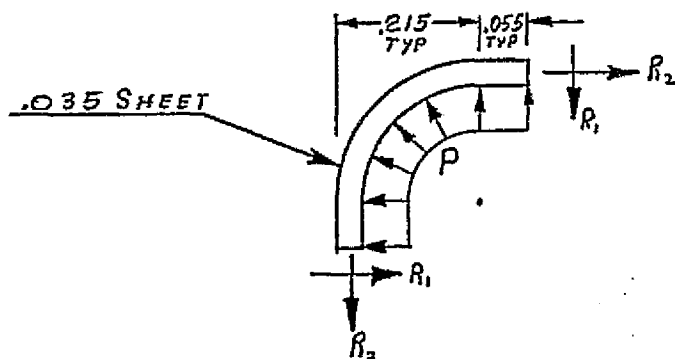FLASH EVAPORATOR
U-408780

FIGURE E-4
CYLINDER TO FLAT JOINT

WELD ASSUMED TO
DEVELOPE 75% OF
PARENT MATERIAL

LOADS ON OUTER FACE SHEET SPLICE

ASSUME $R_{2A} = (P_{AP})(.215)$ = $(\% E_{FF})(A)(F_{ZY})$ = $(.035)(5000)(.75) = 131.25$

$R_{1A} = (P_{AP})(.055)$ = $(\% E_{FF})(A)(F_{SY})$ = $(.035)(3000)(.75) = 78.75$

$P_{AP_2} = \underline{601\ PSI}$

$P_{AP_1} = \underline{1430\ PSI}$

E-8

PRELIMINARY STRUCTURAL ANALYSIS
FLASH EVAPORATOR
U-408781

THIS EVAPORATOR IS OF THE SAME CONSTRUCTION AS U-408780, EXCEPT FOR THE INLET MANIFOLD WHICH IS ANALYZED BELOW.
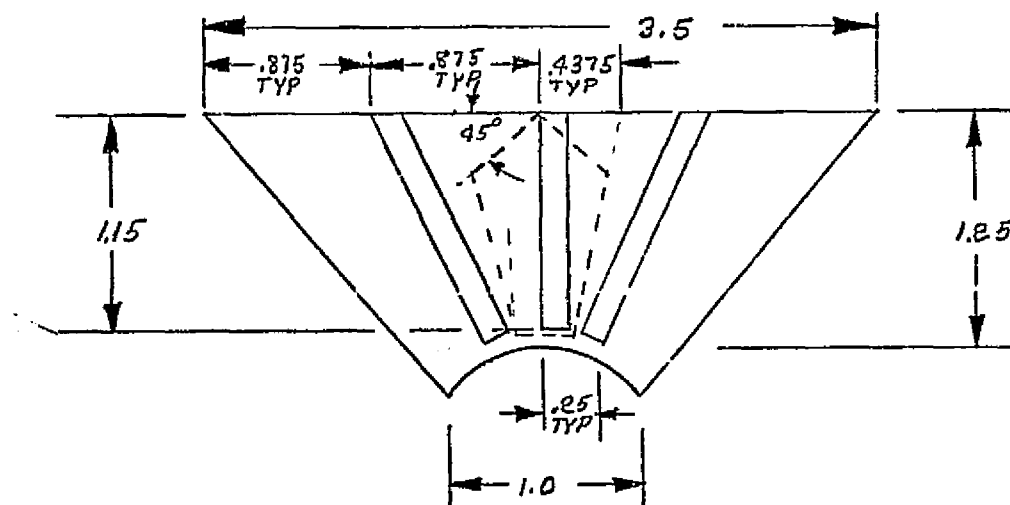

FIGURE E-5

$\underline{AREA}$ LOADING CENTER WEB SHOWN IN DASHED AREA

$$A_p = (2)\left[(1.15)\left(\frac{.4375 + .125}{2}\right) - (.4375)(.4375 \sin 45°)(.5) - (.4375 \sin 45°)\right.$$

$$\left. (.4375 \sin 45°)(\tan 15.6°)(.5)\right]$$
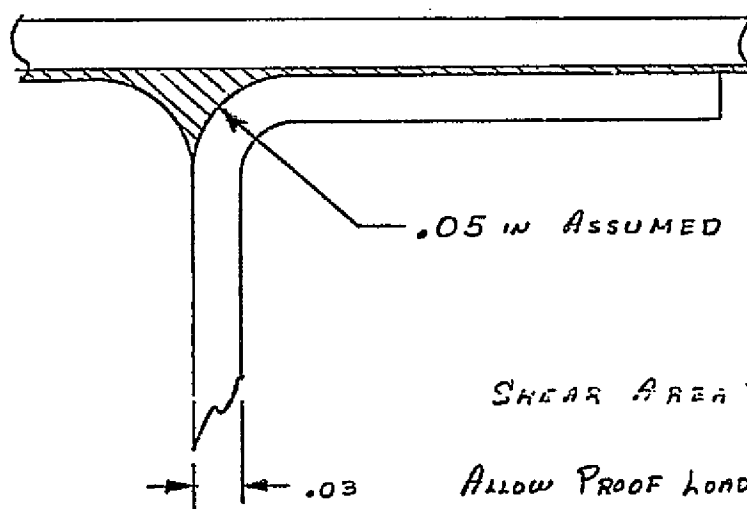
$$A_p = (2)[.3234 - .0675 - .013] = .4858 \, IN^2$$

FOR TENSION ALLOWABLE IN WEB

$$\text{PROOF PRESSURE} = \frac{A_t F_{ty}}{A_p} = \frac{(1.15)(.03)(5000)}{.4858} = \underline{356 \, PSI}$$

$$\text{OPERATING PRESSURE ALLOWABLE} = \frac{356}{1.5} = \underline{237 \, PSI}$$

PRELIMINARY STRUCTURAL ANALYSIS
FLASH EVAPORATOR
U-408781

THE JOINT BETWEEN THE WEB AND THE FLAT
OF THE MANIFOLD IS ASSUMED TO BE BRAZED
AS SHOWN.

.05 IN ASSUMED

.03

FIGURE E-6

$$SHEAR\ AREA = \frac{\pi \cdot D(.115)}{4} = .0722$$

$$ALLOW\ PROOF\ LOAD = (.0722)(3000)$$

$$= 216\ \#$$
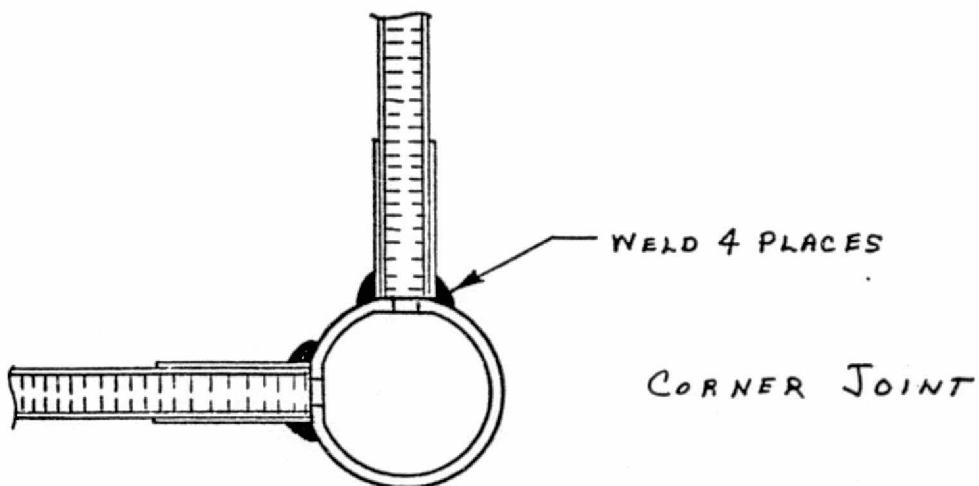
$$ALLOW\ PROOF\ PRESS = P/A = \frac{216}{.4858} = \underline{445\ psi}$$

$$ALLOWABLE\ OPERATING\ PRESSURE = \frac{445}{1.5} = \underline{296}\ psi$$

PRELIMINARY STRUCTURAL ANALYSIS
FLASH EVAPORATOR

WELD
TWO PLACES

.08 OR SMALLER HOLES
FOR FLOW CONTROL
WITH 2 D SPACING
MINIMUM IN 3003-
MATERIAL

.055
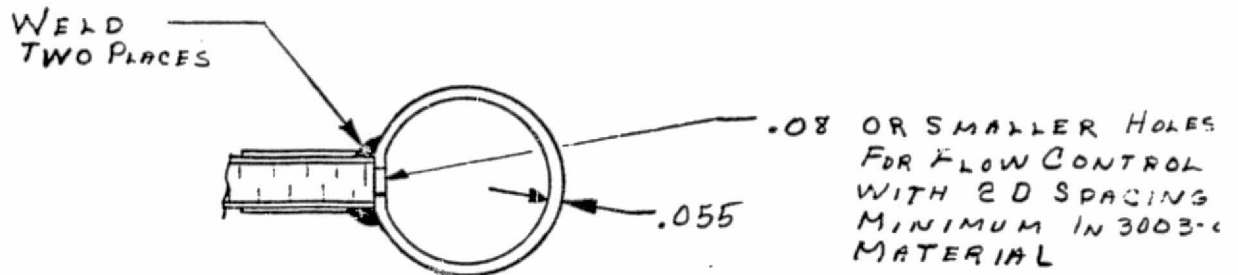
ONE POSSIBLE TUBE ARRANGEMENT
ON MANIFOLD (INTAKE AND EXIT)

WELD 4 PLACES

CORNER JOINT

APPENDIX F

PROTOTYPE 2 WOUND TUBE DESIGN SUMMARY

The Prototype 2 unit design was initially planned to be a refinement
of the Prototype I helically wound tube device shown in Figure F-1 with improve-
ments in nozzle performance, fabrication techniques, valve/nozzle integration,
and reduction in volume. The design requirements, identical to the Prototype I
unit, were 14.6 kw (50,000 BTU/hr) heat rejection capability with a 277.5°K
(40°F) controlled outlet temperature device which incorporated redundant transport
passages and water spray nozzles (see Reference 2). Additionally, the same
Prototype I approach to heat load control and exhaust duct design was to be used.
A short summary of the design effort conducted is described in this Appendix.

The results of initial nozzle testing (reported in Section 3.0 of
Appendix A) indicated that the wound tube Prototype 2 evaporator could be reduced
in volume by 25% primarily by positioning the spray nozzle 30 cm (12 inches) from
the device floor. The sidewalls could be reduced in height by 50 mm (2 in.), and
a rather flat backcone with a 50 mm (2 in.) depth could be fabricated to which a
valve nozzle mounting plate could be mounted.

After careful consideration, the sidewall height of the Prototype I
device was retained, and a flat backcone was designed which incorporated the valve/
nozzle mounting plate was selected for simplicity of design, and cost of fabrication.
The valve/nozzle was mounted to this back plate with provisions for removal for
servicing.

The valve/nozzle design used a similar approach as used in the Prototype
I unit. The holdup volume was reduced, however, from 0.5 cc of the Prototype I
to 0.15 cc by redesign of the valve/nozzle method of attachment and method of nozzle
distributor holding technique, (the design goal was 0.10 cc). This reduction in
holdup volume resulted in approximately 1/3 less volume of holdup "ice chip" during
cyclic operation.

Manufacturing and fabrication design improvements were the major dif-
ferences between the wound tube Prototype 2 and 1 device designs. Seamless drawn
tubing of rectangular cross section were to replace the structurally unreliable
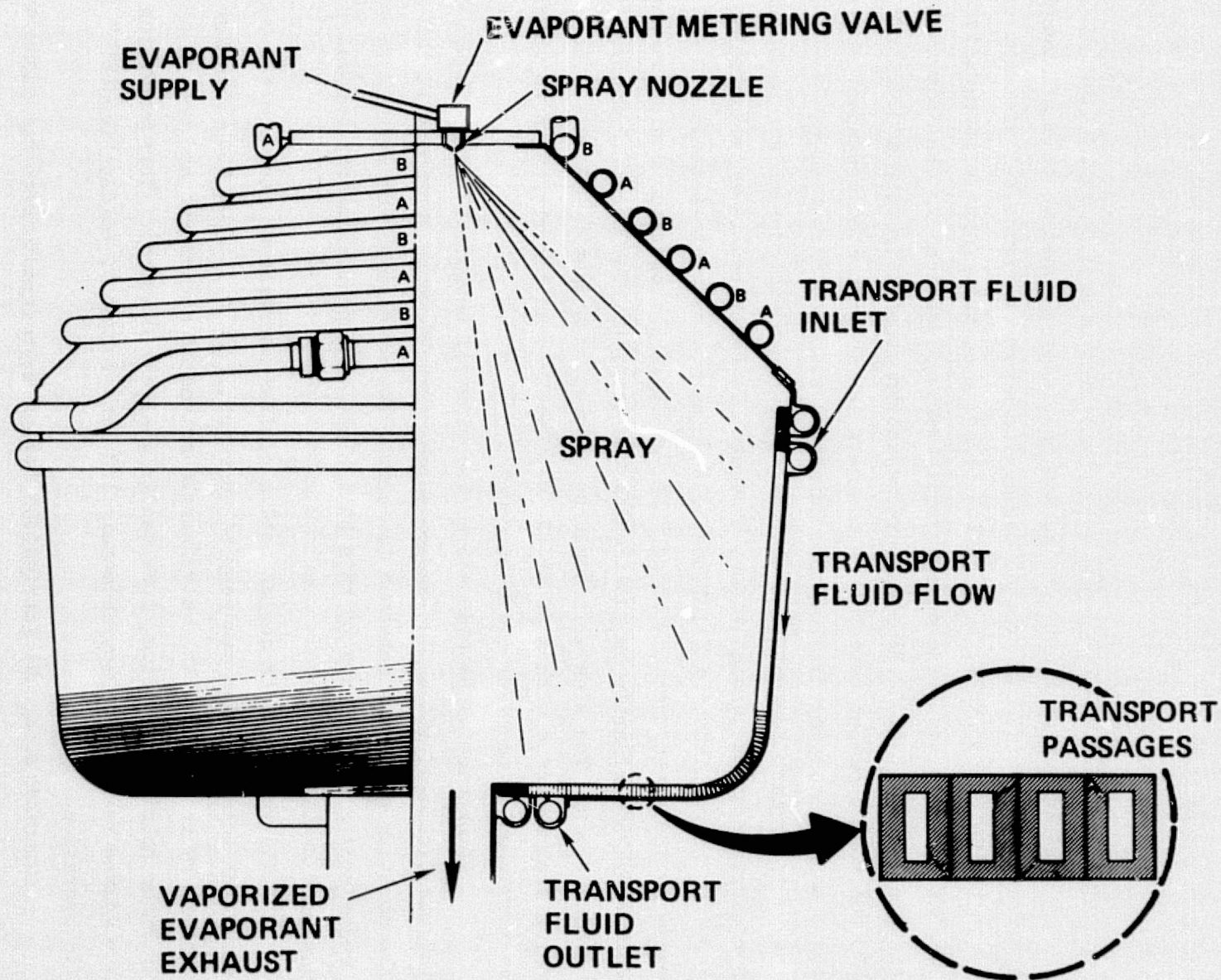port hole die extruded tubes used on the Prototype I device. Assembly techniques

FIGURE F-1   PROTOTYPE I FLASH EVAPORATOR

(including draw forming, tube performing, etc.) were investigated with the hand formed tube procedure selected, as in the previous fabrication, with little additional tooling identified due to cost and technical risks involved. Six structural supports were designed to be tack welded and subsequently brazed to the assembly to provide a structurally sound method of mounting the device.

An experimental program was conducted to determine the most promising approach of brazing the wound tube assembly to meet the current (1972) Shuttle materials specification. The program included investigation of pre-assembly cleaning, pre-braze cleaning, brazing and post braze cleaning procedures. The feasibility of brazing the wound tube evaporator using standard vacuum fluxless braze and vacuum brazing employing a volatile cleaner were experimentally investigated. Although successful brazes were obtained using both techniques, the salt pot brazing process employed in the Prototype I fabrication was selected because the state-of-the-art status of brazing the complicated wound tube assembly was not developed and a high degree of technical risk would have been involved.

A structural analysis of the wound tube Prototype 2 design indicated the proposed design was adequate for Shuttle application of the device. The launch vibroacoustic environment loads could be met providing a 90% braze between the wound tubes could be obtained. The seamless drawn tubing had adequate strength to withstand the Shuttle fluid internal pressures expected. Six mounting lugs/ structural support members were identified to carry the expected pressure and vibration loadings.

The design of the wound tube Prototype 2 unit was completed during March 1973. During a thorough design review with NASA-JSC, however, it was decided to forego fabrication of the device since the heat load requirements of the Space Shuttle had become better defined as much higher values, and the need for a top-off evaporator for supplementing radiator heat rejection and for water management became firmly identified. It was also desired to optimize the device weight (because of Shuttle weight problems) and cost by fabricating the unit from compact heat exchanger core. The results of this approach are reported in Section 4.0 of this report.